UNIVERSITY OF OKLAHOMA

GRADUATE COLLEGE

DESIGN AND ANALYSIS OF BUILDING THERMAL MODEL FOR GRID-INTERACTIVE EFFICIENT OPERATIONS

A DISSERTATION

SUBMITTED TO THE GRADUATE FACULTY

in partial fulfillment of the requirements for the

Degree of

DOCTOR OF PHILOSOPHY

By

JUNKE WANG
Norman, Oklahoma
2020

DESIGN AND ANALYSIS OF BUILDING THERMAL MODEL FOR GIRD-INTERACTIVE EFFICIENT OPERATIONS

A DISSERTATION APPROVED FOR THE
SCHOOL OF AEROSPACE AND MECHANICAL ENGINEERING

BY THE COMMITTEE CONSISTING OF

Dr. Li Song, Chair

Dr. Choon Yik Tang, Co-Chair

Dr. Dean Hougen

Dr. Jie Cai

Dr. Wilson Merchan-Merchan

Acknowledgements

At this moment, a lot of thoughts and feelings start emerging in my mind. Time flies like an arrow. The process of pursing a Ph.D. is coming to an end. Looking back, there have the joy of success, frustration of failure, confusion about the future, and confidence in the future. There have passions, and there have tears, but they have been engraved in the current thoughts. This period of no regrets made me lucky to meet my advisor, teammates, and friends and your care and help allowed me to spend these golden years of youth. I sincerely thank you!

I would like to thank my advisor Dr. Li Song for bringing me into her research team and all her tremendous support, advice, and encouragement in my research work and daily life. Your mentorship and guidance have enabled me to complete my Ph.D. and become a better researcher. Your profound knowledge, broad academic vision, pragmatic work style, and amiable attitude not only increase my academic knowledge and professional skills, but also help me learn how to deal with people and things in work and life. It has been a very pleasant experience to work with you during my Ph.D. I want to express my sincerest thanks to you. I am very thankful to my co-adviosr Dr. Choon Yik Tang for mentoring me in my research works. Your guidance and support have enabled me to gain extra knowledge from different fields. I am also very thankful to my committee members Dr. Jie Cai, Dr. Dean Hougen, and Dr. Wilson Merchan-Merchan. Thank you for your time, guidance, advice, and feedback during each stage of my PhD. I greatly appreciate your support and advice.

I am thankful to my current teammates Rodney Hurt and Yilin Jiang, and previous teammates Emmanuel Hakizimana, Oluwaseyi T. Ogunsola, Alejandro L. Rivas Prieto, and Shima Shahahmadi in the Building Energy Efficiency Laboratory (BEEL) at OU. Thank you all for the help and support in the research work. I have gained knowledge and happiness with you all. We had a lot of great time while learning and working together. I also like to thank all AME staffs, Bethany Burklund, Melissa Foster, Martina Ferguson, Ellen E. McKenzie, Billy Mays, and Greg Williams. I would like to thank Drs. Farrokh Mistree and Janet K. Allen for giving me instructions on how to be a professor in academia. I also want to thank my friends Yujie Wei, Zhimin Jiang, Tianyang Zhao, Wenwen Li, and all members of my tennis and badminton teams. Thank you all for the moral support. We spend a lot of wonderful time, full of fun, communicating and helping each other. I really appreciate you all.

I deeply appreciate my family for their support throughout the pursuit of this degree. I am thankful for my grandpa, grandma, uncle, and aunt. You have been silently supporting and encouraging me for many years and have made me feel the warmth of my loved ones. Especially, I am thankful for my parents Deliang Wang and Yinfeng Sun for their love, encouragement, support, and understanding while I was studying abroad. Thank you for caring, supporting, and encouraging me at all times. I have been studying abroad all the year round and have not been able to accompany you. I ignore your concern and miss and feel deeply guilty. If this dissertation counts as a little grade, it is just for you. To my girlfriend Luyao Xie, thank you and your parents for the understanding and the

emotional and spiritual support, which is overwhelming. I really appreciate that. We did it together and we will do it together in the future.

Table of Contents

List of Figures

List of Tables

Abstract

Heating and cooling in residential buildings, provided by Heating, Ventilation, and Air-Conditioning (HVAC) systems, represent a crucial load for electric utilities. Fluctuations of heating and cooling loads in residential buildings have a significant impact on a utility's load profile. Electricity suppliers have introduced time-of-day (TOD) or time-of-use (TOU) electricity pricing, making peak electricity very expensive to consumers, as a means of managing load demand when the grid is near capacity. The impact on the utility's load profile can be mitigated by grid-interactive efficient HVAC operations that reduce the peak load demand. Pre-cooling is a strategy that reduces the load during on-peak hours by shifting cooling operation from on-peak hours to off-peak hours. Accordingly, many manufacturers have built in rule-based pre-cooling operation strategies into their smart thermostats by setting the space temperature a few degrees lower for a period preceding the start of on-peak hours. However, common rule-based pre-cooling operation strategies might not be an optimal solution for a specific home with specific thermal properties and HVAC system cooling capacity under a given utility rate structure and varying weather conditions in terms of cost savings. Moreover, even though the smart thermostat and utility industries have increasingly collected abundant operational data, there is still a lack of a systematic framework that can utilize such data to generate actionable information for advanced home HVAC system diagnosis and control, and for realizing home energy cost savings and grid-interactive efficient operations. Therefore, the primary research question to address in this study is —

What is the fundamental system science underlying the design of such a framework using the data collected from smart devices for the intelligent dynamic management of cooling energy use in a home?

Recognizing that a home thermal model, which is capable of connecting the data such as weather with HVAC operations, is at the heart of this framework, this study first aims to develop such model that is built upon the standard RC (Resistance–Capacitance) approach for one lumped virtual envelope to describe the thermal dynamics of a home. A parameter estimation scheme is also developed that enables automatic, sequential, and optimal estimation of the model parameters, i.e., the thermal properties, of a home, using the data collected through smart thermostats and internet connections. The technical approach includes the development and validation of the home thermal model and its parameter estimation scheme using data collected from a test home. Moreover, with reasonable simplifications to the home thermal model, a model-based envelope performance evaluation method is also proposed to assess the thermal performance of a home envelope in this study. The simplicity of the method allows the parameter to be automatically estimated using a short period of indoor and outdoor air temperature data through data screening without the need for a home's physical information.

Then, an optimal pre-cooling strategy is developed based on an optimization algorithm that is constructed utilizing the automatically identified home thermal model, which is unique for each home, to search optimal HVAC operations for minimizing energy cost with a given TOU utility rate structure,

HVAC system capacity, and weather condition. The algorithm determines the HVAC on/off control signal that minimizes the 24-h energy cost while maintaining thermal comfort and calculates the corresponding optimal indoor air temperature. Through simulations, the results demonstrate that the optimal pre-cooling strategy is indeed significantly more effective than the common rule-based pre-cooling strategies.

Since the optimal pre-cooling is heavily dependent on a specific set of conditions, such as specific thermal properties, HVAC system capacity, utility rate structure, and weather condition, the impact of different sets of conditions on the optimal pre-cooling is investigated by the operation and energy performance analysis on the thermal dynamics, total energy consumption, and energy cost and is also compared with a rule-based pre-cooling through simulations. It is found that the optimal pre-cooling is adaptive based on changing conditions and its performance is significantly dependent on weather conditions and home thermal properties, while its performance may vary for different cooling capacities and utility rate structures. The better the home thermal condition is, the less energy cost the operation requires. In terms of weather condition, it has the dominant impact on the performance of the optimal pre-cooling operation. The hotter the weather is in summer, the more cost savings a good thermal condition home can achieve. Moreover, less energy cost can be achieved for a HVAC system with a higher cooling capacity only when a home has a better thermal condition, and also tends to be achieved for a utility rate structure with a much higher on-peak electricity price than the price during off-peak or/and mid-peak hours. For a home

with a poor thermal condition, however, it is found that the optimal pre-cooling strategy may need more energy consumption, while the least energy consumption can always be achieved without sacrificing thermal comfort for a home with a good or better thermal condition, compared with rule-based operation pre-cooling strategies. The superb energy performance of the optimal strategy is attributed to a longer runtime of the HVAC system in cool outdoor air conditions and to the elimination of deadband in the HVAC operation, which is required by the rule-based operation strategies, to allow the indoor air temperature to stay near the thermal comfort upper bound as much as possible. These observations are in line with the analysis and expectations and experience.

Additionally, this study conducts several experiments through a real test home, including the investigations of the impact of internal heat gains on the home thermal model and cooling load calculations using the mode-based method and the HVAC efficiency. This study also investigates the implementation of the optimal pre-cooling strategy and meanwhile demonstrates the effectiveness of the optimal pre-cooling strategy in terms of the operation and energy performance analysis through experiments.

Overall, this study has helped to answer important questions about effective decision making for the operation of HVAC systems, with tremendous potential for minimizing home energy cost. This study is a fundamental research that has culminated in understanding of thermal interactions and investigation of methodologies for achieving grid-interactive efficient operation of HVAC system. This study also contributes to knowledge through the development of step-by-step

approach that may be followed to achieve optimal operation of HVAC systems, based on consideration of thermal properties, weather condition, HVAC cooling capacity, and utility rate structure in a smart grid environment. Therefore, the developed framework in this study is useful for advanced home HVAC system diagnosis and control, and for realizing home energy savings and grid-interactive efficient operations.

Chapter 1: Motivation and Problem Identification

This chapter introduces the motivation for this study and the background information to building thermal modeling and optimal operation in the presence of smart grid environment. It also includes the state of the art and current challenges with building systems for achieving grid-interactive efficient operations. It concludes with the objectives and overview of this research.

1.1 Motivation

As more variable power supply, such as renewable wind and solar photovoltaic power, has been and will likely continue to be added to the electric grid, there is a mismatch between the power supply and power demand. Energy storage system, such as batteries, is used as one of the ways to compensate for both diurnal variability of solar power and the difficulty to predict stochastic variability of wind power. However, the high cost and relatively fast deterioration of batteries pose an obstacle for the massive adoption of the renewable power supplies.

In buildings, thermal mass, which is equivalent to the thermal capacitance or heat capacity, provides characteristics that enable it to store energy and provide thermal inertia against temperature fluctuations. Since the thermal mass of buildings can absorb thermal energy when the surrounding temperature is higher than building envelope and release thermal energy back when the surrounding temperatures are cooler, the thermal mass of buildings usually can serve to flatten or shift the daily temperature fluctuations when surrounding temperatures are

fluctuating throughout the day. By absorbing and progressively releasing heat, thermal mass helps in the regulation of indoor temperature. This is reflected in the shift of the peak space load. Due to these characteristics of the thermal mass of buildings, there is a large potential for load shifting and peak demand reduction, i.e., moving the building electricity use from on-peak hours to off-peak hours, and has been the most important focus for utilities in order to avoid building more power plants powered by fossil fuels and consequently reduce capital expenses, carbon emissions and environmental pollution.

Consequently, buildings are looked upon to operate in a way to accommodate the variations of grids. In the U.S., about 71% of power on the grids is consumed by buildings (EIA 2012). The infrastructure advancement of smart grids and smart buildings makes it possible to use buildings as thermal storage batteries to accommodate the variability of the renewable power suppliers, dynamic electricity rates, and other auxiliary services to the grids. According to an estimate by U.S. EIA, shown in Figure 1.1, the retail sales of electricity in residential buildings rank the highest among three different sectors and continue to increase year by year. Thus, changes in residential electricity use can have dominant impact on the electricity consumption portfolio in the nation.

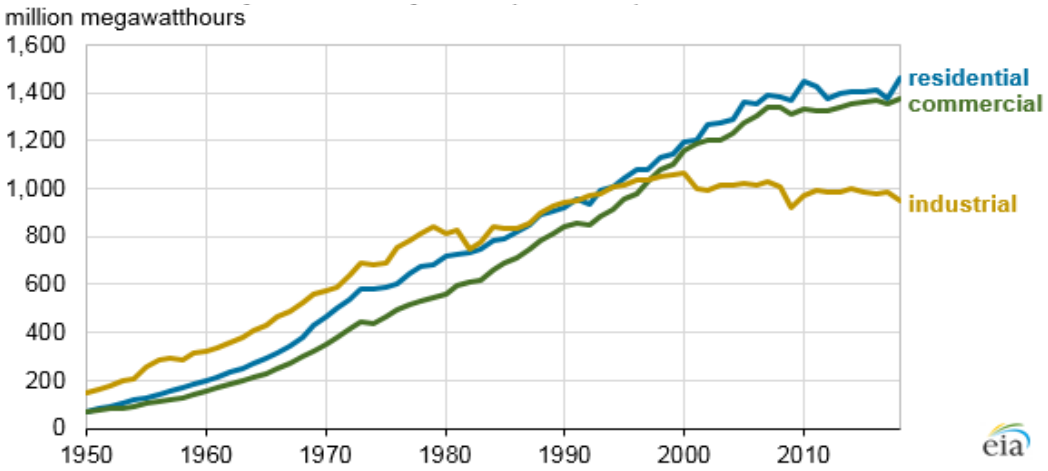

Figure 1.1. U.S. annual electricity retail sales by sector (1950-2018).

(Source: EAI, Electric Power Monthly).

On the other hand, average annual utility expense per household, including electricity, water, and sewage, is between $1400 and $2600 (EIA 2015), which presents an appealing cost-saving incentive for homeowners to invest in smart home devices and lower expenses. Moreover, Figure 1.2 shows the power profile of a test home in a typical summer day. As observed, the measured on-peak demand is close to 20 kW and it occurs at around 5:20 pm, which is the high electricity price period as marked in red circle. Therefore, the merging need for load shifting advocated by utility companies provides significant cost savings opportunity for homeowners.

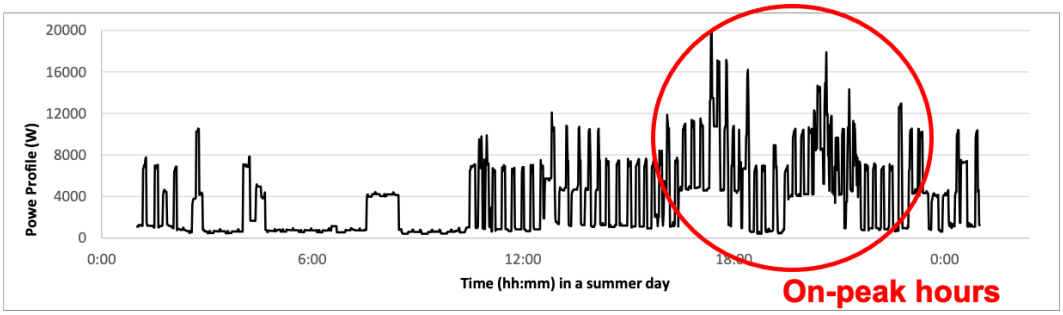

Figure 1.2. The power profile of a test home in a typical summer day.

In terms of energy consumption, about 40% of total U.S. energy was consumed in residential and commercial buildings in 2015 (EIA 2015). Approximately 30% of energy used in building is used inefficiently or unnecessarily (Sherwin 2010). For residential buildings, space heating and cooling annually consumed 11 Quads, nearly 10% of the energy used in the U.S. (DOE 2011), which also provides a significant energy savings opportunity.

Excessive energy consumption and cost in buildings can be explained by failure to operate as intended control strategy, wrong sizing of HVAC system, and lack of understanding of dynamic thermal loads and interactions. Development and implementation of regulations and national policies to encourage reduced building energy consumption and cost have raised worldwide interests from governments. Meanwhile, the dynamic nature of temperature, weather, internal heat gains, occupancy schedules, and the variation of grids, alongside their interactions with the thermal characteristic of a specific building construction continue to provide challenges for optimal operation of HVAC systems.

1.2 Problem Statement

The smart thermostat and utility industries have increasingly provided homeowners with abundant operational data related to advanced HVAC system control and energy usage management in homes (EERE 2016; Lu et. al 2010; Nest 2015). The data include weather and its forecasting, home occupancy, comfort level, time-of-day (TOD) or time-of-use (TOU) electricity pricing, etc., as illustrated in Figure 1.3. These data are usually available to homeowners, smart thermostat manufacturers and utilities through access to the cloud-based servers provided by the latter. *The research gap is a lack of a systematic framework to utilize all the available data. The research hypothesis in this study is that such available data can be used in the systematic framework proposed in this dissertation to produce actionable instruction for advanced home HVAC system diagnosis and control, and for realizing home energy cost savings and grid-interactive efficient operations*.

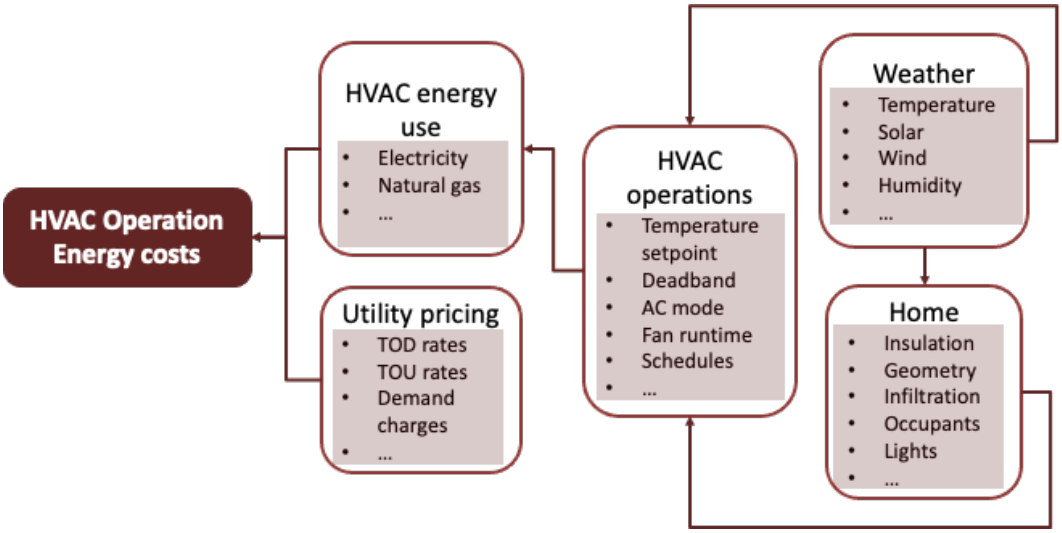

Figure 1.3. Operational data related to advanced HVAC system control and energy usage management in homes.

Heating and cooling in homes, provided by HVAC systems, represent a crucial load for many electric utilities. Fluctuations of heating and cooling loads in buildings also have significant impact on a utility's load profile. This impact can be mitigated by optimal and efficient HVAC operations that shift or reduce the peak load demand. *In this emerging area, to enable grid-interactive and efficient HVAC operations, development of a holistic, physics-based model that describes the dynamics of HVAC system and automatically estimates the thermal properties of buildings for a control purpose is at the heart of this framework.*

Rule-based pre-cooling is a strategy that can reduce the load during peak hours by shifting cooling operation from on-peak hours to off-peak hours. Many thermostat manufactures have built in rule-based pre-cooling operation strategies into their smart thermostats by resetting the indoor air temperature a few degrees lower for a period preceding the start of on-peak hours. Since the electricity use and cost of a HVAC system to maintain the space temperature set point are related to the HVAC system capacity, weather condition, utility rate structure, and home thermal properties that determine the heat transfer rate and thermal capacity of a home, the common rule-based pre-cooling strategies utilized by the smart thermostat manufacturers might not be an optimal solution.

Therefore, two research questions are raised here and need to be answered in this study:

1) to what extend can an optimal pre-cooling strategy outperform common rule-based pre-cooling strategies?
2) how different home thermal properties, HVAC system capacity, weather condition, and utility rate structure impact the optimal pre-cooling?

These will be investigated through both simulations and experiments. The outcome of this research will fill the following knowledge gaps:

1) Lack of a holistic, physics-based model that describes the dynamics of HVAC system for a control purpose and estimates the thermal prosperities of homes for the envelope performance evaluation.
2) Lack of real-time optimization algorithm to generate customized optimal solutions while factoring in specific home thermal properties, HVAC system cooling capacity, weather condition, and utility rate structure for a specific home.
3) No quantitative evaluation of existing common rule-based pre-cooling strategies compared to an optimal pre-cooling strategy that is formulated based on a dynamic thermal model of a home to search for the optimal space air temperature set point solution with specific thermal properties under a given utility rate structure, HVAC cooling capacity, and weather condition.
4) No quantitative study and performance analysis of how different home thermal properties, HVAC system cooling capacities, weather conditions, and utility rate structures impact the pre-cooling strategies in terms of the operation and energy performance.

5) No experimental analysis of how the internal heat gains impact the home thermal model and the corresponding model-based cooling load calculation and optimal pre-cooling strategy and how the optimal indoor air temperature set points from the pre-cooling strategy will be implemented and performed in a real residential building.

1.3 Research Objective

Note that energy cost is determined by energy price and use, while energy use for space heating and cooling is determined by their loads, which are typically influenced by weather, home thermal properties, and occupancy. Therefore, a home thermal model that can estimate heating and cooling loads serves as a bridge that connects the data on the weather, occupancy, HVAC system parameters, and internal gains with the energy use and costs, as illustrated in Figure 1.4. The objective of this research focuses on developing such a framework as mentioned in Section 1.2. The model will facilitate generation of information on deterioration of the home envelope, air distribution, and heating/cooling load, and HVAC system efficiency as well as monetary savings associated with deterioration correction. Moreover, the home thermal model will help home occupants optimize their thermostat settings in response to time-varying electricity prices and in ways that enable occupants to account for trade-offs between indoor temperatures (being an indicator of comfort) and energy cost savings.

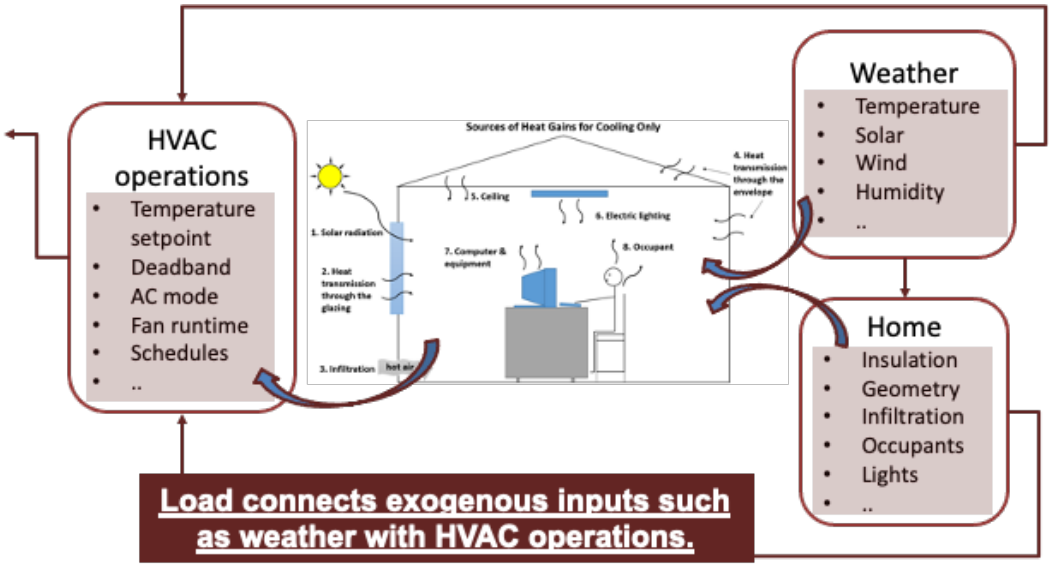

Figure 1.4. Connections between the space cooling load and exogenous inputs.

This research mainly focuses on design and analysis of the building thermal model for grid-interactive efficient operations. Specifically, the five tasks are designed as follows:

1) ***The Thermal Model Construction.*** This task focuses on constructing such a home thermal model. The construction of an accurate and efficient model is challenging because of different heat transfer mechanisms introduced by various weather inputs such as outdoor air temperature, wind, and solar. This challenge is compounded by the lack of detailed home information, such as the orientation, location, layout, floor area, and construction materials. In this study, this challenge is addressed by introducing a model that draws inspiration from traditional network model approaches. The home thermal model that can estimate heating and

cooling loads serves as a bridge that connects all the mentioned operation data.

2) ***Model Parameter Estimation Scheme.*** This task is to develop a real-time model parameter estimation scheme and verify the effectiveness of the scheme. The scheme will enable automatic, sequential, and optimal estimation of the model parameters, i.e., the thermal properties, of a home, using data collected through smart thermostats and internet connections.
3) ***Optimization Formulation.*** The task is to formulate a pre-cooling optimization problem that finds HVAC control signals over a time period and minimizes energy cost subject to maintaining both the indoor air temperature within a pair of bounds for thermal comfort. The formulation of the optimization problem utilizes the home thermal model with specific thermal properties and a given utility rate structure, HVAC cooling capacity, and weather condition to investigate how an optimal strategy outperforms common rule-based operation strategies.
4) ***Performance Analysis of Optimal Pre-Cooling.*** The task is to investigate how different home thermal properties, HVAC system cooling capacities, weather conditions, and utility rate structures impact the optimal pre-cooling strategy in terms of the operation and energy performance.
5) ***Experimental Verification and Implementation.*** The impact of internal heat gains on the home thermal model and the corresponding model-based cooling load calculation and optimal pre-cooling strategy will be

investigated through experiments. The optimal indoor air temperature set points generated from the pre-cooling strategy will be implemented into the study of a residential building in HVAC filed in order to minimize energy cost of the HVAC system through experiments.

This research is therefore a fundamental research that will culminate in the development of methodologies for grid-interactive and efficient HVAC operations. The above tasks will be carried out through the use of a data acquisition system and a software platform built for a smart thermostat which serves to integrate physical sensor measurement with mathematical models for real-time control of HVAC system operations. This research will focus on the following thrust areas:

a) Develop a thermal model that may be used to carry out fundamental study of building thermal interactions.
b) Identify computationally efficient methods to automatically estimate the model parameters.
c) Develop and validate a model-based method for envelope performance evaluation.
d) Formulate a pre-cooling optimization problem that is a quadratically-constrained integer linear program and can be solved through suitable tools.
e) Validate the developed methodologies using case studies in a typical residential building.

1.4 Research Outline

This dissertation begins with motivation and problem identification in Chapter 1 and critical review of literatures on the HVAC system control and optimization and the corresponding methods for building thermal modeling in Chapter 2. This is followed by a description of thermal processes in a home and a traditional 3R2C plus 2R2C model, and the formulation of a home thermal model and its validations in Chapter 3. Next, characterization of U.S. home thermal performance is investigated by a method that utilizes the home thermal model in Chapter 4. Then an optimal pre-cooing strategy is formulated by utilizing the home thermal model and simulations and comparisons are made between the selected rule-based operation cases and the optimal solution in Chapter 5. Moreover, the performance analysis of the optimal strategy is studied by investigations of the impact of different home thermal properties, weather conditions, HVAC cooling capacities, and utility rate structures on the optimal pre-cooling in terms of energy and operation performance in Chapter 6. As followed, experiments are carried out in a real test house to validate the effectiveness of the model and the optimal strategy and meanwhile demonstrate their implementations in Chapter 7. Finally, conclusions and future work are summarized in Chapter 8. Details of the dissertation structure is laid out as shown in Figure 1.5.

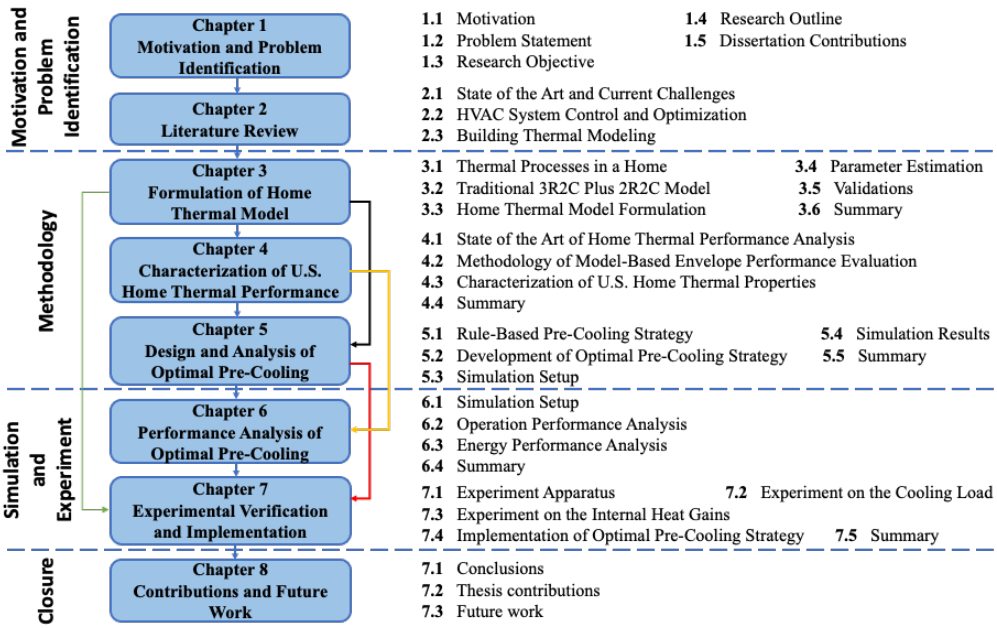

Figure 1.5. Dissertation structure flowchart.

1.5 Dissertation Contributions

Although there are various building thermal models available, the innovation of this research is the construction of the computationally efficient, physics-based model using a data driven method. The model can accurately identify home thermal properties and predict space air temperature dynamics in real time, from which online prediction of home energy costs and comfort levels, along with HVAC system efficiency and home envelope conditions, can be made automatically without homeowner intervention**.**

Additionally, this research is fundamental for developing and delivering a building HVAC control system that provides optimal grid-interactive control of the thermal environment while informing occupants on the impacts of the

changing condition of their buildings and the heating/cooling equipment and actions they take on energy use, comfort, and costs. The framework will generate actionable information for advanced building HVAC system diagnosis and control and for realizing grid-interactive energy-efficient operations using data from various sources such as smart sensors or meters, emerging smart Internet-of-Things (IoT) devices, and the Internet. A building thermal model capable of connecting all these elements is at the heart of the proposed framework.

Specifically, the overall contributions of this research may be summarized as follows:

- Understanding of thermal interactions in buildings, especially for homes.
- Development of a home thermal model that is a core of a systematic framework for realizing home energy cost savings and grid-interactive efficient operations.
- Investigation of the data length needed for the accurate model parameter estimates through an automatically parameter estimation scheme.
- Characterization of U.S. home envelope performance through identification of thermal properties using a data-driven method.
- Development of optimization algorithm for operation and energy performance evaluation.
- Development of model-based cooling load calculation and HVAC system efficiency identification method.

- A benchmark of the energy consumption and cost savings capabilities for different pre-cooling strategies utilizing different thermal properties, weather conditions, HVAC cooling capacities, and utility rate structures.
- Applications of the developed approaches for grid-interactive efficient operations.

Chapter 2: Literature Review

Building operation control and optimization are mainly challenged by dynamic load changes. Unlike lighting and plug loads, the HVAC system load is variable and fluctuates with indoor and outdoor environments. Building systems need to accommodate this characteristic for achieving efficient operations. Inappropriate control strategy and faulty equipment always lead to deficiencies in building system operation. Since buildings are the largest electricity users on the grids, the variations of grids also impose additional challenges, which make operation control and optimization of HVAC systems difficult. To cope with these challenges, lots of operation control and optimization strategies have been proposed and/or tested from literatures.

2.1 State of the Art and Current Challenges

Heating and cooling in homes, provided by HVAC systems, are known to be energy-consuming and costly for homeowners and represent a crucial load for many electric utilities. In 2015, the average end-use energy consumption per household in the U.S. is 42.4 million Btu for heating and cooling alone, which accounts for nearly 55% of total household energy consumption (EIA 2015). In terms of energy cost, the average annual utility expense per household, including electricity, water, and sewage, is between $1400 and $2600, of which more than 43% is spent on heating and cooling spaces in homes (EIA 2015; DOE 2011). Therefore, home space heating and cooling offer considerable potential for energy cost reduction (EERE 2015). Fluctuations of heating and cooling loads also have

significant impact on a utility's load profile. This impact can be mitigated by optimal and efficient HVAC operations that shift or reduce the peak load demand.

As a means of controlling demand when the grid is near its capacity, electricity suppliers have introduced TOD or TOU electricity price in recent years, making peak electricity expensive to consumers (Kamyar and Peet 2017; Tabares-Velasco et al. 2019; Baniasadi 2019). Since electricity is more expensive during on-peak hours, smart thermostat manufacturers have incorporated rule-based pre-cooling strategies into their products, which set the indoor air temperature a few degrees lower for a period preceding the start of on-peak hours (EERE 2016). The resulting lower indoor air temperature, obtained at a lower electricity price, delays the start time of HVAC systems and reduces their runtime during on-peak hours. Such rule-based pre-cooling strategies reduce energy expenditure for homeowners while maintaining reasonable comfort levels in homes because they take advantage of the thermal mass possessed by the building structure. In practice, rule-based pre-cooling strategies vary slightly by setting different pre-cooling runtimes or lowering the indoor air temperature to different levels.

Although rule-based pre-cooling strategies provide a means of shifting or reducing the peak demand, they are guided primarily by intuition and may not be optimal in terms of cost savings. The limitation or/and challenges of rule-based pre-cooling strategies can be accommodated through pre-cooling optimization using model-based strategies. Unlike rule-based pre-cooling strategies, which

keep the same operation schedule for all the applied homes throughout the entire season regardless of home thermal properties or weather conditions, optimal pre-cooling strategies are more adaptive, searching for optimal solutions based on changing conditions, such as home thermal properties, size and efficiency of the HVAC system, weather condition, and utility rate structure. The operations and cost savings of an optimal pre-cooling strategy may vary significantly for different home thermal properties, sizes and efficiencies of the HVAC system, weather conditions, and utility rate structures compared to a rule-based pre-cooling strategy. Therefore, there is a need to investigate and analyze the performance of an optimal pre-cooling strategy regarding the aforementioned various conditions.

Moreover, an optimal pre-cooling strategy is built upon a home thermal model that accounts for the aforementioned conditions. A home thermal model that can be served as this purpose is in urgent need. The home thermal model is expected to be simpler, require fewer measured inputs and less total data, and operate without any homeowner intervention since both precise physical knowledge of the building and a significant amount of data for calibration are generally not available for homes.

2.2 HVAC System Control and Optimization

A summary of HVAC system control methods is introduced in Section 2.2.1 and the corresponding control strategies that minimize building demand and/or energy cost are illustrated in detail in Section 2.2.2.

2.2.1 Summary of HVAC system control methods

Tables 2.1 and 2.2 compare the most common methods that have been used for the HVAC system control (modified from Ogunsola 2016). These tables show the description of the control methods and its limitations to current HVAC system applications. Of all the methods shown in Tables 2.1 and 2.2, the optimal control methods that have the capacity of minimizing the energy cost while maintaining the required thermal comfort, are adopted in this study due to its effectiveness and robustness and reliability in comparison with the classical control methods. It's sufficient to be served as a way to benchmark energy performance focused on this study.

Table 2.1. Comparison of traditional HVAC system control methods.

Control Methods	**Examples**	**Description**	**Limitations**
Classical Control	ON/OFF	Regulates a given process between lower and upper bounds	Unable to control time delay due to thermal inertia. Large swings display in controlled states
	P, PI, PID	Modulates a control variable to achieve control using error dynamics	Controller tuning is cumbersome. Operating conditions should not vary widely from tuning

			conditions

Table 2.2. Comparison of innovative HVAC system control methods.

Control Methods	Examples	Description	Limitations
Hard Control	Gain Scheduling PID	Different set of gains applied to a nonlinear system divided into piecewise liner regions	Inability to handle time varying constraints and disturbances
	Nonlinear Control	Uses a control law to drive a nonlinear system toward a stable state	Requires complex mathematical analysis for the identification of stable states
	Robust Control	Designs a controller that works well with time varying disturbances	Require specification of additional parameters which could be impractical to integrate in HVAC systems
	Optimal Control	Solves an optimization problem to minimize a cost function	The optimal solution may not be easily implemented into current HVAC control system and

			requires a relatively higher computation capacity in some problems.
	Model Predictive Control	Predictive optimal control with disturbance rejection, constraint handling, and slow-moving dynamics integrated into controller design	The controller is able to regulate the system tightly within the given bounds. But it requires accurate predictive model.
Soft Control	Fuzzy Logic	Control actions are implemented in the form of if-then statements	Requires extensive knowledge of system operations and states
	Neural Network	Trained using performance data to fit a nonlinear mathematical model	It's a completely black box approach. Training data must cover a wide range of operating conditions.
Hybrid Control	Adaptive Fuzzy, Fuzzy PID, etc.	It's a fusion of hard and soft control techniques.	Inherits problems associated with soft and hard control methods, such as requiring

			large amounts of data, or problems with controller tuning

2.2.2 Strategies for minimizing building demand and/or energy cost

To provide a means of reducing the peak demand and/or energy cost while maintaining reasonable comfort levels in residential buildings, a variety of rule-based pre-cooling strategies, taking advantage of building thermal mass as a way to shift or reduce the peak load demand by shifting cooling operations from on-peak hours to off-peak hours, have been heavily investigated.

Studies on rule-based pre-cooling strategies using temperature setting schedules have been conducted by a lot of researchers. Specifically, Xu et. al (2004) demonstrated the potential of reducing peak-period electrical demand in a moderate-weight commercial building by modifying the HVAC control systems. With their strategy, zone temperatures were maintained at the lower end of a comfort region before 2 pm and allowed to float to the higher end after 2 pm. As a result, the chiller power was reduced by 80%−100% during on-peak hours (i.e., 2 pm−5 pm) without incurring any complaints on thermal comfort. In a subsequent work (Xu 2009), 11 pre-cooling test schedules that include linear, two-step, and exponential temperature setting strategies and different weather conditions and dates were studied. Through comparison with a baseline operation and analysis of on-site measurement data of two large commercial buildings in California, it was

found that the pre-cooling test schedules were effective in both light and heavy mass buildings. For the light mass building, these schedules significantly reduced the cooling load (35% on cold days, 25% on warm days). For the heavy mass building, the load reduction was even more significant: for example, the peak HVAC load was reduced by 30% on warm days using the exponential temperature setting strategy. This result agreed with the observation that pre-cooling tends to be more effective when the building mass is relatively heavy.

Yin et. al (2010) found that pre-cooling strategies with an exponential or step temperature setting were better compared to those with a linear temperature setting through a study on a commercial building in California. A baseline model equipped with physical information and calibrated with field test data was used to estimate the demand savings. An analysis of factors (e.g., building location, mass level, pre-cooling control strategy, and TOU utility rate) was conducted by Morgan and Krarti (2007) to evaluate the impact of key design and operating conditions on the effectiveness of pre-cooling strategies for peak demand and overall energy cost reduction in office buildings. It was observed that 4–8 hours of pre-cooling were most effective in reducing peak cooling load and operating cost without significantly increasing energy consumption.

Studies on rule-based pre-cooling strategies have also been conducted for residential buildings. Woon and Han (2011) studied pre-cooling strategies characterized by the proper setback period, set point, and setback temperature to achieve peak reduction in residential buildings. Arababadi and Parrish (2015)

compared the performances of five different pre-cooling strategies, similar to those done by Xu (2009), for a wood frame house. The first two strategies each adopted a two-step constant temperature set point, with the first strategy having a lower temperature set point for on-peak hours and a higher one for off-peak hours compared to the second. The third and fourth strategies increased the thermostat temperature linearly and exponentially, respectively, during on-peak hours and behaved the same during off-peak hours. The last one adopted a three-step constant temperature set point and was intended to examine how the house would response to a more complicated pre-cooling design. Through EnergyPlus, it was found that the second strategy could reduce peak energy consumption by up to 7.5% and had the least increase in annual energy consumption while the third and fifth strategies not only did not reduce the on-peak energy consumption, they led to an increase in annual energy consumption during on-peak hours, perhaps due to a low thermal mass of the house.

Surles and Henze (2012) developed an automated thermostat temperature set point control strategy for homes located in different climate zones. The strategy was able to respond to price variations in a TOU tariff and create set points and schedules with varied peak period length, rate ratio, and set point offset through custom scripts written in MATLAB. Through simulation in EnergyPlus using historical weather data, it was found that the total energy saving potential was highly dependent on climate zone. For example, all else being equal, it was possible to consume 50% and 27% less energy consumption during peak hours for

homes in Houston and Los Angeles, which represent ASHRAE Climate Zones 2 and 3, respectively. In terms of monetary saving, the largest test home in Houston yielded more than $200 saving over a four-month period in 2018, whereas the smallest one in Chicago yielded only $10. In addition, homes with different sizes but similar thermal properties and located in similar climate were found to have comparable saving percentages. Turner et. all (2015) found that the effectiveness of pre-cooling was highly dependent on climate zone and the selected pre-cooling strategies for residential buildings with low thermal mass. However, pre-cooling strategies were also found to yield a higher cooling energy consumption in general.

These strategies set the indoor air temperature a few degrees lower for a period preceding the start of on-peak hours with a higher electricity price. The lower indoor air temperature, obtained at a lower electricity price and controlled by a thermostat with a deadband to determine the HVAC on/off signal, delays the start time of HVAC systems and reduces their runtime during on-peak hours. In practice, rule-based pre-cooling strategies vary slightly by setting different pre-cooling runtimes or lowering the indoor air temperature to different levels. Although these rule-based pre-cooling strategies provide a means of shifting or reducing the peak demand, they are guided primarily by intuition and may not be optimal in terms of cost savings, thus leaving room for improvement. To this end, research on how optimization can help enhance the demand response performance, especially in the context of model-based pre-cooling strategies,

attracted widespread attention and has been carried out since the 1990s. In particular, Keeney and Braun (1996, 1997) formulated an optimization problem, based on a simplified building thermal model consisting of plant power, cooling load, comfort, and weather models, to determine an optimal cooling control strategy that minimizes the energy cost for commercial buildings. Simulation results were used to convert the optimal strategy into two simpler, practical pre-cooling strategies, which were subsequently tested with 1008 different building types, weather conditions, cooling plants, and utility rates. It was found that the optimal strategy and the two simplified ones all resulted in 95%–97% saving on cooling cost compared to night setback control. Lee and Braun (2008) developed a model-based approach for minimizing peak cooling demand using energy stored in a commercial building. With this approach, zone temperature setpoints were kept at the lower end of a comfort region before a demand-limiting (DL) period and adjusted upward during the DL period following a trajectory that kept the peak cooling load below a target. To generate the trajectory and target, a building RC (resistance-capacitance) model was utilized, in which its parameters were identified using a global search based on crude building description field data. Such data included temperatures from ambient, ground, and floor as well as solar and internal heat gains. The model was then implemented at a test site to determine zone temperature set points for studying the potential of peak load reduction. Their results showed that a 30% reduction of peak cooling loads was achievable compared to night setback control. Similar work has also been done by

Li and Malkawi (2016), Nikovski et. al (2013), and Chandan et. al (2015), where the common goal was to develop a pre-cooling control strategy that reduces energy demand and cost while maintaining a desired thermal comfort.

Unlike for commercial buildings, model-based pre-cooling optimization in residential buildings have received far less attention (e.g., Reddy et. al 1991; Avci et. al 2012). In one of the earlier works done by Reddy et. al (1991), a simplified 1R1C model was used to study the impact of peak-shaving strategies on the thermal response of a house. The study included examining the time required for the indoor air temperature to increase by 3.6 °F when the HVAC system was off (i.e., temperature float-up) at houses with different time constants. It also included calculating the cooling power used by a linear ramping-up thermostat temperature control and comparing the result with a base case with constant temperature set point. Avci et. al (2012) also used a 1R1C model to develop a residential HVAC load control strategy. However, the model only considered the impact of outdoor air temperature and energy consumed by the HVAC system. In addition, to determine its parameters, the size, structure, and thermal conductivity of the building need to be known. Once determined, an optimal solution that minimizes a weighted sum of cost and thermal comfort is sought, where the latter is reflected by the indoor air temperature. Their results showed that the optimal strategy could improve comfort while reducing electricity cost and energy usage at peak hours compared to a base case without pre-cooling.

Wang et. al (2020) proposed an optimal pre-cooling strategy based on an integer linear programming problem that utilizes a dynamic home thermal model, and its performance was compared with three rule-based control strategies. It was found that the optimal pre-cooling strategy requires the least energy consumption without sacrificing thermal comfort and can save up to 56% of the HVAC electricity cost compared with the rule-based strategies. However, the study was conducted for one summer day only and the conclusions were limited to one envelope thermal condition. Chan and Bashash (2017) developed a mixed-integer quadratic programming (MIQP) problem that utilized a second-order differential equation model to search for optimal HVAC operations that minimize energy cost. The results showed that up to 35% cost savings can be achieved compared with rule-based control. Similar work has also been done by Braun (1990), Kintner-Meyer and Emery (1995), Henze et. al (2008), and Chandan et. al (2015), where the common goal was to develop an optimal pre-cooling strategy that utilizes building thermal models to reduce energy demand and cost while maintaining desired thermal comfort.

To this end, the performance analysis of the optimal pre-cooling strategies on energy consumption and/or energy cost reduction in the context of different weather conditions and TOU or TOD electricity rates has been investigated using different methods (Kamyar and Peet 2016; Yoon et. al 2014; Tabares-Velasco et. al 2019; Surles and Henze 2012; Li and Malkawi 2016; Nelson et. al 2019; Henze et. al 2007). Kamyar and Peet (2016) investigated the impact of different TOU

rates on cost savings. A dynamic programming-based algorithm was proposed to solve the optimal control problem of thermostat programming in the presence of thermal energy storage for consumers with combined demand chargers and TOU electricity rates. The optimization problem was defined as minimization of the total cost of power consumption, subject to the building thermal dynamics and thermal comfort constraints. The thermal dynamics were predicted based on a partial-differential model of diffusion that only considers the conductive heat transfers through the exterior wall of a residential building. By comparing the optimal thermostat programming control with four constant set-point controls, the proposed algorithm can reduce monthly electricity bills by up to 25% in the summer with average savings of 9.2% over a variety of building models by using different TOU electricity rates.

Yoon et. al (2014) investigated the impact of different weather conditions on cost savings. A dynamic demand response controller to reset the thermostat temperature set point was proposed based on real-time retail pricing for residential buildings. The building model was developed using OpenStudio and EnergyPlus, which consider the geometry of a residential building and geographical environment. The controller was implemented into Simulink and connected to EnergyPlus through a building control virtual test bed. The strategy changed the thermostat set-point temperature to control HVAC loads depending on real-time electricity retail pricing for peak load reduction. Simulation results showed that heating and cooling electricity consumption on both the coldest and

hottest months were reduced by 12% and 21% and electricity costs were curtailed by 29% and 31%, respectively, compared to the fixed set-point temperature control strategy. However, the study was not conducted for the optimal pre-cooling strategy.

Using a similar approach proposed by Yoon et. al (2014), Tabares-Velasco et. al (2019) developed a modeling framework for optimization-based thermostat control of a residential building for TOU pricing. The framework integrated EnergyPlus and AMPL (an algebraic modeling language) using MATLAB and Simulink. The impact of different TOU electricity rates on the electricity cost, thermal comfort, and peak demand deduction was analyzed and simulated through the framework. Simulated results showed that the optimization-based control can reduce cooling electricity costs by up to 30% and demonstrated that cost savings and peak demand reduction were highly dependent on the TOU electricity rates. Similar work has also been done by Surles and Henze (2012), Li and Malkawi (2016), and Nelson et. al (2019), where the common goal was to investigate the impact of different size homes under different climates on energy costs, with the help of common modeling tools.

Henze et. al (2007) conducted a sensitivity analysis for evaluating the optimal thermal mass control of an office building and its performance, compared to a nighttime setback control reference case, with respect to utility rate structure, internal gains, occupancy period temperature set-point range, onset and duration of occupancy and on-peak periods, weather, and building thermal mass. The

analysis utilized a dynamic building energy simulation program coupled with a technical computing environment. Through analysis and comparison, it was found that: 1) high utility rate incentives lead to lower pre-cooling temperature set points and larger early morning pre-cooling loads; 2) internal gains largely influence the reference case and the largest savings were observed for small internal gains; 3) the pre-cooling temperature is dependent on whether occupancy and on-peak periods begin or end at the same time; 4) on-peak hours beginning far before or after the beginning of occupancy reduce the effectiveness of load shifting; 5) large diurnal temperature swings reduce cooling loads and ambient humidity has less impact on the cost savings potential; and 6) larger thermal mass reduces cooling loads. All the findings are in line with expectations or experience.

Although the existing pre-cooling strategies provide a means of shifting or reducing the peak demand and/or energy cost in residential buildings, majority of them are rule-based, guided primarily by intuition. The rest of them are model-based but generally do not consider the influence of solar radiation and infiltration due to wind. Wang et. al (2019) showed that the wind impact was not negligible in the formulation of a thermal model for residential buildings. Moreover, previous studies considered the impact of different TOU electricity rates and/or weather conditions but did not include a performance analysis of home conditions, such as different building thermal properties and HVAC system efficiencies. Unlike rule-based pre-cooling strategies, which keep the same operation schedule for all the applied homes throughout the entire season

regardless of home thermal or weather conditions, optimal pre-cooling strategies are more adaptive, searching for optimal solutions based on changing conditions, i.e., they vary not only depending on TOU electricity rates, but also depending on home thermal properties, sizes and efficiencies of the HVAC system, and weather conditions (Wang et. al 2020). The operations and cost savings of the optimal pre-cooling strategy may vary significantly for different home thermal properties, weather conditions, sizes and efficiencies of the HVAC system, and electricity rate structures, compared to a rule-based pre-cooling strategy. Therefore, there is a need to understand to what extent can an optimal strategy outperform common rule-based operation strategies through the development of the optimal pre-cooling strategy that can account for various factors (e.g., the outdoor air temperature, wind, solar, HVAC size and efficiency, and utility rate structure). Moreover, it also needs to investigate and analyze the performance of an optimal pre-cooling strategy regarding the aforementioned various factors. To address these needs, performance analysis of an optimal pre-cooling strategy built upon a home thermal model that accounts for the aforementioned factors are conducted and presented in this study.

2.3 Building Thermal Modeling

This section illustrates the building thermal modeling methods and the selection of building thermal model used in this study. Specifically, review of the building thermal modeling methods is stated in Section 2.3.1. Then advances in

RC modeling approach are present in Section 2.3.2. Finally, inputs to home thermal model are introduced in Section 2.3.3.

2.3.1 Review of building thermal modeling methods

Since the 1970s, a variety of building thermal models have been proposed (Wilson and Templeman 1976; Shaviv and Shaviv 1978; Waters 1980; Zmeureanu 1987), an important subset of which is the thermal network models derived from the standard RC approach. The first such model was a 35-node thermal network simulation model established in 1980 and used at the University of California, San Diego (UCSD) to study room air temperature control of a house (Carroll and Clinton 1987). The model, consisting of various component sub-models that need the physical properties of construction materials and the choice of heat transfer coefficients to simulate each component of the house, was used to calculate the temperatures of the mean radiant temperature (MRT) nodes and the room air for a passive solar house in a given climate. Similarly, in a study done by Achterbosch et. al (1985), physical information on the test buildings was needed for the thermal model, although it is slightly different in the construction of the model elements and the definition of the room air temperature (a weighted average of the indoor air and internal element temperature was used). In a study done by Ogunsola and Song (2012), common challenges facing RC models were reviewed. Their study also identified and evaluated several factors that can impact the accuracy of one of the RC models, i.e., the 3R2C plus 2R2C model where 3R2C is used to describe heat transfers through envelopes and 2R2C is for

internal thermal mass, for building load estimation. Crabb et. al (1987) verified, through a case study at a school, the idea that the thermal dynamics of intermittently occupied buildings can be described by two time constants, namely, a smaller time constant that represents the time needed for the indoor air and wall temperatures to come to an equilibrium, and a one that represents the time needed for the building structure to cool down or warm up. Their results were obtained using a 2R2C model. Other variations of the RC models were also tested, including those reported by Xu and Wang (2008), Bacher and Madsen (2011), Lin et. al (2012), and Tindale (1993). Recently, Ogunsola and Song (2013, 2015) compared several RC structures for heating and cooling season validation in a typical office building. Their results showed that the 2R2C model offers the best overall fit for the internal mass in terms of the R^2 value and error indices such as the mean error (ME), mean bias error (MBE), and coefficient of variation of root mean square error (CVRMSE). Related work has also been done by Underwood (2014), Kircher and Zhang (2015), Hasan et. al (2014), Nassiopoulos et. al (2014), Bueno et. al (2012), Gouda et. al (2002), Goyal and Barooah (2012), Lauster et. al (2014), and Naveros and Ghiaus (2015), in which the common goal was to obtain a simplified and yet accurate building thermal model based on various approaches.

Although RC models are an ideal tool for sufficiently capturing building thermal dynamics under a variety of circumstances, their parameters must be appropriately determined for them to be useful. To this end, a rich collection of

parameter estimation methods has been proposed over the years. For example, Jimenez et al. (2008) showed that the ARMAX (auto-regressive-moving-average with exogeneous inputs) model, together with suitable physical constraints, can be used to accurately estimate the overall heat transfer coefficient (U-value) and solar heat gain coefficient of a simple homogeneous, opaque wall with errors below 0.03 W/(m^2-k) and 0.01, respectively. Wang and Xu (2006) used Genetic Algorithms (GAs) to develop estimators that optimally identify the parameters of a simplified 2R2C model. Their results showed that the average errors between the measured and the predicted cooling load were 7.8% and 9.7% during office hours and non-office hours, respectively, over 14 days. Ogunsola and Song (2014) identified the 3R2C model parameters of building envelopes using theoretical characteristics of building construction in frequency domain and data generated by EnergyPlus. They also identified the 2R2C model parameters of internal masses using GAs. Another popular method for parameter estimation is the least squares method, which has been adopted by Penman (1990), Coley and Penman (1992), Dewson et. al (1993), Chen and Athienitis (2003), and Kramer et. al (2013) and found to be effective for low-order RC models.

Although the aforementioned models and parameter estimation methods are effective, most of them require either precise physical knowledge of the building or a significant amount of data for calibration, both of which are generally not available for homes. Indeed, home thermal models are expected to be simpler, require fewer measured inputs and less total data (from a few days to a

week at a time interval of minutes), and operate without any homeowner intervention. Therefore, one goal of this study is to use the standard RC approach to develop a home thermal model that possesses these desirable features.

2.3.2 Advances in RC modeling approach

The thermal network approach has been modified and applied in different forms (Ogunsola et. al 2014; Ogunsola and Song 2015; Ogunsola et. al 2016; Wang et. al 2019). The general applicability of the thermal network approach has been limited by the identified issues, such as convergence and stability issues due to the need for different time steps, less sensitivity to outliers, and only limited exploration of the thermal network model capabilities permitted because of depending on previous measurements of building load, weather, and usage of several time-steps to forecast future loads (Ogunsola 2016). Moreover, the needed measurements may be unavailable or unreliable due to issues from sensor malfunction or data quality assurance. Most importantly, with increasing building complexity, the thermal network model becomes increasing difficult to develop and optimize.

Even though, the RC thermal network model has been applied for multiple scenarios and case studies of different building constructions and HVAC system operation modes after curtailments and simplifications. Among several models, the RC model IS deemed to be appropriate to capture the dynamics of building construction and HVAC components, with advantages such as:

(1) Capability to represent physical properties of different building constructions in order to investigate the thermal properties on the effectiveness of pre-cooling.

(2) Capability to simulate different HVAC system schedules.

(3) Simulation applicable, in order to investigate multiple scenarios of operations across different weather conditions and controls.

(4) Ability to predict thermal dynamics and cooling/heating loads for thermal comfort control and load estimation.

(5) Ability to determine system stability based on model parameters.

(6) Potential capability as a foundation model to optimize HVAC system peak load and operational control, in response to multiple weather and operation scenario across different climates, since it is simulation-based.

(7) Item (1) to (6) are applicable for residential buildings in this study.

Most of the models used in previous studies in Section 2.3.1 do not meet the requirements. For example, the simulation environment used in a study (Morgan and Krarti 2010) was an integration of a weather predictor and EnergyPlus. It was capable of simulating temperature floats under static schedules, without the flexibility or capability to determine the optimal pre-cooling hour and cooling system size for design purposes. Also, the performance of the simulation model has not been assessed for different constructions and climate types. Likewise, Braun (2002, 2003) estimated zone sensible cooling requirement from on-site measurements. The approach was not suitable for this study, because of the need for simulation scenarios for different weather

conditions. Edmund and Liao (2010) used EnergyPlus in their simulation, but it was not capable of optimizing the system operation based on objectives defined by the user.

2.3.3 Inputs and outputs of building thermal model

As illustrated in Figure 2.1, the inputs to thermal models consist of building geometry, weather condition, HVAC systems and components, internal loads, operating strategies and schedules, and other parameters. Outputs from the RC building thermal model may include interior and exterior surface temperature of walls, zone temperatures, heating or cooling loads, and other thermal variables of interest. Detailed description of these inputs can also be found in Table 2.3.

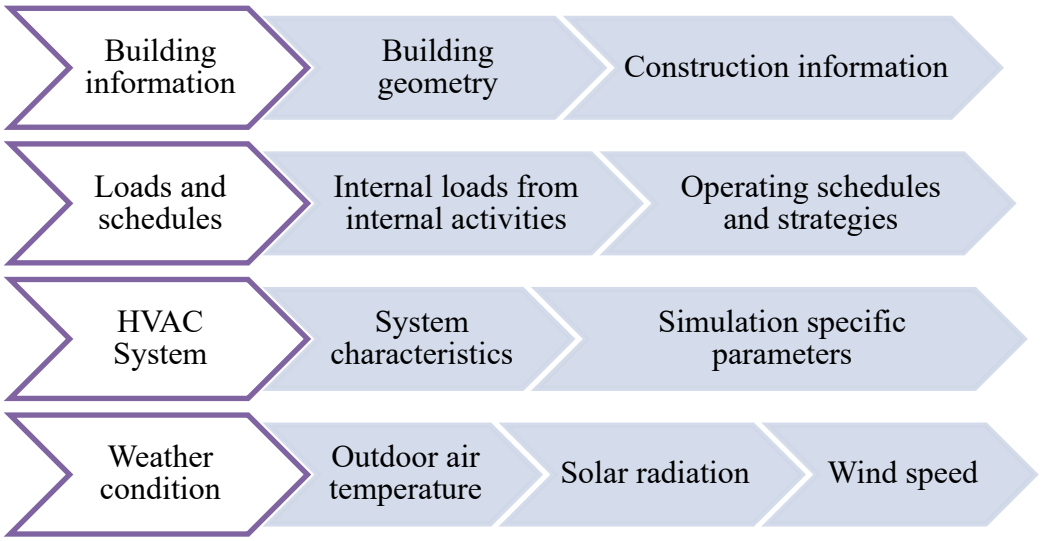

Figure 2.1. Inputs to RC Thermal Models.

Table 2.3. Typical inputs to RC thermal models.

Input	**Description**
Building construction information	The thermal characteristics of building construction determine the temperature fluctuations and thermal delay of radiative heat gains.
Loads and operation schedules and strategies	Internal loads are heat generated within the building, such as from the lightings, computers, office equipment, and occupants and its related activities. The occupancy schedules are the times that occupants are physically present in the thermal zone. The schedules may impact the operation of HVAC system using an on/off control strategy.
HVAC system	The HVAC system operates to maintain thermal comfort within the conditioned space. It compensates for the building heating or cooling loads.
Weather condition	The weather condition includes outdoor air temperature, solar radiation, and wind speed specified by a location being studied.

For homes, however, the precise physical knowledge of the building, such as the orientation, location, layout, floor area, and construction materials, or a significant amount of data for model training are generally not available. Therefore, the RC model needs to be modified appropriately for homes, so that it

can be identified through data training rather than using knowledge about buildings.

Chapter 3: Formulation of Home Thermal Model

In this chapter, a traditional building RC network model is introduced first. Based on the network modeling approaches, a novel home thermal model is developed for representation, modeling, and analysis of the thermal response of a home, and can be used for the home load calculation and HVAC operation optimization. The novel model, which is built upon the energy conservation law, is described through the analysis of heat transfer processes. Then a parameter estimation scheme of the thermal model is established and used to estimate the thermal properties of a test home. Moreover, the stability analysis of the model and the parameter estimation scheme are also included in this chapter.

3.1 Thermal Processes in a Home

The thermal interactions in a home are complex and include all the basic heat transfer processes introduced by the eight exogenous inputs, illustrated in Figure 3.1 using a cooling season, including solar heat gain, heat transfer through opaque envelope elements with the outdoors (driven by the temperature difference between indoors and outdoors), air infiltration, indoor loads (e.g., uses of lighting and appliances), and occupants. The exogenous inputs represent heat gains or losses depending on seasons. For example, the heat gains need to be removed by HVAC systems to maintain the desired home air temperature in summer. The heat extraction rate, i.e., the amount of heat removed, equals the cooling load if the space air temperature is perfectly maintained at a set point. The cooling load

experiences delays from the exogenous inputs at times because of heat storage in the home structure and in furnishings.

Home thermal dynamics, i.e., regulating HVAC energy use and/or room air temperature impacted by the eight exogenous inputs, can be described using a home thermal model. The thermal dynamics of each home are uniquely determined by home design, location, construction materials, air tightness, and home orientation. Thus, each home has its unique thermal characteristics. Therefore, a home thermal model applicable across homes needs to have the capacity to learn these unique characteristics for an individual home.

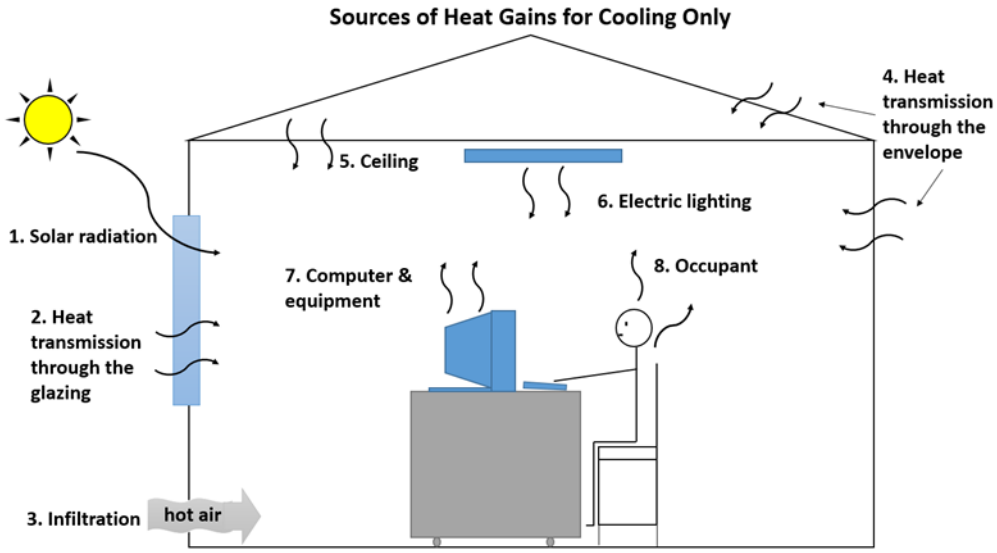

Figure 3.1. Thermal interactions in a home during a cooling season.

3.2 Traditional 3R2C plus 2R2C Model

In this section, a traditional building RC model is introduced and the limitation of the traditional RC model for the home application is discussed.

The most used building envelope model is the 3R2C model, which is based on physical heat transfer and thermodynamic laws (Ogunsola et. al 2014; Ogunsola and Song 2015) but simplified by aggregating parameters and variables that are either costly or impossible to obtain, as shown in Figure 3.2.

The multiple layers of opaque walls and roof of a building, including physical layers such as plywood, insulation, siding, and interior/exterior resistance layers formed by radiative and convective coefficients, are represented in a simplified form as three thermal resistances and two capacitances (3R2C, i.e., R_{e1}, R_{e2}, R_{e3}, and two C_w) by consolidating the layers with similar thermal properties. The indoor surface temperature (T_{iE}) and outdoor surface temperature (T_{oE}) of the exterior wall and the outdoor ambient temperature (T_{amb}) are needed in the model. Heat gains from the outdoor air and the solar energy incident on exterior surfaces are combined and represented as the quotient of the difference between the sol-air temperature (T_{sE}) and the outdoor surface temperature (T_{oE}) and the resistance (R_{e1}), where R_{e1} and T_{sE} are defined so that the quotient equals the combined rate of heat transfer associated with the incident solar energy and convective heat transfer from the air (Ogunsola et. al 2014). The solar energy incident on the outdoor surface of each opaque structural element depends on orientation of the surface and, as a result, T_{sE} varies with the structural component. Therefore, each structural component (wall or roof) is considered separately in this model. Because the thermal capacities of glazing materials are small, the heat transfer through windows is modeled as steady-state and

represented as the quotient of the outdoor-indoor temperature difference (T_{amb} – T_{in}) and a thermal resistance (R_{win1}).

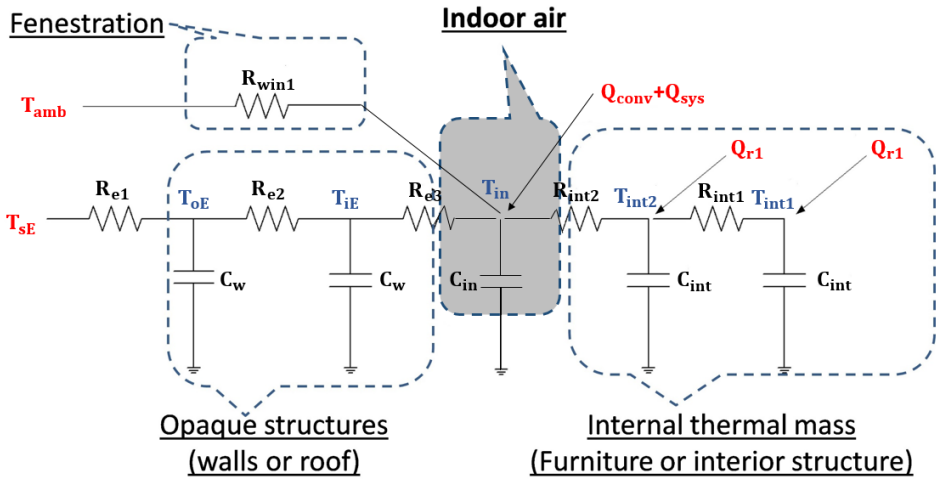

Figure 3.2. 3R2C plus 2R2C thermal model, showing only one exterior wall, solar-air temperature ($\boldsymbol{T_{sE}}$), and HVAC system input ($\boldsymbol{Q_{sys}}$).

The total heat capacity of interior structural components and furniture, which is the product of their mass and specific heat, is lumped into the 2R2C (R_{int1}, R_{int2}, and two C_{int}) circuit on the right-hand side of Figure 3.2, in which T_{int1} and T_{int2} represent two temperature nodes and Q_{r1} represents half of the radiative heat gains (Ogunsola et. al 2014) generated by occupants, solar irradiation through fenestration, lighting or/and appliances, while their convective heat gains (Q_{conv}) directly become the load and have no thermal delays.

Indoor air is represented by one uniform air temperature (T_{in}) in a thermal zone and its associated air thermal capacity (C_{in}). According to the diagram of the thermal model in Figure 3.2, a heat balance at each node yields the following equations:

$$C_w \frac{dT_{oE}}{dt} = \frac{T_{sE}-T_{oE}}{R_{e1}} + \frac{T_{iE}-T_{oE}}{R_{e2}} \tag{3.1}$$

$$C_w \frac{dT_{iE}}{dt} = \frac{T_{oE}-T_{iE}}{R_{e2}} + \frac{T_{in}-T_{iE}}{R_{e3}} \tag{3.2}$$

$$C_{in} \frac{dT_{in}}{dt} = \frac{T_{iE}-T_{in}}{R_{e3}} + \frac{T_{int2}-T_{in}}{R_{int2}} + \frac{T_{amb}-T_{in}}{R_{win1}} + Q_{conv} + Q_{sys} \tag{3.3}$$

$$C_{int} \frac{dT_{int2}}{dt} = \frac{T_{in}-T_{int2}}{R_{int2}} + \frac{T_{int1}-T_{int2}}{R_{int1}} + Q_{r1} \tag{3.4}$$

$$C_{int} \frac{dT_{int1}}{dt} = \frac{T_{int2}-T_{int1}}{R_{int1}} + Q_{r1} \tag{3.5}$$

Equations (3.1) to (3.5) represent an inhomogeneous system of first-order differential equations. In state-space representation, these equations can be re-written as:

$$\dot{T} = AT + BU, \tag{3.6}$$

where A and B are matrices with constant coefficients that are functions of the RC parameters and are given by

$$A = \begin{bmatrix} -\frac{1}{R_{e1}C_w} - \frac{1}{R_{e2}C_w} & \frac{1}{R_{e2}C_w} & 0 & 0 & 0 \\ \frac{1}{R_{e2}C_w} & -\frac{1}{R_{e2}C_w} - \frac{1}{R_{e3}C_w} & \frac{1}{R_{e3}C_w} & 0 & 0 \\ 0 & \frac{1}{R_{e3}C_{in}} & -\frac{1}{R_{e3}C_{in}} - \frac{1}{R_{int2}C_{in}} - \frac{1}{R_{win1}C_{in}} & \frac{1}{R_{int2}C_{in}} & 0 \\ 0 & 0 & \frac{1}{R_{int2}C_{int}} & -\frac{1}{R_{int2}C_{int}} - \frac{1}{R_{int1}C_{int}} & \frac{1}{R_{int1}C_{int}} \\ 0 & 0 & 0 & \frac{1}{R_{int1}C_{int}} & -\frac{1}{R_{int1}C_{int}} \end{bmatrix},$$

$$\mathrm{B} = [B_1 \quad B_2 \quad B_3 \quad B_4 \quad B_5] = \begin{bmatrix} \frac{1}{R_{e1}C_w} & 0 & 0 & 0 & 0 \\ 0 & 0 & 0 & 0 & 0 \\ 0 & \frac{1}{R_{win1}C_{in}} & 0 & \frac{1}{C_{in}} & \frac{1}{C_{in}} \\ 0 & 0 & \frac{1}{C_{int}} & 0 & 0 \\ 0 & 0 & \frac{1}{C_{int}} & 0 & 0 \end{bmatrix},$$

$$\mathrm{T} = [T_{oE} \quad T_{iE} \quad T_{in} \quad T_{int2} \quad T_{int1}]', \tag{3.7}$$

and

$$\mathrm{U} = [T_{sE} \quad T_{amb} \quad Q_{r1} \quad Q_{conv} \quad Q_{sys}]'. \tag{3.8}$$

The indoor air temperature can be represented by

$$T_{in} = CT + DU, \tag{3.9}$$

where C and D are given by

$$\mathrm{C} = [0 \quad 0 \quad 1 \quad 0 \quad 0] \text{ and } \mathrm{D} = [0 \quad 0 \quad 0 \quad 0 \quad 0], \tag{3.10}$$

and T and U are given by Equations. (3.7) and (3.8).

With the Laplace transform of Equations (3.9) and (3.10), Equation (3.9) becomes

$$T_{in}(s) = C(sI - A)^{-1}BU(s) = C(sI - A)^{-1}B_1T_{sE}(s) + C(sI - A)^{-1}B_2T_{amb}(s) + C(sI - A)^{-1}B_3Q_{r1}(s) + C(sI - A)^{-1}B_4Q_{conv}(s) + C(sI - A)^{-1}B_5Q_{sys}(s) \tag{3.11}$$

The coefficients in transfer functions $C(sI - A)^{-1}B_i$ (i =1, 2, …, 5) have products and inverses of the parameters $\mathrm{R}_{(.)}$ and $\mathrm{C}_{(.)}$, which are nonlinear functions of the parameters $\mathrm{R}_{(.)}$ and $\mathrm{C}_{(.)}$. Therefore, estimation of their individual values is extremely difficult, if not impossible. For example,

$$C(sI - A)^{-1}B_1 = [R_{win1} + (C_{int}R_{int1}R_{win1} + 2C_{int}R_{int2}R_{win1})s + C_{int}^2R_{int1}R_{int2}R_{win1})s^2]/\Delta(s) \tag{3.12}$$

where $\Delta(s) = x_5s^5 + x_4s^4 + x_3s^3 + x_2s^2 + x_1s + x_0$, and the coefficients x_0, x_1, x_2, x_3, x_4, and x_5 are very complicated functions, which are not shown here.

To visualize the inner structure of the 3R2C plus 2R2C thermal model, a block diagram of it is shown in Figure 3.3. Most of the blocks involve the sum or convolution of one to five parameters. The diagram provides another view of the complexity of the coefficients that make the estimation of parameters, using five inputs and one output, extremely difficult.

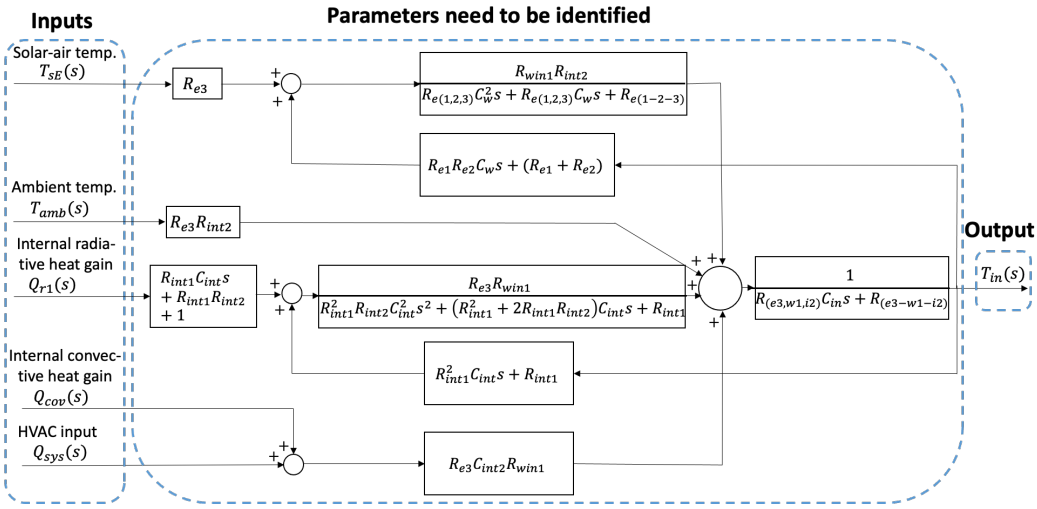

Note: $R_{e(1,2,3)} = R_{e1}R_{e2}R_{e3}$, $R_{e(1-2-3)} = R_{e1} + R_{e2} + R_{e3}$, $R_{(e3,w1,i2)} = R_{e3}R_{win1}R_{int2}$, and $R_{(e3-w1-i2)} = R_{win1}R_{int2} + R_{e3}R_{win1} + R_{e3}R_{int2}$.

Figure 3.3. Block diagram of the 3R2C plus 2R2C thermal system model.

However, the automated parameter estimation is particularly critical for this development, because it allows the model to identify the needed parameters automatically with no need for user inputs. Homes have much smaller footprints, usually with one or two thermal zones, which introduce an opportunity to simplify the 3R2C plus 2R2C model for an automated parameter estimation process. In addition, although homes have similar airtightness compared with commercial

buildings (Sherman and Matson 2002; Emmerich and Persily 2005), infiltration is not negligible. A home usually does not have positive building pressure control and therefore has a large possibility of experiencing outdoor air infiltration. Therefore, a home thermal model that can be automatically estimated and considers air infiltration is needed.

3.3 Home Thermal Model Formulation

In this section, a home thermal model, which is built upon the energy conservation law, is formulated through the analysis of heat transfer processes between indoors and outdoors. The model represented by a second-order dynamic equation is used to capture the thermal dynamics of the indoor space and wall of a home.

3.3.1 Heat transmissions through temperature differences

For a 3R2C model application, the exterior wall shown in Figure 3.2 needs to be replaced by a wall for all exterior walls having different orientations, i.e., different orientations of the walls require them to be modeled individually. However, homes usually have one thermal zone (the entire house in most cases, and generally not more than two zones). Therefore, the home envelope (for a home with one zone) may be consolidated into o*ne virtual envelope* with the orientation-dependent wall temperature (T_{ie}) represented by the weighted-average of the impacts on envelope elements having different orientations, as shown in Figure 3.4. The thermal properties of the virtual envelope are the weighted average of the thermal resistance and heat capacity, i.e., R_{ve} and $C_{ve,in}$ of all the

envelope components. For internal space, the indoor air is represented by one uniform air temperature (T_{in}) in a thermal zone and its associated air thermal capacity (C_{air}) and thermal resistance (R_{air}). Therefore, the heat transmissions through all the envelope components and internal space can be represented by two heat transfer relationships driven by the temperature difference between the outdoor air temperature (T_o) and the wall temperature (T_{ie}), and driven by the temperature difference between the interior wall surface temperature (T_{ie}) and indoor air temperature (T_{in}), along with the consolidated thermal properties of all the envelope components and internal space, to be estimated using home operational data, shown in Equations (3.13) and (3.14), respectively.

$$C_{ve,in}\frac{dT_{ie}}{dt} = \frac{T_o - T_{ie}}{R_{ve}} + \frac{T_{in} - T_{ie}}{R_{air}} \tag{3.13}$$

$$C_{air}\frac{dT_{in}}{dt} = \frac{T_{ie} - T_{in}}{R_{air}} \tag{3.14}$$

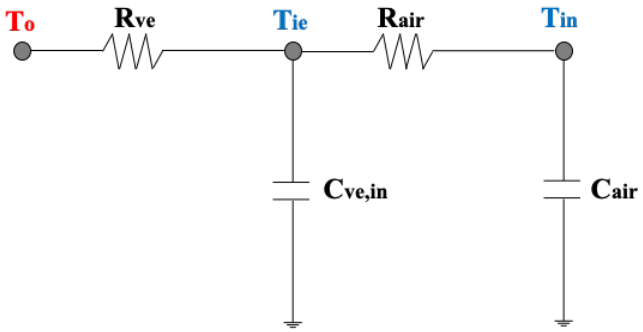

Figure 3.4. One virtual envelope.

3.3.2 Solar impacts

Solar radiation transfers heat inside a home through an envelope, consisting of all structural elements that separate the conditioned indoor spaces

from unconditioned indoor spaces and the outdoors, by two mechanisms. One is to heat the exterior opaque surfaces of the home. The heat received by the opaque envelope elements is absorbed by the total heat capacity of the opaque envelopes first and then released into the indoor air through conduction and convection. The other mechanism is to heat indoor structural components and furnishings through which solar radiation transmitted through glazing, such as windows and skylights. Some of the solar heat gain absorbed by interior furnishings and structural components (e.g., walls) are immediately transferred to the indoor air by convection, and the rest is conducted into the structure or furnishings and gradually released later, thus heating the indoor air. In a traditional RC thermal model, the two mechanisms are described separately. The heat transfer of solar radiation on the exterior surfaces of opaque structural components is described by the sol-air temperature, which is orientation-dependent, while the solar gain through fenestration is separately described as radiative heat gains (McQuiston et. al 2000). In this home model, however, a third-order polynomial, shown in Equation (3.15), is used to describe the overall attenuation from the global horizontal irradiation to the solar heat received by all the envelope components, including opaque and fenestration components, and eventually contributed to the internal space. The coefficients in the polynomial in Equation (3.15), representing the home thermal responses to solar inputs, are estimated using a parameter estimation scheme introduced in Section 3.4.

$$Q_{sol}(G) = a_1 G + a_2 G^2 + a_3 G^3 \quad (3.15)$$

where G is the global horizontal irradiation; $Q_{sol}(G)$ is the space air temperature increase that represents solar impacts on a home; and a_1, a_2, and a_3 are empirically-determined coefficients using home operational data.

3.3.3 Wind impacts

Wind impacts home thermal load through two mechanisms: changes in convection heat transfer coefficient and infiltration. Wind impact is not considered in Equations (3.1)–(3.5). To investigate the wind impacts, a preliminary study was carried out in March 2016 in an unoccupied home, and distinctive heat losses were observed for different wind speeds for the same outdoor air temperature. As shown in Figure 3.5, when the wind speed was at 3 mph, the heat loss rates were approximately 10% higher than the loss rates at 1.5 mph wind speed and more than 50% higher than the loss rates at close to 0 mph. This proves that wind impacts cannot be ignored for home thermal load studies and suggests that the amount of heat gains or losses can be related to wind speeds. The heat loss rates were calculated using operational data of a gas-heater logged over one-minute intervals.

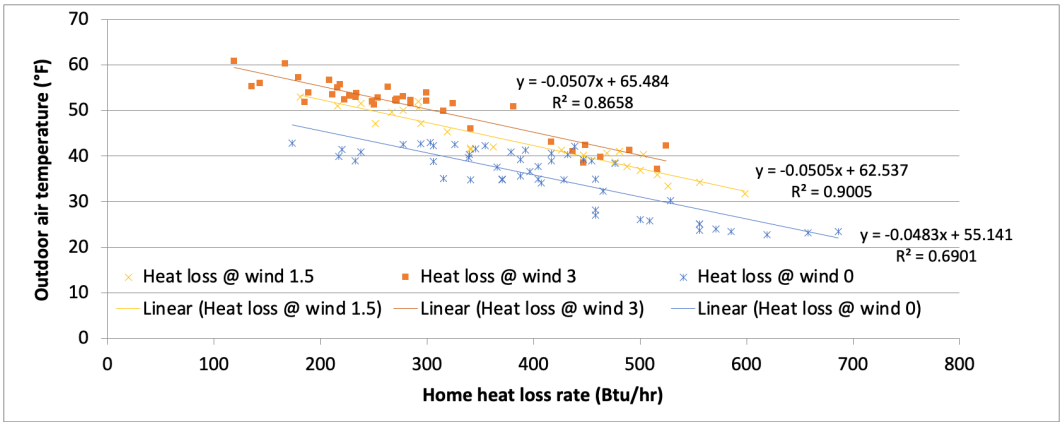

Figure 3.5. Home heat loss rate vs. outdoor air temperature for three different wind speeds.

Due to the difficulties in directly calculating the infiltrated air flow rate (Gowri et. al 2009; Waite and O'Brien 2010) and quantifying the convection heat transfer coefficient changes, in this study the quadratic equation, $b_1'W + b_2'W^2$, is used to capture the wind impacts for each specific home with the values of its parameters estimated through data training. Therefore, the rate of heat transfer by wind effects can be expressed by

$$q'_{vw} = \frac{T_o - T_{in}}{1/(b_1'W + b_2'W^2)} = \frac{T_o - T_{in}}{R_{vw}} \tag{3.16}$$

where q'_{vw} is the heat transfer rate by wind effects; W is the wind speed; b_1' and b_2' are the empirical coefficients; and R_{vw} is a variable resistance dependent on the wind speed and the airtightness of a specific home.

3.3.4 Internal heat gain impacts

For homes, the dominant thermal mass (the product of the mass and the specific heat capacity) comes from the envelopes (Kosny et. al 2001; Johra and Heiselberg 2017), because the heat capacity per specific volume of concrete, glass and wood/plastic, and materials for envelope elements is 1000 times higher than the heat capacity per volume of air while interior structure of a house is much smaller than a commercial building given the need for corridor, stairs, and elevator in addition to interior zones in a building. Meanwhile, for residential buildings, the volume of the envelope is significantly larger than the volume of

the partition walls and furnishings. Therefore, internal thermal mass, represented by 2R2C in Equations (3.1)–(3.5), is ignored. On the other hand, internal heat gains have relatively small impacts compared with envelope heat gains/losses (Kim and Moon 2009). Herein, the internal heat gains are simply treated as one input Q_{int} in this study.

3.3.5 Formulate heat transfer processes

By integrating the contributions of Sections 3.3.1–3.3.4, the governing equation for the home thermal model can be expressed as

$$C_{ve,in}\frac{dT_{ie}}{dt} = \frac{T_o - T_{ie}}{R_{ve}} + \frac{T_{in} - T_{ie}}{R_{air}} \tag{3.17}$$

$$C_{air}\frac{dT_{in}}{dt} = \frac{T_{ie} - T_{in}}{R_{air}} + q'_{vw} + Q_{sol} + Q_{int} + Q_{sys} \tag{3.18}$$

where Q_{int} represents the sum of all internal heat gains and Q_{sys} is the HVAC system output.

Compared with Equations (3.1)–(3.5), Equations (3.17) and (3.18) are expressed in a 2R2C model format which eliminates the exterior wall surface temperatures (T_{oE}) by using *one virtual envelope* assumption and meanwhile uses Q_{sol} to represent the solar impacts instead of the traditional solar-air temperature (T_{sE}). Furthermore, the heat transfer impacted by wind is included as a function of wind speed. R_{ve}, $C_{ve,in}$, R_{air}, and C_{air} are time-invariant parameters, but R_{vw} varies with time as wind speeds change. The circuit diagram for Equations (3.17) and (3.18) are shown in Figure 3.6.

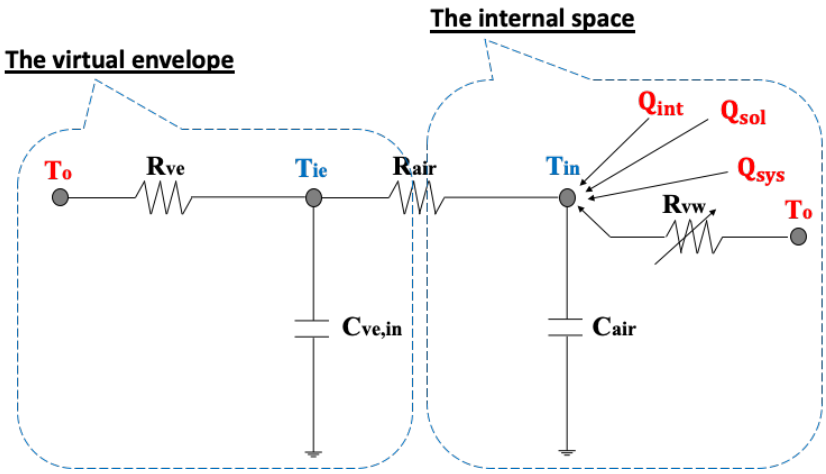

Figure 3.6. Schematic diagram of the 2R2C network.

Applying the Laplace transform to Equations (3.17) and (3.18) yields

$$C_{ve,in}sT_{ie}(s) = \frac{T_o(s)-T_{ie}(s)}{R_{ve}} + \frac{T_{in}(s)-T_{ie}(s)}{R_{air}} \tag{3.19}$$

$$C_{air}sT_{in}(s) = \frac{T_{ie}(s)-T_{in}(s)}{R_{air}} + q'_{vw}(s) + Q_{sol}(s) + Q_{int}(s) + Q_{sys}(s) \tag{3.20}$$

Rearranging Equations (3.19) and (3.20), these become

$$T_{ie}(s) = \frac{1}{s}\left(\frac{T_o(s)}{R_{ve}C_{ve,in}} + \frac{T_{in}(s)}{R_{air}C_{ve,in}} - \frac{T_{ie}(s)}{R_{ve}C_{ve,in}} - \frac{T_{ie}(s)}{R_{air}C_{ve,in}}\right) \tag{3.21}$$

$$T_{in}(s) = \frac{1}{s}\left[\frac{T_{ie}(s)}{R_{air}C_{air}} - \frac{T_{in}(s)}{R_{air}C_{air}} + \frac{\left(q'_{vw}(s)+Q_{sol}(s)+Q_{int}(s)+Q_{sys}(s)\right)}{C_{air}}\right] \tag{3.22}$$

Similarly, a block diagram of the home thermal model in Figure 3.6 is constructed and shown in Figure 3.7.

Compared with the block diagram of the 3R2C plus 2R2C thermal model in Figure 3.3, the home thermal model has the same number of inputs but different outputs and expressions of solar impacts. Furthermore, it includes infiltration impacts. Each block in the model (see Figure 3.7) is a straightforward

transfer function. Therefore, parameter estimation using measured input and output data is easier than for the model in Figure 3.3.

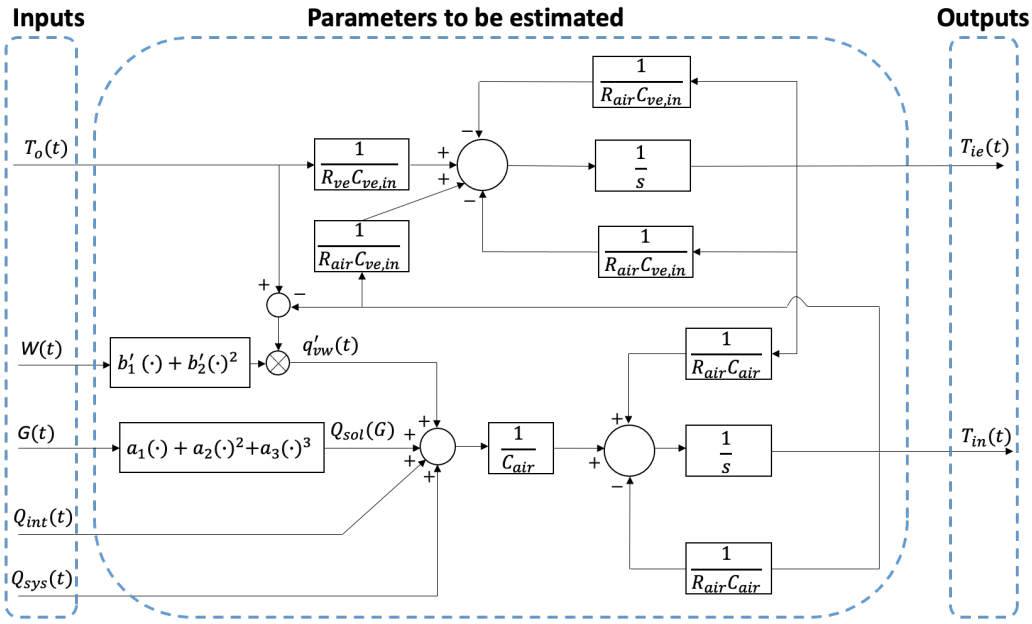

Figure 3.7. Block diagram of the home thermal model.

3.3.6 Summary

Substituting Equations (3.15) and (3.16) into Equation (3.18) and rearranging Equations (3.17) and (3.18), the equations are the time-continuous model

$$\frac{dT_{ie}(t)}{dt} = \frac{1}{\tau_1}[T_o(t) - T_{ie}(t)] + \frac{1}{\tau_2}\left[\left(T_{in}(t) - T_{ie}(t)\right)\right] \tag{3.23}$$

$$\frac{dT_{in}(t)}{dt} = -\frac{1}{\tau_3}T_{in}(t) + \frac{1}{\tau_3}\Big[T_{ie}(t) + \left(T_o(t) - T_{in}(t)\right)\left(b_1W(t) + b_2W^2(t)\right) +$$

$$\left(a_1G(t) + a_2G^2(t) + a_3G^3(t)\right) + \left(Q_iu_i(t) + Q_su_s(t)\right)\Big], \tag{3.24}$$

where $\tau_1 = C_{ve,in}R_{ve}$ and $\tau_3 = C_{air}R_{air}$ are the time constants of the envelope and indoor air of a home, respectively; $\tau_2 = C_{ve,in}R_{air}$, $a_1 = a_1'R_{air}$, $a_2 =$

$a_2' R_{air}$, $a_3 = a_3' R_{air}$, $b_1 = b_1' R_{air}$, and $b_2 = b_2' R_{air}$ are the corresponding coefficients associated with R_{air}; and $Q_i = Q_{int} R_{air}$ and $Q_s = Q_{sys} R_{air}$, where the internal heat gain Q_{int} and HVAC system output Q_{sys} are treated as constant associated with the internal activity schedules u_i and HVAC system on/off signal u_s, respectively.

All the coefficients in Equations (3.23) and (3.24), representing the thermal responses of the envelope and indoor air of a home to the inputs of outdoor air temperature, interior wall surface temperature, wind, solar, internal heat gains, and HVAC system output, are estimated using a parameter estimation scheme introduced in Section 3.4.

3.4 Parameter Estimation

The formulated home thermal model in Equations (3.23) and (3.24) includes several unknown parameters that need to be estimated. In this section, a parameter estimation scheme is introduced using Euler's approximation and the least squares method.

3.4.1 Model discretization

Because the home thermal model in Equations (3.23) and (3.24) is time-continuous, it must be discretized in order to use measured input and output data for the parameter estimation. The continuous-time model is converted into a discrete-time model by applying Euler's method. As an example, the left-hand sides in Equations (3.23) and (3.24) become

$$\frac{dT_{ie}(t)}{dt} = \frac{T_{ie}(t) - T_{ie}(t-1)}{\Delta t} \tag{3.25}$$

$$\frac{dT_{in}(t)}{dt} = \frac{T_{in}(t) - T_{in}(t-1)}{\Delta t} \tag{3.26}$$

where Δt is the sampling interval between measurements.

By substituting Equations (3.25) and (3.26) into Equations (3.23) and (3.24), respectively, the continuous-time state equations are approximately converted in discrete time to

$$T_{ie}(k) - T_{ie}(k-1) = \frac{\Delta t}{\tau_1}[T_o(k) - T_{ie}(k)] + \frac{\Delta t}{\tau_2}[(T_{in}(k) - T_{ie}k)] \tag{3.27}$$

$$T_{in}(k) - T_{in}(k-1) = -\frac{\Delta t}{\tau_3}T_{in}(k) + \frac{\Delta t}{\tau_3}\Big[T_{ie}(k) + \big(T_o(k) - T_{in}(k)\big)\big(b_1 W(k) + b_2 W^2(k)\big) + \big(a_1 G(k) + a_2 G^2(k) + a_3 G^3(k)\big) + (Q_i u_i(k) + Q_s u_s(k))\Big] \tag{3.28}$$

where k denotes discrete time, i.e., each measurement sampling time, k=1, 2, 3, ….

The right side of Equations (3.27) and (3.28) refers to the linear, quadratic, and polynomial terms. Due to the complexity of the model, a stepwise data parameter estimation scheme is proposed and shown in Section 3.4.2. To identify the values of these parameters, the least squares method is used. Herein, as an example, Equation (3.27) in the first-step parameter estimation can be written in a matrix form as

$$X\beta = Y \tag{3.29}$$

where X and Y are the matrices containing measured variables, whose elements are the inputs and output of the home thermal model, and β is the matrix of constant coefficients, which are the unknown parameters to be estimated.

Assuming that X has full column rank, the least squares solution to Equation (3.29) is:

$$\hat{\beta} = (X^T X)^{-1} X^T Y \tag{3.30}$$

where $\hat{\beta}$ is the optimal estimate of the unknown parameters, and

$$X = \begin{pmatrix} x_{11} & \cdots & x_{1m} \\ \vdots & \ddots & \vdots \\ x_{n1} & \cdots & x_{nm} \end{pmatrix}; \qquad \beta = \begin{bmatrix} \beta_1 \\ \vdots \\ \beta_m \end{bmatrix}; \qquad Y = \begin{bmatrix} y_1 \\ \vdots \\ y_n \end{bmatrix}. \tag{3.31}$$

where n represents sampling data in time steps and m represents different combination of measured variables involved in Equation (3.27). Detailed definitions can be found in Equations (A.1) to (A.4) in the **Appendix A**.

3.4.2 Parameter estimation scheme

The home thermal model in Equations (3.23) and (3.24) requires estimation of ten parameters using a data set of seven known inputs: indoor air temperature (T_{in}), outdoor air temperature (T_o), interior wall surface temperature (T_{ie}), wind speed (W), global horizontal irradiation (G), internal activity schedules (u_i), and HVAC system on/off signal (u_s). Among all the parameters to be estimated, the accuracy of the time constants (τ_1 and τ_3) in Equations (3.23) and (3.24) are the most dominant parameters for ensuring the accurate representation of the home thermal properties, including the home envelope and internal space, which stay the same in HVAC on/off mode for a specific home. To

minimize the errors introduced by the indoor air and wall surface temperature in HAVC on/off mode in Equations (3.23) and (3.24), a stepwise data estimation scheme based on the least squares method described in Equations (3.29) to (3.31) is used. The parameter estimation process consists of two steps:

(1) Identify τ_1 and τ_2 through solving a least squares problem that is formed in Equation (3.27) and the measurements of indoor air temperature $T_{in}(k)$, outdoor air temperature $T_0(k)$, and interior wall surface temperature $T_{ie}(k)$, focusing on time periods when HVAC system is off; and

(2) Identify τ_3, b_1, b_2, a_1, a_2, a_3, Q_i, and Q_s by solving another least squares problem that is formed in Equations (3.28) and all the measurements at each time step, completing the parameter estimation process.

Figure 3.8 shows a schematic diagram of the parameter estimation process. Details of the parameter estimation are presented in Equations (A.1) to (A.8) in the **Appendix A**.

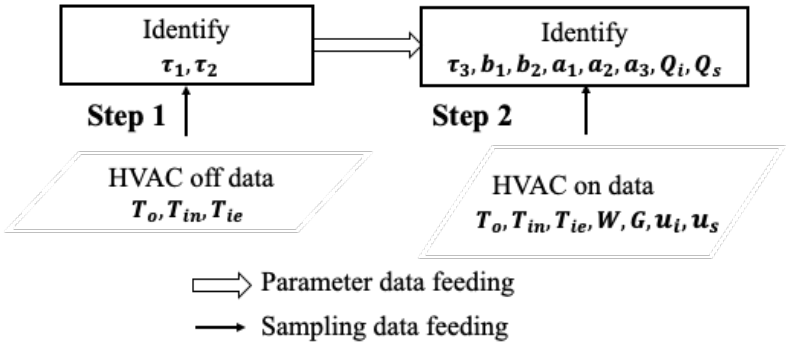

Figure 3.8. A schematic diagram of parameter estimation.

3.5 Validations

The indoor air temperature predication for a typical home located in Norman, Oklahoma was used to validate the home thermal model and the parameter estimation scheme. To mitigate the impacts of occupancy disturbances that may cause uncertainties in the model validation, two experiments were conducted, where the first one was from May 7 to May 21, 2020 (15 days) when the HVAC system was forced to shut down and another was from May 28 to June 11, 2020 (15 days) when the HVAC system was on. The home description, measurements, and data collection and analysis are introduced in this section.

3.5.1 The experimental home and data acquisition system

Validations were performed in the home shown in Figure 3.9(a); it is a single-family, one-story home with a floor area of 1,658 ft^2, built in 1940. The home is equipped with 3.5 tons (42,000 Btu/h) of cooling capacity and 1,400 cfm of air flow rate. The home includes three bedrooms and one living room. The thermostat is in the living room. The measured inputs include the indoor and outdoor air temperature, interior wall surface temperature, wind speed, global horizontal irradiation, return air flow rate, used to represent the HVAC on/off status. All temperature data were measured using T-type thermocouple and logged using the connected Raspberry Pi and its associated thermocouple hat, shown in Figure 3.9(b), and air velocity sensors were installed on the return air ducts shown in Figure 3.9(c). All the thermocouples were calibrated according to the ASTM standard E220 (ASTM 2019). An outdoor weather station, shown in

Figure 3.9(d), was set up for the outdoor temperature, wind, and solar measurements at thirty-second intervals, which were compared with the data downloaded from Mesonet (Oklahoma Mesonet 2016) at five-minute intervals. The comparison shows that the Mesonet data provided more consistent results. Therefore, the Mesonet data were used in the study. For the experimental period, there were total 30 days, including 20 sunny days, 8 cloudy days, and 2 rainy days. The outdoor temperature varied from 38.1 °F to 94.5 °F during the experiment. All the measured weather conditions were plotted and shown in Figures B.1 and B.2 in the **Appendix B**. Table 1 lists the specifications of the sensors used in the experiment.

(a)

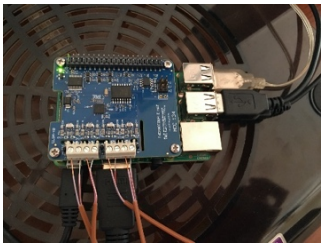

(b)

(c)

(d)

Figure 3.9. Test home and data acquisition device: (a) Outside view of the front of the test home; (b) Raspberry Pi and thermocouple hat; (c) Flow rate sensor; (d) Outdoor weather station.

Table 3.1. Specifications of the sensors in the experiment.

Sensors	Measurement	Range	Accuracy
Indoor thermocouple	Temperature	32 – 392 °F	±0.9 °F
Air velocity transducer	Air speed	25 – 1500 fpm	±2%
Outdoor weather station	Temperature	-40 – 167 °F	±0.38 °F from 32 to 122 °F
	Wind speed	0 – 125 mph	±4%
	Solar radiation	0 – 1250 W/m^2	±5%

3.5.2 Validation of the parameter estimation scheme

To predict the indoor air temperature using the thermal model, the model parameters in Equations (3.23) and (3.24) need to first be estimated using the stepwise parameter estimation scheme discussed in Section 3.4.2. In general, more training data provide more robust results, although collection of more data will need more waiting time for the model to function properly. Therefore, the number of data collection days required to obtain sufficiently reliable results for the parameter estimation was first examined using the two sets of the collected 15 days' data.

Two examinations were conducted based on Equations (3.23) and (3.24) of the model using the two sets of data separately. Each examination was initiated by using one day's training data to estimate the parameters. The parameter estimation was repeated for increased training data sets by incrementally adding one-day's (24-hour) data per trial, i.e., the first trial uses one day of training data, the second trial uses two days of training data, and the n^{th} trial uses training data for n days. For the first trial, by applying the 15-day operational data one-by-one, a total number of 15 sets of parameters were obtained, one set for each day's data collected at 30-second intervals. For the second trial, two consecutive days of training data were applied to train the parameters for each set, and a total of 14 (15-2+1) sets of parameters were obtained. The process continued by adding one day to increase the training data length per trial, so that the 15^{th} trial only generated one set (15-15+1) of parameters.

The results of the trials were compared to determine the minimum number of data points needed to obtain stable results. According to the model formulation shown in Equations (3.23) and (3.24), the values of τ_1 and τ_3 represent the physical home thermal properties, i.e., area-weighted average thermal properties of all envelope elements and internal space, which are supposed to be a relatively constant numbers regardless of the home operation conditions. Therefore, the consistency of the estimated values of τ_1 and τ_3 are used to determine the number of days needed for training data collection. Figure 3.10 shows example results of

values of the time constants (τ_1 and τ_3) for all the trials. Results of values of other model parameters are shown in the **Appendix C**. Note that the spikes in the 1st trials indicate less robust results using a relatively small amount of data. As can be seen from the mean values of τ_1 and τ_3 in Figure 3.10, by 6 consecutive days of data per set (6th trial), the values of τ_1 and τ_3 have already reached relative constant values compared with the values obtained from less than 6 consecutive days of data. Therefore, 6 or more consecutive days' data length is suggested for the estimation of the model parameters τ_1 and τ_3. Moreover, when reaching the first available 15 consecutive days of data, the value of τ_1 and τ_3 still vary after 6 consecutive days of data. Hence, in the next section, the thermal model is constructed twice, using the parameters τ_1 and τ_3 estimated with 6 and 15 consecutive days of data from the two sets of data, respectively, to show the impacts of different lengths of the training data sets on the model accuracy.

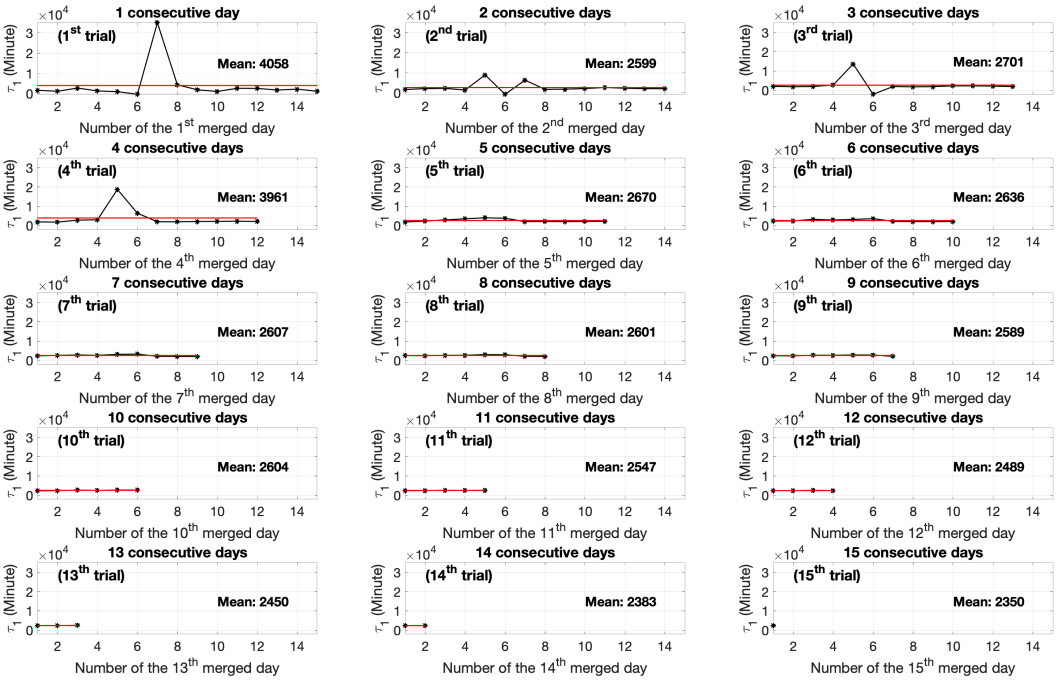

(a) Parameter τ_1

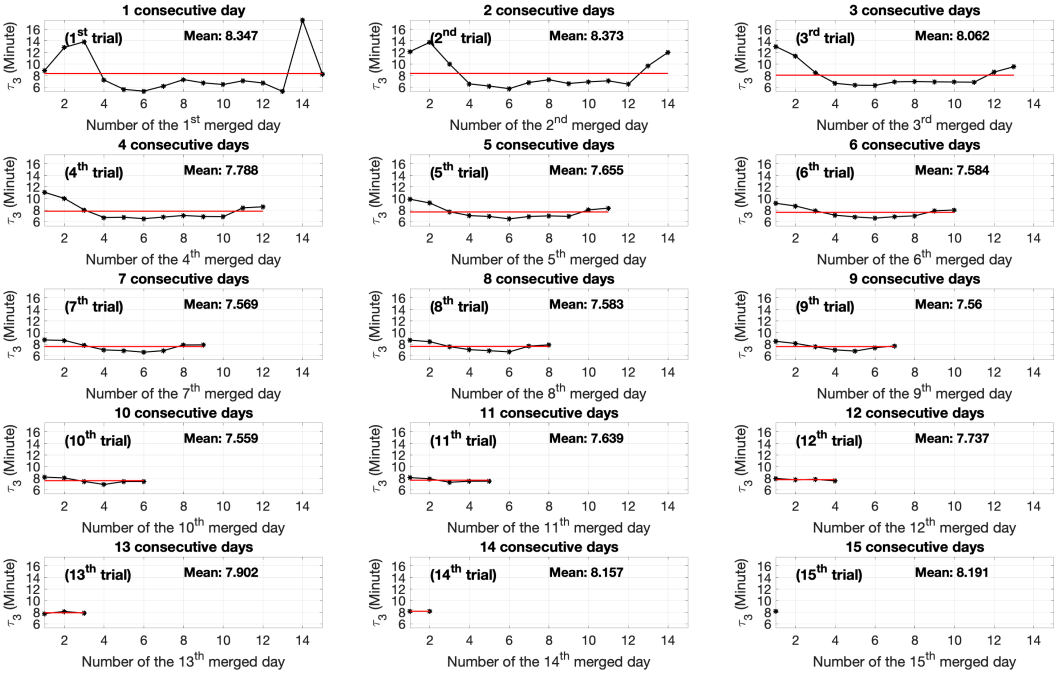

(b) Parameter τ_3

Figure 3.10. Empirically-determined values of parameters $\boldsymbol{\tau_1}$ and $\boldsymbol{\tau_3}$ for different numbers of days in each data set, used for validation.

3.5.3 Analysis and validation for two identified models

Table 3.2 shows the results of estimating the home thermal model parameters using the first 6 and 15 consecutive days of training data. The first 6 or 15 consecutive days of the training data are chosen because they would be the earliest available data while generating relatively reliable model parameters through the estimation scheme. Using these sets of estimated parameters in Equations (3.23) and (3.24) yields two home thermal models with different parameters that can be used for simulation.

Table 3.2. Estimated parameters for two identified models.

Length of training data	$\boldsymbol{\tau_1}$	$\boldsymbol{\tau_2}$	$\boldsymbol{\tau_3}$	$\boldsymbol{b_1}$	$\boldsymbol{b_2}$
First 6 consecutive days	2636	278.6	7.584	0.01272	-0.0002349
First 15 consecutive days	2350	272.1	8.191	0.01488	-0.0007994
Length of training data	$\boldsymbol{a_1}$	$\boldsymbol{a_2}$	$\boldsymbol{a_3}$	$\boldsymbol{Q_s}$	
First 6 consecutive days	4.331	-8.457	5.218	-2.200	
First 15 consecutive days	5.361	-10.33	6.264	-2.267	

Figures 3.11 and 3.12 show the measured and predicted indoor air temperatures and interior wall surface temperatures using the two identified models. These temperatures were predicted for every 24-hour ahead of the current time. In terms of the indoor air temperature, the predicted temperatures match the measured temperatures well, with a mean absolute error of 0.82 °F and 0.80 °F and an absolute error of 1.85 °F and 1.90 °F at 95% confidence interval for the two models, respectively. Similar to the indoor air temperature predictions, the interior wall surface temperatures follow the trend of the measured ones that show small fluctuations due to the HVAC system on/off. Figure 3.13 compares the histogram of absolute error distribution of indoor air temperature for the two models. This tends to indicate that the home thermal model is effective at capturing the home thermal dynamics through learned thermal properties for a specific home.

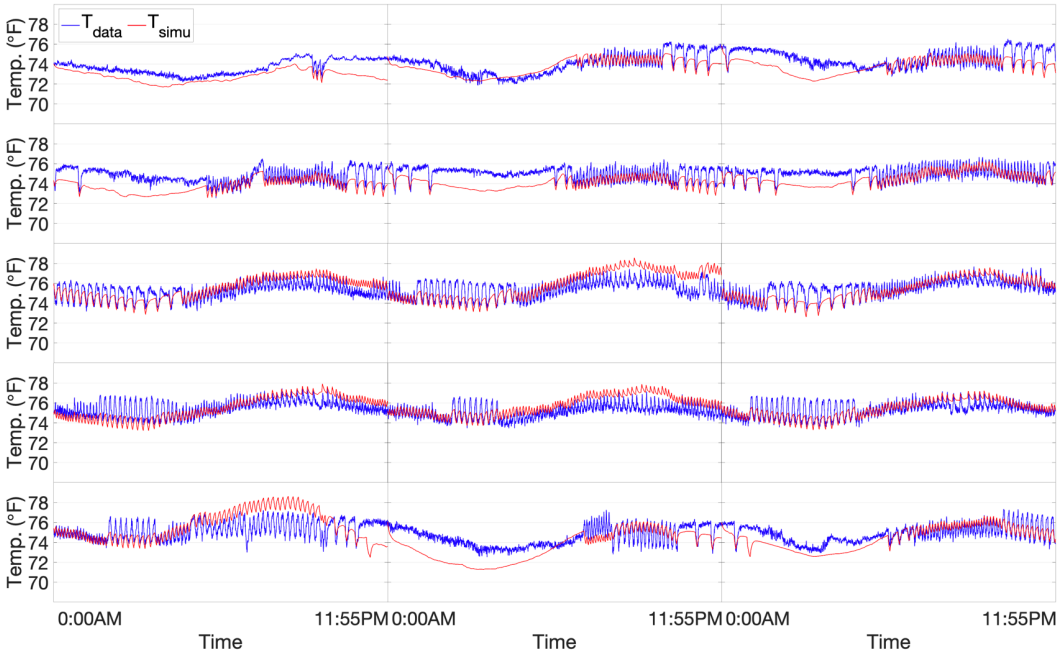

(a) for the home thermal model trained by first 6 consecutive days' data

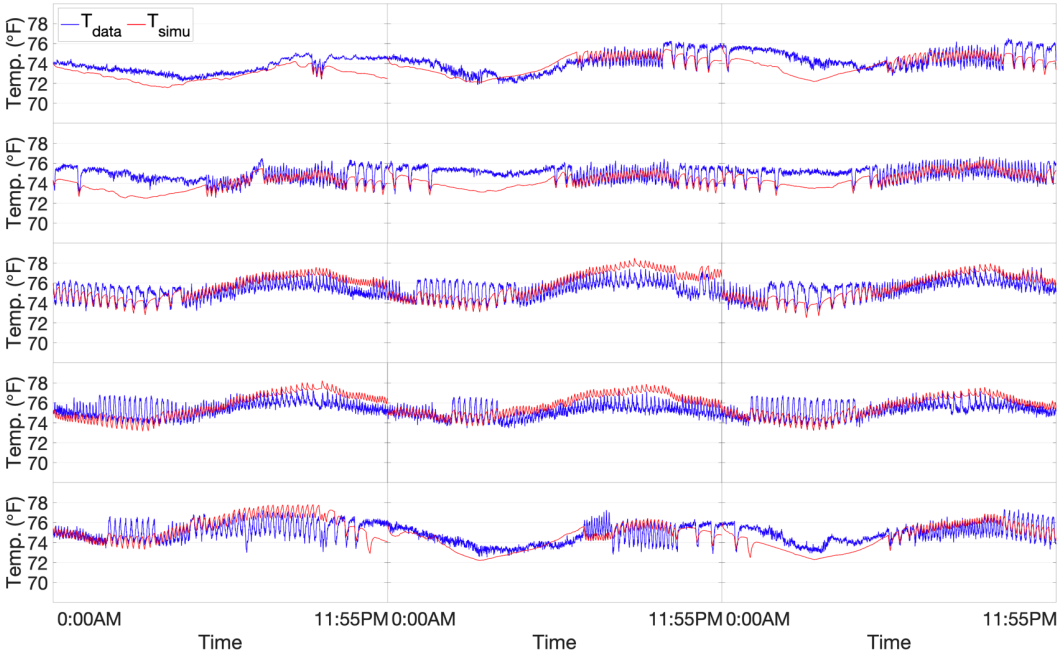

(b) for the home thermal model trained by first 15 consecutive days' data

Figure 3.11. Measured and predicted indoor air temperature comparison using the data from the first 6 and 15 consecutive days to estimate the thermal model parameters.

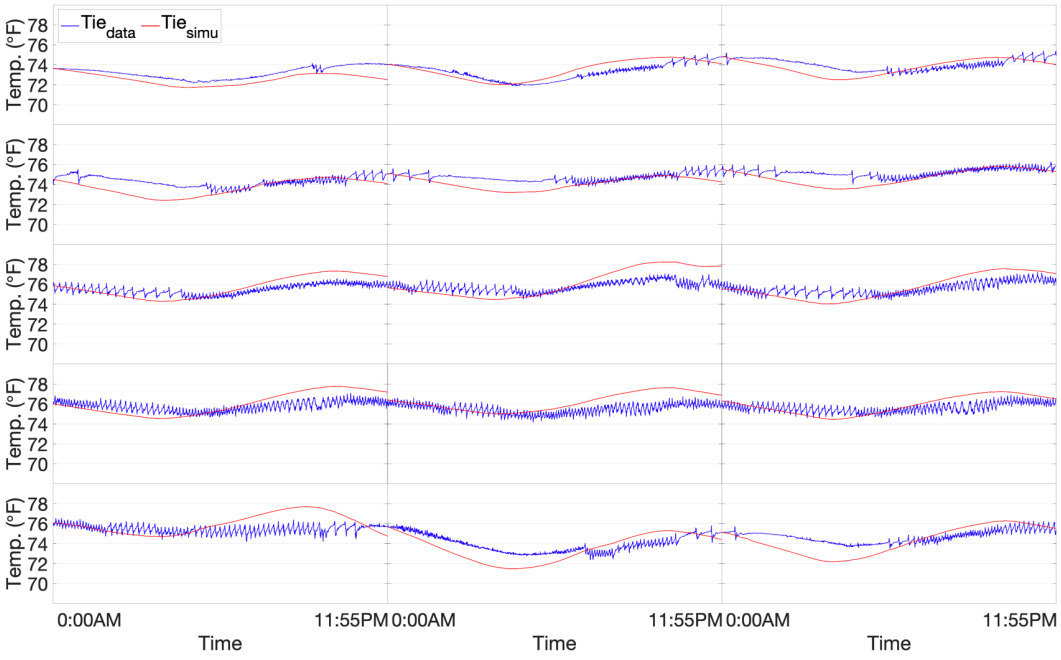

(a) for the home thermal model trained by first 6 consecutive days' data

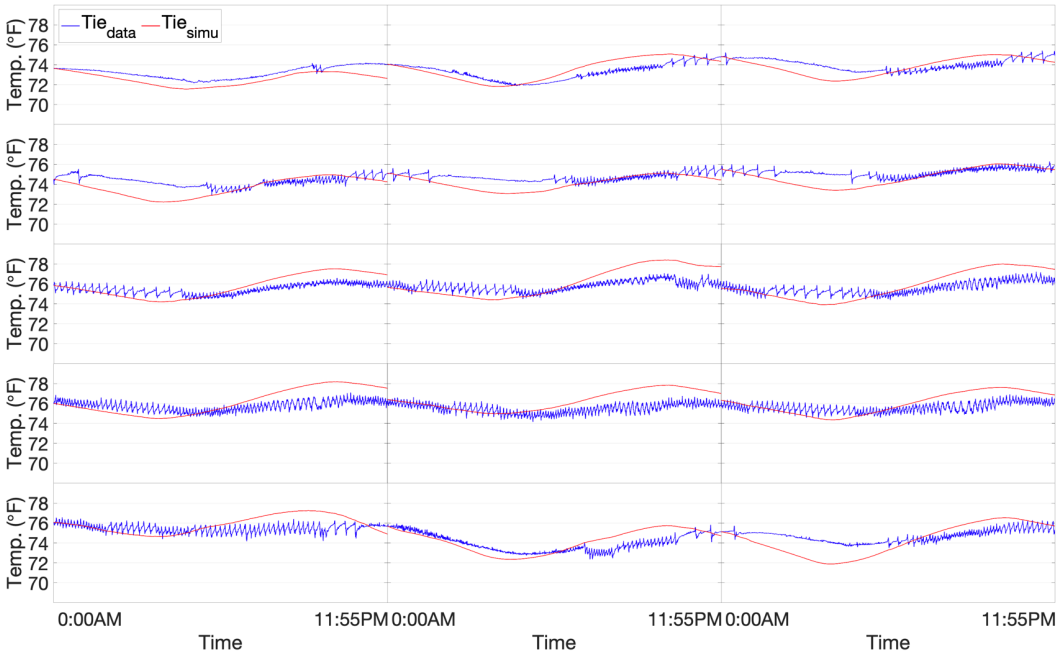

(b) for the home thermal model trained by first 15 consecutive days' data

Figure 3.12. Measured and predicted interior wall surface temperature comparison using the data from the first 6 and 15 consecutive days to estimate the thermal model parameters.

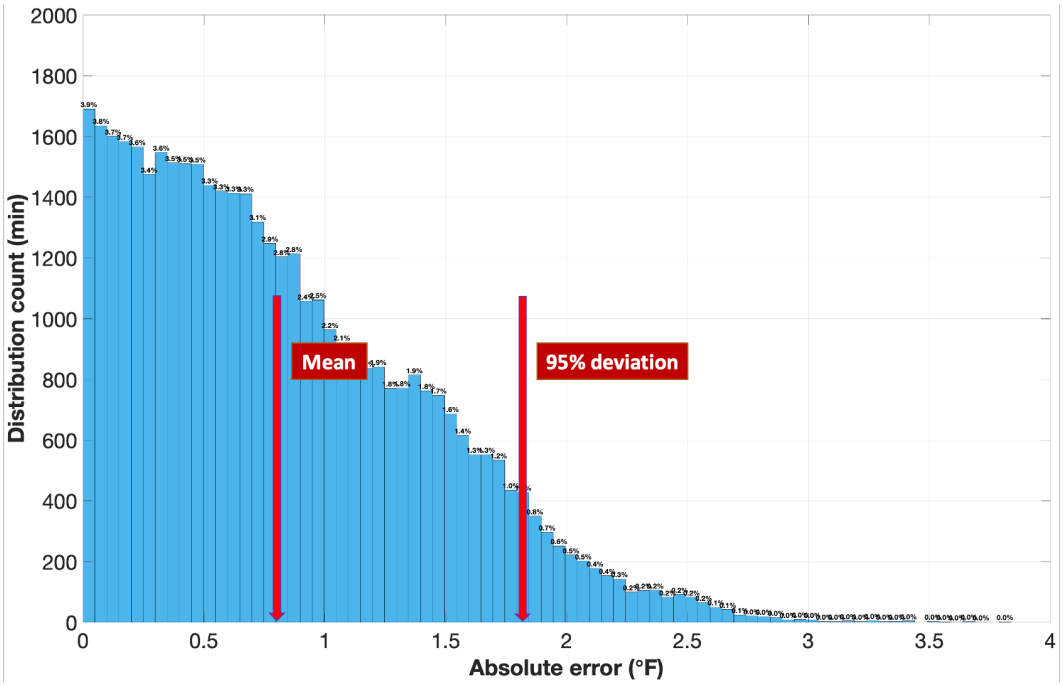

(a) for the home thermal model trained by first 6 consecutive days' data

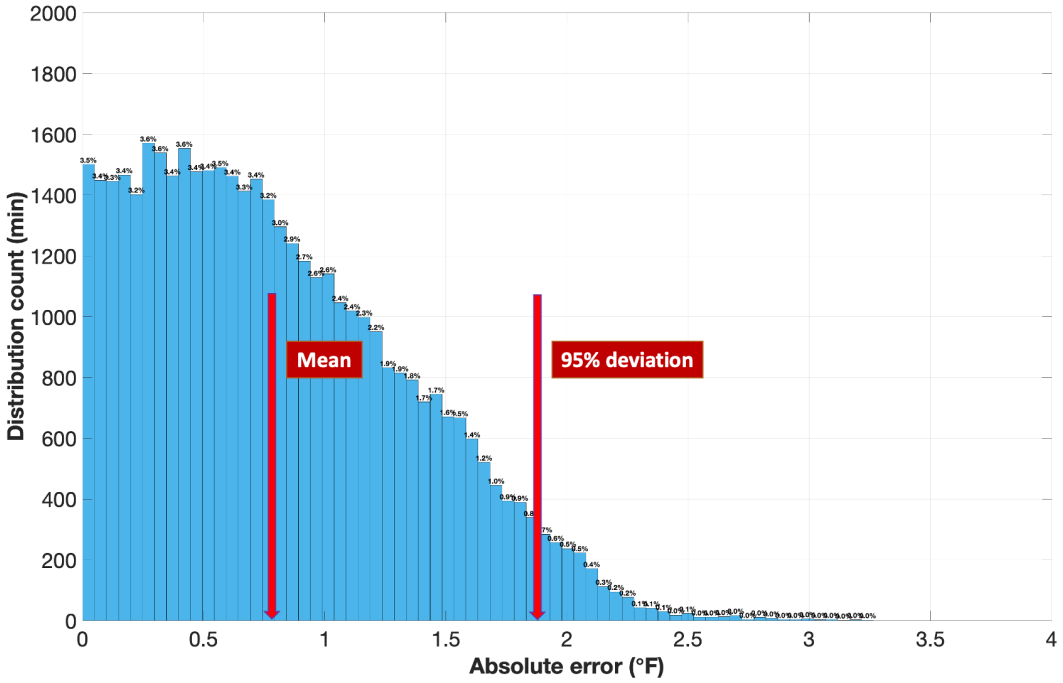

(b) for the home thermal model trained by first 15 consecutive days' data

Figure 3.13: Absolute error distribution for the indoor air temperature with predictions based on the home thermal model parameters estimated using data for the first 6 and 15 consecutive days. The red arrows identify the mean error and the error at 95% confidence interval.

The simulation results for the thermal model trained using data for 6 and 15 consecutive days are very close to each other, as presented in Figures 3.11 and 3.12. In addition, as shown in Table 3.3, the mean, maximum, and absolute error at 95% confidence interval of the model trained using data from 15 consecutive days are slightly better than the errors in indoor temperature prediction for the model trained using data from the first 6 consecutive days. Both models have similar accuracy in predicting the indoor air temperature 24 hours into the future and successfully verify the effectiveness of the proposed home thermal model and the parameter estimation scheme.

Table 3.3. Absolute error comparison for two identified models.

Length of training data	**Mean absolute error, °F**	**Maximum absolute error, °F**	**Absolute error at 95% confidence interval, °F**
First 6 consecutive days	0.82	3.84	1.85

First 15 consecutive days	0.80	3.26	1.90

3.6 Summary

With *one virtual envelope* node to describe the heat transfer processes between the indoor and outdoor environments of a home, the home thermal model is successfully formulated to capture the home thermal dynamics with reasonable accuracy. The simplicity of the model also allows its parameters to be automatically estimated using a short period of home operational and weather data and therefore eliminates the need for user inputs. The validation results for the test home show that training data for 6 consecutive days are needed to generate reliable parameters, i.e., the thermal properties of the home. More data improve the model robustness and therefore accuracy, but only marginally. In this study, the accuracy of the home thermal model is validated by applying it to predict the home indoor temperature for the test home. By utilizing on the model, the calculations of cooling load and cooling efficiency of the HVAC equipment will be investigated in Section 7.3. As conclusions, the novelty of the study resides in the successful self-identification of the parameters of the thermal model for each specific home using the parameter estimation process presented. The automatically identified model can effectively connect weather data with home operations and capture the home thermal dynamics with reasonable demands on

training data. The successful development of the model provides a key to achieve system operation optimization and reduce the energy cost needs for homes, which is the critical first step to realize model-based intelligent home HVAC system operations. However, since the model is simplified under the assumptions that the internal heat gains and HVAC system output are treated as two constant inputs and latent heat is not considered, there is room for improvement in the prediction of the dynamics of space air temperature, which will be the focuses of future studies (but while keeping the model sufficiently simple for compatibility with actual application in homes).

Chapter 4: Characterization of U.S. Home Thermal Performance

This chapter introduces the state of the art of home thermal performance analysis firstly. Then a model-based envelope performance evaluation method is proposed based on the home thermal model in Chapter 3 through some simplifications. Three sequential experiments are conducted to validate the effectiveness of the method. Finally, the characterization of U.S. home thermal properties is investigated through using data collected from 1,676 homes.

4.1 State of the Art of Home Thermal Performance Analysis

Energy usage for heating and cooling homes is known to account for a significant share of energy consumption in the United States. Indeed, in 2015 the 118.2 million housing units in the United States consumed 4.67 quads, or 4.67×10^{15} BTUs (4.93×10^{15} kJ), of end-use energy for heating and cooling alone, which was nearly 10% of the total energy use in the country (DOE 2011; EIA 2015). The energy consumption in homes is affected by multiple factors, such as the overall envelope thermal performance, HVAC system efficiency, weather conditions, and occupants' behavior. Among these factors, the overall envelope thermal performance, reflected by the integration of thermal properties (thermal transmittance and capacity) and airtightness, has a critical impact on the energy performance due to a large percentage of the total energy demand on the heating and cooling by envelope (Caffey 1979; Dickerhoff 1982; Harrje and Born 1982; Cooperman et al. 2011).

Although the thermal properties are provided in the design phase, performance can deteriorate and vary in practice due to the impacts caused by irregular construction, workmanship quality, multi-dimensional heat and moisture flow, and material degradation (Atsonios et al. 2017). Thus, envelope performance evaluation, namely evaluation of the thermal properties (thermal transmittance and capacity) and airtightness are becoming increasingly important for achieving energy efficient homes.

Over the past half century, a variety of envelope performance evaluation methods have been proposed. This section introduces the state of the art of home thermal performance analysis methods, such as those based on initial design data, measured structure data from sampling, and in-situ measurements using a heat flow meter. Unlike traditional evaluation methods, the model-based envelope performance evaluation method proposed in this section is based on a simplified home thermal model.

4.1.1 In-situ measurement methods

In-situ measurement methods are further categorized into two types: destructive and non-destructive (or invasive and non-invasive) testing methods. The destructive testing method adopts an auxiliary analysis method that obtains the values of the thickness and conductivity of each envelope components by using instrumental measurements of each layer for the selected sampling, which is acquired using a hollow drill. Then the thermal resistance (or R-value) and thermal transmittance (or U-value) can be calculated in accordance with the ISO

6946 (ISO 2017). With this method, the in-situ values of the envelope components can be directly compared with the design parameters. The destructive method provides a means of understanding ground-truth of an operational wall from inside to outside surfaces. Therefore, this method can be adopted to obtain the U-value as a reference to calibrate or evaluate other methods. However, uncertainties could happen when calculating the U-values for multilayer walls due to the error accumulation of measurements caused by instruments and/or users (ISO 2014).

Currently, on the other hand, many non-destructive methods are widely used and available for building envelope performance evaluations due to the rapid development of measurement tools such as heat flow meters (HFMs) and infrared (IR)/thermographic cameras. Such tools are broadly used for in-situ measurements and diagnostics of building envelope performance in many applications (Desogus et al. 2011; Ficco et al. 2015; ISO 2018; Albatici and Tonelli 2010; Fokaides and Kalogirou 2011; Lehmann and Wakili 2013; Fox et al. 2014; Kylili et al. 2014; Nardi et al. 2016). Briefly, the HFMs are designed for the measurements of heat flux using the heat flux sensors and thermocouples. A heat flux sensor is a thin plate with a known thermal conductivity λ (Btu/(h·ft·°F) and thickness d (ft), which is mounted perpendicular to the surface of building envelope component, to monitor the amount of heat energy loss/gain through the plate. The plate is also equipped with thermocouples with multiple contacts on both sides to measure the temperature difference ΔT (°F). When reaching stable

temperature difference, i.e., thermal equilibrium, the heat flux q (Btu/(h·ft^2)) can be calculated by:

$$q = \lambda \frac{\Delta T}{d} \tag{4.1}$$

Then the HFM method simplifies the calculation of the U-value (Btu/(h·ft^2)) by dividing the sum of heat flux of all the measurement points using the sum of differences between indoor air temperature T_{in} (°F) and outdoor air temperature T_o (°F), i.e., the calculated U-value is obtained using a progressive mean method or an average method (ISO 2014), as given by:

$$U = \frac{\sum_{i=1}^{n} q_i}{\sum_{i=1}^{n} (T_{in,i} - T_{o,i})} \tag{4.2}$$

where the subscript i represents the i^{th} measurement.

Moreover, if the internal surface temperature T_{is} (°F) and external surface temperature T_{es} (°F) are available, the HFM method can also calculate the U-value by using the thermal conductance C (Btu/(h·ft^2·°F)), the internal total heat transfer coefficient h_{it} (Btu/(h·ft^2·°F)) (including both convective and radiative heat transfer coefficient), and the external total heat transfer coefficient h_{et} (Btu/(h·ft^2·°F)), shown in:

$$U = \frac{1}{\frac{1}{h_{it}} + \frac{1}{C} + \frac{1}{h_{et}}} \tag{4.3}$$

where the calculation of the thermal conductance is similar to the U-value calculation using Equation (4.2), but the temperature difference is replaced by the ones between internal and external surface temperatures, shown in:

$$C = \frac{\sum_{i=1}^{n} q_i}{\sum_{i=1}^{n} (T_{is,i} - T_{es,i})} \tag{4.4}$$

The HFM method (Atsonios et al. 2017; Desogus et al. 2011; Ficco et al. 2015) was also adopted by the ISO 9869-1 (ISO 2014). The comparisons of the R-values (Desogus et al. 2011) or U-values (Ficco et al. 2015) measured by the HFM method and the one calculated from the destructive method were also conducted and concluded. From Desogus et al. (2011), the results verified that the R-value measured by the HFM was significantly affected by environmental conditions, especially by the temperature difference between the indoor and outdoor air. The results also showed that the HFM method was reliable if the indoor and outdoor air temperature difference was equal to or higher than 50 °F in their tests. In addition, the result from Ficco et al. (2015) showed that the in-situ U-value could be considerably influenced by many operative conditions such as high temperature gradient variation and heat flow inversion, whereas other factors, such as sampling time and heat flow meter plate dimensions, seemed to be less significant. Similar work was also done by Atsonios et al. (2017), who implemented two methods, the average and summation method and the dynamic and sum of least squares method, in three representative walls measured at different conditions in terms of surface temperature difference and direction of

heat flow. For the average and summation method, high temperature differences between the indoor and outdoor surfaces of the tested wall were required to provide R-values in a short measurement period with low variability. For the dynamic and sum of least squares method, however, the required measuring period is independent of the measuring conditions and R-values can still have low variability when only considering that the direction of heat flow is stable during the measurements.

The IR method, however, is another way to estimate the U-value. The IR method considers the heat flux that is obtained by measuring the total heat transfer coefficient, environment temperature, and surface temperature of the building element. Then the U-value is determined by the difference between the indoor and outdoor temperature of the building element that is in steady-state. Thus, the U-value can be calculated from (ISO 2018):

$$Q = h_t(T_{ie} - T_{is})A \tag{4.5}$$

$$U = \frac{Q}{(T_{ie} - T_{oe})A} \tag{4.6}$$

where h_t is the total heat transfer coefficient of the surface of the building element (Btu/(h·ft^2·°F)), which is measured by using a heat transfer coefficient sensor; T_{ie} and T_{oe} are the indoor and outdoor environment temperature (°F), which are conceptual quantities defined as a weighted average of the radiative temperature and air temperature and measured by environmental temperature (ET) sensors installed on the surfaces of the building element; T_{is} is the internal

surface temperature of the building element (°F), which is measured with an IR camera; and A is the heat transfer area of the building element (ft^2).

From Albatici and Tonellli (2010), the IR method was proposed to obtain the U-value of the building envelope in a quasi-steady state condition in three case studies, through a comparison with the HFM and theoretical calculation method, where the overall R-value is calculated based on the wall material thickness and thermal properties. Their results indicated that the IR method could estimate the U-value in existing buildings. However, Case A showed that the average U-value by IR was 31% higher than the theoretically calculated one and 21% lower than the one measured with the HFM method. Case B showed the average U-value by IR was 29.6% and 80% different from the calculated one when wind speed was 0 to 2.2 mph, and Case C showed a 27% difference compared to the calculated one. Fokaides and Kalogirou (2011) stated that the IR method was a reliable measurement method and validated that the absolute deviation percentage of the measured U-values was in the range of 10–20% in comparison with the use of the HFM method. Similar works have also been done by Lehmann and Wakili (2013), Fox et al. (2014), Kylili et al. (2014), and Nardi et al. (2016), whose common goal was to prove the IR was a useful and yet effective method based on various case studies. However, limitations of the IR method are that the emissivity and the reflective temperature of the envelope need to be known for calibrations; meanwhile, the thermal image analysis requires professionals (Kylili et al. 2014).

To overcome these strict requirements, especially for the HFM method, a frequency response method was introduced by Peng and Wu (2008), who calculated the overall R-values using the 0^{th} order of the frequency responses of heat conduction, the mean indoor and mean solar-air temperatures, and the average of the indoor air and inside surface temperatures of the building envelope elements, with no need for the heat flux measurements. Their result showed a good agreement in comparison with the design values. Additionally, an Excitation Plus Method (EPM) based on the transient response factors (RFs) method was investigated and tested by Rasooli et al. (2016) through three case studies. Basically, a triangular temperature pulse was applied to the interior surface and the measured heat flux responses on both the interior and exterior surfaces of the walls with constant surface temperatures were used to calculate the RFs and then to obtain the R-values. Their results showed that the U-values could be calculated with less than 2% error by using only one and a half hours of in-situ measurements compared with the required measurements in the ISO 9869-1 (ISO 2014). Evangelisti et al. (2018), using a finite-element analysis method, verified that an equivalent homogeneous wall could be used to represent a multilayer wall by producing the same behavior when exposed to the same weather conditions.

As a conclusion, for these above methods, it is difficult to apply in practice due to unavailability of requisite temperatures and required weather conditions as well as long measurement periods. In addition, the in-situ measurement methods are designed to measure the thermal resistance of an

envelope element that is associated with steady-state heat transfer only and therefore do not provide an overall integrated performance evaluation of an envelope, i.e., thermal resistance and thermal capacity through dynamic heat transfer study, and its associated airtightness.

4.1.2 Model-based methods

To overcome the disadvantages of in-situ measurement methods, model-based methods have been proposed and studied. A recent model-based approach was proposed by Zeifman and Roth (2016), who developed a coarse grade thermal response model to evaluate the envelope performance. The model used nighttime data to correlate the interval indoor temperature changes over a heater's runtime to evaluate the thermal properties for a home. It assumed that the indoor temperature increased linearly with a constant outdoor temperature in each runtime, in addition to ignoring wind and internal heat gains. However, Wang et al. (2019) proved that it was not appropriate to ignore the wind impacts and suggested that the amount of heat gains or losses could be related to wind speeds; for example, the heat loss rate at wind speed of 0.6 mph was approximately 50% higher than the rates at close to 0 mph for the same outdoor air temperature. Therefore, the model will unavoidably cause large errors in the real practice of envelope performance evaluation. Similar work was done by Newsham et al. (2017), in which a model-based method was expressed as a simple linear equation to estimate the integrated U-values. On the other hand, their work assumed the indoor temperature dropped linearly with the temperature difference between the

average indoor and outdoor air within the setback period. Therefore, these models are only applicable for nighttime heating or nighttime indoor temperature floating period (temperature setback period in this case). Siemann (2013) applied the RC network approach and physics-based solar and infiltration method to model the thermal dynamics in homes, along with 12 parameters to be estimated by applying the data, such as the indoor and outdoor temperature, wind speed, solar irradiation, and HVAC signal, to train the model using the Genetic Algorithm (GA) method. Although the model is complicated and difficult to be applied, and wind and solar data usually are unavailable for homes, thermal conductivity and thermal mass of the envelope—described by two parameters in the model—can be used to evaluate the performance of the envelopes.

Inspired by the previous work, this study has developed a model-based envelope performance evaluation method that uses a home thermal model through reasonable simplifications. The development of an accurate and effective model-based envelope performance evaluation method is challenging because of the different heat transfer mechanisms introduced by different weather inputs, e.g., outdoor air temperature, wind, and solar, and availability and quality of the data. In this study, the challenges are addressed by simplifications of a home thermal model in Section 4.2 and construction of an automated data screening procedure in Section 4.3. More specifically, in this study it first briefly introduces the formulation of a home thermal model that is able to account for the heat transfers between indoor and outdoor temperatures as well as the impacts of infiltration and

solar in Section 4.2.1. Secondly, a model-based envelope performance evaluation method is proposed through the simplification of the model by applying it to the nighttime data in Section 4.2.2, along with an introduction of a data screening procedure. Finally, three sequential experiments are conducted to validate the effectiveness of the method in Section 4.3.

4.2 Methodology of Model-Based Envelope Performance Evaluation

Building thermal dynamic models have been intensively studied and used for a long time. For the home envelope evaluation application, there are unique features to be considered to formulate a home thermal model. In this section, a model-based envelope performance evaluation method, which is built upon the standard RC network approach, is introduced through the analysis of heat transfer processes.

4.2.1 A simplified home thermal model for performance evaluation

A home thermal model, which can account for the heat transfer between indoors and outdoors using *one virtual envelope* as shown in Figure 4.1(a), is constructed in Chapter 3, where the impacts of infiltration and solar energy are described using two polynomial regressions, as expressed by

$$C_{ve,in}\frac{dT_{ie}(t)}{dt} = \frac{T_o(t)-T_{ie}(t)}{R_{ve}} + \frac{T_{in}(t)-T_{ie}(t)}{R_{air}} \tag{4.7}$$

$$C_{air}\frac{dT_{in}(t)}{dt} = -\frac{1}{R_{air}}T_{in}(t) + \frac{1}{R_{air}}\Big[T_{ie}(t) + \big(T_o(t) - T_{in}(t)\big)\big(b_1 W(t) + b_2 W^2(t)\big) + \big(a_1 G(t) + a_2 G^2(t) + a_3 G^3(t)\big) + (Q_i u_i(t) + Q_s u_s(t))\Big] \tag{4.8}$$

The home thermal model can be further simplified by using the thermostat temperature (T_{TSTAT}), which directly reflects the dynamics of space air temperature (T_{in}), and by ignoring the node for the interior wall surface temperature (T_{ie}), shown in Figure 4.1(b), when using HAVC off data at nighttime only. Because the only excitation is outdoor air and the indoor air presents a very small time constant, for its small heat capacity (C_{air}) and thermal resistance (R_{air}) compared with the home envelope (ASHRAE Handbook: Fundamentals 2017; ASHRAE Standard 90.2 2007) when the interests of investigation lie in envelope heat transfer performance. Moreover, the error of ignoring the node for the interior wall surface temperature can be effectively minimized through the best-fit search in the parameter estimation. Therefore, the heat transmission through all the envelope components can be represented by one heat transfer relationship driven by the single temperature difference between the indoor air temperature (in this case, the thermostat temperature) and outdoor air temperature, along with the consolidated thermal properties of all the envelope components.

Thus, the home thermal model in Equations (4.7) and (4.8) can be simplified into:

$$\frac{dT_{in}(t)}{dt} = -\frac{1}{\tau}T_{in}(t) + \frac{1}{\tau}\Big[T_o(t) + \big(T_o(t) - T_{in}(t)\big)\big(b_1 W(t) + b_2 W^2(t)\big) + \big(a_1 G(t) + a_2 G^2(t) + a_3 G^3(t)\big) + \big(Q_i u_i(t) + Q_s u_s(t)\big)\Big] \quad (4.9)$$

where $\tau = C_{ve,in}R_{ve}$ is the time constant of the virtual envelope of a home; $R_{vw} = 1/(b_1'W + b_2'W^2)$; b_1' and b_2' are the empirical-determined coefficients; and $b_1 = b_1'R_{ve}$ and $b_2 = b_2'R_{ve}$.

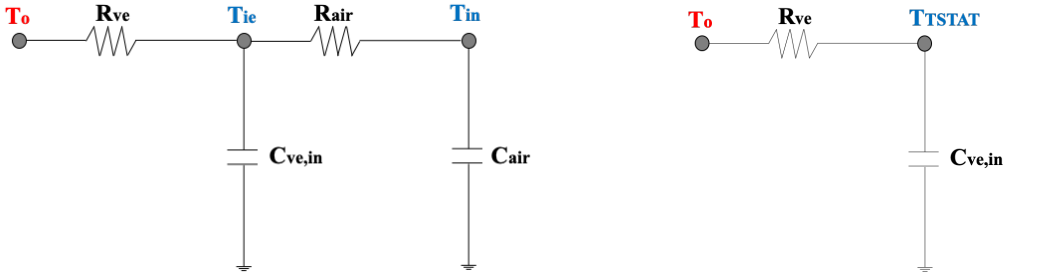

(a) One virtual envelope (b) Simplified one virtual envelope

Figure 4.1. Schematic diagram of the one virtual envelope. (a) one virtual envelope; (b) simplified one virtual envelope where the heat capacity of the indoor air and interior thermal resistance are ignored.

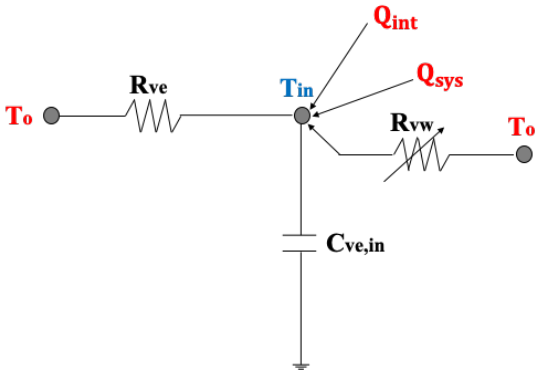

Figure 4.2. Modified RC home thermal model with simplified one virtual envelope.

4.2.2 Model-based envelope performance evaluation method

In Equation (4.9), τ is the time constant of the home virtual envelope. It describes the time needed for a home to thermally respond to the indoor and

outdoor air temperature differences. The unit of τ is the same as the time unit of the data sampling time interval. Physically, it represents the product of thermal resistance R_{ve} (i.e., the reciprocal of U) and thermal capacity $C_{ve,in}$ of the home envelope.

Because the internal heat gains (due to marginal occupant activities) and solar are both negligible at nighttime, only nighttime home operational data are used for model simplification. Therefore, only heat transmission through indoor and outdoor air temperature differences and infiltration needs to be considered. Note that τ reflects the heat transfer rate only by temperature difference. The infiltration impacts are accounted for by the wind term in Equation (4.9), $\big(T_o(t) - T_{in}(t)\big)\big(b_1 W(t) + b_2 W^2(t)\big)$. Using only intermittent data when the HVAC system is off, Equation (4.9) can be simplified into:

$$\frac{dT_{in}(t)}{dt} = -\frac{1}{\tau}T_{in}(t) + \frac{1}{\tau}\big[T_o(t) + \big(T_o(t) - T_{in}(t)\big)\big(b_1 W(t) + b_2 W^2(t)\big)\big] \quad (4.10)$$

Rearranging Equation (4.10), it becomes

$$\frac{dT_{in}(t)}{dt} = \frac{1}{\tau}\big[1 + \big(b_1 W(t) + b_2 W^2(t)\big)\big]\big(T_o(t) - T_{in}(t)\big) \quad (4.11)$$

However, for the cases when wind data are not available or when the wind term is ignored, Equation (4.10) further reduces to:

$$\frac{dT_{in}(t)}{dt} = -\frac{1}{\tau'}T_{in}(t) + \frac{1}{\tau'}T_o(t) = \frac{1}{\tau'}\big(T_o(t) - T_{in}(t)\big) \quad (4.12)$$

where τ is replaced by τ', which reflects the heat transfer rate by both heat transmission and infiltration.

Therefore, the difference between τ and τ' represents the impacts of infiltration. Note here that τ' is a wind speed-dependent parameter, while τ is independent of wind. As observed in Equations (4.11) and (4.12), τ' should always have a smaller value than τ because τ' represents the heat loss from both the heat transmission by temperature difference and air infiltration caused by wind. With given wind speeds, the smaller the difference between the values of τ and τ', the better the airtightness of a home.

The simplified models represented by Equations (4.10) and (4.12) are a time-continuous model. To use the measured data for parameter estimation, discretization of the models is needed. Thus, the continuous-time models are converted using Euler's method into the discrete-time models, given by:

$$T_{in}(k+1) = (1-\alpha)T_{in}(k) + \alpha\left[T_o(k) + \left(T_o(k) - T_{in}(k)\right)\left(b_1 W(k) + b_2 W^2(k)\right)\right] \quad (4.13)$$

$$T_{in}(k+1) = (1-\alpha')T_{in}(k) + \alpha' T_o(k) \quad (4.14)$$

which can be rewritten as:

$$T_{in}(k+1) - T_{in}(k) = \alpha\left(T_o(k) - T_{in}(k)\right) + \alpha\left(T_o(k) - T_{in}(k)\right)\left(b_1 W(k) + b_2 W^2(k)\right) \quad (4.15)$$

$$T_{in}(k+1) - T_{in}(k) = \alpha'\left(T_o(k) - T_{in}(k)\right) \quad (4.16)$$

where $\alpha = \frac{T_s}{\tau}$ and $\alpha' = \frac{T_s}{\tau'}$; T_s is the sampling interval; and k denotes discrete time.

Detailed identification of the parameters, using α (corresponding to τ) as an example, can be found in Equations (A.9) to (A.11) in the **Appendix A**. The

least squares method is adopted to minimize the sum of squared differences between the data values.

4.3 Characterization of U.S. Home Thermal Properties

Three sets of experiments were conducted in this section, which were designed to test the effectiveness of the method. In the first experiment that conducted in 2016, an unoccupied home located in Norman, OK was used to validate the method. All the data in this test home were collected by lab meters with good data quality. In the second experiment, four occupied homes located in Tulsa and Oklahoma City, OK were selected to compare their envelope performance and the data was obtained through a smart thermostat provider collected in 2015, 2016, and 2017 respectively. The indoor and outdoor air temperatures were measured on site and obtained through their home smart thermostats. Wind speed data were obtained through local weather stations. Since the physical addresses of the four homes were unknown due to privacy protection given to the homeowners, there are uncertainties how proximate the four homes were to the local weather stations and how accurately the wind data could reflect the real wind speed surrounding the test homes. In the third experiment, operational data in 7,000+ homes located in the United States were obtained through a smart thermostat provider. Because there were no wind data available for these homes, only τ', shown in Equation (4.12), was estimated. To understand the results of the third experiment with missing wind data, the wind impacts were first examined in the first two experiments.

For all three experiments, data quality was examined. For example, outdoor temperature that increases after midnight when the solar effects are supposed to diminish was considered a bad measurement. Moreover, to eliminate the random sensor noise impacts, only the data that contain such abnormal patterns over one hour were eliminated.

4.3.1 The first experiment

In the first experiment, validation of the proposed model-based envelope performance evaluation method was performed in a typical home located in Norman, Oklahoma as shown in Figure 4.3. The home is a single-family, two-story home with a floor area of 3,160 ft^2, built in 2003. All bedrooms and a living room are located on the first floor, with a game room on the second floor. The thermostat is in the living room. The measured inputs include the outdoor air temperature, wind speed, global horizontal irradiation, and the indoor air temperature represented by the thermostat temperature. An outdoor weather station starter kit, shown in Figure 4.4(a), was set up for the outdoor temperature, wind, and solar measurements at one-minute intervals. Additionally, the air conditioner (A/C) return air temperature and on/off signal from the thermostat were measured and logged using the temperature and current transducer data-loggers shown in Figures 4.4(b) and 4.4(c). Table 1 lists the specifications of the sensors and data loggers used in the experiment.

Figure 4.3. Profile of the front of the test home.

(a) (b) (c)

Figure 4.4. Data acquisition device: (a) Indoor temperature sensor; (b) Current transducer data-loggers; (c) Weather station starter kit.

Table 4.1. Sensor specifications in the experiment.

Sensor Name	Measurement	Measuring Range	Measurement Accuracy
Weather station starter kit	Outdoor air temperature	-40 – 167 °F	±0.38 °F from 32 to 122 °F
	Wind speed	0 – 170 mph	±2.4 mph
	Solar radiation	0 – 406 Btu/(h·ft^2)	± 3 Btu/(h·ft^2)
Temperature sensor	Indoor/return air temperature	-40 – 158 °F	±0.63 °F from 32 to 122 °F
Current transducer	Fan current	0 – 20.1 mA	±0.001 mA

To mitigate the impacts of occupancy disturbances that may cause uncertainties in the method validation, the first experiment was conducted from September 27 to November 28, 2016 (63 days), when the home was unoccupied. In addition, nighttime data when the HVAC system was off were selected for the experiments. Due to the fact that randomly selected 10-day consecutive data can provide robust parameter estimation through data training (Wang et al. 2019), the earliest available data, the first available 10 days' data, were selected for the first experiment. Then the values of τ and τ', were estimated by using the 10 days' home operational data at one-minute intervals for two cases: with and without wind data. By implementing the proposed envelope performance evaluation method, the estimated values of τ and τ' were 3,357 and 2,868, respectively. Therefore, the value of τ' estimated without wind data, representing the integrated heat loss rate caused by heat transfer and infiltration, was 14.57% smaller than the value of τ estimated with wind data, representing the heat loss rate by heat transfer only. The difference between these two values can be used to evaluate the airtightness of the home envelope. Moreover, the fact that smaller value indicated a larger heat loss rate validated that the model is effective in capturing thermal behaviors of a home. By plotting the temperature data together with the value of τ'estimated from no wind data as shown in Figure 4.5, where the black squares represent the indoor air temperature and the grey dots represent the outdoor air temperature, the indoor air temperature was shown to decrease by 1.3 to 3.6 ºF over night, when the outdoor air temperature was between 40 ºF and 80 ºF.

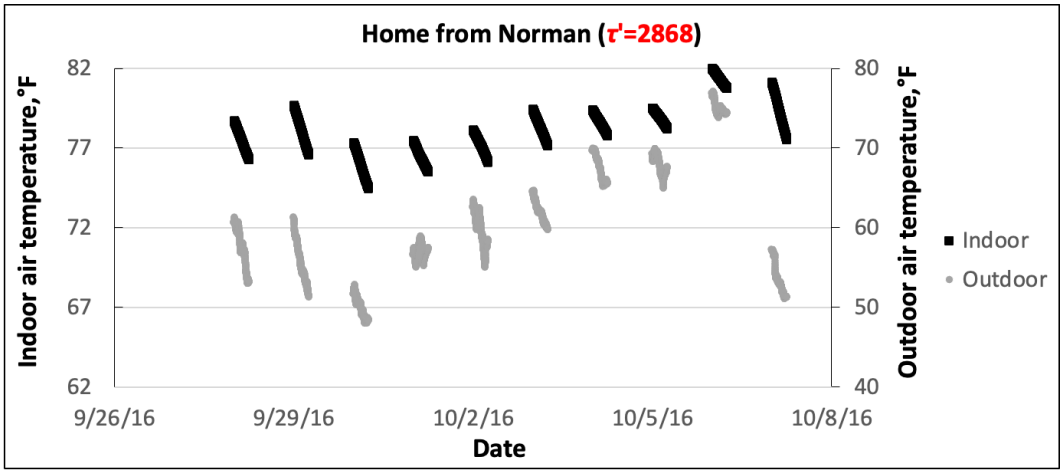

Figure 4.5. τ' value and its training data, i.e., indoor and outdoor temperatures, for a test home in Norman, OK.

4.3.2 The second experiment

Four homes located in Oklahoma were tested for the second experiment. Of these, two were in Tulsa, one in Oklahoma City east (OKCE), and one in Oklahoma City north (OKCN). Nighttime data when the HVAC system was off were used for the experiments. Meanwhile, the extent of the impact of wind on the τ value of the test homes was also investigated using data collected from city weather stations. The values of τ and τ' were estimated using the 10 days' home operational data sampled at five-minute intervals for two cases: with and without wind data. Two sets of the values were obtained, as shown in Table 4.2, from which differences of 2% to 10% were observed. However, an opposite pattern was observed in Table 4.2, i.e., the values of τ'estimated with no wind data were larger than the values of τ with wind data. For the four test homes, the physical addresses were not known. The experiment results indicated the wind data

obtained through a city weather station might not be accurate to reflect the true wind conditions near the homes. Therefore, for the third experiment where the wind data were not measured onsite, only the values of τ' were calculated.

Table 4.2. Variations in $\boldsymbol{\tau}$ and $\boldsymbol{\tau'}$ for four homes.

	Home 1 from Tulsa	**Home 2 form Tulsa**	**Home 3 form OKCE**	**Home 4 form OCKN**
Values of τ' without wind data (minute)	4361	2757	3323	1862
Values of τ with wind data (minute)	4270	2625	3017	1812
Error percentage (%)	2.13	5.03	10.14	2.76

By plotting the temperature data together with the values of τ', the variation of indoor air temperatures along with outdoor air temperature changes is shown for the four homes in Figure 4.6, where the black squares represent the indoor air temperature and the grey dots represent the outdoor air temperature. In general, larger values of τ' indicate better envelopes. As evident in Figure 4.6(a) and (b), although the outdoor air temperature is in a similar range, the indoor air temperature drops more drastically for Home 2 than for Home 1. The poorest envelope in Home 4 with the lowest value of τ' is observed by the fact that the

indoor air temperature almost drops vertically in Figure 4.6(d) in similar outdoor air conditions.

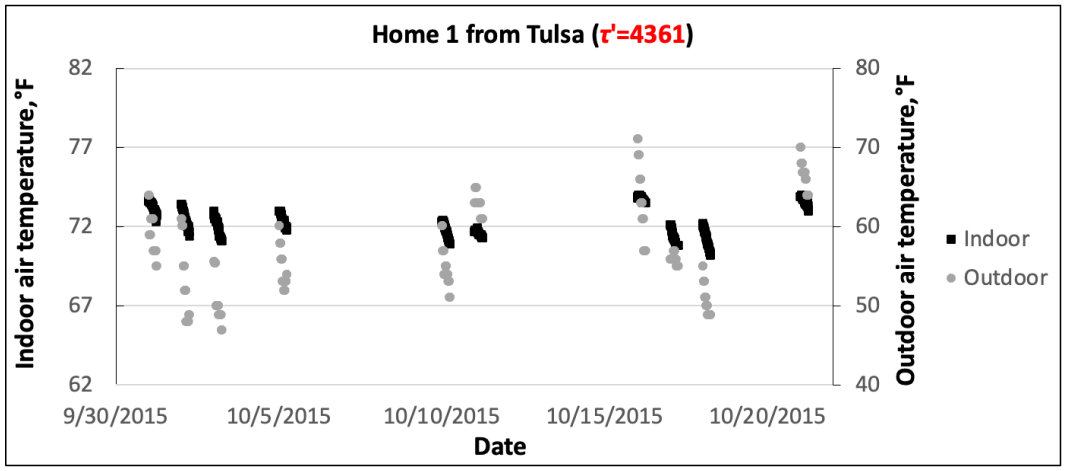

(a)

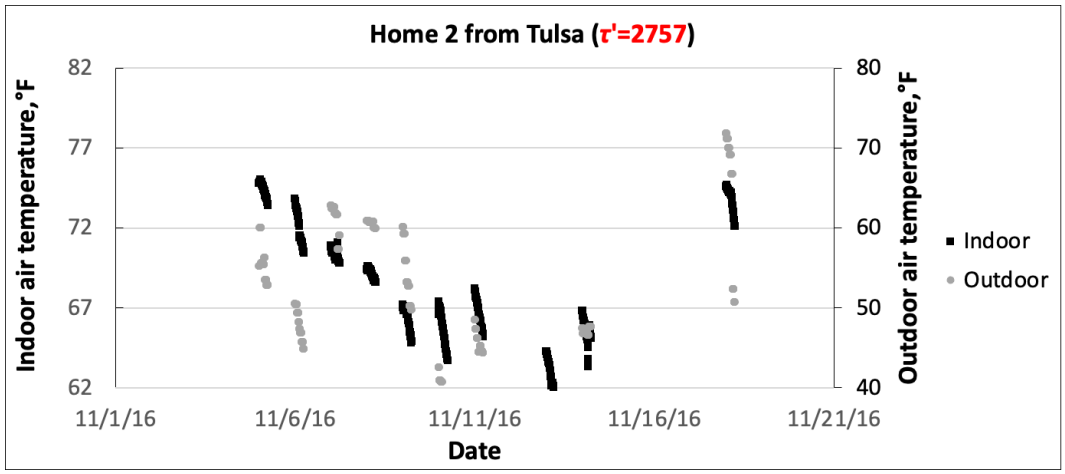

(b)

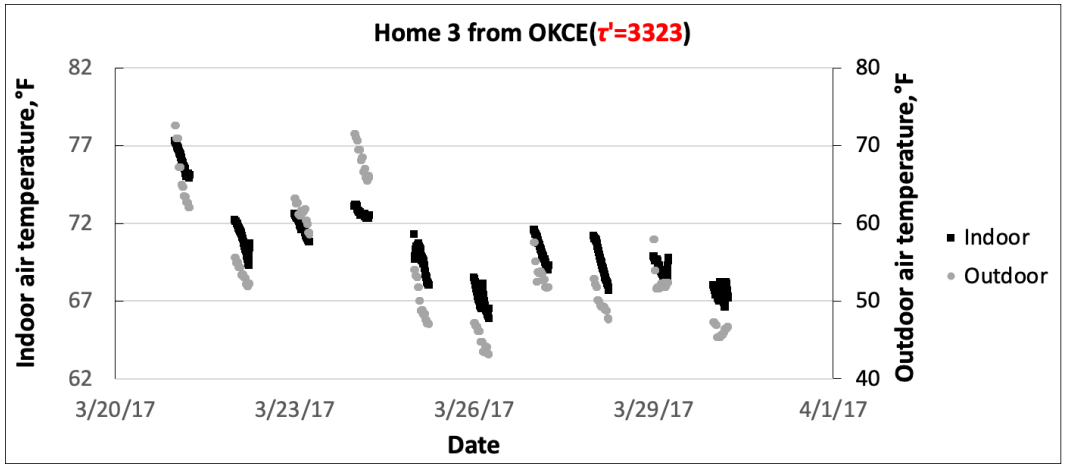

(c)

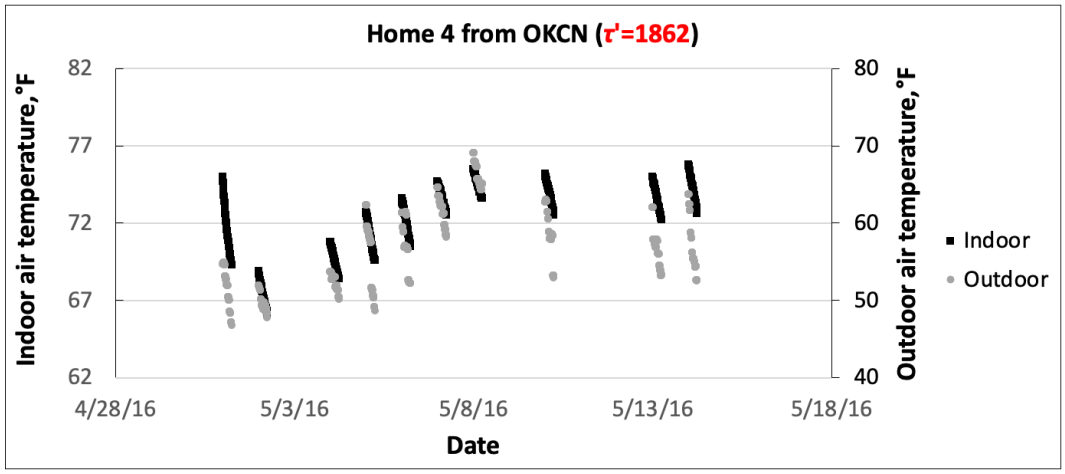

(d)

Figure 4.6. Comparison of the values of τ' for four homes in the state of Oklahoma. (a) Home 1 from Tulsa; (b) Home 2 from Tulsa; (c) Home 3 from OKCE; (d) Home 4 from OKCN.

4.3.3 The third experiment

Due to inconsistent quality in the data provided by a smart thermostat manufacturer, in the third experiment data screening was first applied. The

screening also allowed for intermittent data selection, where only nighttime data and the HVAC system was off were selected.

Data Screening. Home operational data from 10,000+ homes worldwide were provided by a smart home thermostat manufacturer. Among these homes, 7,000+ homes across the United States were selected. Figure 4.7 shows the location of the test homes on an U.S. map (only city-level information is known). All the homes were equipped with smart thermostats that provide five-minute interval data. Information and operational data for the past three years in these 7,000+ real homes were collected. The **operational data** included the indoor and outdoor air temperature, humidity, HVAC system on/off (from fan signals), occupancy and so on, while **home information data** included year built, square footage, story, city, state and so on. Figure 4.8 shows a screenshot of part of the data of home information as an example. As can be seen, there are missing data with blank or dashes and differently labelled country names (for example, some homes are labelled as United States while others are as U.S.), marked with red circles in Figure 4.8. Unavoidably, these undesirable situations increased the time and difficulty of data screening.

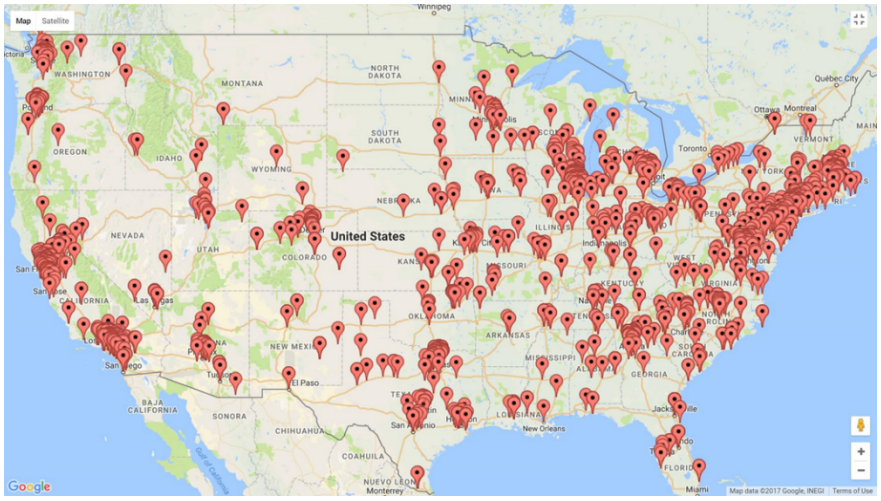

Figure 4.7. The 7,000+ real homes distribution from the U.S. shown by Google map.

Identifier	Country	Province/State	City	Floor Area [ft2]	Style	Number of Floors	Age of Home [years]	Number of Occuapants	filename
511aed9e	United States	WV	Wheeling	1800	other	3	0	0	511aed9e3f96eb67beeda1995d8bbc29ce882f01.csv
8751972c	CA	ON	Toronto	3500	detached	3	0	0	8751972c08b8b82c685dc75e44e92f97e0cb6f2f.csv
df99740f5	CA	ON	Lambton Shores	456	other	1	0	0	df99740f5db9a79add56323d472ed4db85591d16.csv
f59964d5		ON	Toronto	1700	townhouse	3	36	0	f59964d5cd71463a83187846ae36ee6fecdfd2a7.csv
aac4200e	CA	ON	Mississauga	3000	semiDetached	3	45	2	aac4200e0300753e7ece2b8d1b02f8ecca6c0f9b.csv
86801627	CA	ON	Mississauga	2000	townhouse	2	20	0	86801627a0e393bef7eed528ab998d27196a1aaf.csv
fa942d18	US	IL	Dundee	2000	detached	3	45	4	fa942d1820fc79d181c1ec6fb813d2dea45f4087.csv
5847d0fd		ON	Toronto	0		0	0	0	5847d0fd5ed46c8752b6be20425405cc50e33cc4.csv
baa79903	US	MD	Walkersville	2500	detached	3	45	3	baa799039ab623a0b84415413f5dd1c132b80506.csv
d0e417e9	US	MA	Dighton	2500	other	2	20	3	d0e417e9cc297fc3527f1010139fbd24663ce0ab.csv
765fbdc5	CA	ON	Toronto	0		0	0	0	765fbdc569c08a2fd4cdd794a85a0493b6c7d442.csv
b73e63ff5	US	TX	Garland	3500	detached	2	20	4	b73e63ff502c1f08b663a85e38997c4384c00873.csv
0691391	US	NH	Milford	2000	detached	3	55	4	0691391881a28a5ab2d1a76edb9a8f165c552c2b.csv
808c687f	US	PA	Pittsburgh	2000	apartment	1	105	1	808c687f6a9adad3ec843395f672e40f791b3014.csv
db703e93	US	IL	Groveland	2000	detached	2	10	2	db703e93dce79b24f318f36e8b49db07a47284f2.csv
62670834	US	CA	Garden Grove	1500	detached	1	55	3	62670834eee9b0860f312f49c751a7280790a980.csv
c5454ab7	CA	ON	Pickering	2000	townhouse	3	30	3	c5454ab7187afc928e0bd80e16ce1c4620badb51.csv
1d71ad64	US	IN	Shelbyville	1500	rowHouse	1	10	4	1d71ad640f7e35f2e71d447659f86b48010c755f.csv
0d47ee3a	US	NC	Charlotte	1500	detached	1	60	2	0d47ee3a9d795a68f20e6e97f213b4ed367020d0.csv
9304ddc3	US	OH	Brunswick	2000	detached	3	40	2	9304ddc3ffca3e8e8b840dde142bb0616bf7c3ee.csv
cf20df47f	US	UT	Murray	2500	detached	2	40	5	cf20df47fe41535bf983a4ee8794bb9164ba8ae0.csv
b3f0b5d7	US	MI	Dearborn	3000	detached	2	55	0	b3f0b5d78f417c649eed691aa2d5eb991d3fb300.csv
e830374d	US	PA	-	3000	detached	3	20	5	e830374de64ddd452d8c881bc40221a2ef738491.csv
682f209e	US	AZ	Tucson	2000	detached	2	25	2	682f209e67b7a8a1bd7b4b5a20dab6f81d097dd0.csv
af051697	US	CA	Irvine	3500	detached	2	35	2	af0516978127d470a9f32ef4263a01a17ad54d2b.csv
cb592d0f	US	CA	La Mirada	1500	Semi-Detached	1	60	0	cb592d0fae4663d77f393035597dd6672d7a95da.csv
c1febf99a	US	TX	Grand Prairie	2300	detached	2	0	0	c1febf99acb39eb86dd5d27000638940e64506f5.csv

Figure 4.8. The known real home information.

To qualify and implement the proposed model-based envelope performance evaluation method, several data-processing steps are needed for data selection. They are briefly described below:

(1) Data processing for data quality control

To simplify the experiments, only single-family detached homes with no auxiliary heat were selected. To further eliminate the undesired situations as mentioned above, for the home information data file, a standard name format that includes country, state, and home style was created to replace the inconsistent names, e.g., using US to replace the United States or us for countries, OK to replace Oklahoma or oklahoma for cities, and semidetached to replace Semi-Detached or semidetached for home style, and then to eliminate the homes with incompatible data and missing data labelled with blanks and/or dashes. The homes that successfully passed the home information data screening were used for the operational data screening.

A large amount of operational data files was provided by the smart thermostat manufacturer for three-year home operations. Each data file, consisting of one-month operational data for each home, was stored in the folder named by the month for which the data were collected. Therefore, there were a total 36 folders (for three years) with a total of three years' operational data, and each folder contained the operational data files for that month for all the test homes. The files were named by the unique home ID, shown by the green rectangle in Figure 4.8. Therefore, the first step was to combine all the data files that have the same filenames but were in different folders into one file, i.e., each home operational data file only contained all the operational data for one specific home in the past three years. Then, for each constructed home operational data file, similar processing procedures to the home information data screening were

carried out to eliminate the undesirable situations. Therefore, the desired data that included the date and time, indoor and outdoor temperatures, and fan signals (0 or 1) remained. Meanwhile, the homes with undesired data, such as missing data, were eliminated.

(2) Data processing for selecting the data in appropriate periods

To use Equation (4.16), only data, including the date and time, indoor and outdoor temperatures, and HVAC off signals, were selected. Then, the nighttime data from 12:00am to 6:00am were selected. The selection criteria made the length of each time segment contain 73 time points. More than 10 days of data were selected due to the requirements of parameter estimation (Wang et al. 2019).

To automatically manipulate the data processing procedures described above, automated data screening codes were programmed to execute the data processing steps. Finally, 1,676 homes passed the screening criteria and qualified operational data were obtained and ready for use.

Data Testing. By implementing the training data into Equation (4.16), 1,676 sets of the values of τ' were estimated and generated for the test homes. Since there was no information about the home conditions and no ground-truth of each test home envelope, to validate the effectiveness of the method, the values of τ' versus the ages of the homes were plotted in Figure 4.9, with the expectation that older homes would have poorer envelope thermal performance, presented by lower values of τ'.

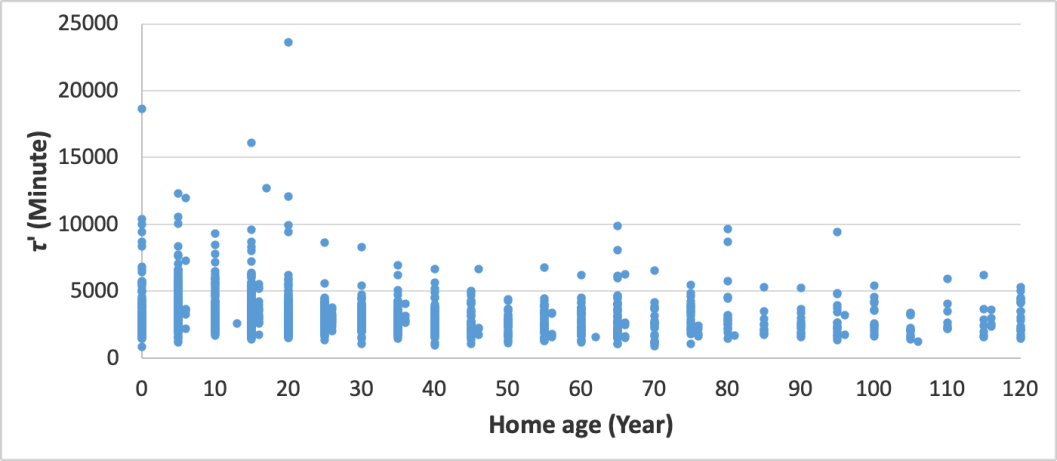

Figure 4.9. τ' value estimation using nighttime and AC off.

Although slight improvement can be seen for younger homes in Figure 4.9, the improvement pattern is not distinctive. To further investigate the values of τ' in Figure 4.9, the test homes were divided into two groups, according to the sample sizes of each age group: homes 40 years or younger and homes more than 40 years old. The sample sizes for the age group for 40 years or younger ranged from 72 to 278 homes, while the sample sizes for the age groups older than 40 years old ranged from 7 to 54 homes. The values of τ' for homes less than 40 years old are plotted in Figure 4.10(a), which shows the average values of τ' with error bars that represent the distribution of the τ' values in the age group, as well as a trend line together with the coefficient of determination (R^2 value). As can be seen, a distinctive correlation between the values of $\tau'$and the age of the test homes can be observed with a high correlation coefficient. This observation is in line with the facts that the older homes with older technologies result in poorer thermal performance of the envelopes in design and construction phase as well as

the thermal performance of home envelopes deteriorate as the age increases. Moreover, the value of τ' for the first experiment home, 15 years old, is plotted and represented by using a red dot as shown in Figure 4.10(a), in which the value is slightly lower than, but in the range of, the average value of τ' for its age. However, no obvious pattern was observed for the values of τ' for the homes older than 40 years, as shown in Figure 4.10(b). This observation also aligns well with our expectations due to two reasons: 1) A much smaller sample size provides greater randomness; and 2) older homes have a better chance for renovations, through which the home envelope thermal performance can be greatly enhanced.

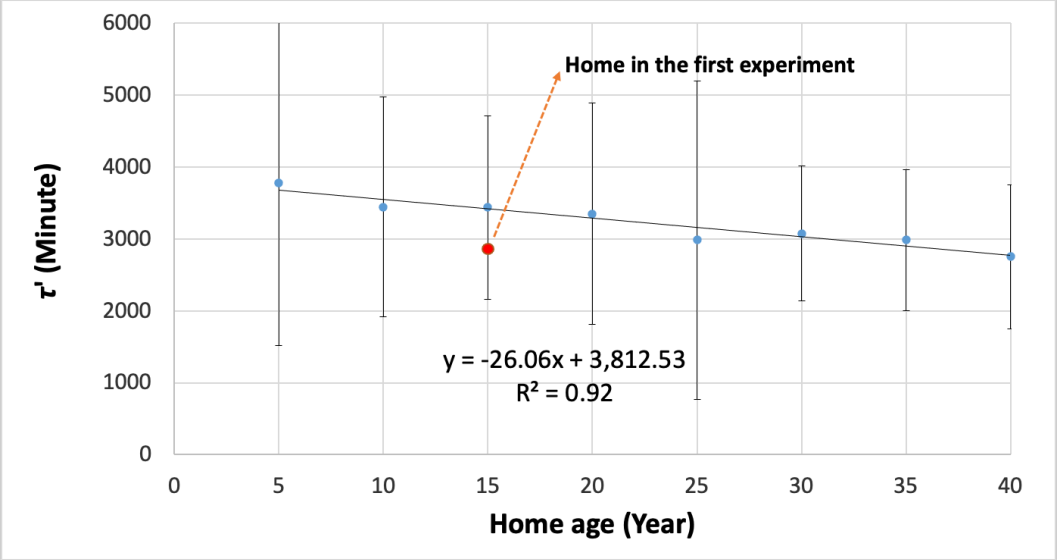

(a)

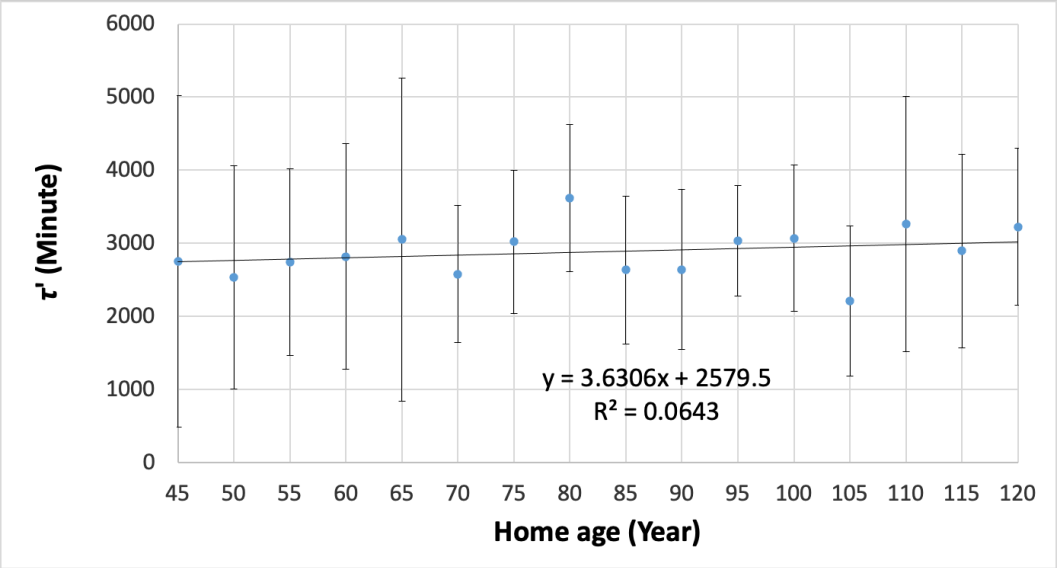

(b)

Figure 4.10. τ' distribution versus home ages: (a) from 0 to 40 years old; (b) from 45 to 120 years old.

4.4 Summary

With reasonable simplifications to the home thermal model that describes the heat transfer processes between the indoor and outdoor conditions in a home, a model-based envelope performance evaluation method is proposed to assess the thermal performance of a home envelope. The simplicity of the method allows the parameter to be automatically estimated using a short period of indoor and outdoor air temperature data through data screening without the need for a home's physical information. Depending on the availability of the wind or not, the method can also evaluate the integrated heat transfer rate of an envelope through both heat transmission and infiltration together or the heat transfer rate through heat transmission only. Three sequential experiments are conducted to validate

the effectiveness of the method. The first experiment shows the wind effect can cause around 15% difference in envelope thermal property estimations; the second experiment suggests that wind data collected from a city weather station might not be accurate to represent the local wind conditions near the test homes; and the third experiment, using data collected from 1,676 homes, demonstrates that the envelope performance decreases proportionally as the home age increases for homes that are 5 to 40 years old, while there is no distinctive patterns for homes older than 40 years due, perhaps, to a small sample size. The demonstrated results of the third experiment align well with the expectation that younger homes experience better home envelope thermal performance. Therefore, the experimental results show that the thermal properties can be estimated and evaluated using the simplified model-based method. Moreover, the proposed method also shows that the estimated thermal properties are effective across homes. As a conclusion, although more experiments with the knowledge of the ground-truth of test home envelope conditions are needed, the proposed method can possibly be an effective alternative to traditional methods, which require intensive labor for measurements and calculations, for the evaluation of the home envelope properties using only short-period measurements of the indoor and outdoor air temperatures and HVAC on/off status. In addition, wind impact is not negligible for the data-driven envelope evaluation method if high-precision estimation is desired.

Chapter 5: Design and Analysis of Optimal Pre-cooling

Although the existing pre-cooling strategies provide a means of shifting or reducing the peak demand and/or energy cost in residential buildings, majority of them are rule-based, guided primarily by intuition. The rest of them are model-based but generally do not consider the influence of various factors (e.g., the outdoor air temperature, wind, solar, HVAC size and efficiency, and utility rate structure). Therefore, there is a need to understand to what extent can an optimal strategy outperform common rule-based pre-cooling strategies through the development of an optimal pre-cooling strategy that can account for the various factors. To address this need, a pre-cooling optimization problem built upon a home thermal model that is able to account for the aforementioned factors is presented in this chapter.

As will be shown, the pre-cooling optimization problem is a quadratically-constrained integer linear program concerned with finding the HVAC on/off control signal over a 24-hour period that minimizes energy cost subject to maintaining the indoor air temperature within a pair of bounds. To eliminate the need to know the detailed specifications of a home which is often impractical, the model parameters are determined through data training that can be performed in real time. Finally, through simulation using real data collected from a test home and a local weather station, the performance of the proposed optimal pre-cooling strategy is compared with those of three rule-based operation strategies in terms

of their thermal dynamics, total and on-peak energy consumption, energy cost, and potential cost savings. Summary is given at the end.

5.1 Overview of Rule-Based Pre-Cooling Strategy

Heating and cooling in homes, provided by HVAC systems, are known to be energy-consuming and costly for homeowners and represent a crucial load for many electric utilities. In 2015, the average end-use energy consumption per household in the U.S. is 42.4 million Btu for heating and cooling alone, which accounts for nearly 55% of total household energy consumption (U.S. EIA 2015). In terms of energy cost, the average annual utility expense per household, including electricity, water, and sewage, is between $1400 and $2600, of which more than 43% is spent on heating and cooling spaces in homes (U.S. EIA 2015; U.S. DOE 2011). Therefore, home space heating and cooling offer considerable potential for energy cost reduction (U.S. EERE 2015; U.S. EERE 2016). Fluctuations of heating and cooling loads also have significant impact on a utility's load profile. This impact can be mitigated by an optimal and efficient HVAC operation that shifts or reduces the peak load demand. As a means of controlling demand when the grid is near its capacity, electricity suppliers have introduced time-of-day or time-of-use electricity price in recent years, making peak electricity expensive to consumers (Kamyar and Peet 2017; Tabares-Velasco et. al 2019; Baniasadi et. al 2019). Since electricity is more expensive during on-peak hours, smart thermostat manufacturers have incorporated rule-based pre-cooling strategies into their products, which set the indoor air temperature a few

degrees lower for a period preceding the start of on-peak hours (U.S. EERE 2016). The resulting lower indoor air temperature, obtained at a lower electricity price, delays the start time of HVAC systems and reduces their runtime during on-peak hours. Such rule-based pre-cooling strategies reduce energy expenditure for homeowners while maintaining reasonable comfort levels in homes because they take advantage of the thermal mass possessed by the building structure.

As reviewed in Section 2.2.2, three common rule-based operation strategies, studied by Xu et. al (2004), Xu (2009), Yin et. al (2010), Morgan and Krarti (2007), Moon and Han (2011), Arababadi and Parrish (2015), Surles and Henze (2012), and Turner et. al (2015), were selected as references to compare with an optimal pre-cooling strategy proposed in Section 5.2. The profiles of the three rule-based operation strategies are shown in Figure 5.1. As depicted in the figure, the first strategy—referred to as Base Case I (BC I)—has no pre-cooling and utilizes a uniform indoor air temperature set point $T_{set}[k]$ of 78 °F. The second and third strategies—referred to as Base Cases II and III (BC II and BC III)—both have pre-cooling with different profiles. Specifically, BC II starts out with a $T_{set}[k]$ of 78 °F, reduces it later to 73 °F for 6 hours, and returns it to 78 °F when on-peak hours begin. BC III behaves similarly but has a shorter and more aggressive pre-cooling, i.e., $T_{set}[k]$ is reduced for only 5 hours but to a lower 71 °F. For each of these strategies, the selected $T_{set}[k]$ was used by the thermostat to determine the HVAC on/off control signal $u_s[k]$ following the description in Section 5.2.1, where the deadband width $\pm\sigma$ was $\pm$1 °F.

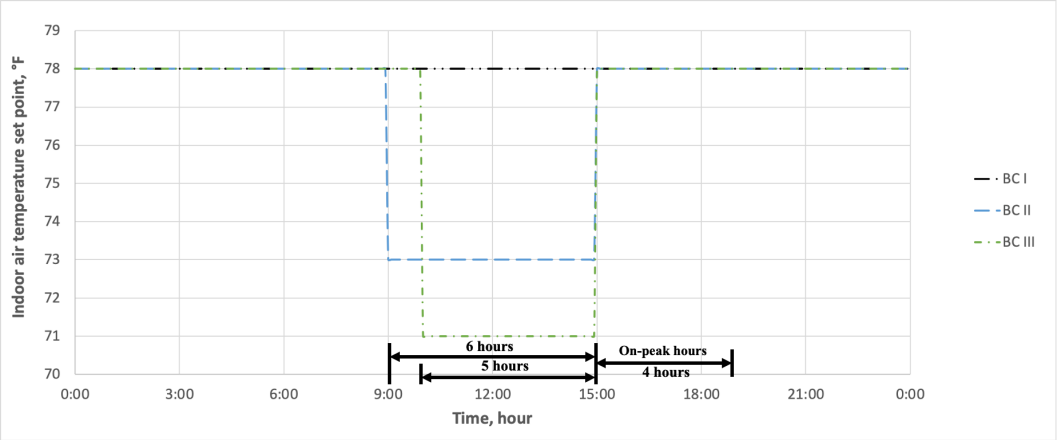

Figure 5.1. Profile of the indoor air temperature set point for the three rule-based operation strategies.

5.2 Development of Optimal Pre-Cooling Strategy

Figure 5.2 depicts an approach to formulating the aforementioned pre-cooling optimization problem. As can be seen from the figure, key to the formulation is a home thermal model that takes into account the weather conditions, HVAC system capacity, and home thermal properties that characterize the heat transfer rate and thermal capacity of a home. This model will be briefly introduced in Section 5.2.1. The model, along with the thermal comfort criteria, utility rate, and cooling capacity and total power use of the HVAC system, will be utilized to formulate a pre-cooling optimization problem in Section 5.2.2.

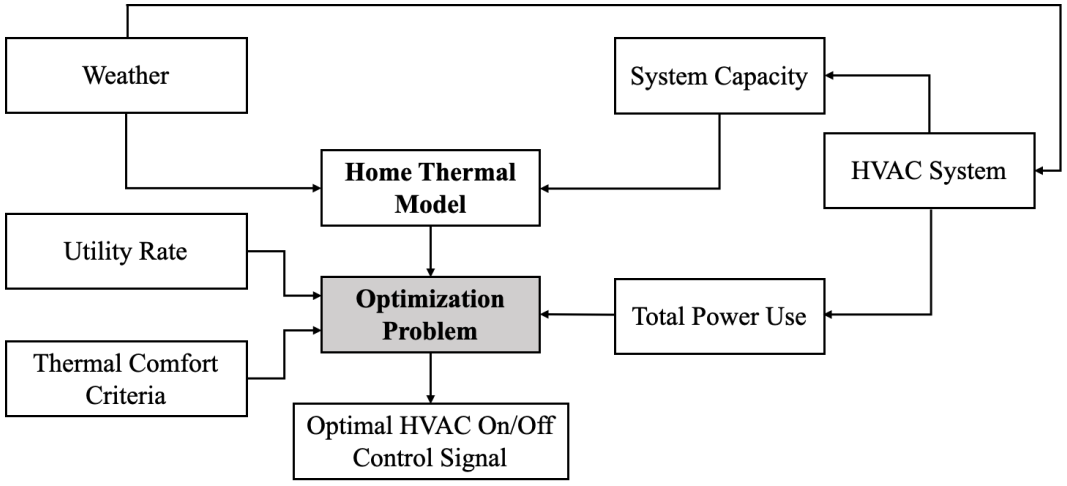

Figure 5.2. An approach to formulating a pre-cooling optimization problem.

5.2.1 Home thermal dynamic modeling

Consider a home equipped with a HVAC system. Let $T_{in}(t)$ and $T_{ie}(t)$ denote the indoor air temperature and interior wall surface temperature of the home at time t and suppose their dynamics are described by the following lumped home thermal model, as shown in Equations (5.1) and (5.2), which was formulated and detailed in Chapter 3.

$$\frac{dT_{ie}(t)}{dt} = \frac{1}{\tau_1}[T_o(t) - T_{ie}(t)] + \frac{1}{\tau_2}\left[\left(T_{in}(t) - T_{ie}(t)\right)\right] \tag{5.1}$$

$$\frac{dT_{in}(t)}{dt} = -\frac{1}{\tau_3}T_{in}(t) + \frac{1}{\tau_3}\left[T_{ie}(t) + \left(a_1G(t) + a_2G^2(t) + a_3G^3(t)\right) + \left(T_o(t) - T_{in}(t)\right)\left(b_1W(t) + b_2W^2(t)\right) + \left(Q_i(t)u_i(t) + Q_s(t)u_s(t)\right)\right] \tag{5.2}$$

where $\tau_1 = C_{ve,in}R_{ve}$ and $\tau_3 = C_{air}R_{air}$ are the time constants of the envelope and indoor air of a home, respectively; $\tau_2 = C_{ve,in}R_{air}$, a_1, a_2, a_3, b_1, and b_2 are the corresponding coefficients associated with R_{air}; R_{ve} and $C_{ve,in}$ are the thermal resistance and thermal capacitance of the home envelope; $T_o(t)$ is the outdoor air

temperature; $G(t)$ is the global horizontal irradiation; $W(t)$ is the wind speed; $Q_i(t)$ and $Q_s(t)$ are the scaled internal heat gain and HVAC system output (determined by the HVAC system capacity) associated with R_{air}; u_i is the internal activity schedule; $u_s(t) \in \{0, 1\}$ is the HVAC system on/off control signal; and a_1, a_2, a_3, b_1, and b_2 are the model parameters. These parameters together with τ_1, τ_2, and τ_3 may be empirically identified using operational data and the least-squares method, as detailed in Section 3.4.2 and also summarized in Section 5.3.1. In addition, note that $T_{in}(t)$ in Equation (5.2) is influenced by several exogenous inputs, involving all three basic heat transfer modes (conduction, convection, and radiation) separately.

Typically, the HVAC on/off control signal $u_s(t)$ is determined by a control algorithm (i.e., thermostat) that attempts to regulate the indoor air temperature $T_{in}(t)$ around a set point $T_{set}(t)$. To avoid high frequency cycling, a deadband of width $\pm\sigma$ is often inserted, leading to a hysteresis behavior as illustrated in Figure 5.3. For the cooling mode, this hysteresis behavior can be expressed as

$$u_s(t) = \begin{cases} 1, & \text{if } u(t-\delta) = 0 \text{ and } T_{in}(t-\delta) > T_{set}(t-\delta) + \sigma \\ 0, & \text{if } u(t-\delta) = 1 \text{ and } T_{in}(t-\delta) < T_{set}(t-\delta) - \sigma \\ u_s(t-\delta), & \text{otherwise} \end{cases} \quad (5.3)$$

where $t - \delta$ is the 'previous' time instant based on which the 'current' $u_s(t)$ is determined.

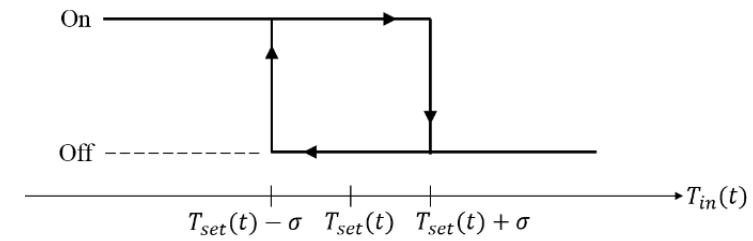

(a)

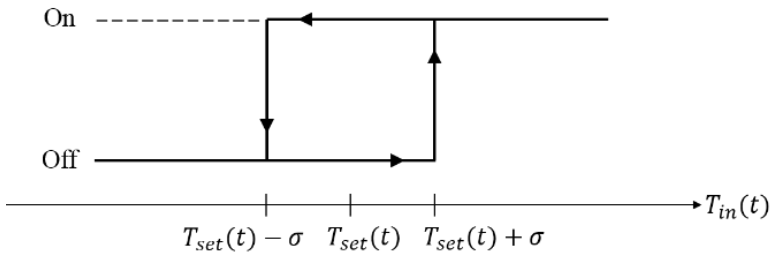

(b)

Figure 5.3. A typical HVAC on/off control algorithm in the (a) heating mode and (b) cooling mode.

5.2.2 Optimization problem formulation

In this study, the HVAC on/off control signal $u_s(t)$ in Equation (5.2) is treated as an optimization variable as opposed to being determined by Equation (5.3). Specifically, $u_s(t)$ for $t \in [0, t_f]$ will be chosen to minimize the objective function

$$J(u_s) = \int_0^{t_f} P(t)E(t)u_s(t)\,dt \tag{5.4}$$

subject to the constraints

$$u_s(t) \in \{0, 1\} \text{ for all } t \in [0, t_f] \tag{5.5}$$

$$T_{lb} \leq T_{in}(t) \leq T_{ub} \text{ for all } t \in [0, t_f] \tag{5.6}$$

dynamics Equations (5.1) and (5.2) with

$$T_{in}(0) = [0 \quad 1]\begin{bmatrix} T_{ie}(0) \\ T_{in}(0) \end{bmatrix} = [0 \quad 1]\begin{bmatrix} T_{ie,0} \\ T_{in,0} \end{bmatrix} \tag{5.7}$$

where $[0, t_f]$ is the optimization time horizon; $P(t)$ is the electricity price at time t; $E(t)$ is the total power use of the HVAC system; T_{lb} and T_{ub} are lower and upper bounds on $T_{in}(t)$ that ensure thermal comfort; and $T_{in,0}$ and $T_{ie,0}$ are the initial values of $T_{in}(t)$ and $T_{ie}(t)$, respectively. Accordingly, a solution $u_s^*(t)$ for $t \in [0, t_f]$ to the optimization problem Equations (5.4)−(5.7) is the HVAC on/off control signal that minimizes energy cost over the time horizon $[0, t_f]$ while maintaining an acceptable level of thermal comfort.

Moreover, to maintain a proper HVAC operation cycle time for safe operations, the number of the total operation cycles is limited by N/2, which becomes another constraint of the optimization problem, and can be expressed by

$$\sum_1^{t_f}[u_s(t) - u_s(t-1)]^2 \leq N \tag{5.8}$$

Although Equations (5.4)−(5.8) represent a meaningful optimization problem, it is formulated in continuous-time and, thus, is not amenable to practical implementation. To address this issue, the problem will be discretized as follows: let Δt denote the sampling period, $K = t_f/\Delta t$ denote the number of discrete time slots, and $x[k]$ for k =1, 2, …, K denote the sampled values of a generic continuous-time signal $x(t)$ at time t =0, Δt, …, $(K-1)\Delta t$. By applying the forward Euler method, the continuous-time model in Equations (5.1) and (5.2) can be converted into a discrete-time model

$$T_{ie}[k+1] = (1-\alpha_1-\alpha_2)T_{ie}[k] + (\alpha_1 T_o[k] + \alpha_2 T_{in}[k]) \quad (5.9)$$

$$T_{in}[k+1] = (1-\alpha_3)T_{in}[k] + \alpha_3(T_{ie}[k] + (a_1 G[k] + a_2 G^2[k] + a_3 G^3[k]) +$$

$$(T_o[k] - T_{in}[k])(b_1 W[k] + b_2 W^2[k]) + Q_i[k]u_i[k] + Q_s[k]u_s[k]) \quad (5.10)$$

where $\alpha_1 = \frac{\Delta t}{\tau_1}$, $\alpha_2 = \frac{\Delta t}{\tau_2}$, and $\alpha_3 = \frac{\Delta t}{\tau_3}$. Equations (5.9) and (5.10) can be combined and further be expressed in the form of a linear time-varying system

$$x[k+1] = A[k]x[k] + B[k]u_s[k] + d[k] \quad (5.11)$$

where $x[k]$, $A[k]$, $B[k]$, and $d[k]$ are matrices given by

$$x[k] = \begin{bmatrix} T_{ie}[k] \\ T_{in}[k] \end{bmatrix}$$

$$A[k] = \begin{bmatrix} 1-\alpha_1-\alpha_2 & \alpha_2 \\ \alpha_3 & (1-\alpha_3) - \alpha_3(b_1 W[k] + b_2 W^2[k]) \end{bmatrix}$$

$$B[k] = \begin{bmatrix} 0 \\ \alpha_3 Q_s[k] \end{bmatrix}$$

$$d[k] =$$

$$\begin{bmatrix} \alpha_1 T_o[k] \\ \alpha_3(T_o[k](b_1 W[k] + b_2 W^2[k]) + (a_1 G[k] + a_2 G^2[k] + a_3 G^3[k]) + Q_i[k]u_i[k]) \end{bmatrix}$$

As is known (Brogan 1991), the solution $T_{in}[k]$ of the linear time-varying system Equation (5.11) is given by

$$x[k] = \left(\prod_{p=1}^{k-1} A[p]\right) x[1] +$$

$$\sum_{j=2}^{k} \prod_{p=j}^{k-1} A[p](B[j-1]u_s[j-1] + d[j-1]) \quad (5.12)$$

where $\prod_{p=m}^{n} A[p] = A[m]\, A[m+1] \cdots A[n]$ if $m \leq n$, and $\prod_{p=m}^{n} A[p] = 1$ otherwise. Equation (5.12) can be alternatively written as

$$x[k] = \Phi(k,1)x[1] + \sum_{j=2}^{k} \Phi(k,j)\,(B[j-1]u_s[j-1] + d[j-1]) \quad (5.13)$$

where $\Phi(k,j) = \prod_{p=j}^{k-1} A[p]$ is the so-called state transition matrix (Brogan 1991).

With the above discretization, the continuous-time problem Equations (5.4)–(5.8) can be reformulated in discrete-time as follows: find a HVAC on/off control sequence $u_s[k]$ for k =1, 2, …, K that minimizes the objective function

$$J(u_s) = \sum_{k=1}^{K} P[k]E[k]u_s[k] \quad (5.14)$$

subject to the constraints

$$u_s[k] \in \{0,1\} \text{ for } k = 1, 2, \ldots, K \quad (5.15)$$

$$\sum_{k=2}^{K} (u_s[k] - u_s[k-1])^2 \le N \quad (5.16)$$

$$T_{lb} \le T_{in}[k] \le T_{ub} \text{ for } k = 1, 2, \ldots, K \quad (5.17)$$

$$T_{in}[k] = [0 \quad 1]\left\{\Phi(k,1)\begin{bmatrix} T_{ie}(1) \\ T_{in}(1) \end{bmatrix} + \sum_{j=2}^{k} \Phi(k,j)\,(B[j-1]u_s[j-1] + d[j-1])\right\} \text{ for } k = 1, 2, \ldots, K \quad (5.18)$$

Note that the discrete-time problem Equations (5.14)–(5.18) is a quadratically-constrained integer linear programming problem (Schrijver 1998) that may be solved, for example, using CVX, a MATLAB-based modeling system for convex optimization (Mathworks 2019; Grant and Boyd 2014), based on the MOSEK solver for convex optimization (MOSEK ApS 2019). This method of determining the optimal HVAC on/off control sequence $u_s^*[k]$ for k =1, 2, …, K is referred to as the proposed optimal pre-cooling strategy. With such $u_s^*[k]$ and with Equation (5.18), the corresponding optimal indoor air temperature $T_{in}^*[k]$ for

k =1, 2, …, K may be calculated, as is done in Section 5.4. Moreover, different from the typical HVAC on/off control algorithm in Figure 5.3, $u_s^*[k]$ is not determined based on a set point with a deadband control. Because set point control makes the optimization problem Equation (5.14) extremely difficult, if not impossible, to solve. In contrast, optimal HVAC on/off control has the advantage of controlling thermostats directly via the generated $u_s^*[k]$. The disadvantage, however, is that currently available thermostats may not have this function.

5.3 Simulation Setup

This section describes a simulation setup that allows one to evaluate the effectiveness of the optimal pre-cooling strategy proposed in Section 5.2 by comparison with three rule-based operation strategies introduced in Section 5.1. Section 5.3.1 introduces the selection of home thermal parameters. Section 5.3.2 states the relevant thermal comfort criteria and utility rate structure. Finally, Section 5.3.3 presents a method for calculating the HVAC system output and its total power use. Upon completing this section, details about the simulation setup would have been provided.

5.3.1 Selection of home thermal parameters

In Section 3.5.2, a two-step parameter estimation scheme along with the first 6 consecutive days of data and the available 15 consecutive days of data was used to identify the parameters τ_1, τ_2, τ_3, a_1, a_2, a_3, b_1, b_2, and Q_s of the discrete-time home thermal model in Equations (5.9) and (5.10). When the test home was unoccupied, the term $Q_i[k]u_i[k]$ in Equation (5.10) was zero and,

hence, did not affect the identification. In practice, when the HVAC system is on, however, the term $Q_s[k]$ in Equation (5.10) varied with the outdoor air temperature $T_o[k]$ instead of a constant value identified in Section 3.5.2. Therefore, the relationship between $Q_s[k]$ and $T_o[k]$ is investigated in Section 5.3.3.

In Section 3.5.2, the accuracy of the identified model was validated by comparing 24-hour-ahead prediction of indoor air temperature with the measured one. Indeed, by using 15 consecutive days of data, the resulting mean, maximum, and 95%-confidence-interval absolute errors were found to be relatively better than the one by using the first 6 consecutive days of data. Hence, this section adopts the model parameters that were trained by the 15 consecutive days of data, as shown in Table 5.1. With the parameter values from Table 5.1, the home thermal model in Equations (5.9) and (5.10) becomes ready for simulation use.

Table 5.1. Identified values of the home thermal model.

Parameter	$\boldsymbol{\tau_1}$	$\boldsymbol{\tau_2}$	$\boldsymbol{\tau_3}$	$\boldsymbol{b_1}$
Value	2350	272.1	8.191	0.01488
Parameter	$\boldsymbol{b_2}$	$\boldsymbol{a_1}$	$\boldsymbol{a_2}$	$\boldsymbol{a_3}$
Value	-0.0007994	5.361	-10.33	6.264

5.3.2 Thermal comfort criteria and utility rate structure

In the simulation, 70 °F and 79 °F were selected as the lower bound T_{lb} and upper bound T_{ub} on the indoor air temperature $T_{in}[k]$ in Equation (5.17),

respectively, following the ASHRAE thermal comfort requirements (ANSI/ASHRAE Standard 55 2017). In addition, the time-of-day utility rate structure that defines the 24-hour electricity price $P[k]$ in Equation (5.14) is provided by a utility supplier in the state of Oklahoma. This rate structure is shown in Figure 5.4, from which it can be seen that the on-peak hours are 15:00−19:00 (3 pm−7 pm), and the on-peak electricity price of \$0.22/kWh is much higher than its off-peak counterpart of \$0.05/kWh.

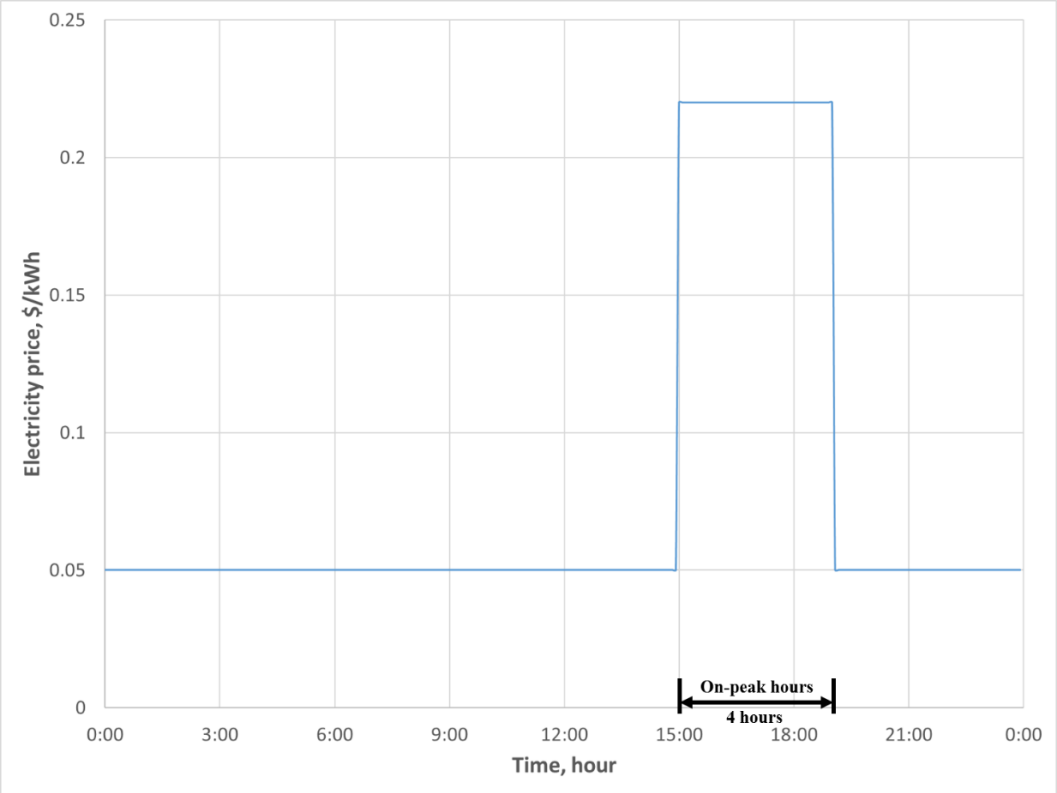

Figure 5.4. Time-of-day utility rate structure from a utility supplier.

5.3.3 HVAC system output and total power use

As shown in Equation (5.10), the HVAC system output, determined by the HVAC system capacity, affects the dynamics of $T_{in}[k]$ through the term $Q_s[k]u_s[k]$, where $Q_s[k] = R_{air}Q_{sys}[k]$ represents the scaled cooling capacity by R_{air}. $Q_s[k]$ was assumed to be constant and the estimated value of Q_s equals -2.267 for the HVAC equipment of a manufacturer with 3.5 tons (42,000 Btu/h) of cooling capacity and 1,400 cfm of flow rate, as identified in Section 3.5.3. Ideally, the HVAC cooling capacity varies with weather conditions, but is not affected as much by the changes in the indoor dry bulb (DB) and wet bulb (WB) temperatures. To investigate how the HVAC cooling capacity, $Q_s[k]$, in Equation (5.10) changes with weather conditions, the cooling capacity data from a HVAC manufacturer, as shown in Figure D.1 in the **Appendix D,** was converted into $Q_s[k]$ based on the assumption that $Q_s = -2.267$ at 3.5 tons was achieved under median weather conditions. Figure 5.5, which was generated using such data, displays the relationships between the HVAC cooling capacity $Q_s[k]$ at 3.5 tons and outdoor air temperature $T_o[k]$ for five different indoor DB and WB temperatures. As observed, the relationships are sensitive to changes in both the outdoor air temperatures and indoor DB and WB temperatures. According to the ASHRAE thermal comfort requirements (ANSI/ASHRAE Standard 55 2017), the conditioned indoor space air is close to the DB temperature at between 75 °F and 80 °F and WB temperature at 62 °F, and the two relationships (75DB62WB and 80DB62WB) are very close as observed in the figure. Therefore, the relationship

was adopted based on the indoor DB and WB temperatures at 80 °F and 62 °F, respectively. Moreover, the relationship may be approximated by a second-order polynomial,

$$Q_s[k] = -0.00005982T_o^2[k] + 0.00200312T_o[k] + 2.25981693 \quad (5.19)$$

with a coefficient of determination (R^2) of 0.99883293. Therefore, for simplicity, $Q_s[k]$ in Equation (5.10) is replaced by Equation (5.19) in the simulation.

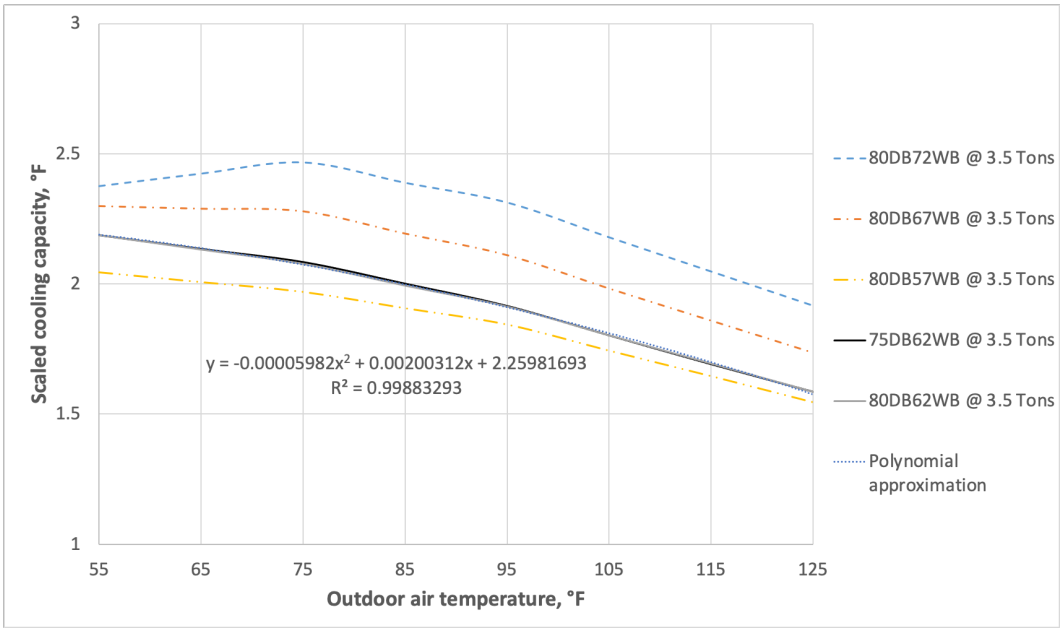

Figure 5.5. HVAC system scaled cooling capacity versus outdoor air temperature for different indoor DB and WB temperatures.

Similarly, to investigate how total HVAC power use, $E[k]$, in Equation (5.14) varies with weather conditions, power data from the same HVAC manufacturer were used. Figure 5.6 shows the relationship between HVAC total power use $E[k]$ and outdoor air temperature $T_o[k]$ for five different indoor DB and WB temperatures. As observed, the relationship is insensitive to changes in

the indoor DB and WB temperatures. Moreover, the relationship may be accurately approximated by a second-order polynomial,

$$E[k] = 0.00019940T_o^2[k] - 0.00353571T_o[k] + 1.96209821 \quad (5.20)$$

with a coefficient of determination (R^2) of 0.99938409. Therefore, for simplicity, $E[k]$ in Equation (5.14) is replaced by Equation (5.20) in the simulation.

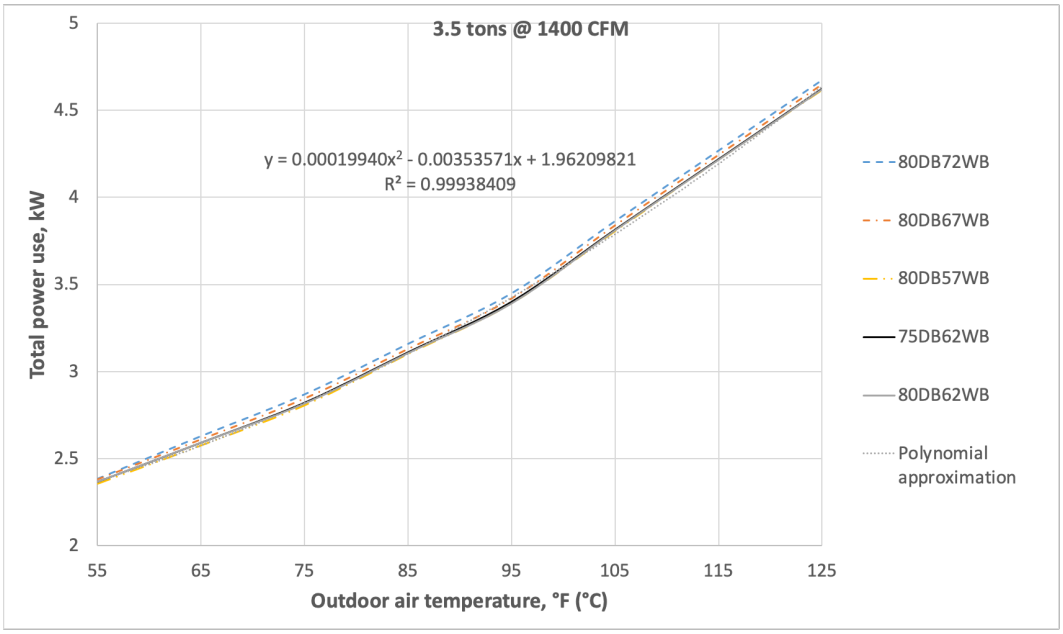

Figure 5.6. HVAC total power use versus outdoor air temperature for different indoor DB and WB temperatures.

5.4 Simulation Results

This section presents and compares the simulation results for BC I, II, III, and the proposed optimal pre-cooling strategy (OPS). In particular, Section 5.4.1 analyzes the simulated indoor temperature and control signal, Section 5.4.2 examines the resulting total and on-peak energy consumption, and Section 5.4.3 compares the resulting energy cost and saving potential.

5.4.1 Comparison of indoor temperature and control signal

Based on the simulation setup described in Section 5.3, a 24-hour simulation with a sampling period Δt of 10 minutes has been carried out for BC I, II, III, and OPS. The simulation utilized weather data from August 2, 2020, as shown in Figure B.3 in the **Appendix B**, which was selected as an example to show a summer day in Norman, Oklahoma. Figures 5.7–5.10 show the simulation results for BC I, II, III, and OPS, respectively. Each figure includes three graphics, in which the top one represents different temperatures, the middle one represents the HVAC on/off control signal $u_s[k]$, and the bottom one represents the electricity price $P[k]$, along with 24-hour time. Moreover, the gray, blue, red, black dotted, and magenta dashed curves in the top graphic of each figure represent the outdoor air temperature $T_o[k]$, interior wall surface temperature $T_{ie}[k]$, indoor air temperatures and $T_{in}[k]$, lower bound T_{lb}, and upper bound T_{ub}. In addition, to enable a better comparison, the four red and blue curves representing $T_{ie}[k]$ and $T_{in}[k]$ from Figures 5.7–5.10, respectively, were superimposed on Figure 5.11, where the top graphic represents $T_{ie}[k]$ and the bottom one represents $T_{in}[k]$ (using different colors to distinguish among them).

For BC I shown in Figure 5.7 which had no pre-cooling, the HVAC system had to stay on for the whole on-peak hours to cope with the relatively high $T_o[k]$. Because BC I did not try to avoid the high on-peak electricity price, it incurred a high energy cost. With this strategy, $T_{in}[k]$ was allowed to float to the upper bound T_{ub} and exceed T_{ub} for some times and hence the HVAC system

cannot maintain the thermal comfort, at which the system was turned on to keep $T_{in}[k]$ bouncing between ± 1 °F of the uniform set point $T_{set}[k]$ of 78 °F. Since the thermal mass of the wall is larger than that of air, $T_{ie}[k]$ showed slow fluctuations and had some time delay to rise to the upper bound T_{ub}.

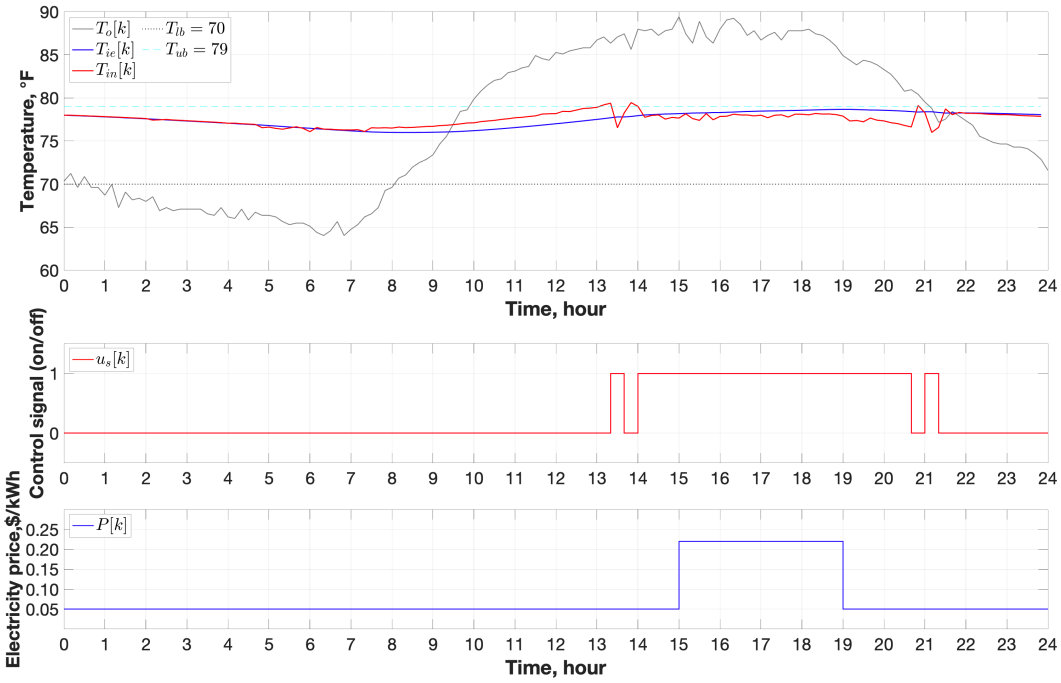

Figure 5.7. Simulation result for BC I.

Unlike BC I, for BC II shown in Figure 5.8 which had pre-cooling, the HVAC system could be kept off for 2 hours and 30 minutes during part of the on-peak hours, i.e., it was off two times from 15:00 to 17:10 and from 17:30 to 17:50 for the total of 2 hours and 30 minutes, despite the high $T_o[k]$. Thus, BC II was capable of avoiding part of the high on-peak electricity price. To accomplish this cost saving, however, the HVAC system had to start running at 9:00 and remain on for all 6 hours to try to bring $T_{in}[k]$ down for pre-cooling before the on-peak

hours. However, due to limited cooling capacity, $T_{in}[k]$ still increased slightly when $T_o[k]$ kept increasing and became high. During the on-peak hours, the HVAC system was turned on two times for 20 minutes from 17:10 to 17:30 and 1 hours and 10 minutes from 17:50 to 19:00. Following the latter operation starting at 17:50, the system had to continually stay on for 20 minutes until 19:20 after the on-peak hours end at 19:00. Furthermore, the system was turned on twice times for 20 minutes from 19:40 to 20:00 and for 20 minutes from 20:20 to 20:40 during the off-peak hours, to prevent $T_{in}[k]$ from exceeding T_{ub}. Due to the effect of pre-cooling, the wall could store cooling energy and gradually release to the indoor air. Therefore, the HVAC system did not run much time during both the on-peak hours and off-peak hours at nighttime.

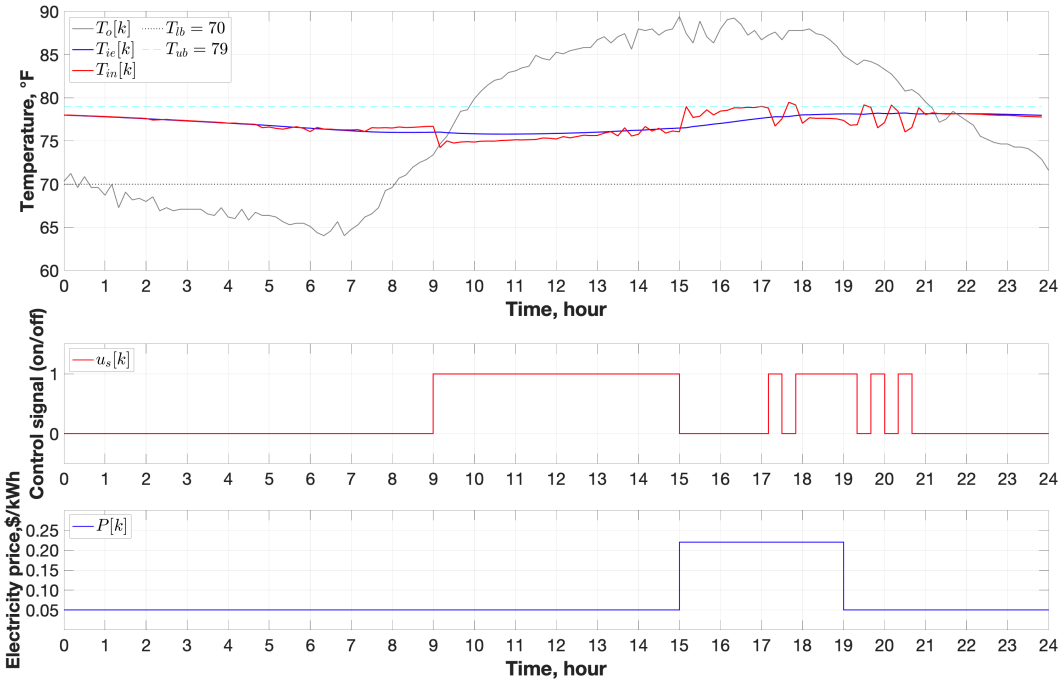

Figure 5.8. Simulation result for BC II.

Similar to BC II, for BC III shown in Figure 5.9 which also had pre-cooling, the HVAC system could be kept off for 1 hour and 50 minutes during the on-peak hours, i.e., it was off four times for 20 minutes, 50 minutes, 20 minutes, and 20 minutes from 15:00 to 15:20, from 15:40 to 16:30, from 16:50 to 17:10, and from 17:30 to 17:50, respectively. Following the latter operation starting at 17:50, the system had to continually stay on for 20 minutes until 19:20 after the on-peak hours end at 19:00. Furthermore, the system was turned on twice times for 20 minutes from 19:40 to 20:00 and for 20 minutes from 20:20 to 20:40 during the off-peak hours, to prevent $T_{in}[k]$ from exceeding T_{ub}. The HVAC system start running at 10:00 with lower $T_{set}[k]$ of 71 °F and remained on for all 5 hours to try to bring $T_{in}[k]$ down for pre-cooling before the on-peak hours. Similar to BC II, due to limited cooling capacity, $T_{in}[k]$ still keep rising slightly when $T_o[k]$ kept increasing and became high. Moreover, the system had a longer turn-on time than BC II during the on-peak hours. This is because with BC II, its 6 hours of pre-cooling was able to slightly lower $T_{ie}[k]$ and $T_{in}[k]$ than its shorter, 5 hours of pre-cooling with BC III, despite its lower $T_{set}[k]$ of 71 °F. The fact that the HVAC system with BC III was kept on more times during and after the on-peak hours suggests that BC III had a higher energy cost than BC II for this specific home thermal condition on this particular day.

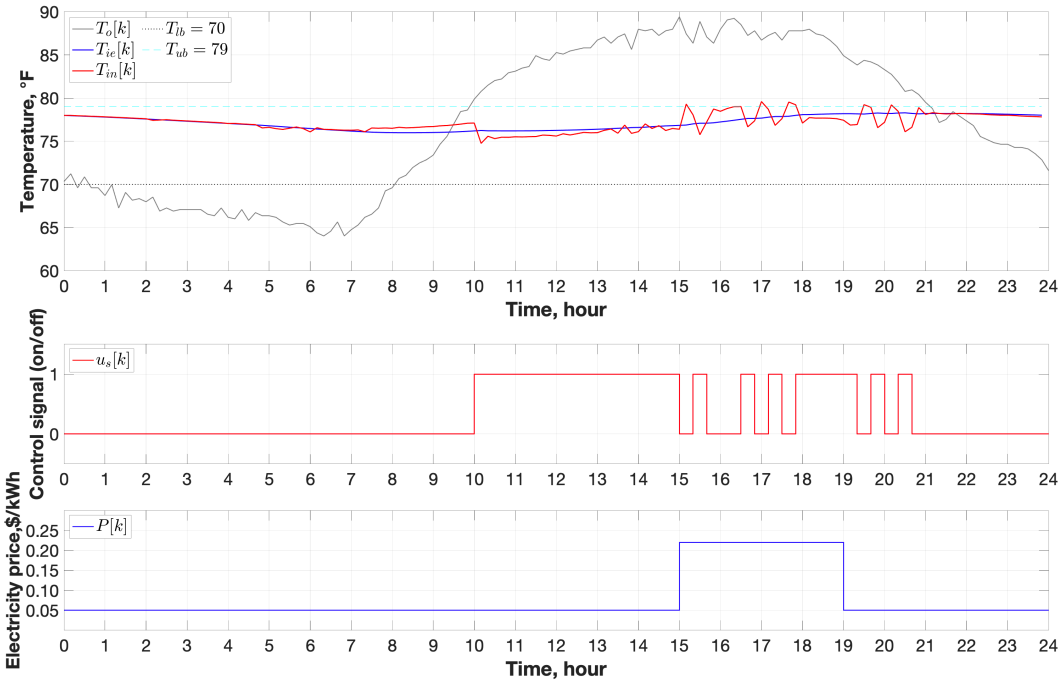

Figure 5.9. Simulation result for BC III.

Finally, for OPS shown in Figure 5.10 which selected $u_s[k]$ to minimize energy cost while keeping $T_{in}[k]$ between T_{lb} and T_{ub}, the HVAC system was turned off during the entire on-peak hours unlike other operation cases. In addition, pre-cooling began in the early morning at 3:20 (compared to 9:00 and 10:00 for BC II and III) and lasted for 6 hours and 30 minutes until 9:50, reducing $T_{in}[k]$ and $T_{ie}[k]$ to as low as 72.5 °F and 73.6 °F, respectively, which was actually able to lower $T_{in}[k]$ and $T_{ie}[k]$ before on-peak hours compared with BC I, II, and III (see Figure 5.11). This behavior was due to OPS exploiting the fact that between 3:20 and 9:50, the higher HVAC efficiency produced by cooler outdoor air enabled the HVAC system to run more economically. Because pre-cooling ended earlier at 9:50, three additional rounds of pre-cooling, of which the

first two lasted for only 10 minutes and the latter lasted for 2 hours and 20 minutes, took place before the on-peak hours started at 15:00. After the on-peak hours ended at 19:00, the HVAC system was kept off entirely to take fully use of the upper bound T_{ub} of thermal comfort, which was different from the three operation cases that required to be turned on. Note that unlike the rigid, rule-based BC II and III, OPS was able to optimally adapt its pre-cooling pattern to all relevant factors including specific home thermal properties, HVAC system capacity, utility rate structure, and weather conditions.

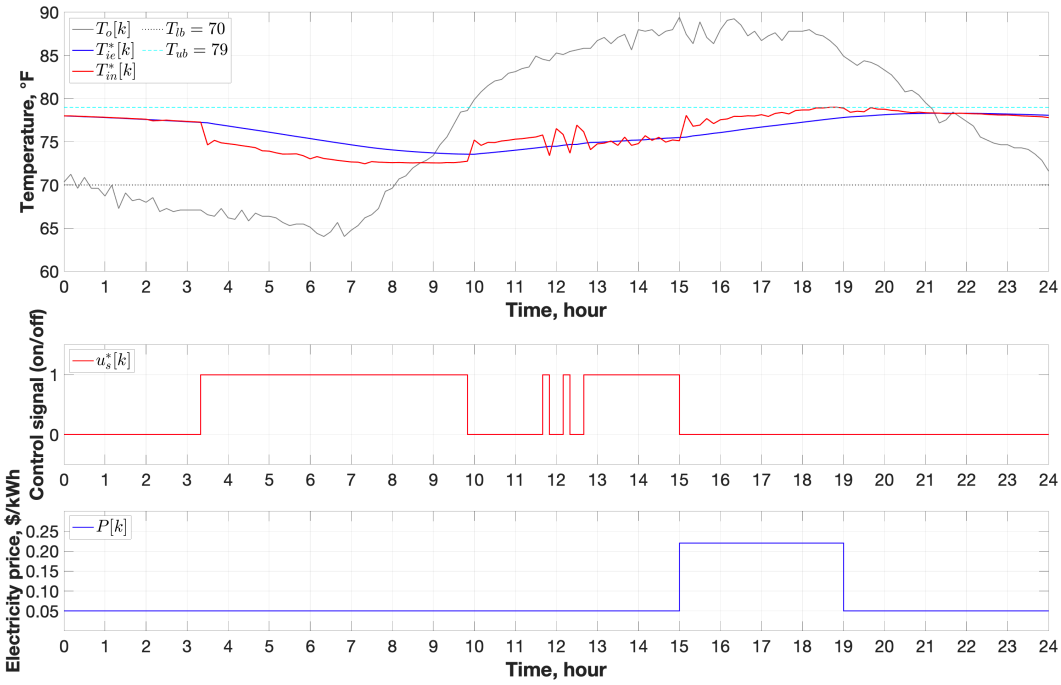

Figure 5.10. Simulation result for the proposed optimal pre-cooling strategy (OPS).

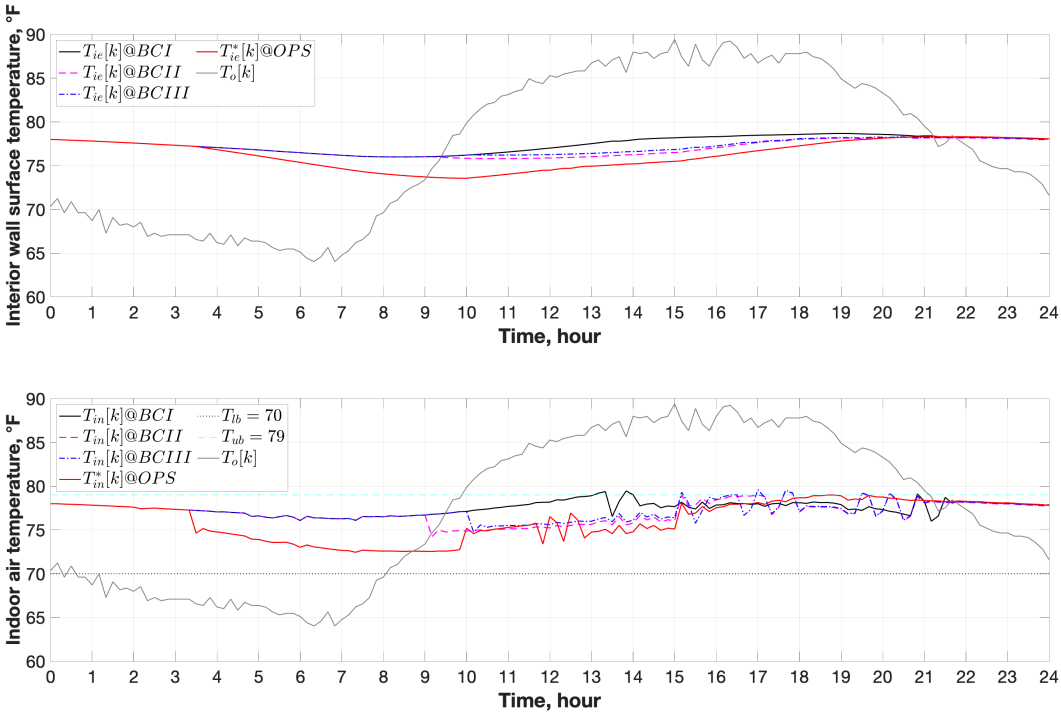

Figure 5.11. Comparison of the interior wall surface temperatures and the indoor air temperatures for BC I, II, III, and OPS.

5.4.2 Comparison of total and on-peak energy consumption

The total and on-peak energy consumption are defined as $\Delta t \sum_k E[k]u_s[k]$ where k is taken over the whole day and over the on-peak hours, respectively. Table 5.2 lists the total and on-peak energy consumption for BC I, II, III, and OPS. Observe from the table that BC I requires less total energy consumption compared to BC II, BC III, and OPS due to both no pre-cooling and not maintaining the thermal comfort. The observation is in line with conclusions, made in the literature, that pre-cooling tends to reduce cost but consume more energy. In terms of pre-cooling operations, even if OPS has much longer runtime and strictly maintains the thermal comfort, it only requires a slightly higher total

energy consumption than BC III but less than BC II. This can be attributed to: 1) running the HVAC system more in cool outdoor air conditions when the HVAC efficiency is high; and 2) eliminating the 1 °F deadband in operation, which is required by the rule-based strategies, to allow $T_{in}[k]$ to stay near T_{ub} as much as possible. As additional observations, BC II needs more total energy consumption than BC III—likely because BC II has a lowered $T_{set}[k]$ for one more hour than BC III. As for on-peak energy consumption, OPS requires none, while all of BC I, II, and III require some with BC I needing more. These observations agree with the discussions in Section 5.4.1.

Table 5.2. Comparison of total and on-peak energy consumption for BC I, II, III, and OPS.

Operation strategy	BC I	BC II	BC III	OPS
Total energy consumption, kWh	23.04*	26.20*	25.47*	25.63
On-peak energy consumption, kWh	12.73	4.76	6.89	0.00

Note: * represents that the thermal comfort cannot be maintained.

5.4.3 Comparison of energy cost and saving potential

The energy cost is defined by the objective function Equation (5.14). Table 5.3 lists the 24-hour energy cost for BC I, II, III, and OPS as well as the percentage of cost saving that can be achieved when OPS is used in place of BC I, II, and III. Notice from the table that the percentage of saving enabled by using OPS is 39.62% compared with BC II and may be as high as 61.45% compared with no pre-cooling operation BC I, confirming its benefit.

Table 5.3. Comparison of energy cost and saving potential for BC I, II, III, and OPS.

Operation strategy	BC I	BC II	BC III	OPS
Energy cost	$3.32*	$2.12*	$2.44*	$1.28
Percentage of OPS cost saving	61.45%	39.62%	47.54%	0%

Note: * represents that the thermal comfort cannot be maintained.

5.5 Summary

This chapter formulates a pre-cooling optimization problem that accounts for the thermal properties of a home, HVAC system capacity, utility rate structure, and weather conditions and makes use of a home thermal model. The effectiveness and energy performance of the proposed optimal pre-cooling strategy is investigated and compared with three rule-based operation strategies that differ in whether they have pre-cooling and their pre-cooling characteristics. It is found that on a hot summer day in Norman, Oklahoma, the optimal strategy requires more total energy consumption than no pre-cooling operation but requires a less or similar total energy consumption compared with the two rule-based pre-cooling strategies without sacrificing thermal comfort, agreeing with conclusions reached in the literatures. Moreover, even if the optimal pre-cooling has much longer runtime compared with the rule-based pre-cooling operations, the energy consumption almost keeps same, which is attributed to the longer runtime of the HVAC system in cool outdoor air conditions and to the elimination of the deadband operation, which is required by the rule-based strategies, to allow

the indoor air temperature to stay near the thermal comfort upper bound as much as possible after on-peak hours. After on-peak hours, even if the HVAC system is still in high cooling demand, the system can still be kept off for the optimal pre-cooling strategy. In terms of 24-hour energy cost, the three rule-based operation strategies require $3.32, $2.12, and $2.44, respectively, whereas the optimal strategy only requires $1.28. These figures represent a saving of 61.45%, 39.62%, and 47.54%, respectively. The results suggest that the optimal strategy is indeed significantly more effective than the existing rule-based operation strategies.

The successful development of the pre-cooling optimization algorithm for homes provides a way to benchmark energy performance of the optimal pre-cooling strategy. However, it is found that the optimization is heavily dependent on a specific set of conditions (i.e., specific thermal properties, HVAC system capacity, utility rate structure, and weather conditions). The impact of different sets of conditions on the energy performance of optimal pre-cooling operation needs to be investigated. This will be the focus in Chapter 6.

Chapter 6: Performance Analysis of Optimal Pre-Cooling

To provide a means of reducing the peak demand and/or energy cost from on-peak hours to off-peak hours in residential buildings, an optimal pre-cooling strategy is proposed in Chapter 5 as an alternative to rule-based pre-cooling strategies that are intuitive and may not provide optimal cost savings. Since the optimal pre-cooling strategy is heavily dependent on a specific set of conditions, such as specific thermal properties, HVAC system cooling capacities, weather conditions, and utility rates, an analysis of different sets of conditions on the performance of the optimal pre-cooling strategy will be conducted in this chapter, as illustrated in Figure 6.1.

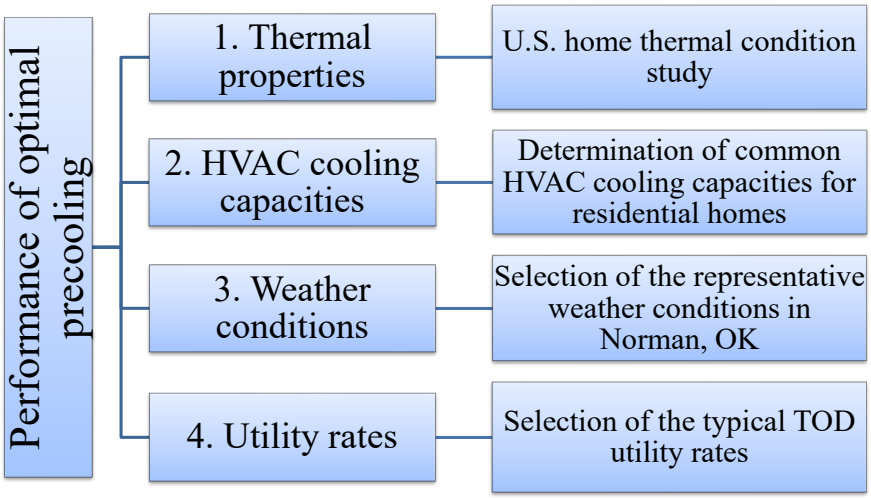

Figure 6.1. Performance analysis of optimal pre-cooling by different influencing factors.

6.1 Simulation Setup

A simulation setup that allows one to conduct a performance analysis of the optimal pre-cooling strategy proposed in Chapter 5 is described in this section. The parameters of the home model adopted for various home thermal conditions are described in Section 6.1.1. A method for calculating different HVAC system outputs is presented in Section 6.1.2. The calculation method of different HVAC system total power uses is introduced in Section 6.1.3. The varying weather conditions that are adopted are described in Section 6.1.4. Finally, the selections of different lower and/or upper bounds and utility rate structures are stated in Section 6.1.5.

6.1.1 Determine home thermal model parameters for various home thermal conditions

In Chapter 3, the parameters τ_1, τ_2, τ_3, a_1, a_2, a_3, b_1, and b_2 of the discrete-time home thermal model, as shown in Equations (3.27) and (3.28), were identified using a two-step parameter estimation scheme and 15 consecutive days of data collected at an unoccupied test home in Norman, Oklahoma. Table 6.1 lists the identified values of the model parameters. The identified model showed a good performance in validations with the resulting mean, maximum, and 95%-confidence-interval absolute errors of 0.80 °F, 3.26 °F, and 1.90 °F, respectively.

Table 6.1. Identified values of the home thermal model parameters.

Parameter	$\boldsymbol{\tau_1}$	$\boldsymbol{\tau_2}$	$\boldsymbol{\tau_3}$	$\boldsymbol{b_1}$	$\boldsymbol{b_2}$

Value	2350	272.1	8.191	0.01488	-0.0007994
Parameter	$\boldsymbol{a_1}$	$\boldsymbol{a_2}$	$\boldsymbol{a_3}$	$\boldsymbol{Q_s}$	
Value	5.361	-10.33	6.264	-2.267	

In Chapter 4, using 1,676 homes across the U. S., it was found that the average Tau (i.e., τ_1) value ranged from 2000 to 5000, with 5000 representing a good thermal condition and 2000 a poor condition, as shown in Figure 4.10 in Chapter 4, by the distribution of Tau values versus home ages. Since the Tau value represents the physical home thermal properties, i.e., the area-weighted average thermal properties of all envelope elements, and the impacts of wind and solar are relatively small (Wang et. al 2019; Wang et. al 2020), variations of the Tau value are adopted in this study to represent different home thermal conditions.

6.1.2 Determine HVAC system output for different units

Similar to method used in Section 5.3.3, to investigate how the HVAC cooling capacity, $Q_s[k]$, of 3.5 tons, 4 tons, and 5 tons in Equation (5.10) changes with weather conditions, the cooling capacity data from a HVAC manufacturer, as shown in the **Appendix D**, were converted into $Q_s[k]$ based on the assumption that $Q_s = -2.267$ at 3.5 tons was achieved under median weather conditions. Figure 6.2, which was generated using such data, displays the relationships between the HVAC cooling capacity $Q_s[k]$ at 3.5 tons, 4 tons, and 5 tons and outdoor air temperature $T_o[k]$ for five different indoor DB and WB temperatures,

respectively. As observed, the relationships are sensitive to changes in both the outdoor air temperatures and indoor DB and WB temperatures. According to the ASHRAE thermal comfort requirements (ANSI/ASHRAE Standard 55 2017), the conditioned indoor space air is close to the DB temperature at between 75 °F and 80 °F and WB temperature at 62 °F, and the relationships (75DB62WB and 80DB62WB) are very close as observed. Therefore, the relationships are adopted based on the indoor DB and WB temperatures at 80 °F and 62 °F, respectively. Moreover, the relationships may be approximated by second-order polynomials,

$$Q_s[k] = -0.00005982T_o^2[k] + 0.00200312T_o[k] + 2.25981693 \quad (6.1)$$

$$Q_s[k] = -0.00006027T_o^2[k] + 0.00064772T_o[k] + 2.66622436 \quad (6.2)$$

$$Q_s[k] = -0.00013254T_o^2[k] + 0.01099916T_o[k] + 2.82327276 \quad (6.3)$$

with coefficients of determination (R^2) of 0.99883293, 0.99915505, and 0.998477398, representing the HVAC scaled cooling capacity at 3.5 tons, 4 tons, and 5 tons, respectively. Therefore, for simplicity, $Q_s[k]$ in Equation (5.10) is replaced by Equations (6.1)–(6.3) to represent the HVAC scaled cooling capacity at 3.5 tons, 4 tons, and 5 tons in the simulation, respectively.

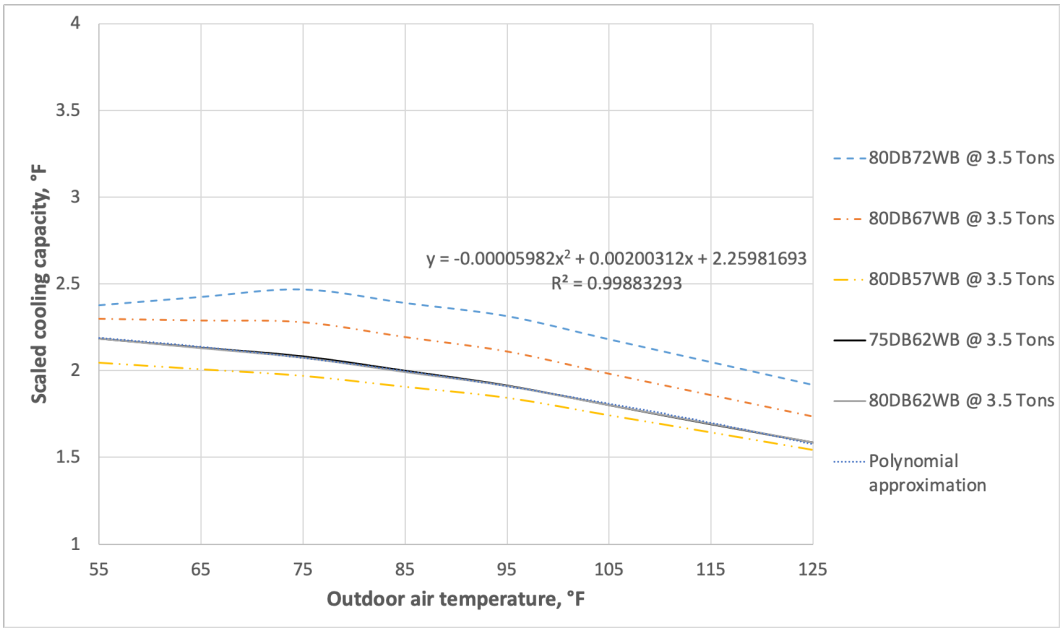
Scaled cooling capacity, °F
Outdoor air temperature, °F
y = -0.00005982x² + 0.00200312x + 2.25981693
R² = 0.99883293
80DB72WB @ 3.5 Tons
80DB67WB @ 3.5 Tons
80DB57WB @ 3.5 Tons
75DB62WB @ 3.5 Tons
80DB62WB @ 3.5 Tons
Polynomial approximation

(a)

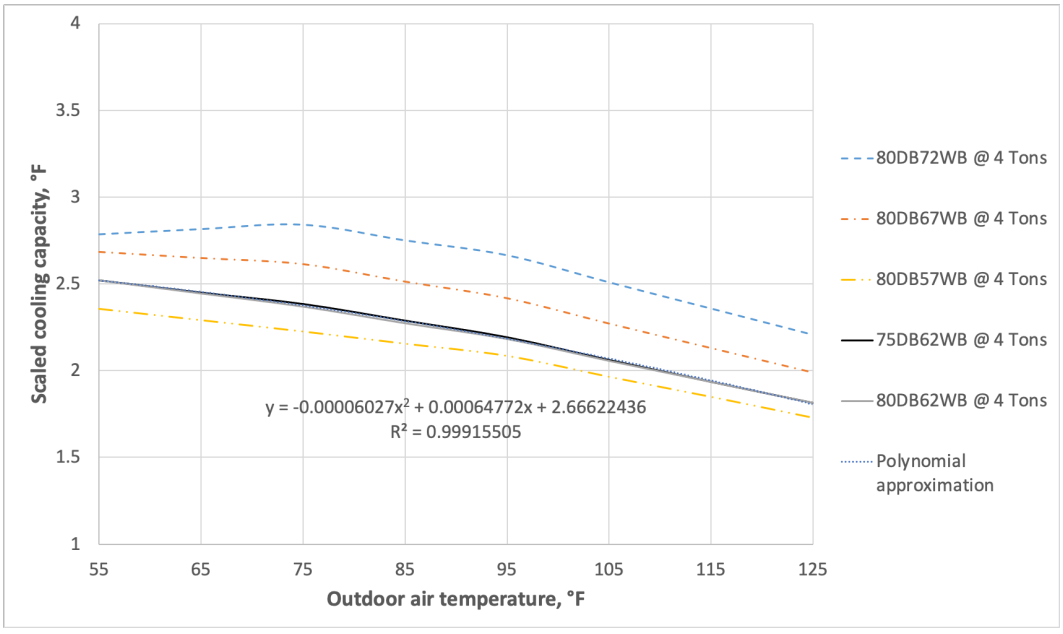
Scaled cooling capacity, °F
Outdoor air temperature, °F
y = -0.00006027x² + 0.00064772x + 2.66622436
R² = 0.99915505
80DB72WB @ 4 Tons
80DB67WB @ 4 Tons
80DB57WB @ 4 Tons
75DB62WB @ 4 Tons
80DB62WB @ 4 Tons
Polynomial approximation

(b)

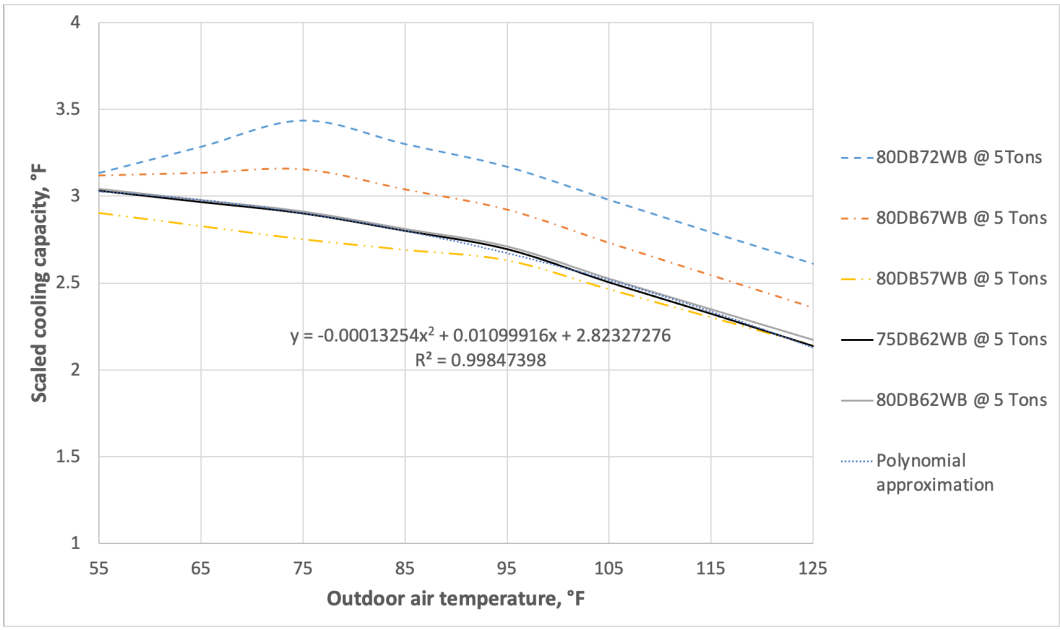

(c)

Figure 6.2. HVAC system scaled cooling capacity versus outdoor air temperature for different indoor DB and WB temperatures in different units: (a) 3.5 tons; (b) 4 tons; and (c) 5 tons.

6.1.3 Determine HVAC system total power use for different units

Similar to the method used in Section 6.1.2, to investigate how the HVAC system total power use, $E[k]$, in Equation (5.14) varies with weather conditions, power data from the same HVAC manufacturer were used. Figure 6.3 shows the relationships between the HVAC total power use $E[k]$ and outdoor air temperature $T_o[k]$ for five different indoor DB and WB temperatures from different cooling capacity HVAC units. As observed, these relationships are insensitive to changes in the indoor DB and WB temperatures. Moreover, these relationships may be accurately approximated by second-order polynomials,

$$E[k] = 0.00019940T_o^2[k] - 0.00353571T_o[k] + 1.96209821 \quad (6.4)$$

$$E[k] = 0.00023631T_o^2[k] - 0.00500000T_o[k] + 2.26308036 \quad (6.5)$$

$$E[k] = 0.00029583T_o^2[k] - 0.00678571T_o[k] + 2.71790179 \quad (6.6)$$

with coefficients of determination (R^2) of 0.99938409, 0.99937370, and 0.99935438, representing the HVAC system total power use at 3.5 tons, 4 tons, and 5 tons, respectively. Therefore, for simplicity, $E[k]$ in Equation (5.14) is replaced by Equations (6.4)–(6.6) to represent the HVAC system total power use at 3.5 tons, 4 tons, and 5 tons in the simulation, respectively.

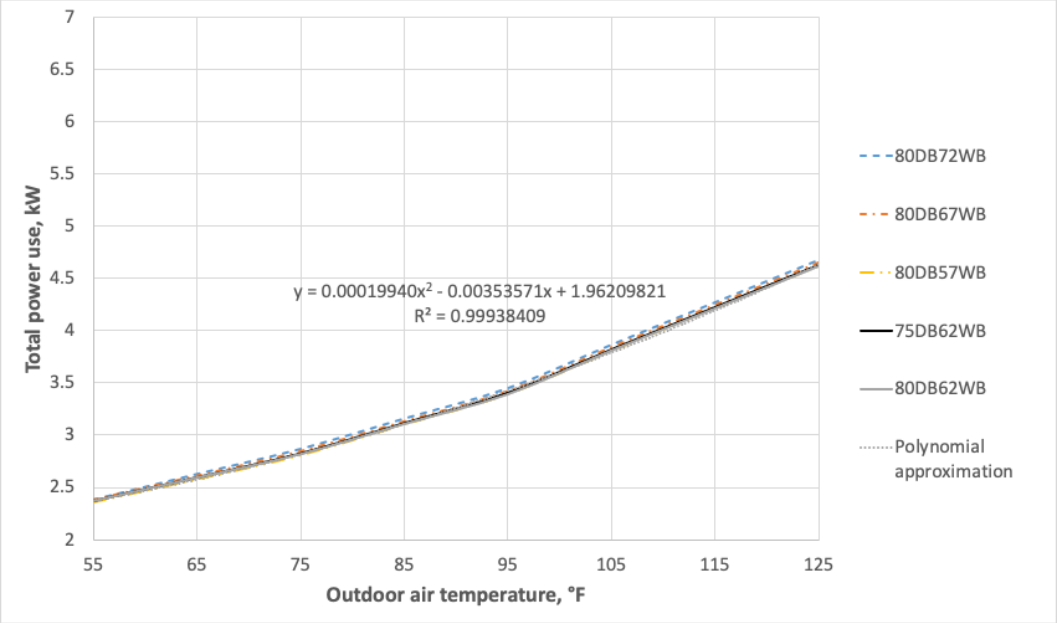

(a)

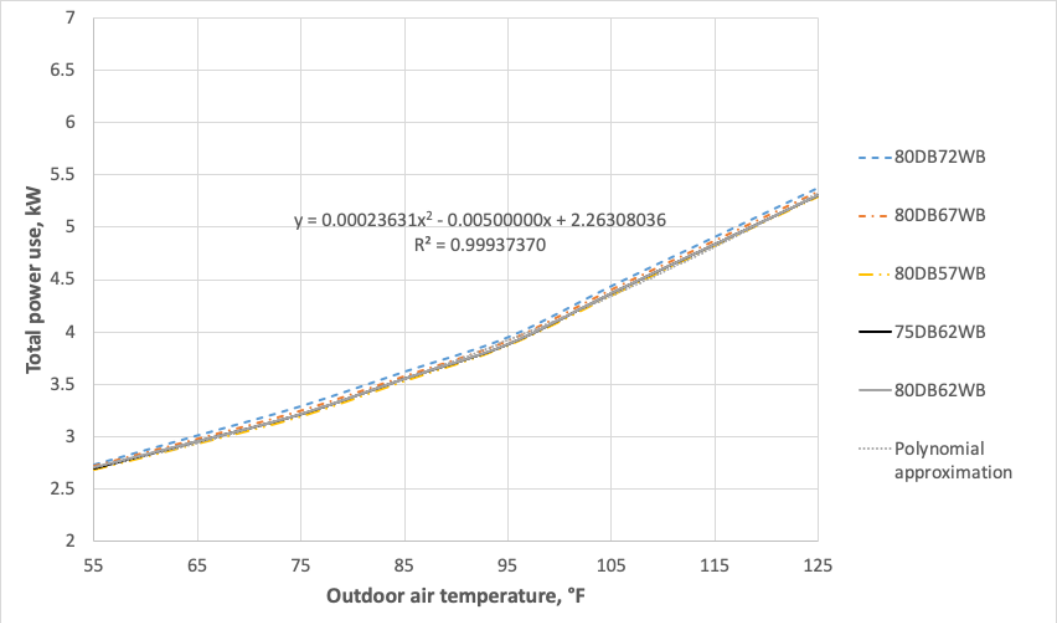
y = 0.00023631x² - 0.00500000x + 2.26308036
R² = 0.99937370
Total power use, kW
Outdoor air temperature, °F
80DB72WB
80DB67WB
80DB57WB
75DB62WB
80DB62WB
Polynomial approximation

(b)

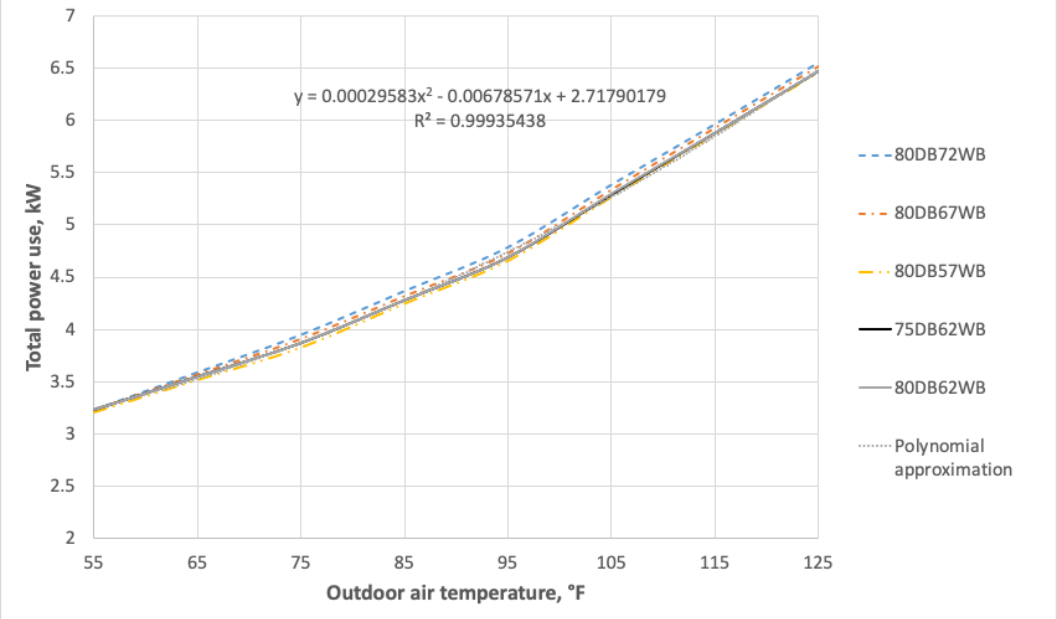
y = 0.00029583x² - 0.00678571x + 2.71790179
R² = 0.99935438
Total power use, kW
Outdoor air temperature, °F
80DB72WB
80DB67WB
80DB57WB
75DB62WB
80DB62WB
Polynomial approximation

(c)

Figure 6.3. HVAC total power use versus outdoor air temperature for different indoor DB and WB temperatures in different units: (a) 3.5 tons; (b) 4 tons; and (c) 5 tons.

6.1.4 Selection of different weather conditions

To investigate the performance of the optimal pre-cooling strategy under different weather conditions, three typical summer days, i.e., July 16, July 20, and August 2, 2018, were adopted to represent a medium hot summer, the hottest summer day, and a cool summer day, respectively, in Norman, Oklahoma. Their outdoor temperature profiles are shown in Figure 6.4. The profiles of wind speed and solar radiation can be found in Figures B.4–B.6 in the **Appendix B**. As observed in the figure, $T_o[k]$ varied between 75.5 ºF and 95.5 ºF on July 16, between 77.2 ºF and 108.3 ºF on July 20, and between 66.2 ºF and 90.5 ºF on August 2.

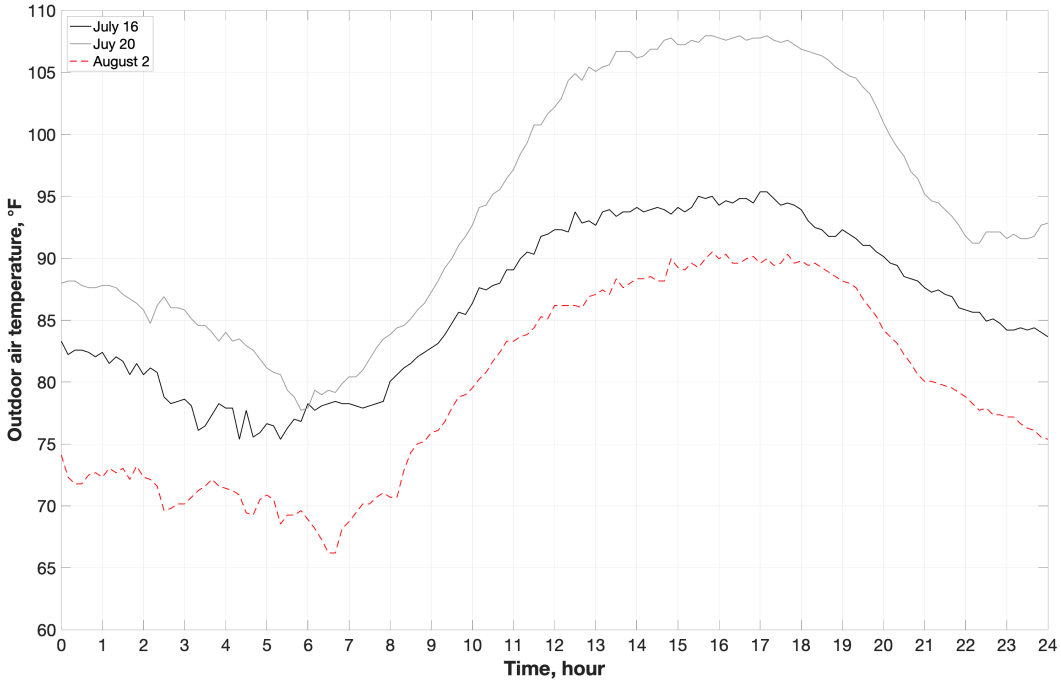

Figure 6.4. Profile of the outdoor temperature for the three summer days.

6.1.5 Selection of different lower and upper bounds and utility rate structures

As introduced in Section 5.3.2, 70 °F and 79 °F were selected as the lower bound T_{lb} and upper bound T_{ub} of the indoor air temperature $T_{in}[k]$ in Equation (5.17), respectively, following the ANSI/ASHRAE Standard 55 (2017), in the simulation. If no optimal solution is found, the lower bound at 70 °F will keep same while the upper bound will be released to 83 °F for the purpose of comparison and analysis. In addition, three TOD utility rate structures, referred to RI, RII, and RIII, that define the 24-hour electricity price $P[k]$ in Equation (5.14) are provided from a utility supplier in the state of California, which were selected to investigate the impact of different time periods and rates of off-peak, mid-peak, and on-peak hours on different pre-cooling strategies, respectively. The profiles of

the three TOD utility rate structures are shown in Figure 6.5, from which it can be seen that RI has on-peak hours from 16:00 to 21:00 and its on-peak electricity price of $0.42/kWh is much higher than its off-peak counterpart of $0.24/kWh. Compared with RI, RII and III have the same on-peak hours, but different from the mid-peak hours. RII has it on-peak electricity price of $0.43/kWh compared with its off-peak price of $0.23/kWh and mid-peak price of $0.19/kWh, while RIII has the electricity prices of $0.31/kWh, $0.22/kWh, and $0.30/kWh for on-peak, off-peak, and mid-peak hours, respectively.

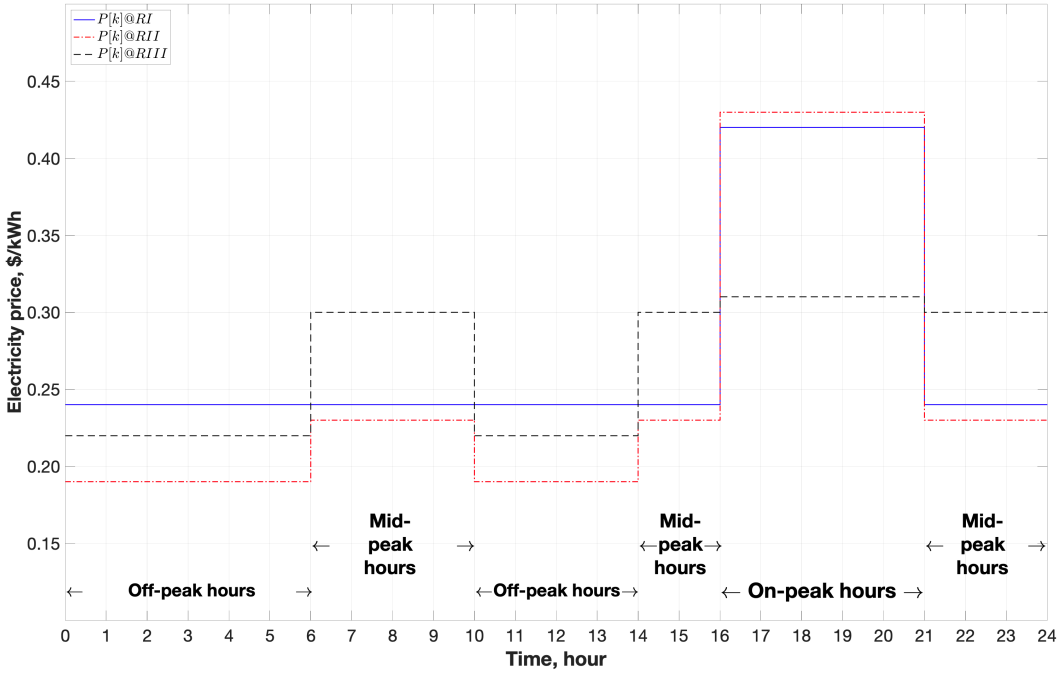

Figure 6.5. Profiles of three TOD utility rate structures from a utility supplier.

6.2 Operation Performance Analysis

This section presents a comparison of simulation results for operation performance analysis by using different sets of home thermal properties, HVAC

cooling capacities, and weather conditions in the presence of different TOD utility rate structure data. More specifically, the comparison of the operation performance by different home thermal properties and HVAC cooling capacities is conducted in Section 6.2.1 and 6.2.2. Then the comparison of the operation performance by different weather conditions and utility rate structures is carried out in Section 6.2.3 and 6.2.4. Finally, the comparison of the operation performance with a rule-based pre-cooling strategy is stated and analyzed in Section 6.2.5.

Based on the simulation setup described in Section 6.1, a 24-hour simulation with a sampling period Δt of 10 minutes was carried out for different sets of home thermal properties, HVAC cooling capacities, and weather conditions in the presence of different time-of-day utility rate structure data. The simulation utilized weather data from three summer days on July 16, July 20, and August 2, 2018, representing a medium hot summer day, the hottest summer day, and a cool summer day, respectively, in Norman, Oklahoma. Tau (i.e., τ_1) values of 2000, 3500, and 5000 were selected to represent a home with poor, medium, and good thermal conditions, respectively. Moreover, the 3.5, 4, and 5 tons of HVAC unit, referred to CC=3.5, 4, and 5, were selected to represent different cooling capacities and three utility rate structures, i.e., RI, RII, and RIII, were selected to represent different profiles of utility rates in the state of California.

In addition, Figures 6.6–6.15 show the simulation results of the optimal pre-cooling strategy when considering different home thermal properties, HVAC

cooling capacities, weather conditions, and utility rate structures. Each figure includes three graphics. On the bottom graphic, the black, red, and blue solid curves represent the HVAC on/off control signals $u_s[k]$ under different conditions; on the top and middle graphics, the black curve with point markers, red curve, and blue curve with cross markers represent the resulting indoor air temperatures $T_{in}[k]$ and interior wall surface temperatures $T_{ie}[k]$, and the magenta dashed and purple dash-dot curves represent the upper bound T_{ub} and lower bound T_{lb} at Tau=2000, 3500, and 5000, respectively. In addition, Figure 6.17 shows the comparison of the simulation results of the optimal pre-cooling strategy with a rule-based pre-cooling strategy based on the same thermal properties, cooling capacity, and weather condition but different from the utility rate structures, where the gray solid curves represent the resulting $T_{in}[k]$ and $u_s[k]$ of a rule-based pre-cooling operation for each graphic of the figure.

6.2.1 Comparison of the performance by different home thermal properties

For HVAC operations on July 16 (the medium hot summer day), shown in Figure 6.6, the three graphics at the bottom of the figure indicate that the optimal pre-cooling strategy results in completely avoiding HVAC operations during on-peak hours for the medium and good thermal condition homes (Tau=3500 and 5000), except for the poor thermal condition home (Tau=2000), taking advantage of low electricity rates during off-peak hours. For the medium and good thermal condition homes (Tau=3500 and 5000), the HVAC system was turned on in the very early morning and cooled down $T_{in}[k]$ first, taking advantage of lower utility

rate by pre-cooling before on-peak hours. The higher HVAC efficiency produced by the cooler outdoor air enabled the HVAC system to run more economically and allowed $T_{in}[k]$ floating during on-peak hours. For the poor thermal condition home, the HVAC system was on at 3:30 and almost ran for the rest of day and cannot avoid the on-peak hours. More specifically, the HVAC system started pre-cooling at 3:30, 0:00, and 0:10 and ran a total of 11 hours and 10 minutes, 15 hours and 40 minutes, and 13 hours and 20 minutes, respectively, before on-peak hours for different thermal condition homes. The resulting lowest pre-cooling temperature $T_{in}[k]$ was reached at 74.85 °F, 73.20 °F, and 73.25 °F for the Tau values of 2000, 3500, and 5000, respectively. For the home thermal conditions that could avoid the on-peak hours, it appears that the larger the Tau value, the less pre-cooling runtime and temperature drop the system requires.

After on-peak hours, the HVAC system kept on for the rest of day for the poor thermal condition home (Tau=2000). On the contrary, for the medium and good thermal condition homes (Tau=3500 and 5000), the HVAC system was able to completely turn off to allow $T_{in}[k]$ to approach T_{ub} as much as possible at nighttime to balance between the cost and thermal comfort. The peak of $T_{in}[k]$ was reduced and shifted from the afternoon to the night where the system was kept off for the rest of day after on-peak hours. This demonstrates the advantage of a home with good thermal mass. This situation is likely to occur many days per year if $T_o[k]$ is not too high and the envelope is in a good thermal condition.

In addition, these observations are in line with expectations: 1) The optimal pre-cooling operation could delay heat transfer and attenuate/shift peak load from the late afternoon to the nighttime after on-peak hours; 2) the envelope with good thermal condition has a shorter pre-cooling runtime and the corresponding HVAC system has a earier pre-cooling start time with lower $T_o[k]$ and better HVAC efficiency and therefore correspondingly leads to lower energy cost for optimization; and 3) the optimal operation is adaptive for different home thermal properties.

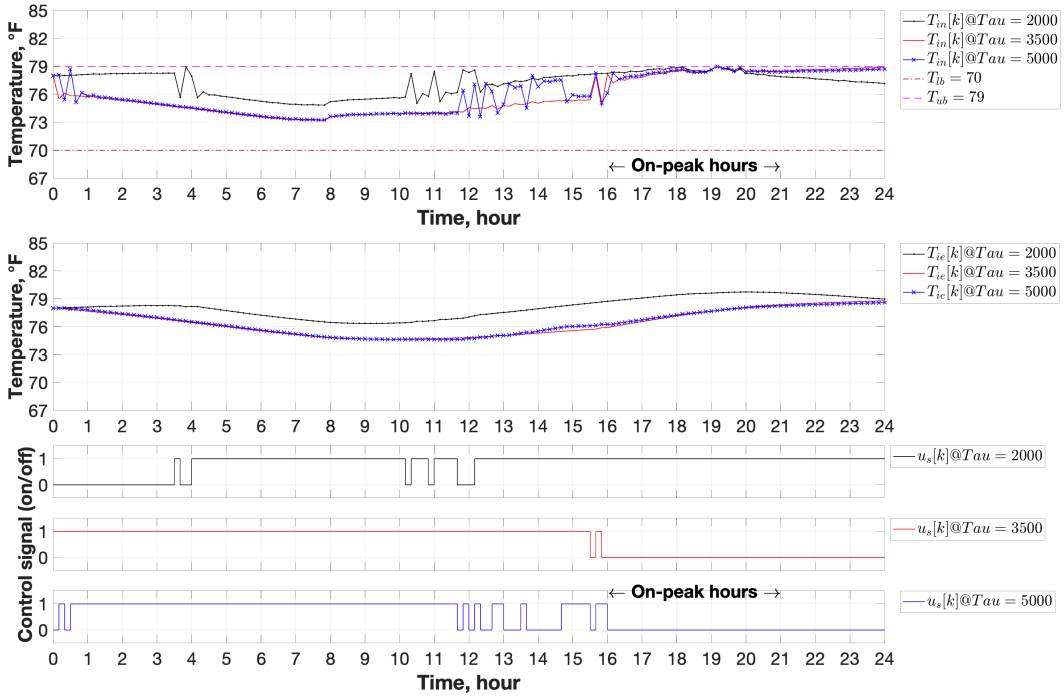

Figure 6.6. Fluctuations of the temperature and operation control signals for different thermal properties based on the 3.5-ton unit and RI on July 16 (a medium hot summer day).

6.2.2 Comparison of the performance by different HVAC cooling capacities

To investigate how the impact of different HVAC cooling capacities on the performance of the optimal pre-cooling operation, the simulation results that use the HVAC cooling capacity of 3.5, 4, and 5 tons, i.e., CC=3.5, 4, and 5, on July 16 are shown in Figure 6.7. Moreover, the impact of different cooling capacities on the optimal pre-cooling operation was further investigated based on different thermal condition homes as shown in Figures 6.8 and 6.9. As these figures show that different behaviors in control signals and indoor air temperatures were observed for the operations.

For operations in the poor thermal condition home (Tau=2000), shown in Figure 6.7, the HVAC system was completely on during on-peak hours for CC=3.5 and 4, while the system was off for most of time for CC=5. Therefore, the results showed that the operation for CC=5 had a much earlier pre-cooling start time, more pre-cooling runtime, a lower pre-cooling temperature $T_{in}[k]$ that can be reached, and a quicker pre-cooling temperature drop, compared to the operations for CC=3.5 and 4. More specifically, the HVAC system had the pre-cooling starting at 3:30, 5:20, and 0:00 and running a total of 11 hours and 10 minutes, 8 hours and 30 minutes, and 15 hours and 50 minutes before on-peak hours for CC=3.5, 4, and 5, respectively. The resulting lowest pre-cooling temperature $T_{in}[k]$ was reached at 74.85 °F, 74.74 °F, and 71.03 °F for each cooling capacity, respectively. Similar patterns were observed for the corresponding wall interior surface temperature $T_{ie}[k]$. Moreover, the resulting

pre-cooling temperature $T_{in}[k]$ for the cooling capacity of 5 tons was maintained to approach T_{lb} as much as possible before on-peak hours to lower the energy cost while maintaining required thermal comfort.

After on-peak hours, the HVAC system was turned on for the entire 8 hours for the cooling capacities of 3.5 and 4 tons, while the system was only on two times for 40 minutes for the cooling capacity of 5 tons, to keep $T_{in}[k]$ slightly below T_{ub} to maintain thermal comfort. These results showed that cooling capacity of 5 tons had much impact on the performance of the pre-cooling operations compared with the ones of 3.5 and 4 tons. Note that the system still cannot completely avoid the on-peak hours even with a 5-ton cooling capacity.

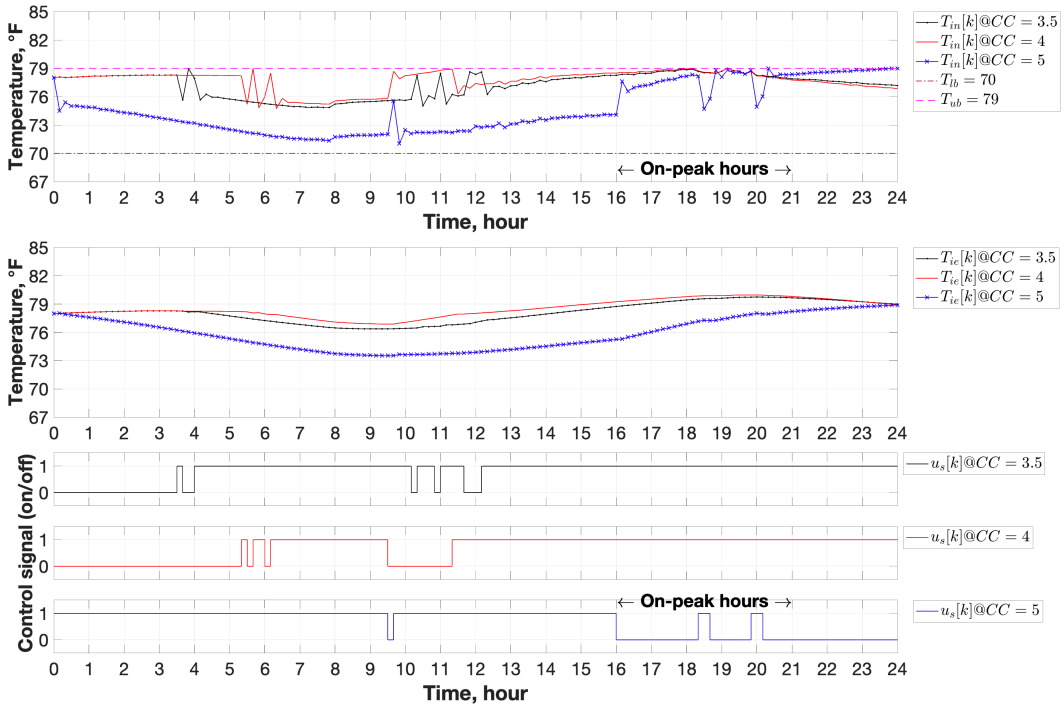

Figure 6.7. Fluctuations of the temperature and operation control signals for different cooling capacities based on Tau=2000 and RI on July 16 (a medium hot summer day).

For the operations in medium and good thermal condition homes (Tau=3500 and 5000), shown in Figures 6.8 and 6.9, the optimal pre-cooling can completely avoid HVAC operations during on-peak hours for all the cooling capacities. Compared with the corresponding operations at Tau=2000, the system had an earlier pre-cooling start time, longer pre-cooling runtime, and a lower pre-cooling temperature $T_{in}[k]$ that can be reached for cooling capacities of 3.5 and 4 tons due to no operations during the on-peak hours, while the system had a later pre-cooling start time, shorter pre-cooling runtime, and a higher pre-cooling temperature $T_{in}[k]$ for cooling capacity of 5 tons due to a relatively better home thermal condition (Tau=3500). These patterns were more obvious for the good home thermal condition (Tau=5000). More specifically, the optimal pre-cooling is also adaptive for different cooling capacities, i.e., the HVAC system had the pre-cooling starting at 0:00, 1:30, and 2:30 and running a total of 15 hours and 40 minutes, 13 hours and 30 minutes, and 11 hours, respectively, before on-peak hours for different cooling capacities at Tau=3500, while the system had the pre-cooling starting at 0:10, 0:40, and 2:00 and running a total of 13 hours and 20 minutes, 11 hours and 40 minutes, and 9 hours and 30 minutes at Tau=5000. The resulting lowest pre-cooling temperature $T_{in}[k]$ was reached at 73.20 °F, 73.03 °F, and 71.83 °F for the medium thermal condition home (Tau=3500), compared

with the corresponding ones at 73.25 °F, 72.73 °F, and 72.14 °F for the good thermal condition home (Tau=5000). The operation for cooling capacity of 5 tons had the lowest $T_{in}[k]$ due to its better cooling performance, compared to the operations for cooling capacities of 3.5 and 4 tons. After on-peak hours, the HVAC system was switched off for all the cooling capacities to keep $T_{in}[k]$ slightly below T_{ub} to maintain thermal comfort.

These results demonstrate that HVAC cooling capacity had a major impact on the performance of optimal pre-cooling operations only when the system had a better cooling capacity and accommodates with a medium or good thermal condition home since the HVAC runtimes were significantly reduced.

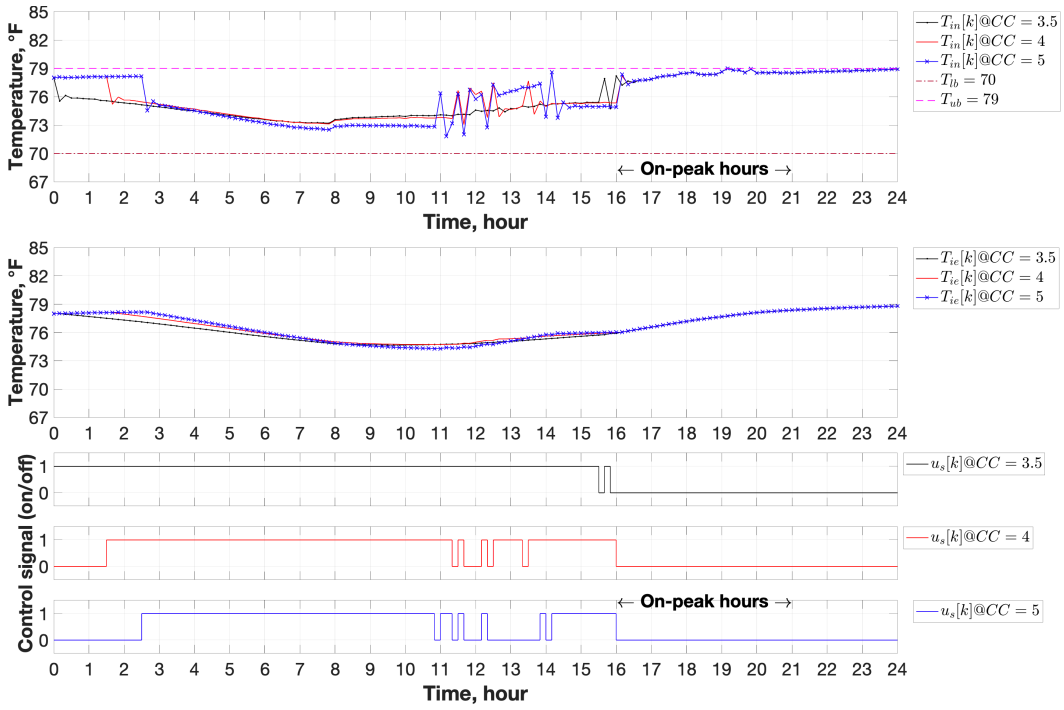

Figure 6.8. Fluctuations of the temperature and operation control signals for different cooling capacities based on Tau=3500 and RI on July 16 (a medium hot summer day).

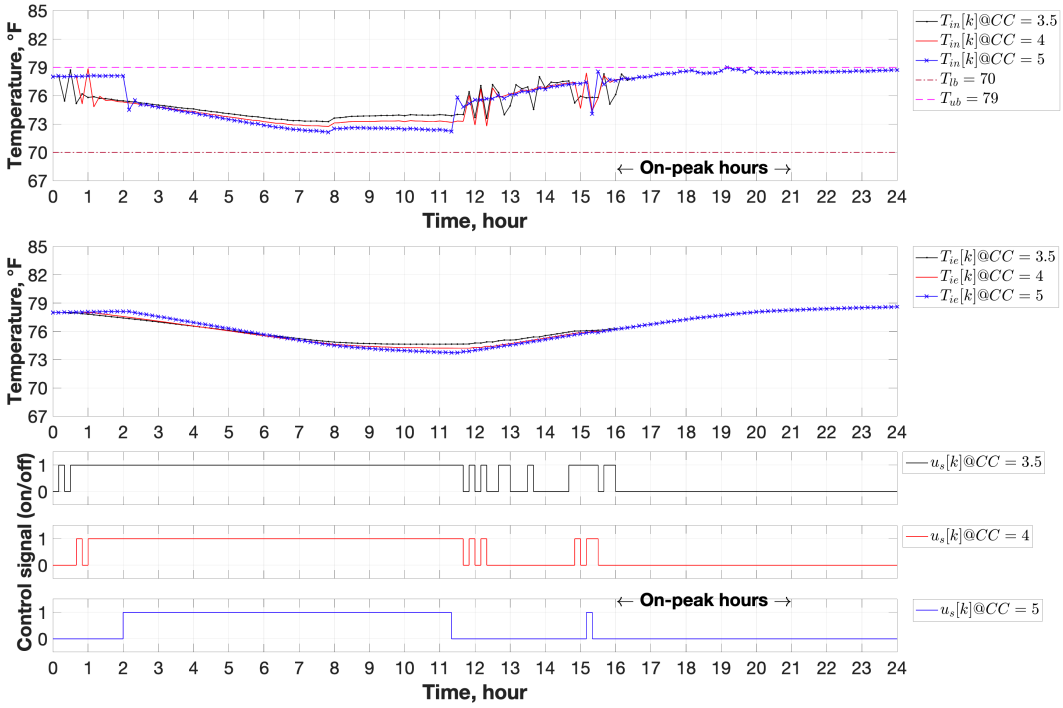

Figure 6.9. Fluctuations of the temperature and operation control signals for different cooling capacities based on Tau=5000 and RI on July 16 (a medium hot summer day).

6.2.3 Comparison of the performance by different weather conditions

To investigate how the impact of different weather conditions on the performance of the optimal pre-cooling operation, the simulation results on July16, July 20, and August 2, representing a medium hot summer day, the hottest summer day, and a cool summer day, respectively, are shown in Figure 6.10, based on the poor thermal condition home (Tau=2000) with HVAC cooling

capacity of 4 tons. Moreover, the weather impact was further investigated with different thermal condition homes under the same cooling capacity of 4 tons and simulation results are shown in Figures 6.11 and 6.12.

For the operations in the poor thermal condition home (Tau=2000), shown in Figure 6.10, the HVAC system could only avoid operations during on-peak hours for the cool summer day (August 2). Note that no optimal result was found when keeping the upper bound of thermal comfort at 79 °F for the operation on the hottest summer day (July 20), where the system still cannot avoid operations during on-peak hours even though the upper bound was released to 83 °F for display purpose. For the operations on July 16, the system cannot avoid the on-peak operations but ran less time and meanwhile maintained the thermal comfort, compared with the operations on July 20. In terms of the operations on August 2, the HVAC system had the pre-cooling starting at 4:40 and running a total of 9 hours before on-peak hours and the resulting lowest pre-cooling temperature $T_{in}[k]$ was reached at 72.48 °F.

After on-peak hours, the HVAC system was kept on continually for the rest of time on July 16 and 20, while the system was completely off to take advantage of T_{ub} as much as possible to lower the energy cost while maintaining required thermal comfort on August 2. These results showed that weather conditions had significant impact on the performance of the pre-cooling operations. Even with optimal pre-cooling operations, the system still cannot completely avoid on-peak hours, especially for operations with the worst thermal

condition home but under much hotter outdoor temperatures. Indeed, the weather had a significant impact on the performance of optimal pre-cooling operations.

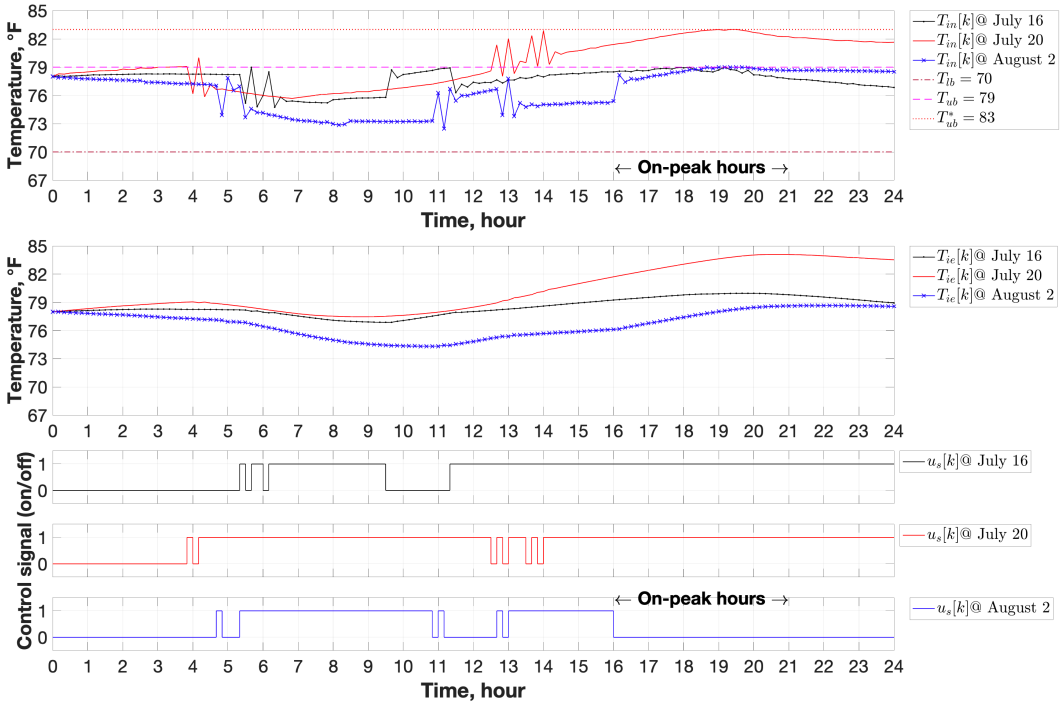

Note: The upper bound was released to 83 °F for the operation on July 20, as represented by T^*_{ub}.

Figure 6.10. Fluctuations of the temperature and operation control signals for different weather conditions based on Tau=2000, CC=4, and RI.

For the operations in the medium and good thermal condition homes (Tau=3500 and 5000), shown in Figures 6.11 and 6.12, the HVAC system can maintain the required thermal comfort for all the days. Moreover, the system can completely avoid HVAC operations during on-peak hours on July 16 and August 2, on which the system had an earlier pre-cooling start time and lower pre-cooling temperature $T_{in}[k]$ that can be reached compared to the operations for the poor

thermal condition home (Tau=2000). More specifically, the optimal pre-cooling was also adaptive for weather conditions, i.e., the HVAC system had the pre-cooling starting at 1:30, 1:30, and 2:30 and running a total of 13 hours and 30 minutes, 14 hours and 20 minutes, and 7 hours and 40 minutes, before on-peak hours for the medium thermal condition home, compared to the corresponding pre-cooling operations starting at 0:40, 0:00, and 2:30 and running a total of 11 hours and 40 minutes, 15 hours and 40 minutes, and 7 hours, respectively. The resulting lowest pre-cooling temperature $T_{in}[k]$ was reached at 73.03 °F, 74.12 °F, and 72.30 °F for the medium thermal condition home (Tau=3500), while $T_{in}[k]$ was reached at 72.73 °F, 73.25 °F, and 72.69 °F for the good thermal condition home (Tau=5000), respectively. For all the thermal condition homes, the operations on August 2 had the lowest $T_{in}[k]$ due to its relatively cooler outdoor temperature, compared to the operations on July 16 and 20.

After on-peak hours, the HVAC system was completely off for the operations on July 16 and August 2 to keep $T_{in}[k]$ slightly below T_{ub} to maintain thermal comfort, while the system was kept on for the rest of time for the medium thermal condition home (Tau=3500) and switched on for two time for a total of 4 hours and 10 minutes for the good thermal condition home (Tau=5000). Additionally, for a cooler summer day, the total of HVAC total runtimes was significantly shorter than a medium and hotter day. These results further demonstrated that weather conditions had a significant impact on the performance of optimal pre-cooling operations.

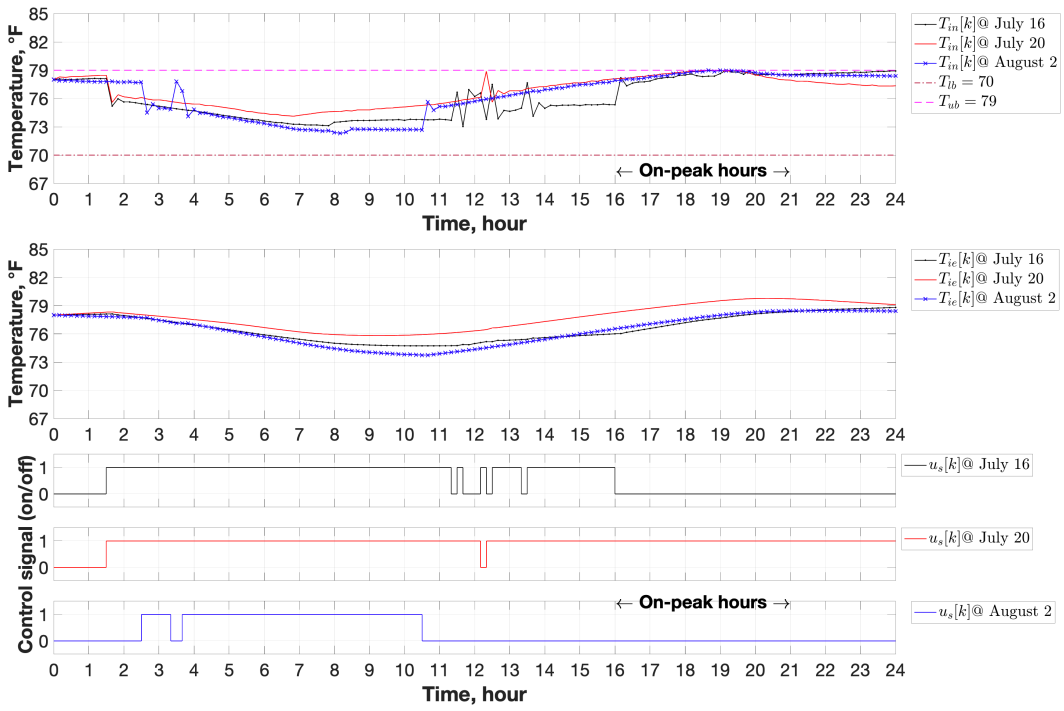

Figure 6.11. Fluctuations of the temperature and operation control signals for different weather conditions based on Tau=3500, CC=4, and RI.

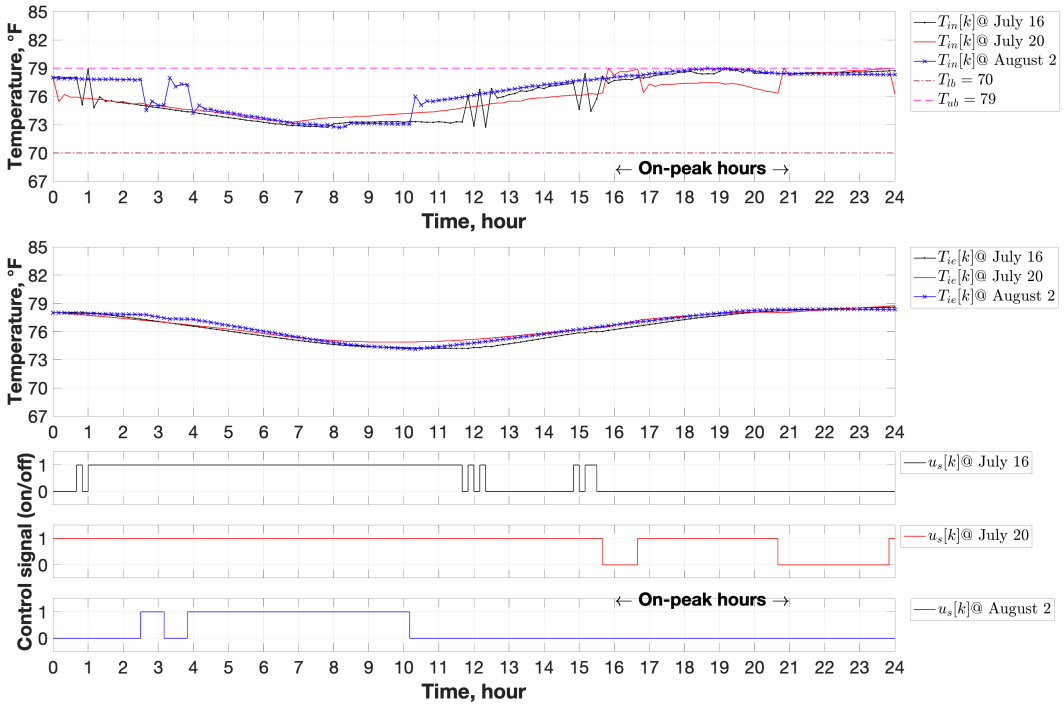

Figure 6.12. Fluctuations of the temperature and operation control signals for different weather conditions based on Tau=5000, CC=4, and RI.

6.2.4 Comparison of the performance by different utility rate structures

To investigate how the impact of different utility rate structures on the performance of the optimal pre-cooling operation, the simulation results are shown in Figure 6.13, which utilize the three utility rate structures, i.e., RI, RII, and RIII, cooling capacity of 4 tons, and weather data on August 2. Moreover, the impact of different utility rate structures on the optimal pre-cooling operation was further investigated in combination with different thermal condition homes as shown in Figures 6.14 and 6.15.

For the operations in the poor thermal condition home (Tau=2000), shown in Figure 6.13, the HVAC system was completely off during on-peak hours and continually kept off after on-peak hours to keep $T_{in}[k]$ slightly below T_{ub} to maintain thermal comfort for all the operations with RI, RII, and RIII. Unlike the system with RI that had no mid-peak hours and was completely on during these hours, the system with RII and RIII tried to avoid operations as less as possible during the mid-peak hours. In terms of the operations with RII and RIII, the system with RII cannot completely keep off for both the first mid-peak hours from 6:00 to 10:00 and the second mid-peak hours from 14:00 to 16:00, while the system with RIII was able to be completely off during the first mid-peak hours but cannot completely avoid the second mid-peak hours. Moreover, the system with RIII ran less time than the system with RII during mid-peak hours due to the mid-

peak electricity price of RIII is higher than the one of RII. Hence, the pre-cooling operation of RIII required to start earlier than the operation with RII.

More specifically, the optimal pre-cooling operation was also adaptive to different utility rate structures, i.e., the HVAC system had the pre-cooling starting at 4:40, 2:10, and 0:20 and running a total of 9 hours, 9 hours and 30 minutes, and 9 hours and 50 minutes before on-peak hours for RI, RII, and RIII, respectively. The resulting lowest pre-cooling temperature $T_{in}[k]$ was reached at 72.48 °F, 71.07 °F, and 71.87 °F for each utility rate structure, respectively. Similar patterns were observed for the corresponding wall interior surface temperature $T_{ie}[k]$ that droped slowly due to the thermal mass of wall was much larger than space air. Moreover, the resulting pre-cooling temperature $T_{in}[k]$ for the operations with RII and RIII were decreased as much as possible even before the mid-peak hours from 6:00 to 10:00 to balance the operation periods under a higher HVAC efficiency and lower electricity cost while minimizing the energy cost and maintaining required thermal comfort.

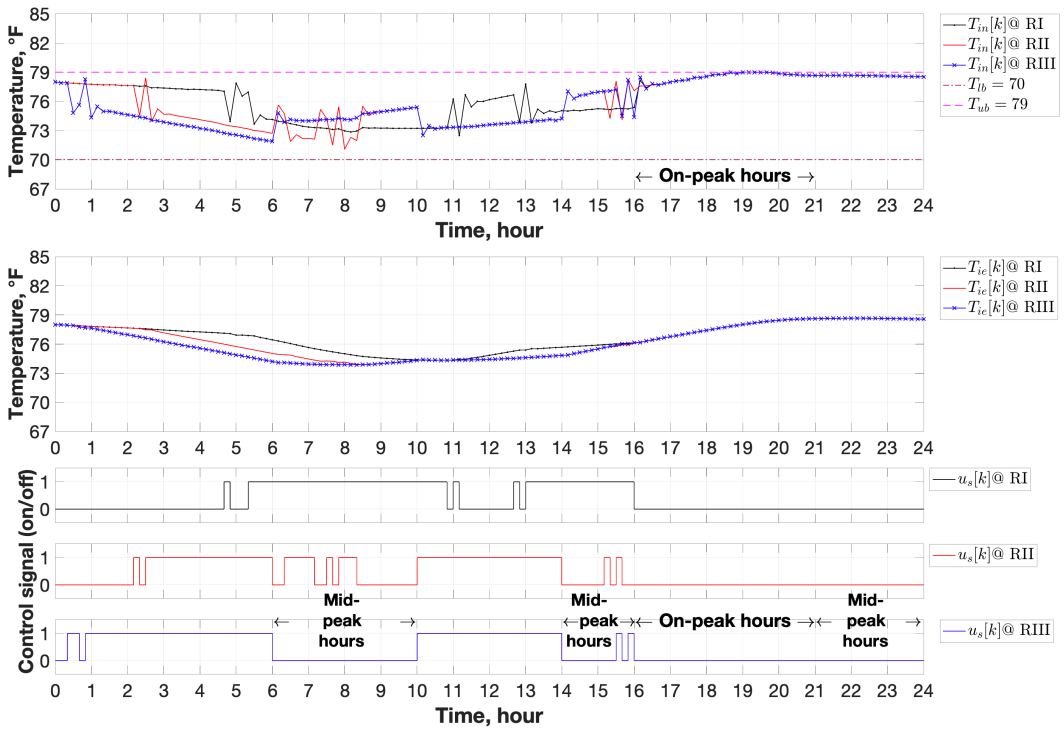

Figure 6.13. Fluctuations of the temperature and operation control signals for different utility rate structures based on Tau=2000 and CC=4 on August 2 (a cool summer day).

Similar to the operations in the poor thermal condition home (Tau=2000), for the operations in the medium and good thermal condition homes (Tau=3500 and 5000), shown in Figures 6.14 and 6.15, the HVAC system also can completely switch off during on-peak hours and continually keep off after on-peak hours to keep $T_{in}[k]$ slightly below T_{ub} to maintain thermal comfort for all the operations with RI, RII, and RIII. Unlike the operations in the poor thermal condition home, the system had an earlier pre-cooling starting time and less pre-cooling runtime for RI and meanwhile can completely avoid all the mid-peak

hours for RII and RIII in the medium and good thermal condition homes. Additionally, the system operations and temperature dynamics with RII and RIII kept same for the medium and good thermal condition homes.

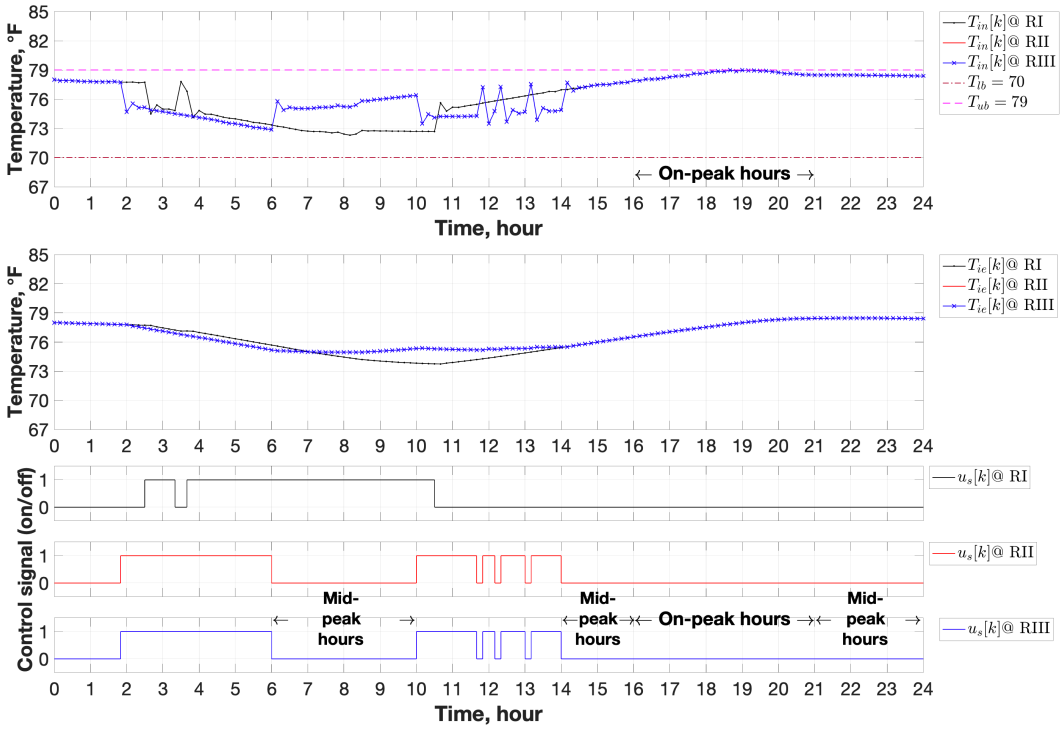

Note: the temperature curves for RII and RIII are overlapped.

Figure 6.14. Fluctuations of the temperature and operation control signals for different utility rate structures based on Tau=3500 and CC=4 on August 2 (a cool summer day).

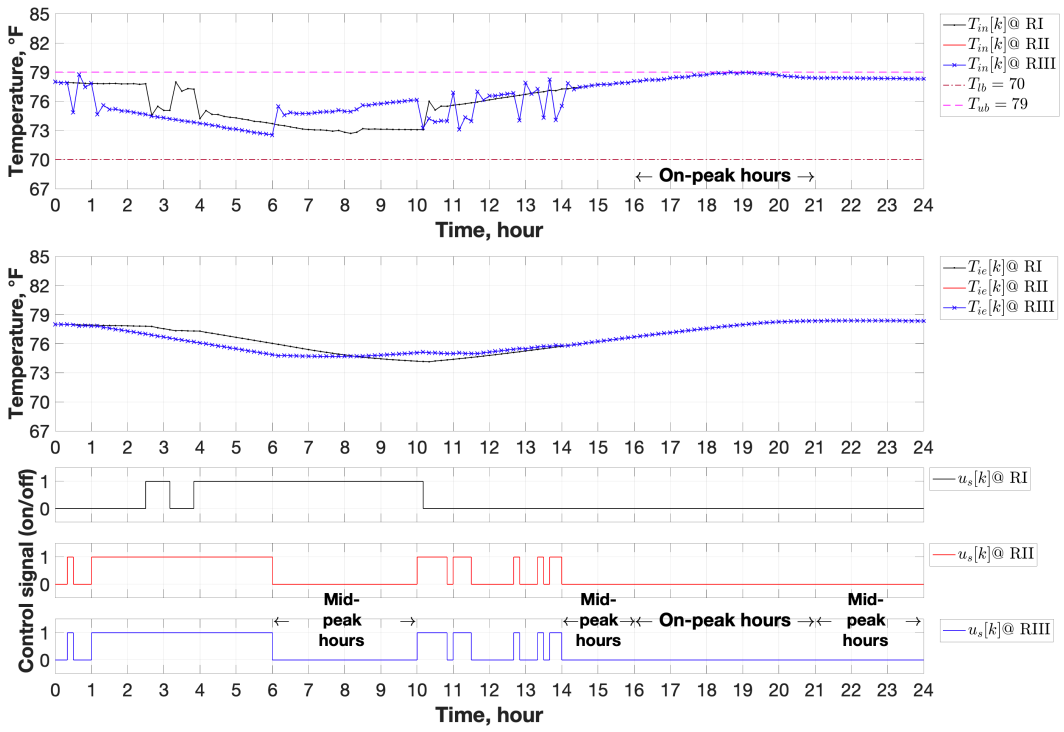

Note: the temperature curves for RII and RIII are overlapped.

Figure 6.15. Fluctuations of the temperature and operation control signals for different utility rate structures based on Tau=5000 and CC=4 on August 2 (a cool summer day).

6.2.5 Comparison of the performance with a rule-base pre-cooling strategy

The performance of the optimal pre-cooling strategy was further investigated and compared with a rule-based pre-cooling strategy, i.e., BC II as descried in Chapter 5, with pre-cooling starting at 9:00 and lasting 6 hours. Because this rule-based pre-cooling strategy showed advantage of energy savings compared with other rule-based operation strategies. Therefore, this rule-based pre-cooling strategy was adopted as base case, referred to BC, for comparison with the optimal pre-cooling strategy in this section. To accommodate with the

three utility rate structures with on-peak hours from 16:00 to 21:00, the rule-based pre-cooling start time was moved forward by one hour, starting at 10:00 and lasting the same 6 hours. The profile of the rule-base pre-cooling strategy is shown in Figure 6.16.

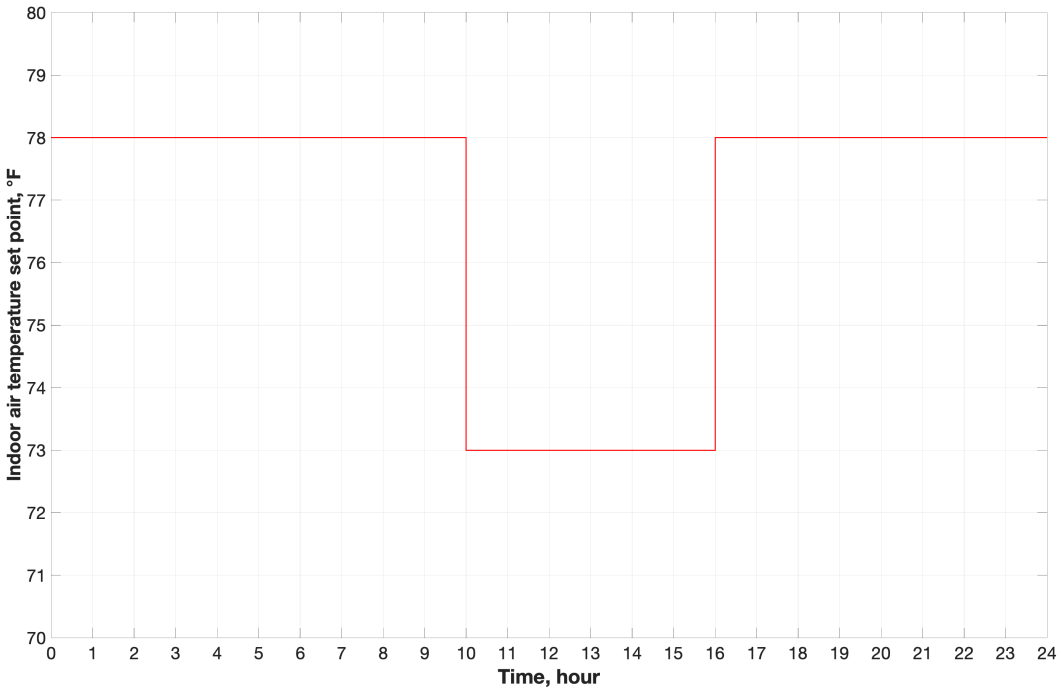

Figure 6.16. Profile of the indoor air temperature set point for the rule-based pre-cooling strategy.

The simulation utilized the same thermal condition home (Tau=3500), cooling capacity of 4 tons, and weather data on July 16, but different from the utility rate structures. Since the rule-based pre-cooling strategy is not adaptive to different utility rate structures, this study just shows the simulation result of the rule-based pre-cooling operation utilizing one of the three utility rate structure profiles (e.g., RI).

Figure 6.17 shows the comparison of the simulation results of the optimal pre-cooling with the rule-based pre-cooling strategy. For the rule-based pre-cooling operation (BC), the HVAC system cannot maintain the thermal comfort in some time periods before and after on-peak hours. The system was almost on during most of the on-peak hours and switched on/off frequency after on-peak hours. Moreover, the rule-based strategy did not enable the HVAC system to run more economically with higher HVAC efficiency produced by the cooler outdoor air in the early morning. In terms of the optimal pre-cooling operations, the system can completely avoid operations with RI and RII during on-peak hours, except for the operations with RIII, with which the system was switched on two times for a total of 30 minutes even if RII and RIII shared the same pattern. Because RII had a lower electricity price than RIII during mid-peak hours and meanwhile had much higher electricity price than RIII during on-peak hours. This explained that the system with RIII did not completely avoid operations during on-peak hours but was switched off for one hour during the mid-peak hours from 6:00 to 10:00, compared to the system with RII that only ran 10 minutes during that mid-peak hours and was kept off during on-peak hours. These results further demonstrated that the optimal pre-cooling strategy was adaptive to different utility rate structures. However, the rule-based pre-cooling strategy cannot cope with the ever-changing electricity prices in a smart grid environment.

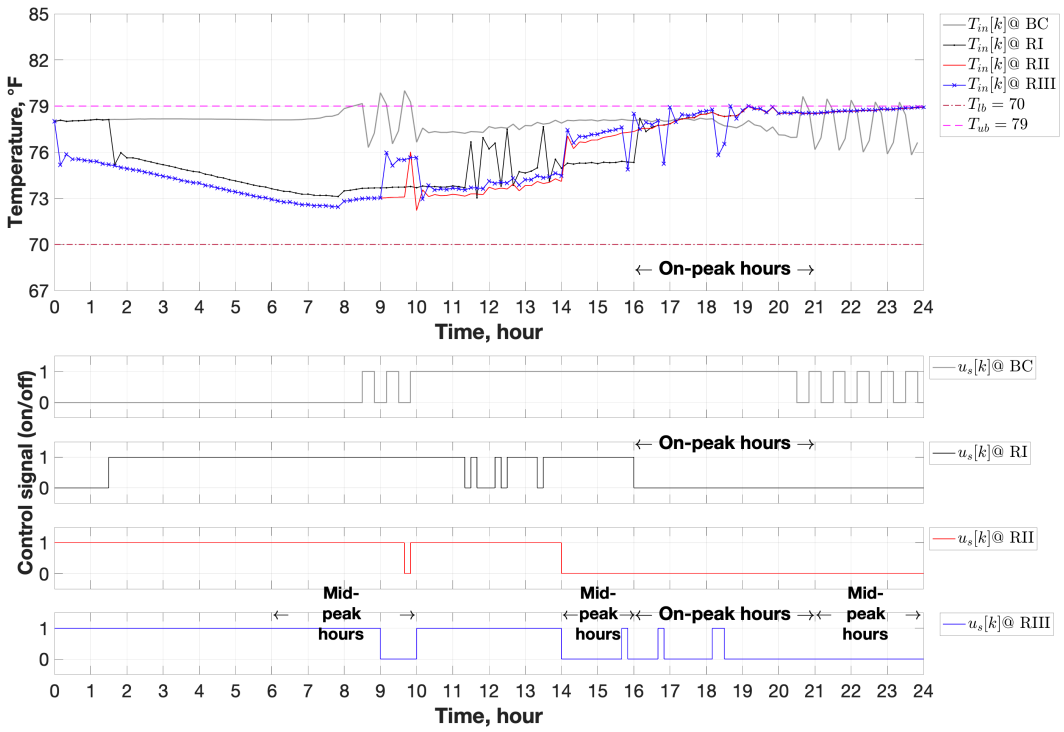

Note: $T_{in}[k]$ @ BC represents the operations with RI, RII, and RIII for BC, which were overlapped.

Figure 6.17. Fluctuations of the temperature and operation control signals for different operation strategies based on Tau=3500 and CC=4 on July 16 (a medium hot summer day).

6.3 Energy Performance Analysis

This section introduces the comparison of energy consumption and cost of the optimal pre-cooling strategy for different thermal properties, weather conditions, cooling capacities, and utility rate structures. The energy performance of the optimal pre-cooling strategy is also compared with the rule-based pre-

cooling strategy based on the same thermal properties, cooling capacity, and weather condition.

6.3.1 Energy consumption comparison

The total energy consumption is defined as $\Delta t \sum_k E[k]u_s[k]$, where k is taken over the whole day. Table 6.2 lists the total energy consumption for the Tau values of 2000, 3500, and 5000, cooling capacities of 3.5, 4, and 5 tons, and three utility rate structures on July 16, July 20, and August 2, respectively. Observe from the table that 1) the operations on July 20 requires the highest total energy consumption than those on July 16 and August 2 when other conditions keep same; 2) the operations with a larger cooling capacity do not always consume more or less energy, which also depend on home thermal condition, utility rate structure, and weather conditions; 3) the better the home thermal condition is, the less energy consumption the system requires; and 4) the selection of a utility rate structure is determined by not only the local weather condition but also the cooling capacity of the HVAC system in a specific thermal condition home for energy saving purpose. These observations are consistent with the analysis in Section 6.2.

Table 6.2. Comparison of total energy consumption for different home thermal properties, cooling capacities, weather conditions, and utility rate structures.

		CC=3.5 tons	CC=4 tons	CC=5 tons

		2000	3500	5000	2000	3500	5000	2000	3500	5000
July 16 High: 95.5 ºF Low: 74.5 ºF	RI	61.39 kWh	48.31 kWh	40.56 kWh	60.66 kWh	47.53 kWh	40.10 kWh	70.53 kWh	46.27 kWh	38.92 kWh
	RII	62.03 kWh	48.31 kWh	41.83 kWh	61.29 kWh	48.14 kWh	41.25 kWh	70.53 kWh	47.76 kWh	40.94 kWh
	RIII	63.10 kWh	47.73 kWh	40.69 kWh	61.29 kWh	47.80 kWh	40.82 kWh	68.60 kWh	47.76 kWh	40.87 kWh
July 20 High: 108.3 ºF Low: 77.2 ºF	RI	78.76* kWh	51.33* kWh	74.03 kWh	76.72* kWh	87.76 kWh	77.40 kWh	74.77* kWh	87.69 kWh	77.41 kWh
	RII	79.56* kWh	51.43* kWh	74.60 kWh	77.59* kWh	88.49 kWh	77.40 kWh	76.82* kWh	95.81 kWh	77.41 kWh

	RIII	79.13* kWh	50.73* kWh	75.30 kWh	78.25* kWh	88.49 kWh	77.24 kWh	76.97* kWh	89.34 kWh	76.11 kWh
August 2 High: 90.7 ºF Low: 65.8 ºF	RI	30.35 kWh	24.26 kWh	22.86 kWh	30.11 kWh	23.97 kWh	21.80 kWh	29.48 kWh	23.43 kWh	21.91 kWh
	RII	31.23 kWh	25.41 kWh	23.27 kWh	31.27 kWh	25.25 kWh	23.02 kWh	31.29 kWh	24.73 kWh	22.50 kWh
	RIII	32.29 kWh	25.51 kWh	23.27 kWh	32.47 kWh	25.25 kWh	23.02 kWh	31.29 kWh	24.73 kWh	22.50 kWh

Note: * represents that the result is available after releasing the upper bound to 83 °F.

Moreover, Table 6.3 lists the comparison of energy consumption of the optimal pre-cooling strategy with the rule-base pre-cooling strategy based on the three different utility rate structures. *Observe from the table that the optimal strategy has the least energy consumption compared with the rule-base strategy*

with RI, RII, and RIII for the same weather condition and cooling capacity of the HVAC system in a medium thermal condition home. It further illustrated the advantage of the optimal pre-cooling strategy. Moreover, the optimal strategy with RII had less energy consumption than the one with RI and RIII. These observations are consistent with the analysis in Section 6.2.

Table 6.3. Comparison of total and on-peak energy consumption and saving potential for the optimal and rule-based pre-cooling strategy.

Operation strategy	Optimal strategy			Rule-based strategy		
Utility rate structure	RI	RII	RIII	RI	RII	RIII
Total energy consumption, kWh	47.53	48.14	47.80	49.00	49.00	49.00
On-peak energy consumption, kWh	0	0	0	17.89	17.89	17.89

6.3.2 Energy cost comparison

The energy cost is defined by the objective function in Equation (5.14). Table 6.4 lists the 24-hour energy cost for the Tau values of 2000, 3500, and 5000, cooling capacities of 3.5, 4, and 5 tons, and three utility rate structures on July 16, July 20, and August 2, respectively. Similar patterns are observed from the table. The larger the Tau value is, the less energy cost the operation requires. In terms of weather conditions, energy cost is highest on July 20 and lowest on August 2 compared with July 16, confirming its dominant impact on the performance of the optimal pre-cooling operation. The hotter the weather is in

summer, the more cost savings a good thermal condition home can achieve. *Moreover, less energy cost can be achieved for a HVAC system with a higher cooling capacity only when a home has a better thermal condition. In addition, less energy cost tends to be achieved for a utility rate structure with a much higher on-peak electricity price than those during off-peak or/and mid-peak hours*. These observations are consistent with the analysis in Section 6.2 and are in line with expectations and experience.

Table 6.4. Comparison of energy cost for different home thermal properties, cooling capacities, weather conditions, and utility rate structures.

		CC=3.5 tons			CC=4 tons			CC=5 tons		
		2000	3500	5000	2000	3500	5000	2000	3500	5000
July 16 High: 95.5 ºF Low: 74.5 ºF	RI	$17.74	$11.59	$9.74	$18.00	$11.41	$9.62	$17.47	$11.11	$9.34
	RII	$16.62	$9.88	$8.39	$16.97	$9.67	$8.08	$15.13	$9.29	$7.78

	RIII	$16.72	$11.89	$9.76	$16.68	$11.55	$9.64	$17.42	$10.93	$8.99
July 20 High: 108.3 ºF Low: 77.2 ºF	RI	$22.31*	$12.32*	$21.17	$22.32*	$24.99	$21.70	$22.68*	$25.78	$18.58
	RII	$20.63*	$10.50*	$19.77	$20.94*	$23.25	$19.76	$21.92*	$24.20	$15.97
	RIII	$21.32*	$12.63*	$20.13	$20.95*	$23.88	$20.33	$21.27	$24.16	$19.24
August 2 High:	RI	$7.29	$5.82	$5.49	$7.23	$5.75	$5.23	$7.08	$5.62	$5.26

90.7 ºF Low: 65.8 ºF	RII	$6.27	$4.85	$4.42	$6.17	$4.80	$4.37	$5.97	$4.70	$4.27
	RIII	$7.44	$5.61	$5.12	$7.24	$5.56	$5.07	$6.93	$5.44	$4.95

Note: * represents that the result is available after releasing the upper bound to 83 °F.

In addition, the energy cost of the optimal pre-cooling strategy is compared with the rule-based pre-cooling strategy in the presence of RI, RII, and RIII as well as the percentage of cost savings that can be achieved when the optimal strategy is used in place of the rule-based strategy with RI, RII, and RIII, respectively. Notice from the table that the percentage of the optimal strategy cost savings is 15.51% compared with BC with RIII and may be as high as 32.93% compared with BC with RII, confirming its benefit. In terms of the optimal pre-cooling strategy, the operation with RII has less energy cost compared with those with RI and RIII. These observations are also in line with the analysis in Section 6.2.5.

Table 6.5. Comparison of energy cost and saving potential for the optimal and rule-based pre-cooling strategy.

Operation strategy	Optimal strategy			Rule-based strategy		
Utility rate structure	RI	RII	RIII	RI	RII	RIII
Energy cost	$11.41	$9.67	$11.55	$14.98	$14.24	$13.67
Percentage of the optimal strategy cost savings	0%	0%	0%	23.83%	32.93%	15.51%

6.4 Summary

This chapter investigates the performance of the optimal pre-cooling strategy, proposed in Chapter 5, that utilizes a home thermal model with diverse home parameters and different weather conditions, HVAC cooling capacities, and utility rate structures. Through simulation, a performance analysis of the optimal pre-cooling on the thermal dynamics, total energy consumption, and energy cost was conducted and compared with a rule-based pre-cooling strategy. It is found that the optimal pre-cooling strategy is adaptive based on changing conditions and its performance is significantly dependent on weather conditions and home thermal properties, while its performance may vary for different cooling capacities and utility rate structures. The larger the Tau value is, the less energy cost the operation requires. In terms of weather conditions, energy cost is highest on the hottest day and lowest on a cool summer day compared with a medium hot summer day, confirming its dominant impact on the performance of the optimal

pre-cooling operation. The hotter the weather is in summer, the more cost savings a good thermal condition home can achieve.

Moreover, less energy cost can be achieved for a HVAC system with a higher cooling capacity only when a home has a better thermal condition, and less energy cost also tends to be achieved for a utility rate structure with a much higher on-peak electricity price than those during off-peak or/and mid-peak hours. In addition, *it is found that the optimal strategy has the least energy consumption and cost while maintaining the required thermal comfort compared with the rule-base strategy with different utility rate structures for the same weather condition and cooling capacity of the HVAC system in a medium thermal condition home*. The superb energy performance of the optimal strategy is attributed to a longer runtime of the HVAC system in cool outdoor air conditions and to the elimination of deadband in HVAC operation, which is required by the rule-based strategies, to allow the indoor air temperature to stay near the thermal comfort upper bound as much as possible. These observations are in line with the analysis and expectations and experience.

Through the performance analysis of the optimal pre-cooling strategy, it provides a quantifiable analysis of the optimal pre-cooling operation in terms of specific thermal properties, HVAC system cooling capacity, weather condition, and utility rate structure. However, since the optimization was formulated based on a simplified home thermal model. The model assumes that the internal heat gains are negligible and not considered. The impact of the internal heat gains on

the model and the optimization problem needs to be investigated. Moreover, the implementation of the optimal pre-cooling strategy needs to be investigated through real homes. These will be the focuses in Chapter 7.

Chapter 7: Experimental Verification and Implementation

To implement the home thermal model and optimal pre-cooling strategy proposed in Chapters 3 and 5, experiments were conducted through the HVAC system of a real test home in this Chapter. The home thermal model is first implemented into the calculations of the cooling load and HVAC efficiency. Since the pre-cooling optimization problem utilizes the model without considering the effect of internal heat gains, the impact of internal heat gains on the thermal model is then investigated through experiments. Finally, the feasibility of implementing the optimal operation schedules of the HVAC system that are obtained through the simulation results of the optimal pre-cooling strategy is tested using the HVAC system through a software platform.

7.1 Experimental Apparatus

This section introduces the devices used for the data acquisition system and an open-source platform for distributed sensing and control.

7.1.1 Devices for data acquisition system

Experiments were performed in the same test house as detailed in Section 3.5.1. The house was equipped with a HVAC system with a cooling capacity of 3.5 tons and air flow rate of 1,400 cfm. Figure 7.1(a) and (b) shows the indoor and outdoor unit of the HVAC system for the house. A data acquisition system was installed in the house, which measured the entering and leaving air temperatures from the outdoor unit of the HVAC system, indoor and outdoor air temperatures, interior wall surface temperatures, supply and return air temperatures from air

ducts, air temperatures from the supply and return air diffusers, wind speed, global horizontal irradiation, return air flow rate, and power consumptions for the indoor and outdoor unit and total power use of the entire home. These data were measured using T-type thermocouples, velocity sensors, anemometer, pyranometer, and power meters, respectively, as shown in Figure 7.1(c)–(h) in addition to Figure 3.9(b)-(d) in Chapter 3. All the data were logged at thirty-second intervals using the connected Raspberry Pis and its associated hats, as shown in Figure 7.1(i). All the thermocouples were calibrated before use.

(a)

(b)

(c)

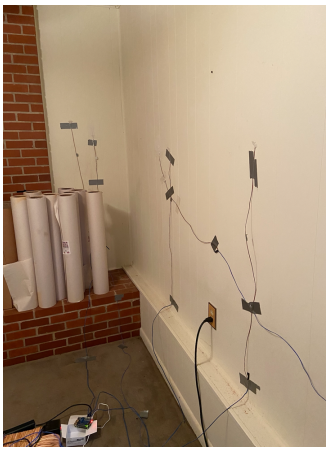

(d) (e) (f)

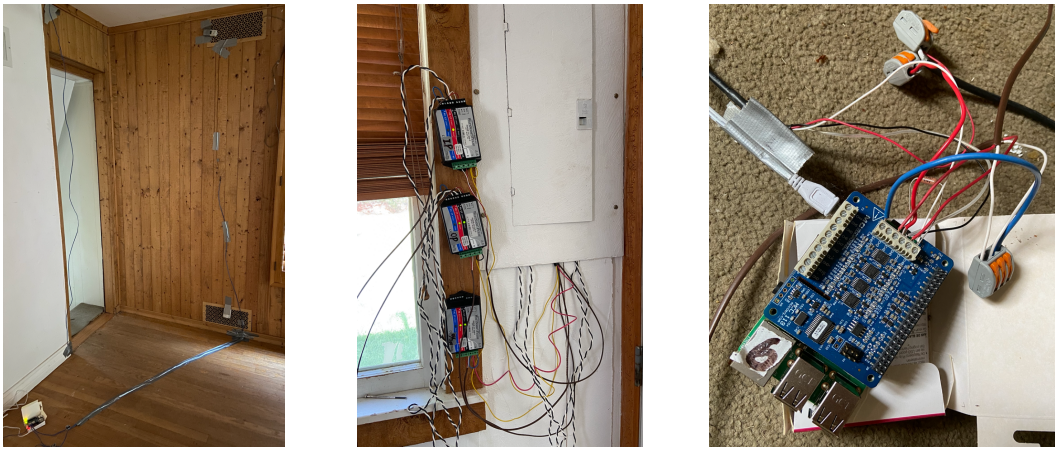

(g) (h) (i)

Figure 7.1. Experimental devices used for data acquisition system.

Note: (a) Indoor unit with the measurements of the relative humidity and temperature from the supply and return air duct; (b) Outdoor unit with the entering and leaving air temperature measurement; (c) Thermocouples for the indoor air temperature measurements; (d) Thermocouples for the interior wall surface temperature measurements; (e) Thermocouples for the exterior wall surface temperature measurements; (f) Thermocouple for the air temperature measurement from one supply diffuser; (g) Thermocouples for the air temperature measurements from two return diffusers; (h) Power meters for the indoor unit and outdoor unit of the HVAC system and total power for the house; and (i) Raspberry Pi and its associated hat.

To further illustrate the sensors and its measurements and locations in the house, a floor plan was drawn as shown in Figure 7.2. Specifications of all the measurements and locations of the sensors with its Pis for the data acquisition

system are shown in Tables 7.1 and 7.2. Since the combination of the indoor air temperature T7 and interior wall surface temperature T11 showed more consistent results, T7 and T11 was used for in the study. Moreover, weather data from the data acquisition system were compared with the data downloaded from Mesonet (Oklahoma Mesonet 2016) at five-minute intervals. The comparison showed that the Mesonet data provided similar, but more consistent results. Therefore, the Mesonet data were used in the study.

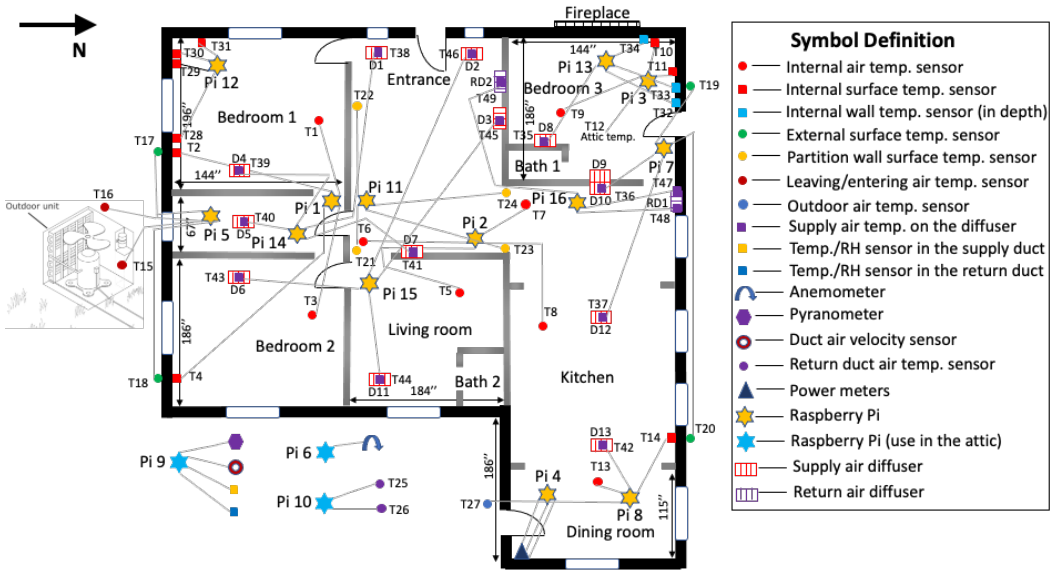

Figure 7.2. House floor plan with the locations of the sensors.

Table 7.1. Specifications of all the measurements for the data acquisition system.

Pi No.	Measurement	Channel	Pi No.	Measurement	Channel
Pi 1	T1	0	Pi 10	T25	0
	T2	1		T26	1

	T3	2		Open	2
	T4	3		Open	3
Pi 2	T5	0	Pi 11	T21	0
	T6	1		T22	1
	T7	2		T23	2
	T8	3		T24	3
Pi 3	T9	0	Pi 12	T28	0
	T10	1		T29	1
	T11	2		T30	2
	T12	3		T31	3
Pi 5	T15	0	Pi 13	T32	0
	T16	1		T33	1
	T17	2		T34	2
	T18	3		T35	3
Pi 6	Wind speed	0	Pi 14	T38	0
	Open	1		T39	1
	Open	2		T40	2
	Open	3		T41	3
Pi 7	T19	0	Pi 15	T43	0
	T20	1		T44	1
	T36	2		T45	2

	T37	3		T46	3
Pi 8	T13	0	Pi 16	T47	0
	T14	1		T48	1
	T27	2		T49	2
	T42	3		Open	3
Pi 4	Indoor frequency	0	Pi 9	Solar radiation	0
	Outdoor frequency	1		Airflow from return duct 1	1
	House frequency	2		Airflow from return duct 2	2
	Indoor power	3		Relative humidity from supply air duct	3
	Outdoor power	4		Air temperature from supply air duct	4
	House power	5		Relative humidity from return air duct	5
	Indoor pulse	6		Air temperature from return air duct	6
	Outdoor pulse	7		Total air flow rate	7
	House pulse	8		Open	8

Table 7.2. Specifications of the location and function of the sensors with its connected Pi for the data acquisition system.

Pi Number	Location	Function
1	Between bedroom 1 and 2	Indoor air temperature measurements
2	Livingroom	Indoor air temperature measurements
3	Bedroom 3	Temperature measurements for indoor air and interior wall surface
4	Dining room	Power measurements
5	Between bedroom 1 and 2	Temperature measurements for the exterior wall surface and leaving and entering air of the outdoor unit
6	Bedroom 3	Wind speed measurement
7	Bedroom 3	Temperature measurements for the exterior wall surface and supply air from diffuser
8	Dining room	Temperature measurements for indoor and outdoor air, exterior wall surface, and supply air from diffuser
9	Bedroom 3	Solar radiation and duct flow rate measurements
10	Attic	Duct temperature measurement

11	Living room	Partition wall surface temperature measurement
12	Bedroom 1	Interior wall surface temperature measurement
13	Bedroom 3	Temperature measurements for interior wall surface and supply air from diffuser
14	Between bedroom 1 and 2	Air temperature measurements from supply diffusers
15	Between bedroom 1 and 2	Air temperature measurements from supply diffusers
16	Living room	Air temperature measurements from return diffusers

7.1.2 Platform for operation control

The house HVAC system was controlled by a smart thermostat, shown in Figure 7.3(a), which uses the common rule-base control algorithm that attempts to regulate the indoor air temperature around a set point with 1 °F deadband as detailed in Section 5.2.1. The thermostat can receive inputs of the indoor air temperature set points at a 30-minute interval for the HVAC system. By trials, however, it was not feasible even when using a 30-minute interval of control signals in practice due to the software malfunction.

In this study, since a better granularity in terms of both the indoor air temperature set points and time duration was required, an open-source software platform, i.e., VOLTTRON (VOLTTRON 2019), for distributed sensing and

control was adopted, as shown in Figure 7.3(b) and (c). On the platform, software modules called “agents” and device driver modules are connected to a message bus to interact. Users may configure included drivers for industry standard device communication protocols, such as BACnet or Modbus, or develop and configure their own. Therefore, VOLLTRON was installed in the thermostat and each Raspberry Pi for the data acquisition and system control use. Through the platform, control signals obtained from the optimal pre-cooling strategy were able to be implemented for testing in the house as described in Section 7.4.

(a) thermostat from a manufacturer

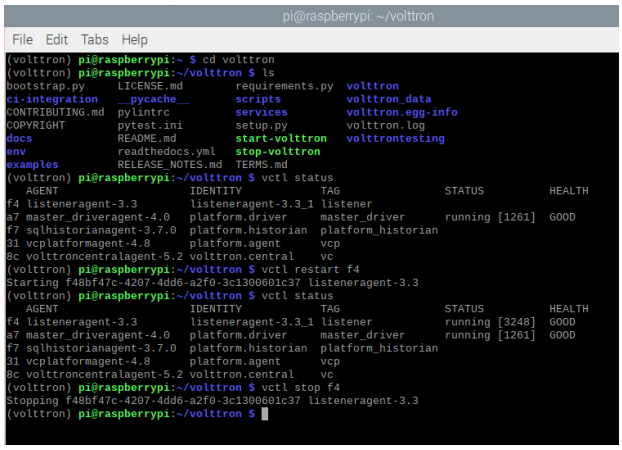

(b) VOLTTRON operation interface

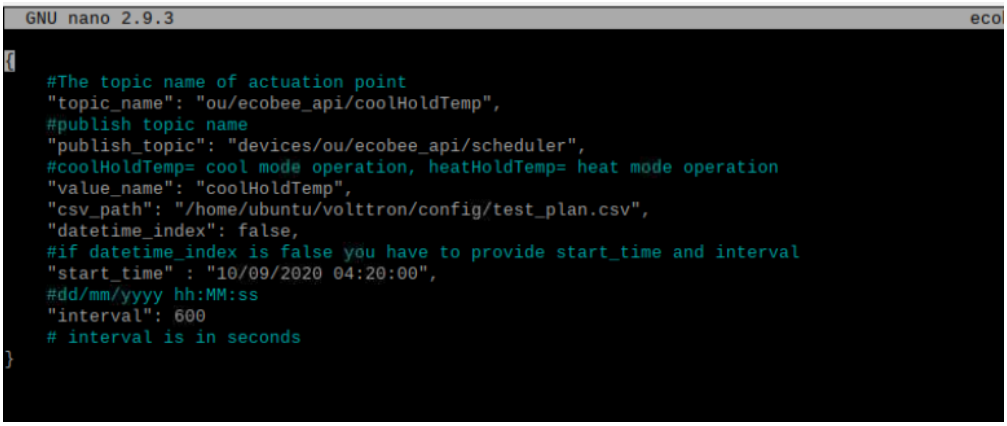

(c) VOLTTRON Thermostat Scheduler

Figure 7.3. The installed thermostat and software platform.

7.2 Experiment on the Cooling Load

This section introduces a model-based method for the calculations of the cooling load and home HVAC efficiency.

7.2.1 Model-based cooling load calculation method

Without considering the internal heat gains, the discrete-time home thermal model proposed in Chapter 3 can be expressed by

$$T_{ie}(k) - T_{ie}(k-1) = \frac{\Delta t}{\tau_1}[T_o(k) - T_{ie}(k)] + \frac{\Delta t}{\tau_2}[(T_{in}(k) - T_{ie}k)] \quad (7.1)$$

$$T_{in}(k) - T_{in}(k-1) = -\frac{\Delta t}{\tau_3}T_{in}(k) + \frac{\Delta t}{\tau_3}\big[T_{ie}(k) + \big(T_o(k) - T_{in}(k)\big)\big(b_1 W(k) + b_2 W^2(k)\big) + \big(a_1 G(k) + a_2 G^2(k) + a_3 G^3(k)\big) + Q_s(k)u_s(k)\big] \quad (7.2)$$

Since the term $Q_s(k)u_s(k)$ in the model represents the scaled sensible cooling load associated with the corresponding heat transfer coefficient and area, the hourly sensible cooling load can be calculated based on either the rearrangement of the model or the term u_s, as expressed by

$$Q_{cl,m} = \frac{hA}{120}\sum_1^K \Big(\tau_3 \frac{T_{in}(k+1) - T_{in}(k)}{\Delta t} + T_{in}(k) - \big[T_{ie}(k) + \big(T_o(k) - T_{in}(k)\big)\big(b_1 W(k) + b_2 W^2(k)\big) + \big(a_1 G(k) + a_2 G^2(k) + a_3 G^3(k)\big)\big]\Big) \quad (7.3)$$

$$Q_{cl,m} = \frac{hA\sum_1^K Q_s(k)u_s(k)}{120} \quad (7.4)$$

where $Q_{cl,m}$ is the hourly sensible cooling load (Btu/h) calculated by the model-based method; K is the length of data point, K=1, 2, 3, ….; h is the overall heat

transfer coefficient (Btu/(hr.ft^2.°F)), using the value of 1.63 in this study in accordance with ASHRAE Standard 90.2 (ASHRAE 2018); A is the heat transfer surface area that can be approximated using the floor area (ft^2); Q_s is the scaled HVAC system output (°F); and u_s is the HVAC system on/off signal (i.e., either 0 or 1) in 30-second interval.

Moreover, the sensible cooling load was also calculated by the theoretical method, i.e., the product of the measured air flow rate and temperature difference between the supply and return air temperature from diffusers for validation, shown by

$$Q_{cl,d} = \dot{m} C_p (T_{sa} - T_{ra}) = \rho \dot{V} C_p (T_{sa} - T_{ra}) \quad (7.5)$$

where $Q_{cl,d}$ is the hourly sensible cooling load distributed to the house space through ducts of the HVAC system (Btu/h); $\dot{m}$ is the mass flow rate from a diffuser (lb/h); ρ is the air density (lb/ ft^3); $\dot{V}$ is the volume flow rate (ft^3/h); C_p is the specific heat capacity of air; T_{ra} is the average temperature from the two return diffusers, i.e., RD1 and RD2, shown in Figure 7.2 (°F); T_{sa} is the average temperature from each supply diffuser weighted by the corresponding flow rate (°F). In this study, the supply air temperature from one diffuser, e.g., D7, was selected for use due to its availability and representativeness through observations.

7.2.2 The home HVAC system efficiency

Similar to Equation (7.5), the cooling capacity of the HVAC system can be calculated by

$$Q_{cc} = \dot{m}_d C_p \left(T_{sa,d} - T_{ra,d}\right) = \rho \dot{V}_d C_p \left(T_{sa,d} - T_{ra,d}\right) \quad (7.6)$$

where Q_{cc} is the sensible cooling capacity of the HVAC system (Btu/h); $\dot{m}_d$ is the mass flow rate from the supply duct (lb/h); $\dot{V}_d$ is the volume flow rate from the supply duct (ft^3/h); and $T_{sa,d}$ and $T_{ra,d}$ are the leaving and entering temperature from the indoor unit of the HVAC system (°F).

Based on Equations (7.5) and (7.6) using the measured data on August 9 and 19, 2020, as shown in Figures B.7 and B.8 in the **Appendix B**, the sensible cooling load $Q_{cl,d}$ was calculated and compared with the cooling capacity Q_{cc} in 30-sencond internal, as shown in Figure 7.4. As observed, approximately 60% of the cooling capacity of the HVAC system (Q_{cc}) was transferred to the indoor space in terms of the sensible cooling load ($Q_{cl,d}$) and meanwhile Q_{cc} accounted for approximately 65%-90% of the design cooling capacity $Q_{cc,d}$ at 3.5 tons (42,000 Btu/h) for the specific days. In this study, 50% of the design cooling capacity, i.e., $0.5Q_{cc,d}$, was adopted as a reference to calculate the absolute error percentage of the model-based cooling calculation using the same month data.

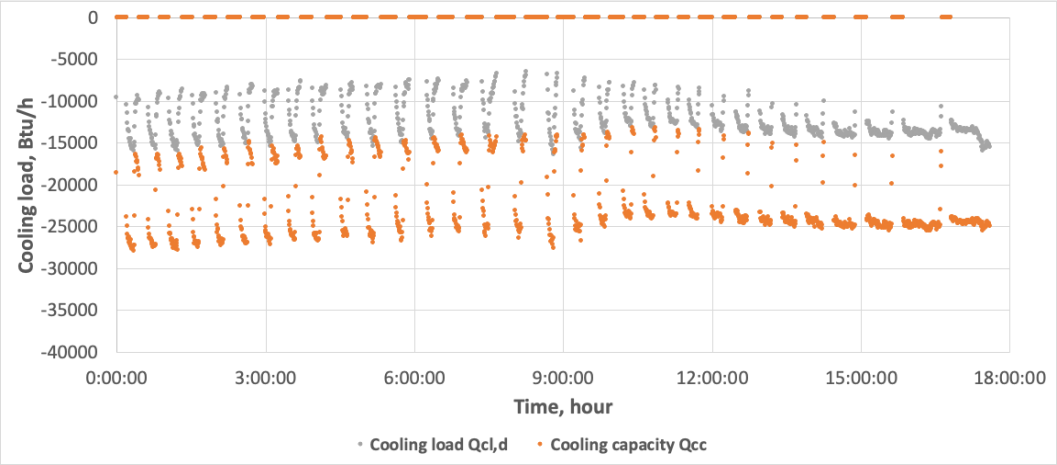

(a) Data on August 9, 2020

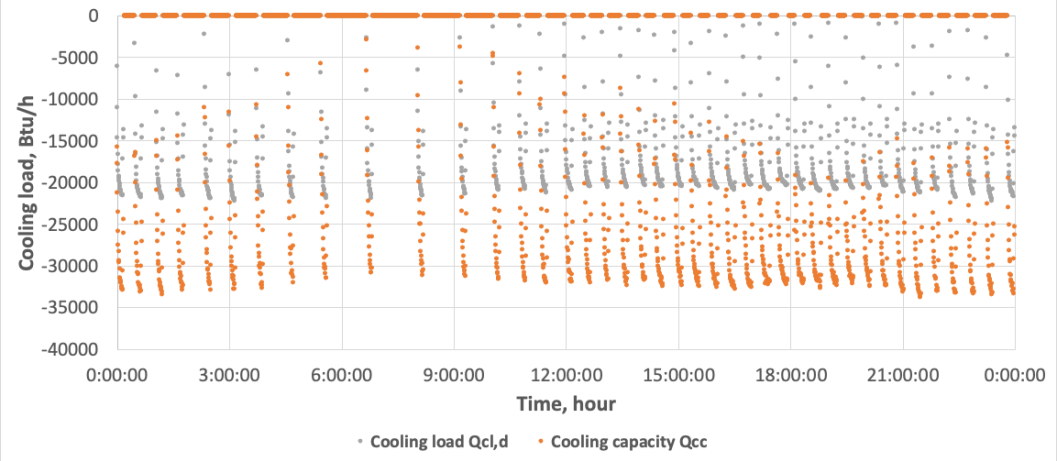

(b) Data on August 19, 2020

Figure 7.4. Comparison of the calculated cooling load and cooling capacity.

Moreover, based on Equation (7.4), the hourly sensible cooling load $Q_{cl,m}$ was calculated using the model-based method and compared with the calculated $Q_{cl,d}$ using the measured data from August 1 to August 7, 2020, as shown in Figure 7.5(a). The detailed weather condition can be found in Figure B.9 in the **Appendix B**. As observed, the cooling load $Q_{cl,m}$ calculated by the model-based

method matched well but far less than Q_{cc}. This indicated that air leakage occurred in the duct and a lot of the cooling energy were lost during duct transmission. Moreover, the absolute error percentage, defined by $|Q_{cl,d} - Q_{cl,m}|/0.5Q_{cc,d}$, was less than 10% during most of the time, as shown in Figure 7.5(b). It validated the effectiveness of the model-based cooling load calculation method.

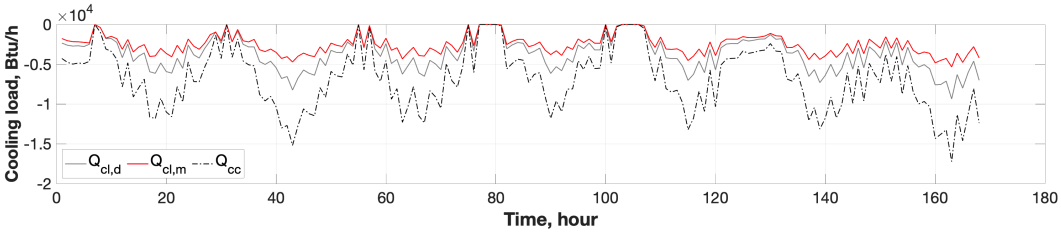

(a) Cooling load and cooling capacity calculation

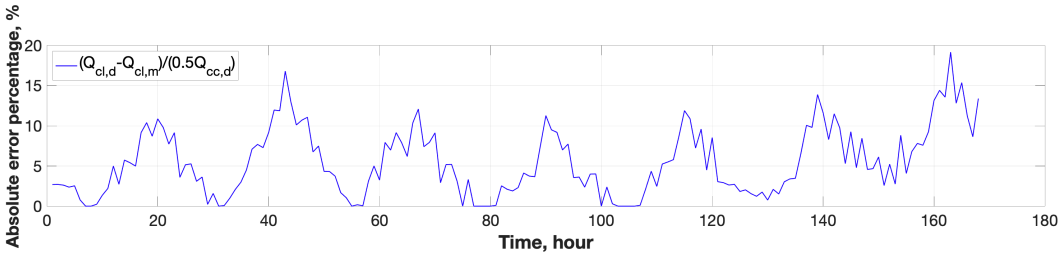

(b) Absolute error percentage

Figure 7.5. Comparison of the cooling load calculation with the cooling capacity using data from August 1 to August 7, 2020.

7.3 Experiments on the Internal Heat Gains

Since the test house was unoccupied, the simulation results in Chapters 5 did not consider the impact of the internal heat gains on the pre-cooling strategies. Moreover, the impact of the internal heat gains on the accuracy of the cooling

load calculation also needs to be investigated. Hence, these effects were investigated in this section.

The internal heat gains are typically generated by occupant and internal activities, for example, the cooking activities using the appliances inside the house. For the house, the total internal loads of 1.5 kW (5,118 Btu/h) and 3 kW (10,236 Btu/h) were selected to represent the moderate and high-intensity internal heat gains generated by the occupant and appliances. In this study, two electric heaters, each with a power of 1.5 kW, were used to simulate the internal loads. Figure 7.6 shows the electric heater of 1.5 kW used for the experiments of internal heat gains.

(a) (b)

Figure 7.6. Electric heaters used for internal heat gain test: (a) one heater representing moderate-intensity heat gains; and (b) two heaters representing high-intensity heat gains.

In Chapter 3, the term Q_i, i.e., the scaled internal heat gains, in Equations (3.23) and (3.24) of the home thermal model proposed in Chapter 3 is similar to the term Q_s, which is the scaled HVAC system output, reflecting the cooling capacity of 3.5 tons (42,000 Btu/h), and was identified through operational data. Since the cooling load and internal loads are similar and impact the thermal dynamics of the house space, the value of Q_i was estimated by the power ratio of the identified value of Q_s, which is available in Chapter 3. Therefore, for one heater with 5,118 Btu/h, $Q_{i,1} = -\frac{5{,}118}{42{,}000} Q_s = -0.122 Q_s$, where the negative represents the heating effect on the house compared to the cooling effect from Q_s (negative). For two heaters with a total of 10,236 Btu/h, $Q_{i,2} = -\frac{10{,}236}{42{,}000} Q_s = -0.244 Q_s$. These values are available for use to investigate the impact of the internal heat gains on the home thermal model, model-based cooling load calculation method, and optimal pre-cooling strategy.

The home thermal model was simulated utilizing weather data on June 10 and 17, 2020, as shown in Figures B.10 and B.11 in the **Appendix B**, and the value of Q_i in addition to the identified model parameters in Chapter 3. During the experiments, both operations of one and two heaters were tested from 2 to 4 pm when the outdoor temperature was relative higher during the day. The validation results were analyzed and compared whether considering the term Q_i of the internal heat gains or not in the model.

Figures 7.7 shows the comparison of the simulation results for two internal heat gain experiments, where the gray solid, blue dash-dot, red dashed, and black solid curves represent the temperatures of the outdoor air, measured indoor air, simulated indoor air without Q_i, and simulated indoor air with Q_i, respectively. As observed in Figure 7.7(a), no obvious difference is observed from the simulated temperatures whether considering the moderate-intensity internal heat gains ($Q_{i,1}$) or not. This is a normal scenario occurring at the house in daily life. However, for the rare scenario where high-intensity internal heat gains ($Q_{i,2}$) were generated, as shown in Figure 7.7(b), the simulated temperatures just deviated from the measured ones during the period from 2 to 4 pm and matched with the measure ones again after the period. In terms of this experiment on June 17, space air temperatures located at different bedrooms in the house were also compared and plotted in Figure 7.8. As observed in Figures 7.7(b) and 7.8, the temperature differences between the simulated and measured ones during the test period were similar to the measured temperature differences between different bedrooms before the test period and were still in a reasonable range. Moreover, to quantitatively observe the differences between the measured and simulated temperatures for these scenarios, the comparison of the absolute errors of the simulation results was listed in Table 7.3, in which the worst scenario was still in a range of 1.02 °F and 3.59 °F of the mean and maximum absolute error and was within the statistic error generated by the thermal model itself.

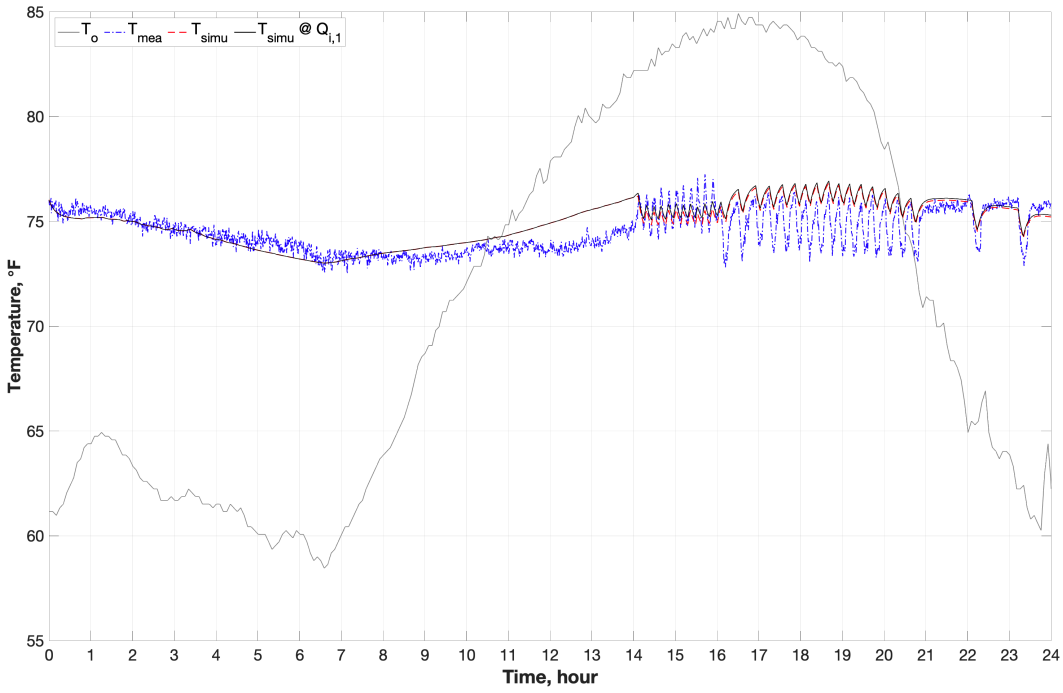

(a) The internal heat gains of 5,118 Btu/h when considering $\boldsymbol{Q_{i,1}}$ or not.

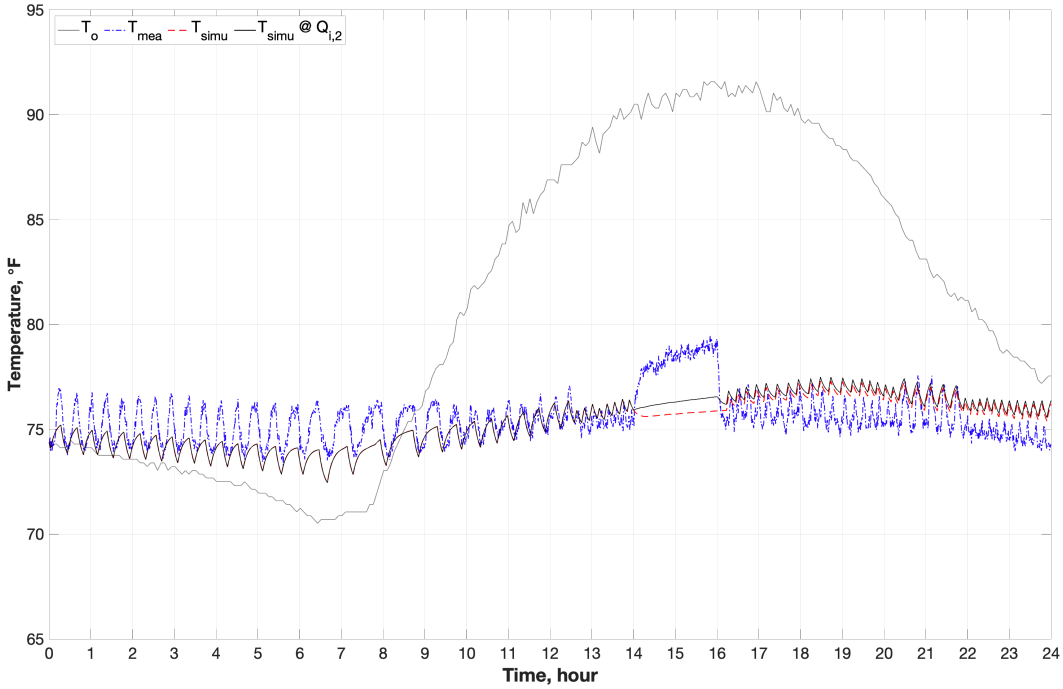

(b) The internal heat gains of 10,236 Btu/h when considering $Q_{i,2}$ or not

Figure 7.7. Validation for two different internal heat gains generated from 2 to 4 pm on June 17, 2020 when considering $\boldsymbol{Q_i}$ or not.

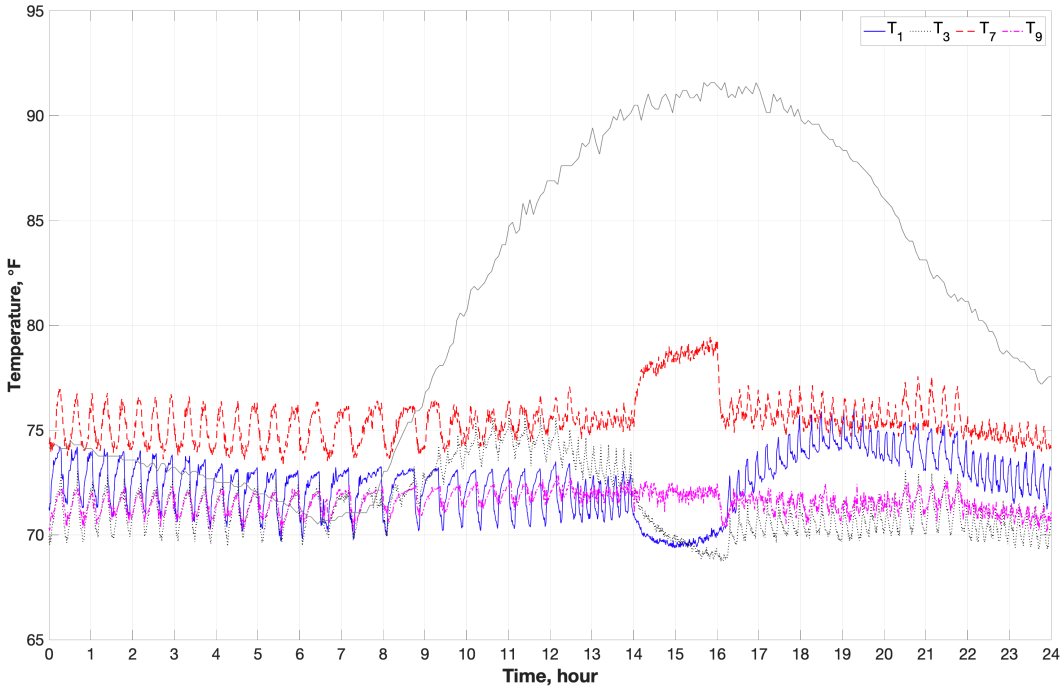

Figure 7.8. Comparison of space air temperatures located at different bedrooms in the house.

Table 7.3. Absolute error comparison for the simulated data.

Scenario / **Day**	**Mean absolute error, °F**		**Maximum absolute error, °F**	
	Without Q_i	With Q_i	Without Q_i	With Q_i
June 10	0.66	0.67	2.80	2.90
June 17	1.02	1.03	3.59	2.93

In addition, to investigate the energy performance of the experimental days whether considering the internal heat gains or not, the corresponding cooling

load $Q_{cl,m}$ (without considering Q_i) and $Q_{cl,m}$ @ Q_i (with considering Q_i) and the absolute error percentage, defined by $|Q_{cl,m} - Q_{cl,m} @ Q_i|/0.5Q_{cc,d}$, were also calculated and compared, as shown in Figures 7.9 and 7.10. As observed from the figures, the cooling load did not show much difference whether considering the internal heat gains or not and the absolute error percentage was less than 10% even for the rare scenario where high-intensity internal heat gains were generated. Through these experiments, it validated that the internal heat gains had little effect on the home thermal model and model-based cooling load calculation in terms of their accuracy and energy performance. Moreover, the simulation results from the optimal pre-cooling operations when considering the internal heat gains or not were plotted in Figure 7.11, of which the HVAC operation performance of pre-cooling was similar and only around 40-minute pre-cooling runtime difference was observed. Hence, the internal heat gains were negligible in this study.

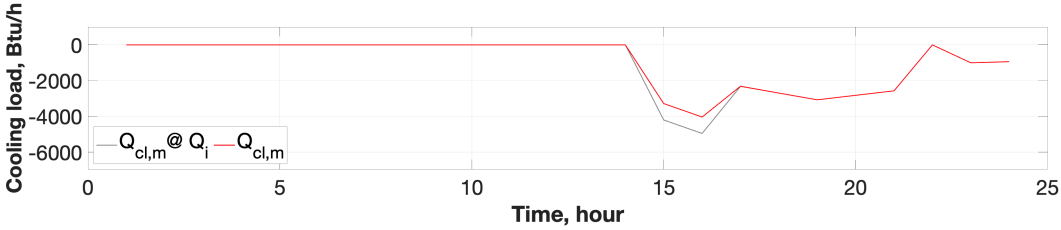

(a) Cooling load calculations

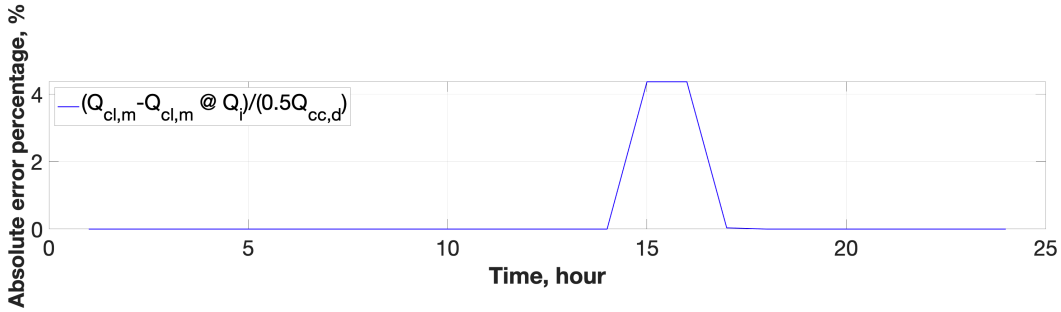

(b) Absolute error percentage

Figure 7.9. Comparison of the cooling load calculations when considering $\boldsymbol{Q_{i,1}}$ or not using data on June 10, 2020.

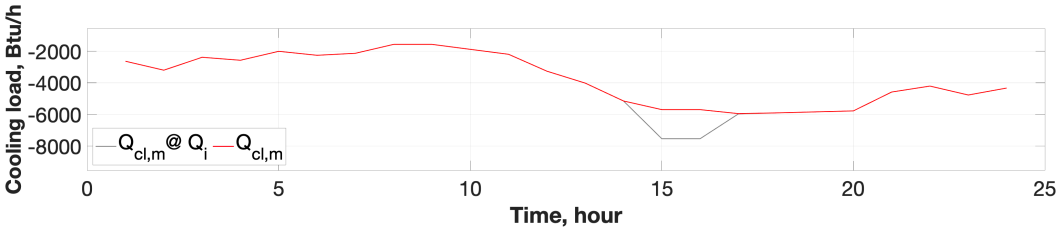

(a) Cooling load calculations

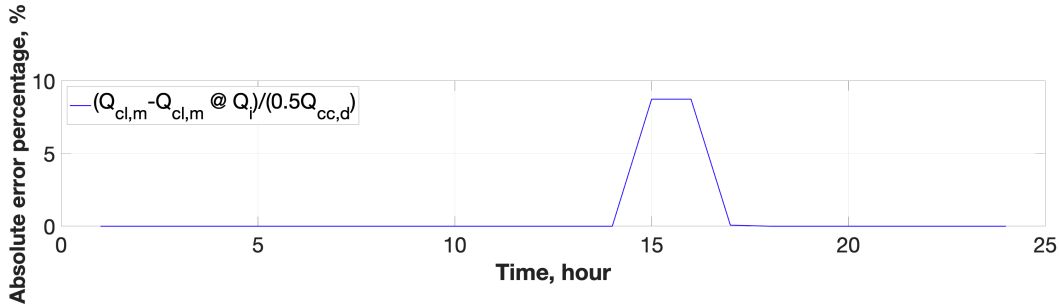

(b) Absolute error percentage

Figure 7.10. Comparison of the cooling load calculations when considering $\boldsymbol{Q_{i,2}}$ or not using data on June 17, 2020.

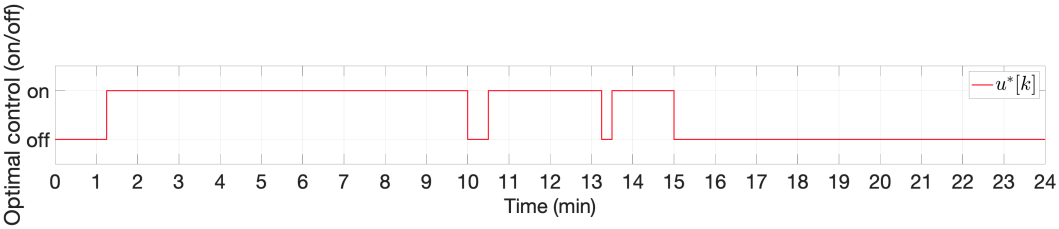

(a) When not considering $Q_{i,2}$

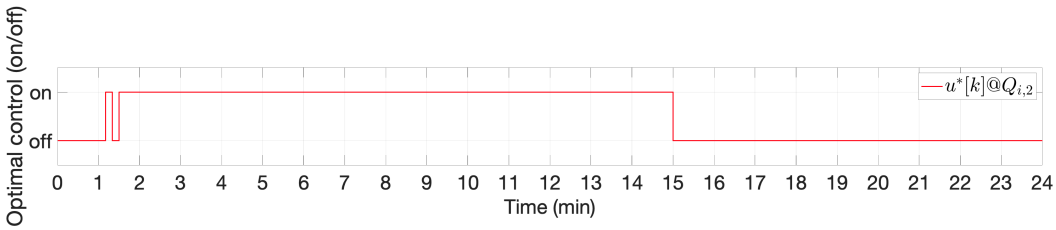

(b) When considering $Q_{i,2}$

Figure 7.11. Comparison of the optimal pre-cooling operations using data on June 17, 2020.

7.4 Implementation of Optimal Pre-Cooling Strategy

This section illustrates the implementation of the simulated results of the optimal pre-cooling strategy (OPS) into on-site operations through the software platform, as described in Section 7.1.2.

7.4.1 Selection of weather conditions

Since the experiments started in September, there were few days suitable for the experiments. Hence, based on weather forecast, weather data on September 5, 2020 was selected as a reference day to generate the operation control signals from the simulation results of OPS and then the signals were implemented into the control system operating in a similar day on September 26, 2020. Figure 7.12 shows the comparison of the outdoor air temperatures for the selected days. The detailed weather conditions can also be found in Figures B.12 and B.13 in the **Appendix B**. As observed, the outdoor temperature of the operation day on September 26 does not matched the reference day on September 5 well, especially before noon. This may cause differences for the operation and

energy performance in the experiment. But this can still serve as the purpose for testing OPS in real operations.

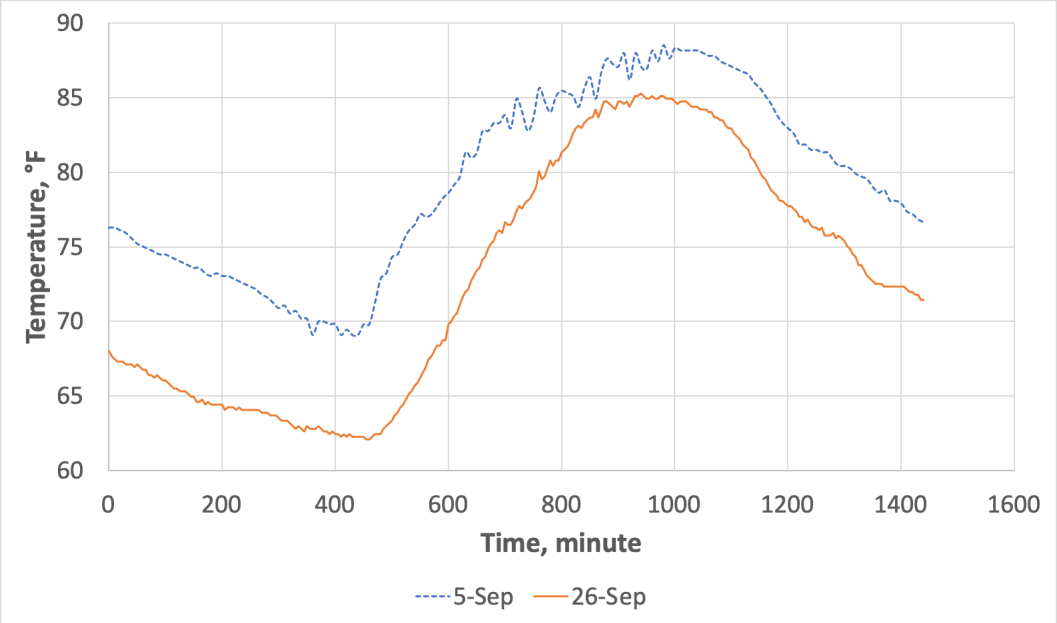

Figure 7.12. Comparison of the outdoor air temperatures from the selected days.

7.4.2 Experiment for optimal operation control

Followed by the same simulation setup described in Section 5.3, a 24-hour simulation with a sampling period Δt of 5 minutes has been carried out for OPS. The simulation utilized weather data as described in Section 7.4.1. The optimal operation control signals from the simulation results of OPS were implemented into the platform to control the thermostat operations as stated in Section 7.1.2. All the simulated and real operation results were compared in terms of the operation and energy performance. These results were plotted in Figures 7.13 and 7.14. Note that the simulations utilized the indoor air temperature T7 while the real operation control was based on the thermostat temperature. Because the data

from T7 had a better granularity (i.e., 30-second interval) than the measured data from thermostat (i.e., 5-minute interval).

As observed from Figure 7.13, both the measured air temperatures from thermostat and T7, located in different locations of the house as shown in Figure 7.2, matched with the thermostat set points with different deadbands during most of the day, except for the times at 15:25 and 15:45 during the on-peak hours from 15:00 to 19:00, at which the system was on two times for around 20 minutes in total, and the times at 21:40, 23:20, and 23:30 after on-peak hours, at which the system was on three times for around 15 minutes in total. The operation differences between thermostat set points and its measured temperatures may be explained by the operation control that used data from T7 instead of the thermostat temperature data. Even if the system was on for a short time during the on-peak hours, the HVAC system was still able to avoid most of the on-peak hours.

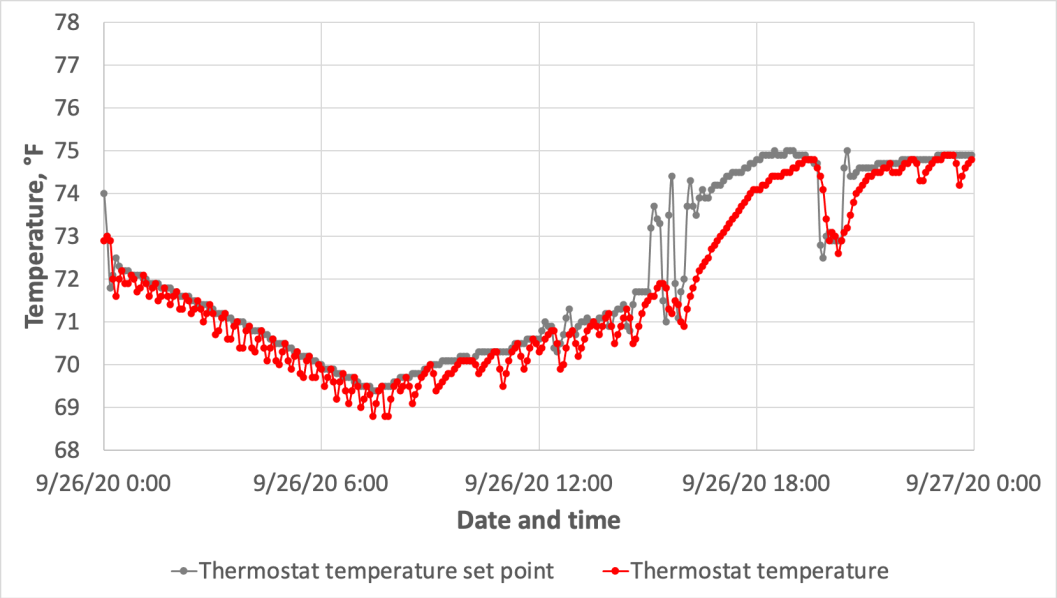

(a) Thermostat set point and thermostat temperature

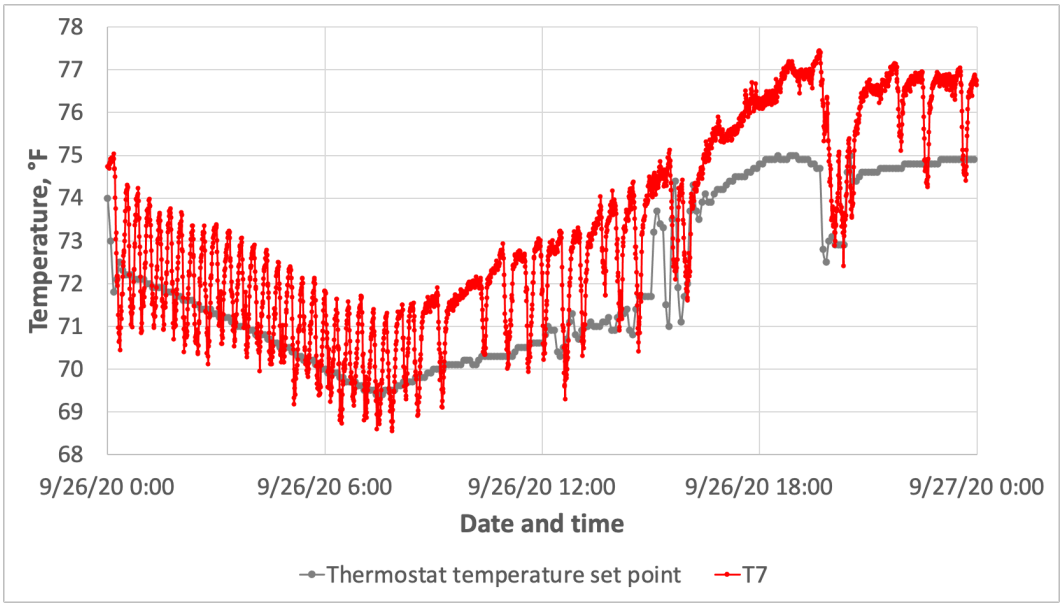

(b) Thermostat temperature and the measured indoor air temperature T7

Figure 7.13. Comparison of the thermostat temperature set points and corresponding indoor temperature T7 for OPS.

Additionally, Figure 7.14 shows the comparison of the simulated and measured total power use, where the simulated one is slightly higher than the measured one. This is because the outdoor temperature for the selected reference day on September 5 was generally higher than the operation day on September 26. The performance is consistent with the analysis in Chapter 5 and experiences. Overall, this experiment tested the implementation successfully and meanwhile demonstrated the effectiveness of the optimal pre-cooling strategy.

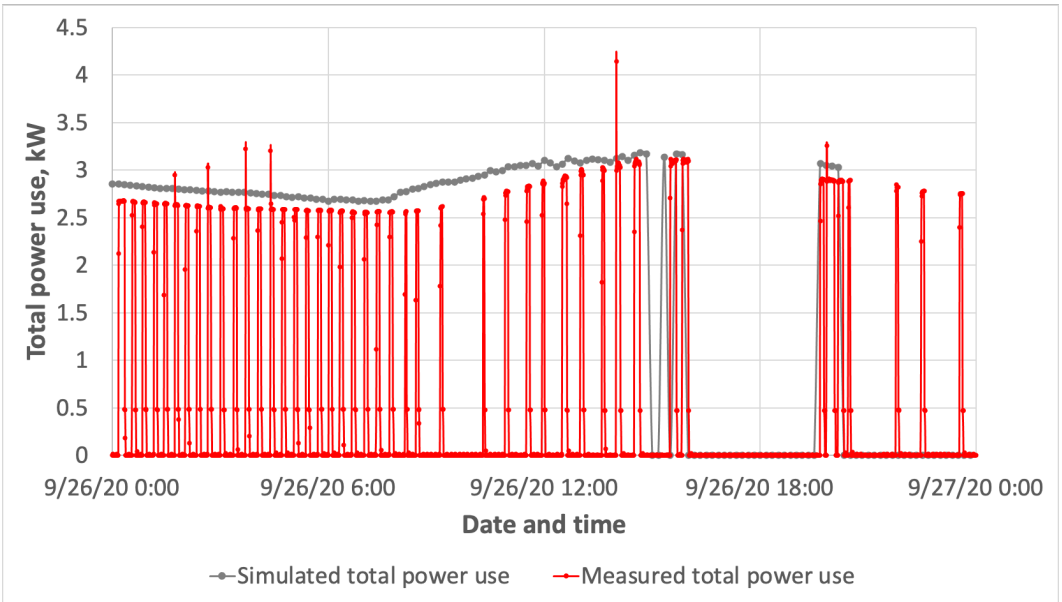

Figure 7.14. Comparison of the HVAC total power uses for OPS.

7.5 Summary

This chapter validates the effectiveness of the home thermal model in Chapter 3 by investigations of the impact of internal heat gains on the thermal model, accuracy of cooling load calculation using the mode-based method, and HVAC efficiency through experiments, which are conducted using the HVAC

system of a real test house. Moreover, it also implements and demonstrates the effectiveness of the optimal pre-cooling strategy proposed in Chapter 5 in terms of the operation and energy performance analysis. The experiments conducted in this chapter are based on assumptions, such as the weather condition used in experiments needs to be similar or identical to the selected reference day from weather forecast, the measured indoor temperature is used to represent the thermostat temperature, and the thermostat has a constant deadband during operation control, which need to be studied in the future work.

Chapter 8: Conclusions and Future Work

In this study, a home thermal model is first successfully formulated to capture the home thermal dynamics with reasonable accuracy to describe the heat transfer processes between the indoor and outdoor environments of a home. The simplicity of the model also allows its parameters to be automatically estimated using a data-driven method. The accuracy of the home thermal model is validated by applying it to predict the home indoor temperature for the test home. The validation results for the test home show that training data for 6 consecutive days are needed to generate reliable parameters, i.e., the thermal properties of the home. More data improves the model robustness and therefore accuracy, but only marginally. The novelty of the study resides in the successful self-identification of the parameters of the thermal model for each specific home using the parameter estimation process presented. The automatically identified model can effectively connect weather data with home operations and capture the home thermal dynamics with reasonable demands on training data. The successful development of the model provides a key to achieve system operation optimization and reduce the energy cost needs for homes, which is the critical first step to realize model-based intelligent home HVAC system operations.

With reasonable simplifications to the home thermal model, a model-based envelope performance evaluation method is proposed to assess the thermal performance of a home envelope in this study. The simplicity of the method allows the parameter to be automatically estimated using a short period of indoor

and outdoor air temperature data through data screening without the need for a home's physical information. Depending on the availability of the wind or not, the method can also evaluate the integrated heat transfer rate of an envelope through both heat transmission and infiltration together or the heat transfer rate through heat transmission only. The effectiveness of the method is validated through three sequential experiments. The experiment results show that the thermal properties can be estimated and evaluated using the proposed method. Moreover, the method also shows that the estimated thermal properties are effective across homes. Although more experiments with the knowledge of the ground-truth of test home envelope conditions are needed, the proposed method can possibly be an effective alternative to traditional methods, which require intensive labor for measurements and calculations, for the evaluation of the home envelope properties using only short-period measurements of the indoor and outdoor air temperatures and HVAC on/off status. In addition, wind impact is not negligible for the data-driven envelope evaluation method if high-precision estimation is desired.

Then this study also develops a pre-cooling optimization algorithm based on a quadratically-constrained integer linear programming problem that accounts for the thermal properties of a home, HVAC system capacity, utility rate structure, and weather conditions and makes use of a home thermal model. The effectiveness and energy performance of the optimal pre-cooling strategy is validated by comparison with three rule-based operation strategies. Through simulations, the results suggest that the optimal strategy is indeed significantly

more effective than the existing rule-based operation strategies. The successful development of the pre-cooling optimization algorithm for homes provides a way to benchmark energy performance of the optimal pre-cooling strategy.

Since the optimal pre-cooling is heavily dependent on a specific set of conditions, such as specific thermal properties, HVAC system capacity, utility rate structure, and weather condition, the impact of different sets of conditions on the optimal pre-cooling is investigated by the operation and energy performance analysis on the thermal dynamics, total energy consumption, and energy cost through simulations, and is also compared with a rule-based pre-cooling strategy. It is found that the optimal pre-cooling is adaptive based on changing conditions and its performance is significantly dependent on weather conditions and home thermal properties, while its performance may vary for different cooling capacities and utility rate structures. The better the home thermal condition is, the less energy cost the operation requires. In terms of weather condition, it has the dominant impact on the performance of the optimal pre-cooling operation. The hotter the weather is in summer, the more cost savings a good thermal condition home can achieve. Moreover, less energy cost can be achieved for a HVAC system with a higher cooling capacity only when a home has a better thermal condition, and less energy cost also tends to be achieved for a utility rate structure with a much higher on-peak electricity price than those during off-peak or/and mid-peak hours. For a home with a poor thermal condition, however, it is found that the optimal pre-cooling strategy may need more energy consumption, while

the least energy consumption can always be achieved without sacrificing thermal comfort for a home with a good or better thermal condition, compared with rule-based operation pre-cooling strategies. The superb energy performance of the optimal strategy is attributed to a longer runtime of the HVAC system in cool outdoor air conditions and to the elimination of deadband in HVAC operation, which is required by the rule-based strategies, to allow the indoor air temperature to stay near the thermal comfort upper bound as much as possible. These observations are in line with the analysis and expectations and experience.

In addition, experiments are conducted in this study through using a real test home to investigate the impact of internal heat gains on the thermal model and cooling load calculations using the mode-based method and the HVAC efficiency. Moreover, experiments are also carried out for the implementation of the optimal pre-cooling strategy and meanwhile demonstrate the effectiveness of the optimal pre-cooling strategy in terms of the operation and energy performance analysis.

Successful development of the home thermal model, model-based envelope performance evaluation method, model-based cooling load calculation method, and pre-cooling optimization algorithm for homes provides a systematic framework underlying an intelligent home HVAC system that can analyze the data to provide actionable instruction for advanced home HVAC system diagnosis and control, and for realizing home energy savings and grid-interactive efficient operations.

8.1 Potential Impact

According to Building America Research to Market Plan (EERE 2015), the HVAC systems in residential buildings along present 27% to 42% energy savings opportunities by using advance monitoring of residential loads and fault detection and diagnosis. Buildings offer considerable potential for energy cost reduction. Grid-interactive and efficient building operations can shift or reduce load during peak hours, resulting in significant savings for both utilities and customers, according to the DOE statistics (EERE 2016).

The pre-cooling optimization algorithm developed in this study could be applied to various HVAC systems and weather conditions for different thermal condition homes under the presence of different utility rate structures in a smart grid environment. Moreover, accuracies of the home thermal model and the related model-based methods have been validated and demonstrated through test homes. Additional thermal model capabilities that have been explored in this study include simulation of temperature fluctuations, study of thermal model parameters for simulation of cooling load, and real-time HVAC efficiency identification. These capabilities present cost-effective solutions and opportunities for fault detection and diagnosis, control, and cost savings in building system operations. The potential impact of this study includes:

- Availability of abundant home operation data has provided a game-changing opportunity to advance home operations.

- A holistic, physic-based model that can sufficiently capture the thermal behaviors is fundamental for optimal control purpose and HVAC system performance evaluations.
- An energy efficient home HVAC system that provides valuable information to homeowners, occupants, and HVAC contractors can be developed based on the framework described.
- Utilities could offer this system as their part of home energy efficiency programs.

This research is therefore a fundamental research that will culminate in the development of methodologies and facilitate corresponding related software platforms built for smart thermostats and devices which serve to integrate physical sensor measurements with mathematical models for enabling grid-interactive and efficient HVAC operations to obtain significant energy cost savings.

8.2 Limitations

The home thermal model is simplified under the assumptions that the internal heat gains are treated as one constant input and latent heat is not considered, there is room for improvement but while keeping the model sufficiently simple for compatibility with actual application in homes.

This study formulates the quadratically-constrained integer linear programming problem that is solved using CVX, a MATLAB-based modeling system for convex optimization, based on the MOSEK solver for nonlinear

convex optimization. A relatively longer runtime is needed for the solver to get solutions for the optimization problem if weather condition is under a medium hot summer with a small diurnal temperature difference. Moreover, the thermal properties of different thermal condition homes were investigated and reflected by one of the model parameters, i.e., the value of the time constant of home envelope, in the simulations. When operational data from different thermal condition homes are available, other model parameters obtained by training process should be considered in practice.

The experiment for optimal pre-cooling operation conducted in this study is based on assumptions, such as the weather condition used in the experiment needs to be similar or identical to the selected reference day from weather forecast, the selected indoor temperature is used to represent the thermostat temperature, and a thermostat needs to keep a constant deadband during operation control but different deadbands are observed during trials.

Moreover, different from the typical HVAC on/off control algorithm based on the indoor air temperature set point with a deadband, optimal HVAC on/off control has the advantage of controlling thermostats directly via the generated optimal solution. However, currently available thermostats may not have this function. Other limitations in this study include the practicability and real-time deployment of the developed methodologies, given the current computational limitations for thermostats and HVAC control systems.

8.3 Future Work

In view of the results from this study and issues encountered during the analysis, further investigation is required in the future. It includes:

- When collecting data from different HVAC seasons for model training, investigations are required to determine whether the model parameter estimates need to be updated seasonally.
- The internal heat gains need to be time-varying variables instead of constant and the latent heat needs to be investigated for home applications.
- The optimal pre-cooling needs to be implemented and validated using additional measurements in more real homes and simulations to extend the results nationwide.
- A prototype for the efficient home HVAC system will be built and tested with an industry partner.
- The impact of the efficient home HVAC system on the utilities needs to be expanded to a neighborhood or a city level.

References

[1] U.S. Energy Information Administration. 2015 Residential Energy Consumption Survey. https://www.eia.gov/consumption/residential/data/2015.

[2] U.S. Energy Information Administration. 2012 Commercial Buildings Energy Consumption Survey. https://www.eia.gov/consumption/commercial/data/2012.

[3] U.S. Department of Energy. 2011 Buildings Energy Data Book (with metadata update on September 3, 2019). https://catalog.data.gov/dataset/buildings-energy-data-book.

[4] Office of Energy Efficiency and Renewable Energy. Building America Research-to-Market Plan. November 2015. https://www.energy.gov/eere/buildings/downloads/building-america-program-research-market-plan.

[5] Office of Energy Efficiency and Renewable Energy. Overview of Existing and Future Residential Use Cases for Connected Thermostats. December 2016. https://www.energy.gov/eere/buildings/downloads/overview-existing-and-future-residential-use-cases-connected-thermostats.

[6] Elton B. Sherwin. Addiction to Energy: A Venture Capitalist's Perspective on how to Save our Economy and our Climate. Energy House Publishing, 2010.

[7] R. Kamyar and M. M. Peet. Optimal Thermostat Programming for Time-of-Use and Demand Charges with Thermal Energy Storage and Optimal Pricing for Regulated Utilities. *IEEE Transactions on Power Systems* 32, no. 4 (2017): 2714–2723.

[8] P. C. Tabares-Velasco, A. Speake, M. Harris, A. Newman, T. Vincent, and M. Lanahan. A Modeling Framework for Optimization-Based Control of a Residential Building Thermostat for Time-of-Use Pricing. *Applied Energy* 242 (2019): 1346–1357.

[9] A. Baniasadi, D. Habibi, O. Bass, and M. A. S. Masoum. Optimal Real-Time Residential Thermal Energy Management for Peak-Load Shifting with Experimental Verification. *IEEE Transactions on Smart Grid* 10, no. 5 (2019): 5587–5599.

[10] O. T. Ogunsola. Investigation of Methodologies for Minimizing Buildings Electricity Demand and Cost. *PhD Dissertation*, 2016.

[11] P. Xu, P. Haves, M. A. Piette, and J. E. Braun. Peak Demand Reduction from Pre-Cooling with Zone Temperature Reset in an Office Building (No. LBNL-55800). Lawrence Berkeley National Laboratory (LBNL), Berkeley, CA, USA, August 2004.

[12] P. Xu. Case Study of Demand Shifting with Thermal Mass in Two Large Commercial Buildings. *ASHRAE Transactions* 115, no. 2 (2009): 586–598.

[13] R. Yin, P. Xu, M. A. Piette, and S. Kiliccote. Study on Auto-DR and Pre-Cooling of Commercial Buildings with Thermal Mass in California. *Energy and Buildings* 42, no. 7 (2010): 967–975.

[14] S. Morgan and M. Krarti. Impact of Electricity Rate Structures on Energy Cost Savings of Pre-Cooling Controls for Office Buildings. *Building and Environment* 42, no. 8 (2007): 2810–2818.

[15] J. W. Moon and S. H. Han. Thermostat Strategies Impact on Energy Consumption in Residential Buildings. *Energy and Buildings* 43, no. 2–3 (2011): 338–346.

[16] R. Arababadi and K. Parrish. Developing and Modeling Potential Precooling Strategies for Residential Buildings in the Phoenix Climate. In *2015 ASHRAE Annual Conference Papers*, Atlanta, GA, USA, June 2015, pp. 1–7.

[17] W. Surles and G. P. Henze. Evaluation of Automatic Priced Based Thermostat Control for Peak Energy Reduction under Residential Time-of-Use Utility Tariffs. *Energy and Buildings* 49 (2012): 99–108.

[18] W. J. N. Turner, I. S. Walker, and J. Roux. Peak Load Reductions: Electric Load Shifting with Mechanical Pre-Cooling of Residential Buildings with Low Thermal Mass. *Energy* 82 (2015): 1057–1067.

[19] K. R. Keeney and J. E. Braun. A Simplified Method for Determining Optimal Cooling Control Strategies for Thermal Storage in Building Mass. *HVAC&R Research* 2, no. 1 (1996): 59–78.

[20] K. R. Keeney and J. E. Braun. Application of Building Precooling to Reduce Peak Cooling Requirements. *ASHRAE Transactions* 103, no. 1 (1997): 463–469.

[21] K. H. Lee and J. E. Braun. Model-Based Demand-Limiting Control of Building Thermal mass. *Building and Environment* 43, no. 10 (2008): 1633–1646.

[22] X. Li and A. Malkawi. Multi-Objective Optimization for Thermal Mass Model Predictive Control in Small and Medium Size Commercial Buildings under Summer Weather Conditions. *Energy* 112 (2016): 1194–1206.

[23] D. Nikovski, J. Xu, and M. Nonaka. A Method for Computing Optimal Set-Point Schedules for HVAC Systems. In *Proceedings of the 11th REHVA World Congress CLIMA*, Prague, Czech, June 2013.

[24] V. Chandan, A. Vishwanath, M. Zhang, and S. Kalyanaraman. Short Paper: Data Driven Pre-Cooling for Peak Demand Reduction in Commercial Buildings. In *Proceedings of the 2nd ACM International Conference*, Seoul, South Korea, November 2015, pp. 187–190.

[25] T. A. Reddy, L. K. Norpord, and W. Kempton. Shaving Residential Air-Conditioner Electricity Peaks by Intelligent Use of the Building Thermal Mass. *Energy* 16, no. 7 (1991): 1001–1010.

[26] M. Avci, M. Erkoc, and S. S. Asfour. Residential HVAC Load Control Strategy in Real-Time Electricity Pricing Environment. In *Proceedings of the 2012 IEEE Energytech*, Cleveland, OH, USA, May 2012, pp. 1–6.

[27] J. Wang, C. Y. Tang, and L. Song. Design and Analysis of Optimal Pre-Cooling in Residential Buildings. *Energy and Buildings* 216 (2020): 109951.

[28] K. Chan and S. Bashash. Modeling and Energy Cost Optimization of Air Conditioning Loads in Smart Grid Environments. In *Proceedings of the ASME 2017 Dynamic Systems and Control Conference*, Tysons, VA, USA, October 2017, pp. DSCC2017-5284.

[29] J. E. Braun. Reducing Energy Costs and Peak Electrical Demand through Optimal Control of Building Thermal Storage. *ASHRAE transactions* 96, no. 2 (1990): 876-888.

[30] M. Kintner-Meyer and A. F. Emery. Optimal Control of an HVAC System Using Cold Storage and Building Thermal Capacitance. *Energy and Buildings* 23 (1995): 19–31.

[31] G. P. Henze, C. Felsmann, and A. R. Florita. Optimization of Building Thermal Mass Control in the Presence of Energy and Demand Charges. *ASHRAE Transactions* 114 (2008): 75–84.

[32] J. H. Yoon, R. Baldick, and A. Novoselac. Dynamic Demand Response Controller Based on Real-Time Retail Price for Residential Buildings. *IEEE Transactions on Smart Grid* 5, no. 1 (2014): 121–129.

[33] J. Nelson, N. G. Johnson, P. T. Chinimilli, and W. Zhang. Residential Cooling Using Separated and Coupled Precooling and Thermal Energy Storage Strategies. *Applied Energy* 252 (2019): 113414.

[34] G. P. Henze, T. H. Le, A. R. Florita, and C. Felsmann. Sensitivity Analysis of Optimal Building Thermal Mass Control. *Journal of Solar Energy Engineering* 129 (2007): 473–485.

[35] J. Wang, C. Y. Tang, M. R. Brambley, and L. Song. Predicting Home Thermal Dynamics Using a Reduced-Order Model and Automated Real-Time Parameter Estimation. *Energy and Buildings* 198 (2019): 305–317.

[36] J. Lu, T. Sookoor, V. Srinivasan, G. Gao, B. Holben, J. Stankovic, E. Field, and K. Whitehouse. The Smart Thermostat: Using Occupancy Sensors to Save Energy in Homes. In *Proceedings of the ACM Conference on Embedded Networked Sensor Systems*, Association for Computing Machinery, Zurich, Switzerland, November 2010, pp. 211–224.

[37] Nest Labs. Energy Savings White Paper. February 2015. http://downloads.nest.com/press/documents/energy-savings-white-paper.pdf.

[38] A. J. Wilson and A. B. Templeman. An Approach to the Optimum Thermal Design of Office Buildings. *Building and Environment* 11, no. 1 (1976): 39–50.

[39] Edna Shaviv and Giora Shaviv. Modelling the Thermal Performance of Buildings. *Building and Environment* 13, no. 2 (1978): 95–108.

[40] J. R. Waters. The Experimental Verification of a Computerised Thermal Model for Buildings. *Building Services Engineering Research & Technology* 1, no. 2 (1980): 76–82.

[41] Radu Zmeureanu, Paul Fazio, and Fariborz Haghighat. Analytical and Inter-program Validation of a Building Thermal Model. *Energy and Buildings* 10, no. 2 (1987): 121–133.

[42] J. A. Carroll and J. R. Clinton. A Thermal Network Model of a Passive Solar House. In *Proceedings of the ISES National Passive Solar Conference*, International Solar Energy Society, Amherst, MA, USA, October 1980, pp. 257–261.

[43] G. G. J. Achterbosch, P. P. G de Jong, C. E. Krist-Spit, S. F. van der Meulen, and J. Verberne. The Development of a Convenient Thermal Dynamic Building Model. *Energy and Buildings* 8, no. 3 (1985): 183–196.

[44] O. T. Ogunsola and L. Song. Review and Evaluation of Using R-C Thermal Modeling of Cooling Load Prediction for HVAC System Control Purpose. In *Proceedings of the ASME International Mechanical Engineering Congress and Exposition*, American Society of Mechanical Engineers, Houston, Texas, USA, November 2012, pp. 735–743.

[45] J. A. Crabb, N. Murdoch, and J. M. Penman. A Simplified Thermal Response Model. *Building Services Engineering Research and Technology* 8, no. 1 (1987): 13–19.

[46] X. H. Xu and S. W. Wang. A Simplified Dynamic Model for Existing Buildings Using CTF and Thermal Network Models. *International Journal of Thermal Sciences* 47, no. 9 (2008): 1249–1262.

[47] P. Bacher and H. Madsen. Identifying Suitable Models for the Heat Dynamics of Buildings. *Energy and Buildings* 43, no. 7 (2011): 1511–1522.

[48] Y. Lin, T. Middelkoop, and P. Barooah. Issues in Identification of Control-Oriented Thermal Models of Zones in Multi-Zone Buildings. In *Proceedings of the IEEE Conference on Decision and Control*, Institute of Electrical and Electronics Engineers, Maui, Hawaii, USA, December 2012, pp. 6932–6937.

[49] A. Tindale. Third-Order Lumped-Parameter Simulation Method. *Building Services Engineering Research and Technology* 14, no. 3 (1993): 87–97.

[50] O. T. Ogunsola and L. Song. Performance Analysis of a Simplified Model of Cooling Load for a Typical Office Building. In *Proceedings of the ASME International Mechanical Engineering Congress and Exposition*, American Society of Mechanical Engineers, San Diego, California, USA, November 2013, pp. V011T06A025.

[51] O. T. Ogunsola and L. Song. Application of a Simplified Thermal Network Model for Real-Time Thermal Load Estimation. *Energy and Buildings* 96 (2015): 309–318.

[52] C. P. Underwood. An Improved Lumped Parameter Method for Building Thermal Modelling. *Energy and Buildings* 79 (2014): 191–201.

[53] K. J. Kircher and K. M. Zhang. On the Lumped Capacitance Approximation Accuracy in RC Network Building Models. *Energy and Buildings* 108 (2015): 454–462.

[54] O. A. Hasan, D. Defer, and I. Shahrour. A Simplified Building Thermal Model for the Optimization of Energy Consumption: Use of a Random Number Generator. *Energy and Buildings* 82 (2014): 322–329.

[55] A. Nassiopoulos, R. Kuate, and F. Bourquin. Calibration of Building Thermal Models Using an Optimal Control Approach. *Energy and Buildings* 76 (2014): 81–91.

[56] B. Bueno, L. Norford, G. Pigeon, and R. Britter. A Resistance-Capacitance Network Model for the Analysis of the Interactions between the Energy Performance of Buildings and the Urban Climate. *Building and Environment* 54 (2012): 116–125.

[57] M. M. Gouda, S. Danaher, and C. P. Underwood. Building Thermal Model Reduction Using Nonlinear Constrained Optimization. *Building and Environment* 37, no. 12 (2002): 1255–1265.

[58] S. Goyal and P. Barooah. A Method for Model-Reduction of Non-Linear Thermal Dynamics of Multi-Zone Buildings. *Energy and Buildings* 47 (2012): 332–340.

[59] M. Lauster, J. Teichmann, M. Fuchs, R. Streblow, and D. Mueller. Low Order Thermal Network Models for Dynamic Simulations of Buildings on City District Scale. *Building and Environment* 73 (2014): 223–231.

[60] I. Naveros and C. Ghiaus. Order Selection of Thermal Models by Frequency Analysis of Measurements for Building Energy Efficiency Estimation. *Applied Energy* 139 (2015): 230–244.

[61] M. J. Jiménez, H. Madsen, and K. K. Andersen. Identification of the Main Thermal Characteristics of Building Components Using MATLAB. *Building and Environment* 43, no. 2 (2008): 170–180.

[62] S. W. Wang and X. H. Xu. Simplified Building Model for Transient Thermal Performance Estimation Using GA-Based Parameter Identification. *International Journal of Thermal Sciences* 45, no. 4 (2006): 419–432.

[63] O. T. Ogunsola, L. Song, and G. Wang. Development and Validation of a Time-Series Model for Real-Time Thermal Load Estimation. *Energy and Buildings* 76 (2014): 440–449.

[64] J. M. Penman. Second Order System Identification in the Thermal Response of a Working School. *Building and Environment* 25, no. 2 (1990): 105–110.

[65] D. A. Coley and J. M. Penman. Second Order System Identification in the Thermal Response of Real Buildings. Paper II: Recursive Formulation for On-Line Building Energy Management and Control. *Building and Environment* 27, no. 3 (1992): 269–277.

[66] T. Dewson, B. Day, and A. D. Irving. Least Squares Parameter Estimation of a Reduced Order Thermal Model of an Experimental Building. *Building and Environment* 28, no. 2 (1993): 127–137.

[67] T. Y. Chen and A. K. Athienitis. Investigation of Practical Issues in Building Thermal Parameter Estimation. *Building and Environment* 38, no. 8 (2003): 1027–1038.

[68] R. Kramer, J. V. Schijndel, and H. Schellen. Inverse Modeling of Simplified Hygrothermal Building Models to Predict and Characterize Indoor Climates. *Building and Environment* 68 (2013): 87–99.

[69] S. Morgan and M. Krarti. Field Testing of Optimal Controls of Passive and Active Thermal Storage. *ASHRAE Transactions* 116 (2010): 134–146.

[70] Braun J.E., T.M. Lawrence, C.J. Klaassen, and J.M. House. Demonstration of Load Shifting and Peak Load Reduction with Control of Building Thermal Mass. In *Proceedings of the 2002 ACEEE Conference on Energy Efficiency in Buildings*, American Council for an Energy-Efficient Economy, Pacific Grove, CA, August 2002.

[71] J. E. Braun. Load Control Using Building Thermal Mass. *Journal of solar energy engineering* 125, no. 3 (2003): 292–301.

[72] E. S. W. Edmund and Z. Liao. Investigating the Impact of Thermal Mass on Building Performance Using Computational Simulation. In *2010 IEEE International Conference on Advanced Management Science*, Institute of Electrical and Electronics Engineer, Chengdu, China, July 2010.

[73] M. H. Sherman and N. E. Matson. Air Tightness of New U.S. Houses: A Preliminary Report. LBNL-48671, Lawrence Berkeley National Laboratory, March 2002.

[74] S. J. Emmerich and A. K. Persily. Airtightness of Commercial Buildings in the US. In *the 16th AIVC Conference*, Air Infiltration and Ventilation Centre, Brussels, Belgium, September 2005.

[75] F. C. McQuiston, J. D. Parker, and J. D. Spitler. Heating, Ventilating, and Air-Conditioning Analysis and Design, 5th ed., John Wiley and Sons, Inc., 2000, ISBN: 0-471-35098-2.

[76] ASHRAE. Handbook 2017: Fundamentals, American Society of Heating, Refrigerating and Air-Conditioning Engineers, Inc., Atlanta, Georgia, USA, July 2017.

[77] ASHRAE. ASHRAE Standard 90.2-2007: Energy Efficient Design of Low-Rise Residential Buildings, American Society of Heating, Refrigeration and Air-Conditioning Engineers, Inc., Atlanta, Georgia, USA, January 2017.

[78] M. B. Waite and S. M. O'Brien. Air Leakage: Difficulties in Measurement, Quantification and Energy Simulation. In *Proceedings of the BEST Building Enclosure Science & Technology Conference*, Portland, Oregon, USA, April 2010.

[79] K. Gowri, D. W. Winiarski, R. E. Jarnagin. Infiltration Modeling Guidelines for Commercial Building Energy Analysis (No. PNNL-18898). Pacific Northwest National Laboratory, Richland, Washington, USA, September 2009.

[80] J. Kosny, T. Petrie, D. Gawin, P. Childs, A. Desjarlais, and J. Christian. Thermal Mass-Energy Savings Potential in Residential Buildings. Oak Ridge National Laboratory, Oak Ridge, Tennessee, USA, 2001.

[81] H. Johra and P. Heiselberg. Influence of Internal Thermal Mass on the Indoor Thermal Dynamics and Integration of Phase Change Materials in

Furniture for Building Energy Storage: A Review. *Renewable and Sustainable Energy Reviews* 69 (2017): 19–32.

[82] J. J. Kim and J. W. Moon. Impact of Insulation on Building Energy Consumption. In the 17th International IBPSA Conference, International Building Performance Simulation Association, Glasgow, Scotland, UK, July 2009.

[83] ASTM. Standard Test Method for Calibration of Thermocouples by Comparison Techniques. ASTM Standard E220. American Society for Testing and Materials, PA, USA, 2019.

[84] Oklahoma Mesonet. Mesonet Data Files. 2016. http://www.mesonet.org/index.php/weather/mesonet_data_files.

[85] G. E. Caffey. Residential air infiltration. *ASHRAE Transactions* 85 (1979): 919–926.

[86] D. J. Dickerhoff, D. T. Grimsrud, and R. D. Lipschutz. Component Leakage Testing in Residential Buildings (No. LBL-14735). Lawrence Berkeley National Laboratory, Berkeley, CA, USA, 1982.

[87] D. T. Harrje and G. J. Born. Cataloguing air leakage components in houses. *Proceedings of the ACEEE 1982 Summer Study*, Santa Cruz, CA, USA. American Council for an Energy-Efficient Economy, Washington, D.C, USA, 1982.

[88] A. Cooperman, J. Dieckmann, and J. Brodrick. Home Envelope Retrofits. *ASHRE Journal* 53, no. 6 (2011):82–86.

[89] I. A. Atsonios, I. D. Mandilaras, D. A. Kontogeorgos, and M. A. Founti. A Comparative Assessment of the Standardized Methods for the In-Situ Measurement of the Thermal Resistance of Building Walls. *Energy and Buildings* 154 (2017): 198–206.

[90] ISO. Building Components and Building Elements — Thermal Resistance and Thermal Transmittance — Calculation Methods. ISO Standard 6946. International Organization for Standardization, Geneva, Switzerland, 2017.

[91] ISO. Thermal Insulation — Building Elements — In-Situ Measurement of Thermal Resistance and Thermal Transmittance — Part 1: Heat Flow Meter Method. ISO Standard 9869. International Organization for Standardization, Geneva, Switzerland, 2014.

[92] G. Desogus, S. Mura, and R. Ricciu. Comparing Different Approaches to in Situ Measurement of Building Components Thermal Resistance. *Energy and Buildings* 43, no. 10 (2011): 2613–2620.

[93] G. Ficco, F. Iannetta, E. Ianniello, F. R. A. Alfano, and M. Dell'Isola. U-Value in Situ Measurement for Energy Diagnosis of Existing Buildings. *Energy and Buildings* 104 (2015): 108–121.

[94] ISO. Thermal Insulation — Building Elements — In-Situ Measurement of Thermal Resistance and Thermal Transmittance — Part 2: Infrared Method for Frame Structure Dwelling. ISO Standard 9869. International Organization for Standardization, Geneva, Switzerland, 2018.

[95] R. Albatici and A. M. Tonelli. Infrared Thermovision Technique for the Assessment of Thermal Transmittance Value of Opaque Building Elements on Site. *Energy and Buildings* 42, no. 11 (2010): 2177–2183.

[96] P. A. Fokaides and S. A. Kalogirou. Application of Infrared Thermography for the Determination of the Overall Heat Transfer Coefficient (*U*-Value) in Building Envelopes. *Applied Energy* 88, no. 12 (2011): 4358–4365.

[97] B. Lehmann, K. G. Wakili, T. Frank, B. V. Collado, and C. Tanner. Effects of Individual Climatic Parameters on the Infrared Thermography of Buildings. *Applied Energy* 110 (2013): 29–43.

[98] M. Fox, D. Coley, S. Goodhew, and P. D. Wilde. Thermography Methodologies for Detecting Energy Related Building Defects. *Renewable and Sustainable Energy Reviews* 40 (2014): 296–310.

[99] A. Kylili, P. A. Fokaides, P. Christou, and S. A. Kalogirou. Infrared Thermography (IRT) Applications for Building Diagnostics: A Review. *Applied Energy* 134 (2014): 531–549.

[100] I. Nardi, D. Paoletti, D. Ambrosini, T. D. Rubeis, and S. Sfarra. *U*-Value Assessment by Infrared Thermography: A Comparison of Different Calculation Methods in a Guarded Hot Box. *Energy and Buildings* 122 (2016): 211–221.

[101] C. Peng and Z. Wu. In Situ Measuring and Evaluating the Thermal Resistance of Building Construction. *Energy and Buildings* 40, no. 11, (2008): 2076–2082.

[102] A. Rasooli, L. Itard, and C. I. Ferreira. A Response Factor-Based Method for the Rapid In-Situ Determination of Wall's Thermal Resistance in Existing Buildings. *Energy and Buildings* 119 (2016): 51–61.

[103] L. Evangelisti, G. Guattari, P. Gori, and F. Asdrubali. Assessment of Equivalent Thermal Properties of Multilayer Building Walls Coupling Simulations and Experimental Measurements. *Building and Environment* 127 (2018): 77–85.

[104] M. Zeifman and K. Roth Residential Remote Energy Performance Assessment: Estimation of Building Thermal Parameters Using Interval Energy Consumption Data. *Proceedings of ACEEE Summer Study on Energy Efficiency in Buildings*, Pacific Grove, CA, USA. American Council for an Energy-Efficient Economy, Washington, D.C, USA, 2016.

[105] G. R. Newsham, Y. Grinberg, A. Pardasani, and K. Bar. Remote Energy Auditing: Energy Efficiency through Smart Thermostat Data and Control. *Proceedings of ECEEE Summer Study on Energy Efficiency: Consumption, Efficiency and Limits*, Belambra Presqu'île de Giens, France. European Council for an Energy Efficient Economy, Stockholm, Sweden, 2017.

[106] M. J. Siemann. Performance and Applications of Residential Building Energy Grey-Box-Models. *PhD Dissertation*, 2013.

[107] C. Y. Shaw. Correlation between Air Infiltration and Air Tightness for Houses in a Developed Residential Area. *ASHRAE Transactions* 87 (1981): 333.

[108] C. P. Crall. Development of the Air Infiltration Model for the Energy Performance Design System. *ASHRAE Transactions* 89 (1983): 201–210.

[109] M. Sherman and D. Dickerhoff. Air-Tightness of US Dwellings. *ASHRAE Transactions* 104 (1998): 1359–1367.

[110] S. Pallin, M. Stockdale, P. Boudereaux, and E. Beuchler. Effects of Air Leakage on Buildings' Overall Thermal Resistances Based on U.S. Climate Zones. *ASHRAE Transactions* 123 (2017): 90–100.

[111] K. Gowri, D. W. Winiarski, and R. E. Jarnagin. Infiltration Modeling Guidelines for Commercial Building Energy Analysis (No. PNNL-18898). Pacific Northwest National Laboratory, Richland, Washington, USA, 2009.

[112] A. K. Persily. Myths about Building Envelopes. *ASHRAE journal* 41 (1999): 39–48.

[113] M. B. Waite and S. M. O'Brien. Air Leakage: Difficulties in Measurement, Quantification and Energy Simulation. In *Proceedings of the BEST Building Enclosure Science & Technology Conference*, Portland, Oregon, USA, 2010.

[114] W. L. Brogan. Modern Control Theory. Prentice-Hall, Inc. 1991.

[115] A. Schrijver. Theory of Linear and Integer Programming. John Wiley & Sons. 1998.

[116] Mathworks. MATLAB *intlinprog*. https://www.mathworks.com/help/optim/linear-programming-and-mixed-integer-linear-programming.html.

[117] ANSI/ASHRAE. ANSI/ASHRAE Standard 55: Thermal Environmental Conditions for Human Occupancy, ASHRAE, January 2017.

[118] M. Grant and S. Boyd. CVX: MATLAB Software for Disciplined Convex Programming, Version 2.1, March 2014. http://cvxr.com/cvx.

[119] MOSEK ApS. The MOSEK Optimization Toolbox for MATLAB Manual, Version 9.1.9, November 2019. https://docs.mosek.com/9.0/toolbox/index.html.

[120] J. Wang, C. Y. Tang, and L. Song. Model-Based Home Envelope Performance Evaluation: A Use Case of Data from Connected Thermostats. *ASHRAE Transactions* 125, no.2 (2019): 67–70.

[121] J. Wang, C. Y. Tang, and L. Song. Home Envelope Performance Evaluation Using a Data Driven Method. *ASHRAE Transactions* 126, no.1 (2020): 713–724.

[122] VOLTTRON. The VOLTTRON Community, Battelle Memorial Institute, Pacific Northwest National Laboratory, USA, 2019.

Appendix A: Model Parameter Estimation

(1) Identify τ_1 and τ_2 in Equation (3.27) in Chapter 3

$$X_1\beta_1 = Y_1 \tag{A.1}$$

The least squares solution to Equation (A.1) is

$$\hat{\beta}_1 = \begin{pmatrix} \hat{\beta}_1(1) \\ \hat{\beta}_1(2) \end{pmatrix} = (X_1^T X_1)^{-1} X_1^T Y_1 \tag{A.2}$$

Thus,

$$\tau_1 = \Delta t/\hat{\beta}_1(1) \text{ and } \tau_2 = \Delta t/\hat{\beta}_1(2). \tag{A.3}$$

where X_1 and Y_1 are known matrices; β_1 is the matrix to be identified; and $\hat{\beta}_1$ is the least squares solution matrix.

$$X_1 = \begin{bmatrix} T_o(2) - T_{ie}(2) & T_{in}(2) - T_{ie}(2) \\ T_o(3) - T_{ie}(3) & T_{in}(3) - T_{ie}(3) \\ \vdots & \vdots \\ T_o(k-1) - T_{ie}(k-1) & T_{in}(k-1) - T_{ie}(k-1) \\ T_o(k) - T_{ie}(k) & T_{in}(k) - T_{ie}(k) \end{bmatrix}, \qquad \beta_1 = \begin{bmatrix} \tau_1 \\ \tau_2 \end{bmatrix},$$

$$Y_1 = \begin{bmatrix} T_{ie}(2) - T_{ie}(1) \\ T_{ie}(3) - T_{ie}(2) \\ \vdots \\ T_{ie}(k-1) - T_{ie}(k-2) \\ T_{ie}(k) - T_{ie}(k-1) \end{bmatrix}. \tag{A.4}$$

(2) Identify τ_3, b_1, b_2, a_1, a_2, a_3, Q_i, and Q_s in Equation (3.28) in Chapter 3

$$X_2\beta_2 = Y_2 \tag{A.5}$$

The least squares solution to Equation (A.5) is:

$$\hat{\beta}_2 = \begin{pmatrix} \hat{\beta}_2(1) \\ \hat{\beta}_2(2) \\ \hat{\beta}_2(3) \\ \hat{\beta}_2(4) \\ \hat{\beta}_2(5) \\ \hat{\beta}_2(6) \\ \hat{\beta}_2(7) \\ \hat{\beta}_2(8) \end{pmatrix} = (X_2^T X_2)^{-1} X_2^T Y_2 \tag{A.6}$$

Thus,

$\tau_3 = \Delta t/\hat{\beta}_2(1)$, $b_1 = \hat{\beta}_2(2)/\hat{\beta}_2(1)$, $b_2 = \hat{\beta}_2(3)/\hat{\beta}_2(1)$, $a_1 = \hat{\beta}_2(4)/\hat{\beta}_2(1)$, $a_2 = \hat{\beta}_2(5)/\hat{\beta}_2(1)$, $a_3 = \hat{\beta}_2(6)/\hat{\beta}_2(1)$, $Q_i = \hat{\beta}_2(7)/\hat{\beta}_2(1)$, and $Q_s = \hat{\beta}_2(8)/\hat{\beta}_2(1)$.

(A.7)

where X_2 and Y_2 are known matrices; β_2 is the matrix needed to identify; and $\hat{\beta}_2$ is the least squares solution matrix.

$$X_2 = \begin{bmatrix} T_{ie}(2) - T_{in}(2) & (T_o(2) - T_{in}(2))W(2) & (T_o(2) - T_{in}(2))W^2(2) & G(2) & G^2(2) & G^3(2) & u_i(2) & u_s(2) \\ T_{ie}(3) - T_{in}(3) & (T_o(3) - T_{in}(3))W(3) & (T_o(3) - T_{in}(3))W^2(3) & G(3) & G^2(3) & G^3(3) & u_i(3) & u_s(3) \\ \vdots & \vdots & \vdots & \vdots & \vdots & \vdots & \vdots & \vdots \\ T_{ie}(k-1) - T_{in}(k-1) & (T_o(k-1) - T_{in}(k-1))W(k-1) & (T_o(k-1) - T_{in}(k-1))W^2(k-1) & G(k-1) & G^2(k-1) & G^3(k-1) & u_i(k-1) & u_s(k-1) \\ T_{ie}(k) - T_{in}(k) & (T_o(k) - T_{in}(k))W(k) & (T_o(k) - T_{in}(k))W^2(k) & G(k) & G^2(k) & G^3(k) & u_i(k) & u_s(k) \end{bmatrix},$$

$$\beta_2 = \begin{bmatrix} \tau_3 \\ b_1 \\ b_2 \\ a_1 \\ a_2 \\ a_3 \\ Q_i \\ Q_s \end{bmatrix},$$

$$Y_2 = \begin{bmatrix} T_{in}(2) - T_{in}(1) \\ T_{in}(3) - T_{in}(2) \\ \vdots \\ T_{in}(k-1) - T_{in}(k-2) \\ T_{in}(k) - T_{in}(k-1) \end{bmatrix}. \tag{A.8}$$

(3) Identify the parameter α (corresponding to τ) in Chapter 4

Equation (4.15) can be written in a matrix form as:

$$X\beta = Y \tag{A.9}$$

where

$X =$

$$\begin{bmatrix} T_o(0) - T_{in}(0) & \big(T_o(0) - T_{in}(0)\big)W(0) & \big(T_o(0) - T_{in}(0)\big)W^2(0) \\ T_o(1) - T_{in}(1) & \big(T_o(1) - T_{in}(1)\big)W(1) & \big(T_o(1) - T_{in}(1)\big)W^2(1) \\ \vdots & \vdots & \vdots \\ T_o(k-2) - T_{in}(k-2) & \big(T_o(k-2) - T_{in}(k-2)\big)W(k-2) & \big(T_o(k-2) - T_{in}(k-2)\big)W^2(k-2) \\ T_o(k-1) - T_{in}(k-1) & \big(T_o(k-1) - T_{in}(k-1)\big)W(k-1) & \big(T_o(k-1) - T_{in}(k-1)\big)W^2(k-1) \end{bmatrix},$$

$$\beta = \begin{bmatrix} \alpha \\ \alpha b_1 \\ \alpha b_2 \end{bmatrix}, Y = \begin{bmatrix} T_{in}(1) - T_{in}(0) \\ T_{in}(2) - T_{in}(1) \\ \vdots \\ T_{in}(k-1) - T_{in}(k-2) \\ T_{in}(k) - T_{in}(k-1) \end{bmatrix}. \tag{A.10}$$

Assuming that X has full column rank, the least squares solution to Equation (A.9) is:

$$\hat{\beta} = \begin{pmatrix} \hat{\beta}(1) \\ \hat{\beta}(2) \\ \hat{\beta}(3) \end{pmatrix} = (X^T X)^{-1} X^T Y \tag{A.11}$$

where $\hat{\beta}$ is the optimal estimate of the unknown parameters.

Thus,

$$\alpha = \hat{\beta}(1),\ b_1 = \hat{\beta}(2)/\hat{\beta}(1), \text{ and } b_2 = \hat{\beta}(3)/\hat{\beta}(1). \tag{A.12}$$

Appendix B: Weather Conditions

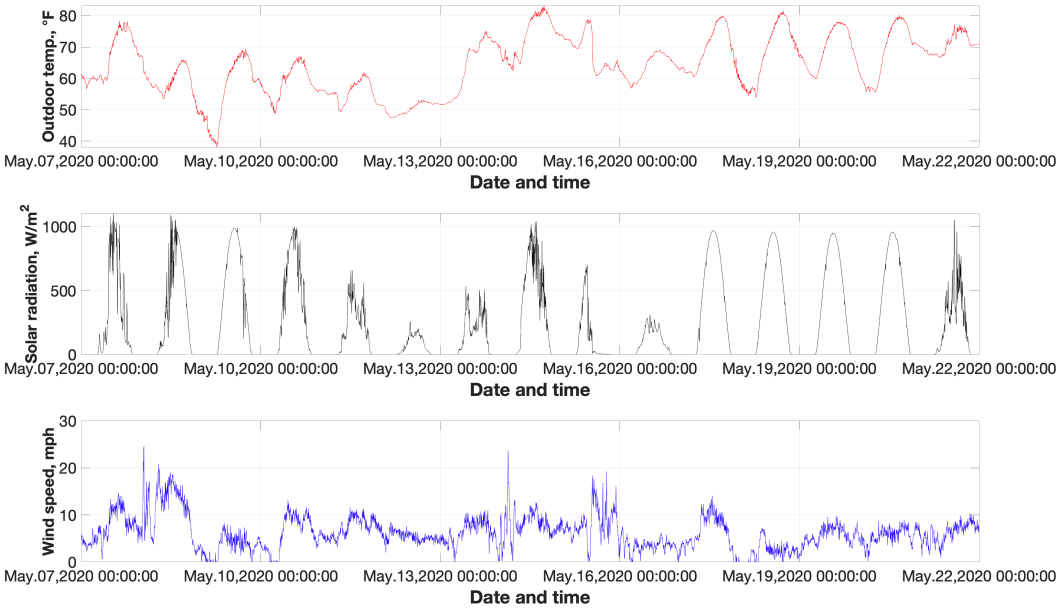

Figure B.1. Weather data from May 7 to May 21, 2020.

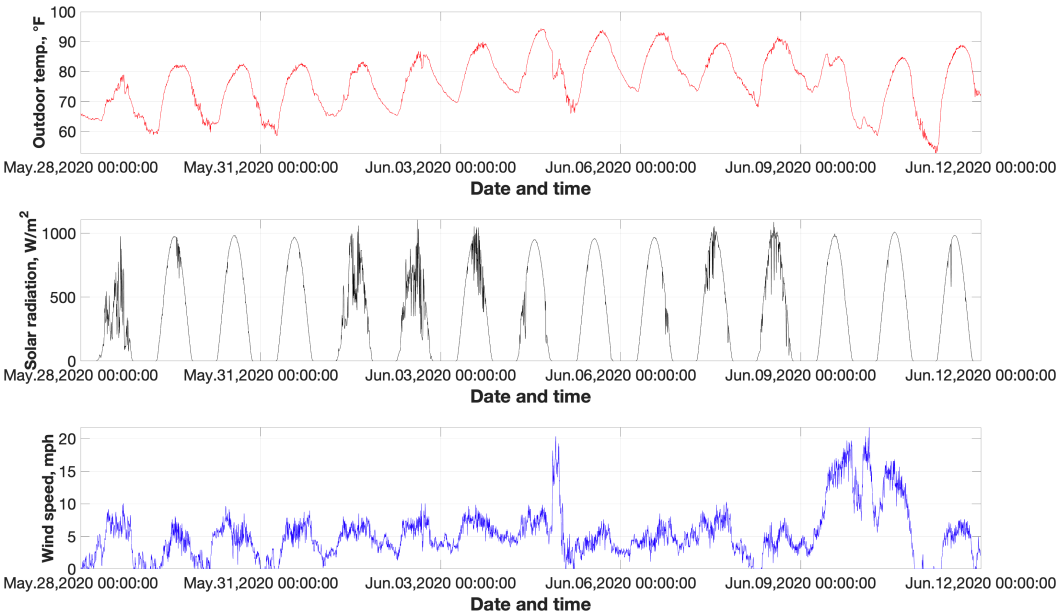

Figure B.2. Weather data from May 28 to June 11, 2020.

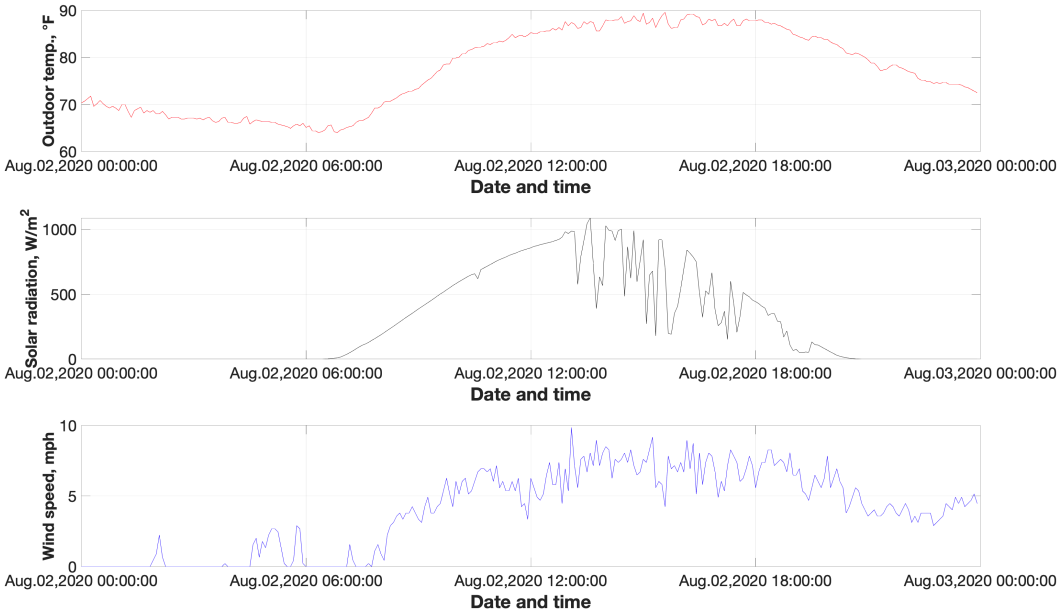

Figure B.3. Weather data on August 2, 2020.

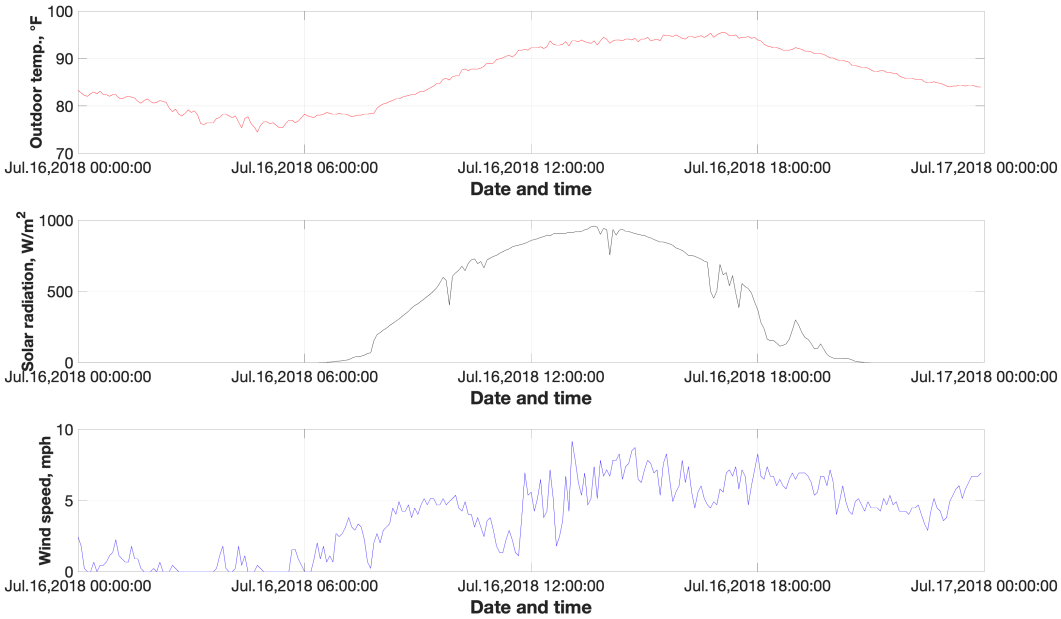

Figure B.4. Weather data on July 16, 2018.

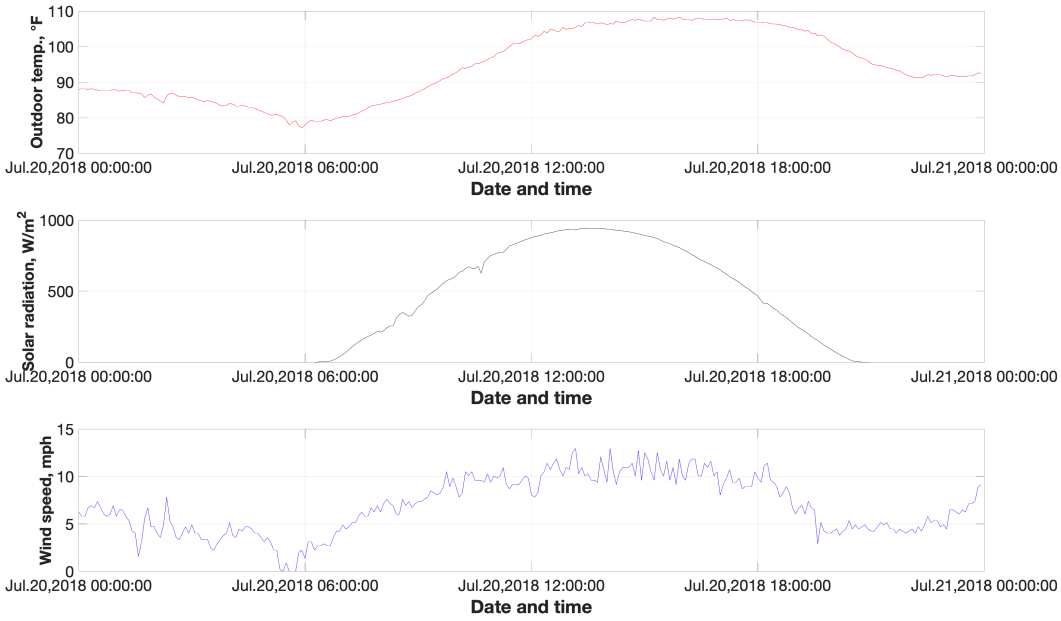

Figure B.5. Weather data on July 20, 2018.

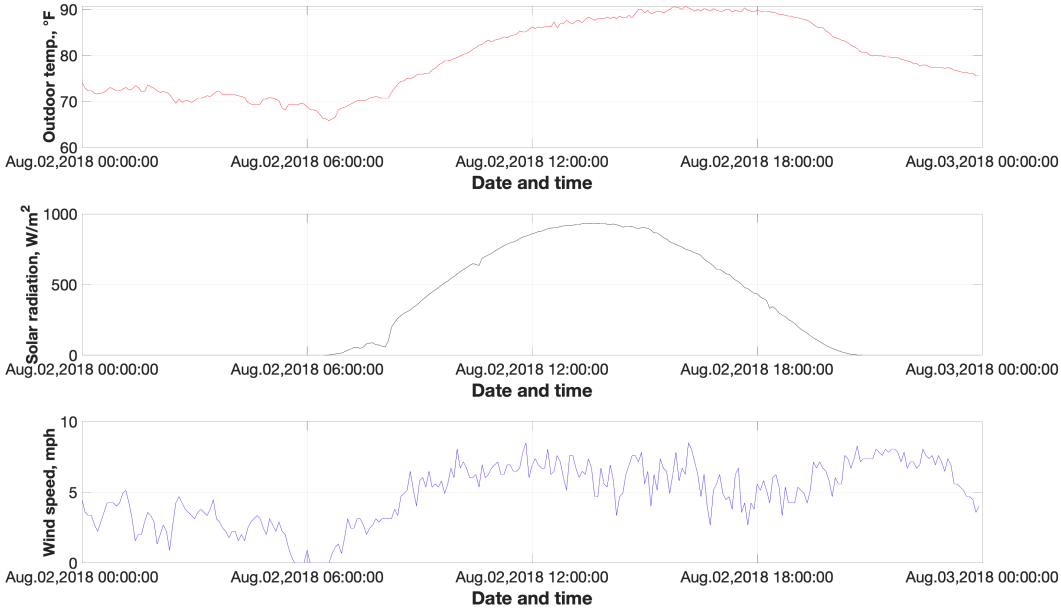

Figure B.6. Weather data on August 2, 2018.

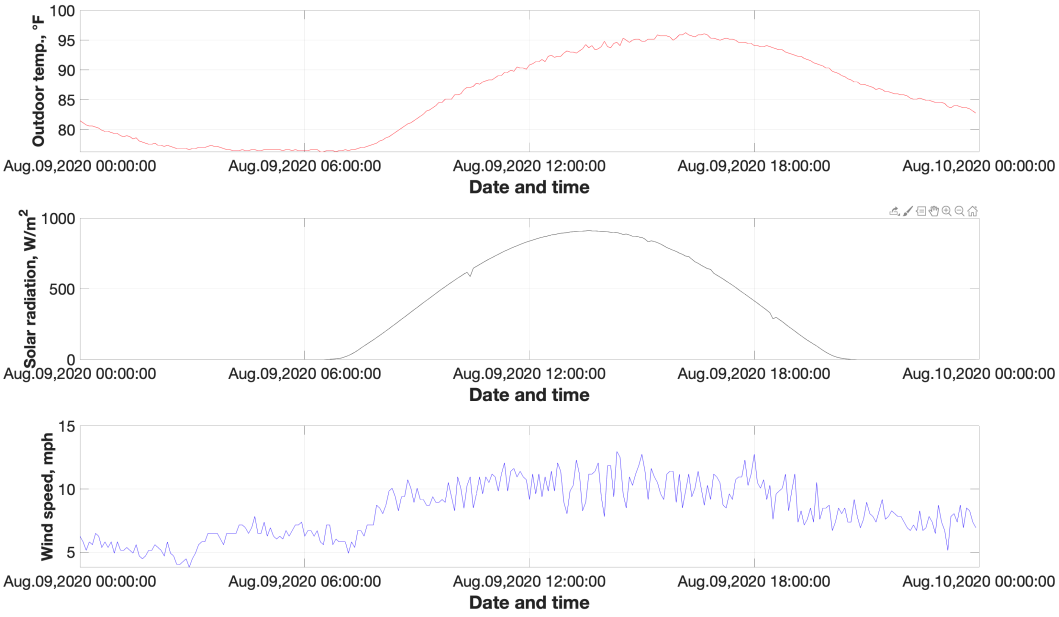

Figure B.7. Weather data on August 9, 2020.

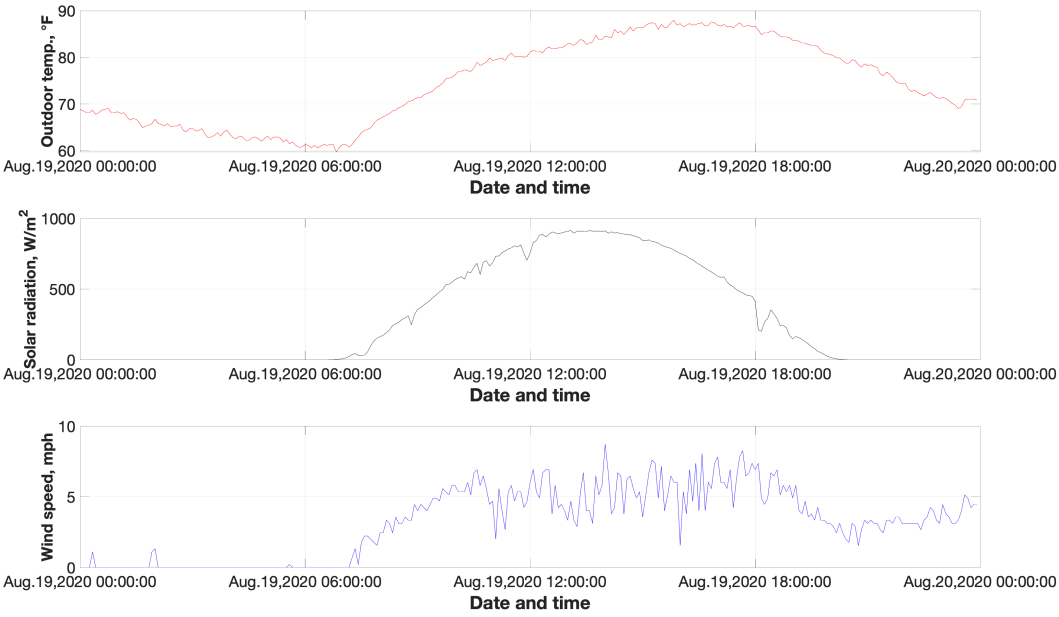

Figure B.8. Weather data on August 19, 2020.

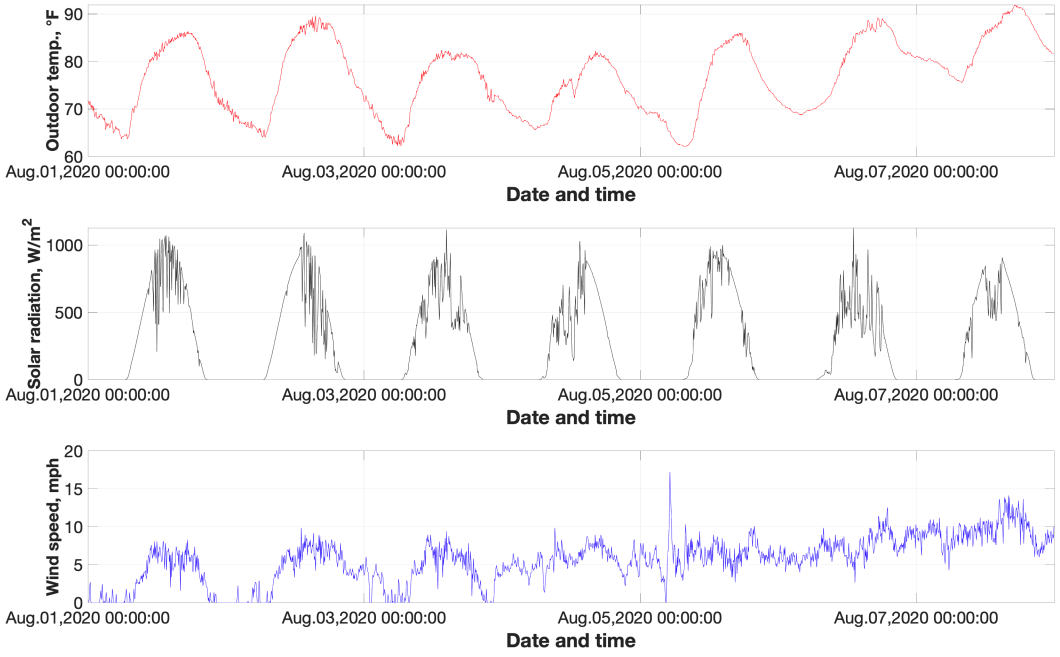

Figure B.9. Weather data on from August 1 to August 7, 2020.

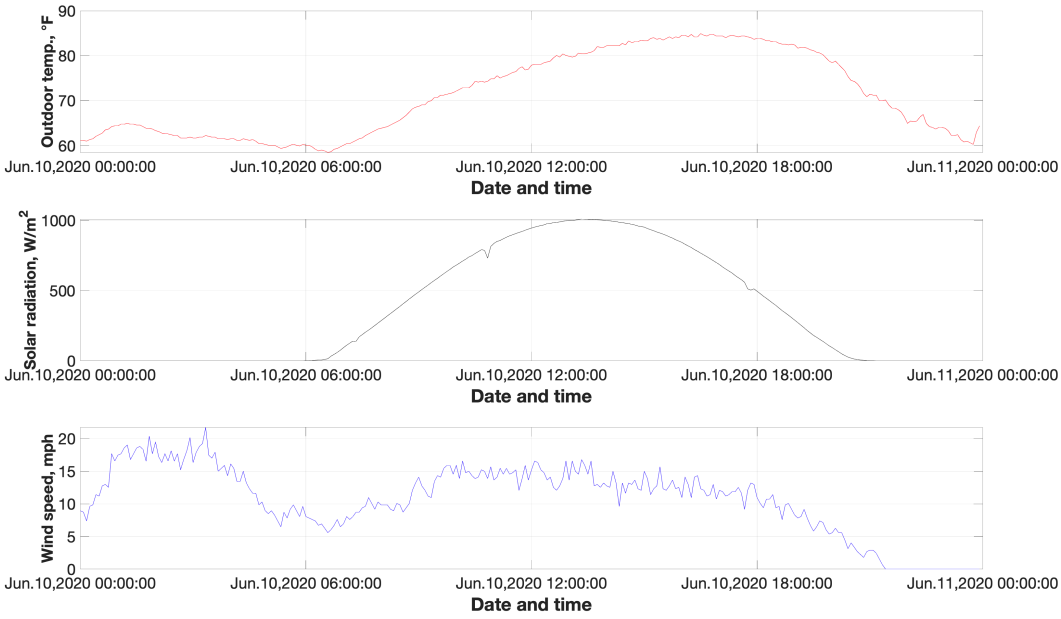

Figure B.10. Weather data on June 10, 2020.

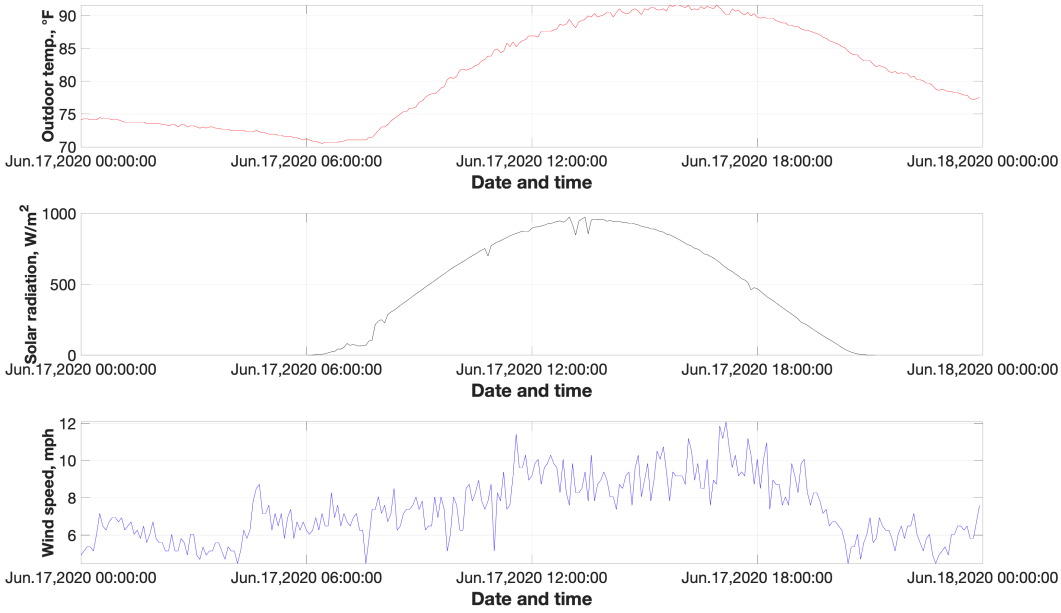

Figure B.11. Weather data on June 17, 2020.

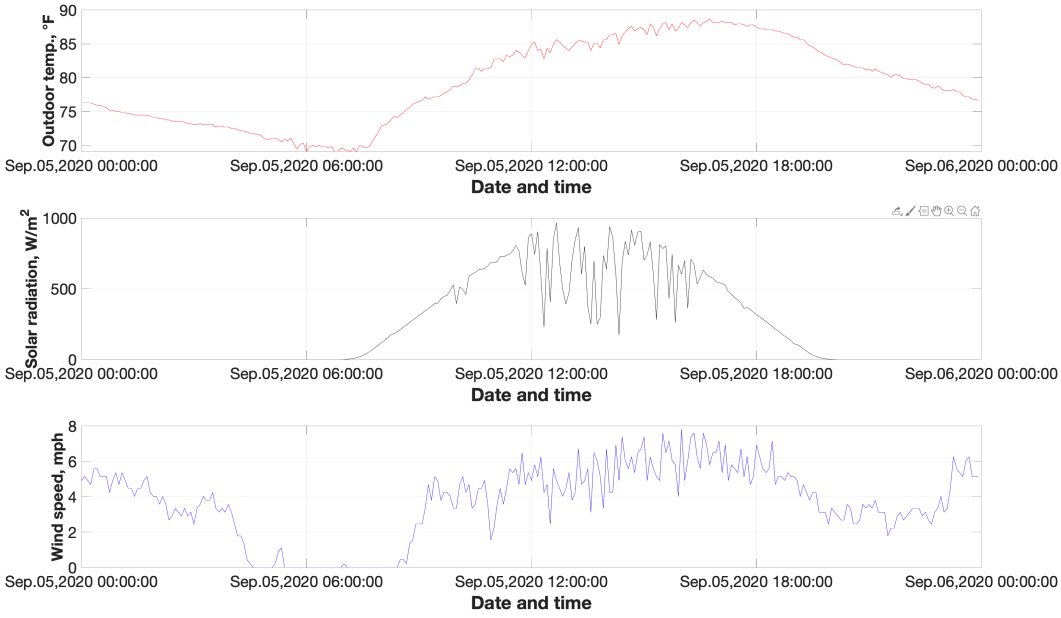

Figure B.12. Weather data on September 5, 2020.

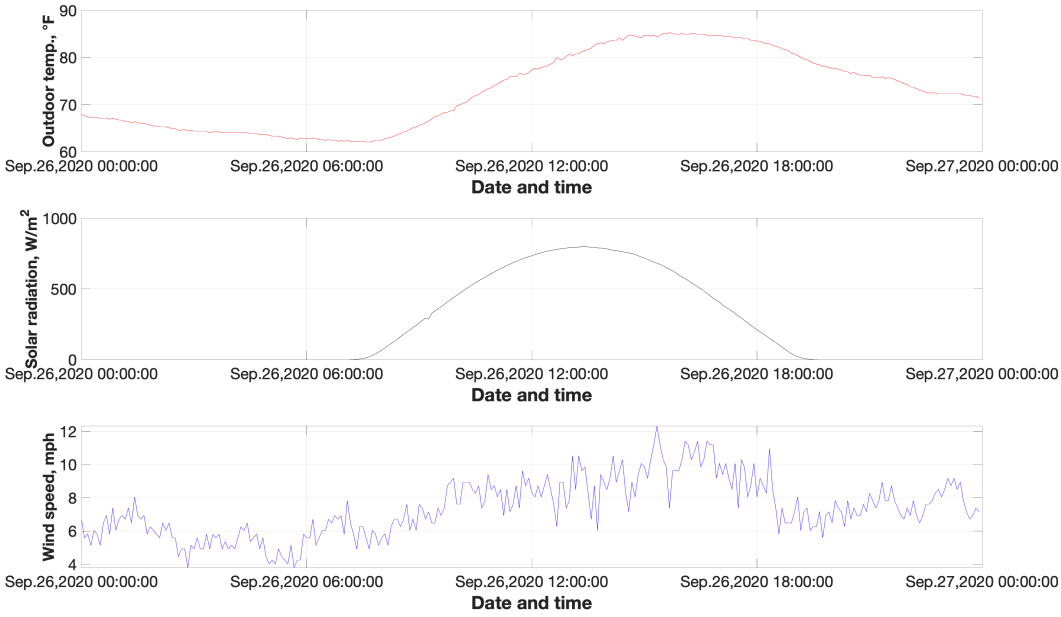

Figure B.13. Weather data on September 26, 2020.

Appendix C: Model Parameter Study Process

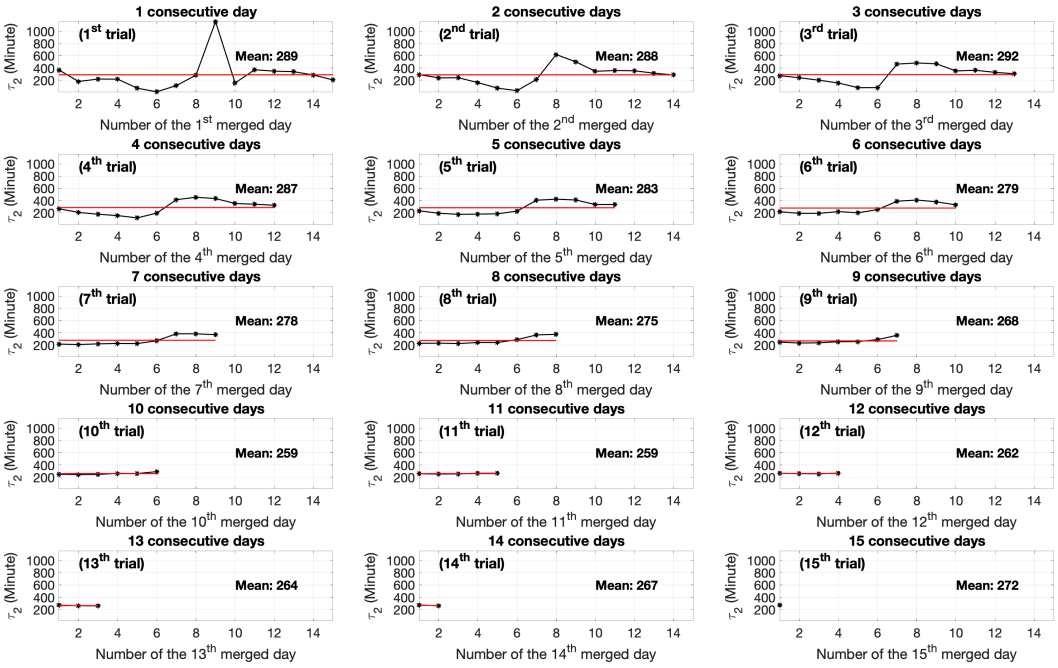

Figure C.1. Study process of the model parameter $\boldsymbol{\tau_2}$.

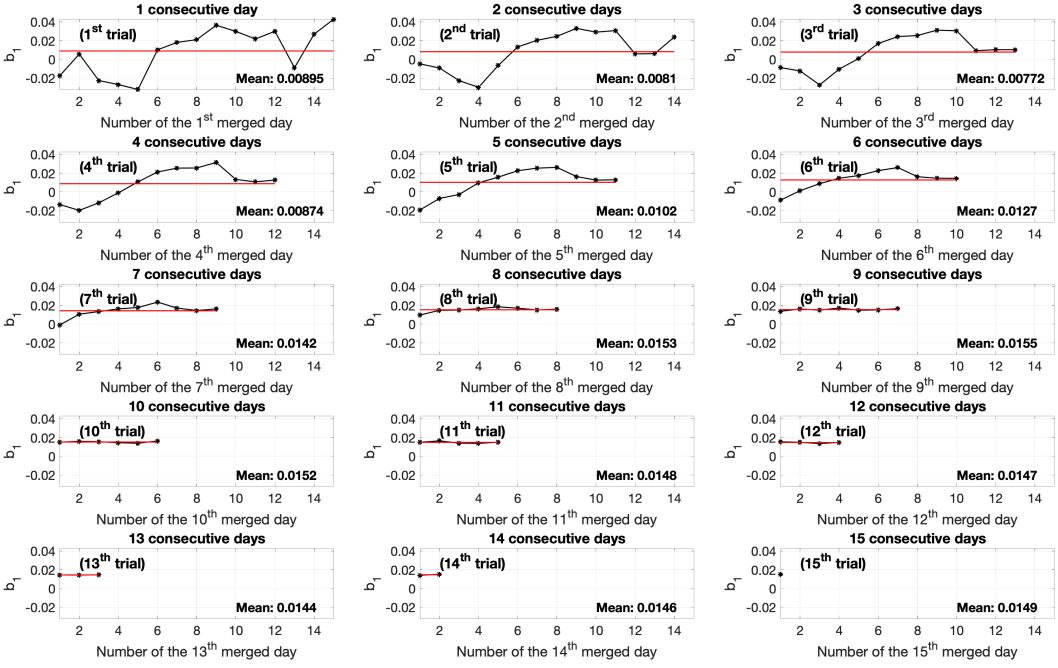

Figure C.2. Study process of the model parameter b_1.

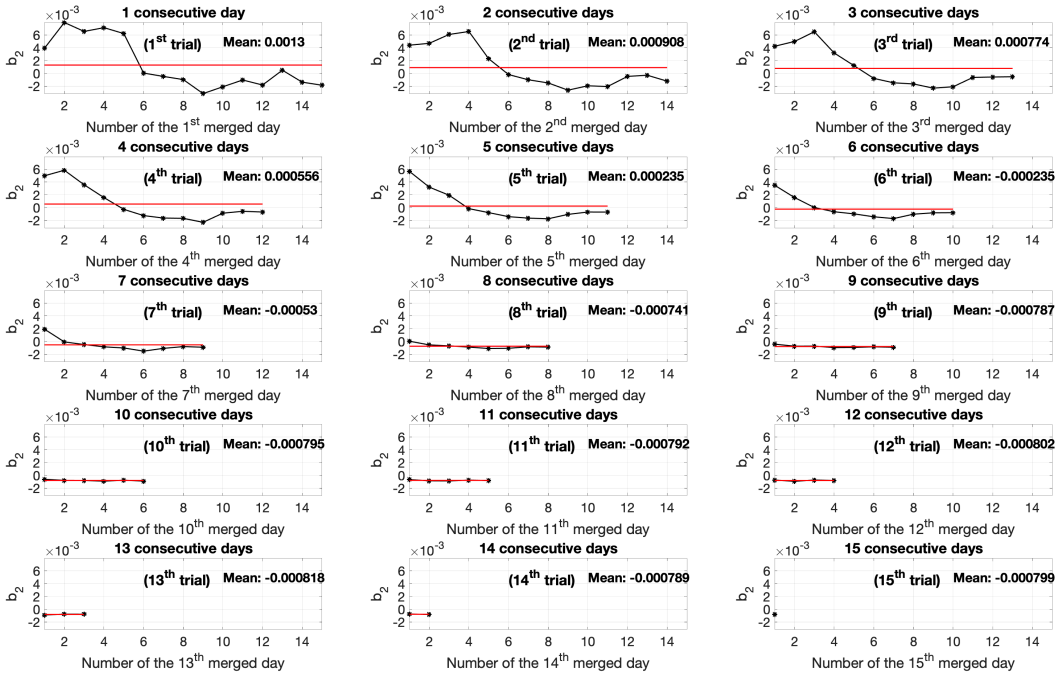

Figure C.3. Study process of the model parameter b_2.

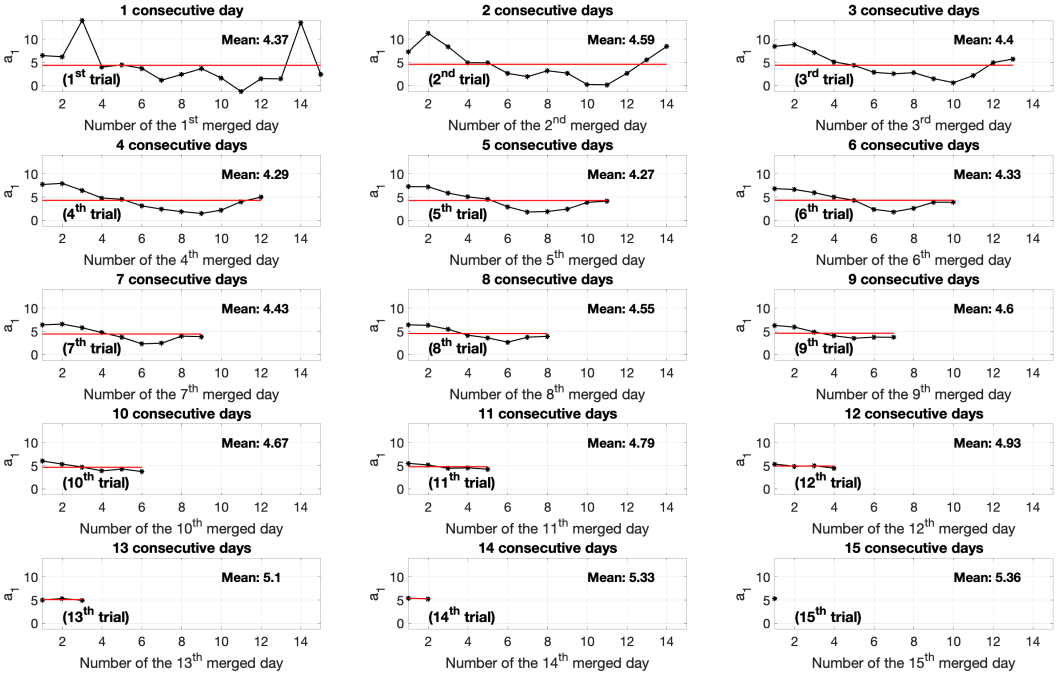

Figure C.4. Study process of the model parameter a_1.

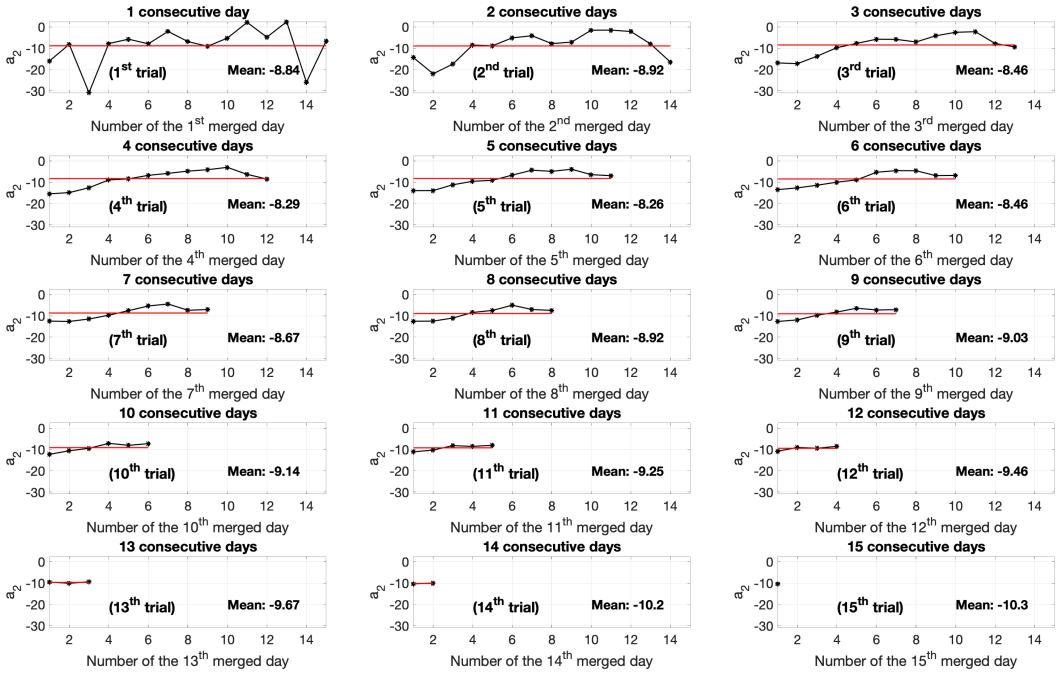

Figure C.5. Study process of the model parameter a_2.

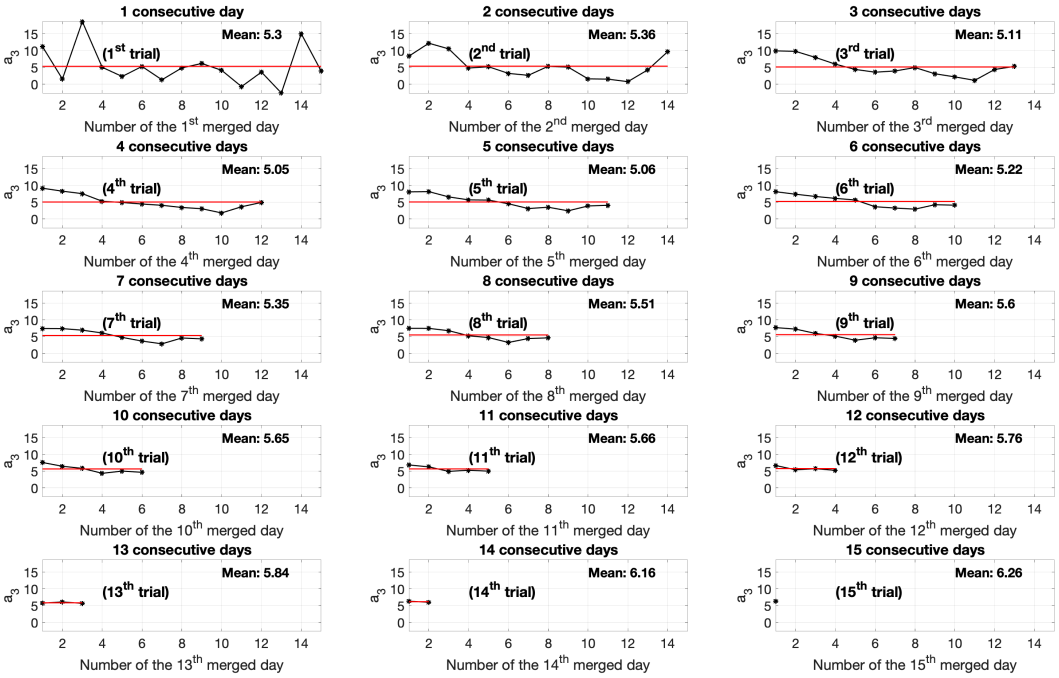

Figure C.6. Study process of the model parameter a_3.

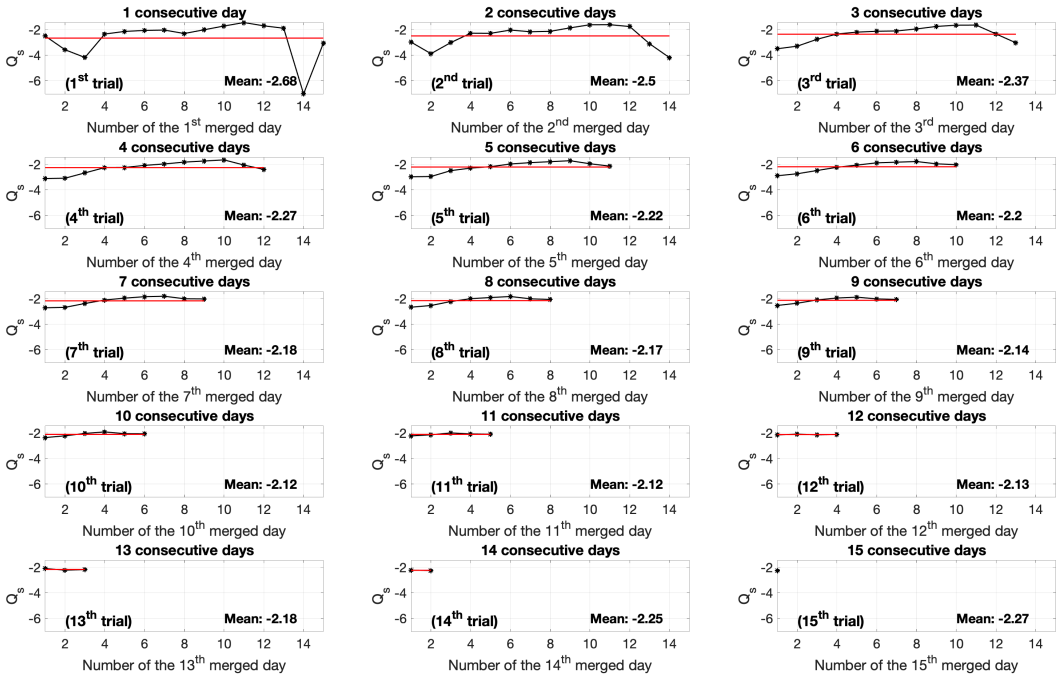

Figure C.7. Study process of the model parameter Q_s.

Appendix D: HVAC System Cooling Performance Data from Different Tons

AIR TEMP. ENTERING OUTDOOR UNIT (°F)	ID CFM	950					1200					1450				
	ID DB (°F)	80	80	75	80	80	80	80	75	80	80	80	80	75	80	80
	ID WB (°F)	57	62	62	67	72	57	62	62	67	72	57	62	62	67	72
55	T.C.	33.4	36.3	36.0	37.7	38.5	34.4	36.8	36.8	38.0	39.0	35.4	37.4	37.5	38.4	39.4
	S.C.	33.4	29.2	24.8	23.6	17.9	34.4	30.4	26.2	24.1	18.1	35.4	31.7	27.5	24.7	18.3
	KW	1.92	1.93	1.94	1.94	1.94	2.03	2.03	2.04	2.04	2.04	2.14	2.14	2.14	2.15	2.14
65	T.C.	32.6	35.1	35.1	37.5	39.5	34.2	36.1	36.1	38.3	40.3	35.8	37.1	37.1	39.2	41.0
	S.C.	32.6	28.9	24.5	23.8	18.6	34.2	31.2	26.4	25.2	19.2	35.8	33.5	28.4	26.5	19.8
	KW	2.11	2.12	2.13	2.13	2.15	2.22	2.23	2.23	2.24	2.25	2.33	2.33	2.34	2.34	2.35
75	T.C.	31.9	33.9	34.1	37.3	40.5	34.0	35.4	35.4	38.6	41.5	36.2	36.8	36.8	39.9	42.5
	S.C.	31.9	28.6	24.1	24.0	19.2	34.0	31.9	26.7	26.2	20.3	36.2	35.2	29.2	28.4	21.3
	KW	2.30	2.31	2.32	2.33	2.35	2.42	2.42	2.43	2.44	2.45	2.53	2.53	2.53	2.54	2.56
85	T.C.	30.9	32.7	32.7	35.9	39.1	32.9	34.0	34.0	37.2	40.2	34.9	35.3	35.2	38.5	41.3
	S.C.	30.9	28.2	23.6	23.5	18.8	32.9	31.4	26.2	25.8	19.8	34.9	34.6	28.7	28.1	20.8
	KW	2.56	2.55	2.56	2.57	2.59	2.67	2.66	2.67	2.68	2.70	2.78	2.77	2.78	2.79	2.81
95	T.C.	30.0	31.5	31.4	34.6	37.7	31.8	32.6	32.5	35.8	38.9	33.6	33.8	33.7	37.0	40.1
	S.C.	30.0	27.8	23.1	23.0	18.4	31.8	30.9	25.7	25.4	19.4	33.6	33.8	28.2	27.8	20.3
	KW	2.81	2.80	2.81	2.81	2.84	2.91	2.90	2.92	2.92	2.95	3.02	3.01	3.02	3.03	3.05
105	T.C.	28.5	29.6	29.6	32.5	35.5	30.2	30.7	30.6	33.6	36.7	31.8	31.8	31.6	34.8	37.8
	S.C.	28.5	26.9	22.3	22.2	17.6	30.2	29.5	24.9	24.5	18.5	31.8	31.8	27.4	26.8	19.5
	KW	3.15	3.14	3.16	3.16	3.19	3.26	3.25	3.26	3.27	3.29	3.37	3.36	3.37	3.38	3.40
115	T.C.	27.1	27.7	27.8	30.4	33.4	28.6	28.8	28.7	31.5	34.5	30.1	29.9	29.6	32.6	35.5
	S.C.	27.1	26.0	21.6	21.3	16.7	28.6	28.0	24.1	23.6	17.7	30.1	29.9	26.6	25.9	18.6
	KW	3.49	3.48	3.49	3.50	3.52	3.60	3.59	3.60	3.61	3.63	3.70	3.70	3.71	3.72	3.73
125	T.C.	25.6	25.8	26.1	28.4	31.3	27.0	26.9	26.9	29.4	32.3	28.4	27.9	27.7	30.4	33.3
	S.C.	25.6	25.1	20.8	20.5	15.8	27.0	26.9	23.3	22.7	16.8	28.4	27.9	25.9	25.0	17.8
	KW	3.82	3.82	3.83	3.84	3.86	3.93	3.93	3.94	3.95	3.97	4.04	4.04	4.05	4.06	4.07

NOTE: ALL CAPACITIES INCLUDE INDOOR FAN HEAT. KW VALUES ARE FOR THE SYSTEM (OUTDOOR + INDOOR).

Green shaded cells are ACCA (TVA) conditions.

Blue shaded cells are AHRI conditions.

Figure D.1. Performance Data – 3 Tons from a Manufacturer.

AIR TEMP. ENTERING OUTDOOR UNIT (°F)	ID CFM	1350					1600					1850				
	ID DB (°F)	80	80	75	80	80	80	80	75	80	80	80	80	75	80	80
	ID WB (°F)	57	62	62	67	72	57	62	62	67	72	57	62	62	67	72
55	T.C.	44.6	48.8	48.8	52.6	54.7	46.8	50.0	50.0	53.3	55.3	48.9	51.1	51.2	54.0	56.0
	S.C.	44.6	39.9	33.9	32.6	24.7	46.8	42.6	35.8	33.5	24.8	48.9	45.4	37.6	34.5	25.0
	KW	2.56	2.59	2.59	2.62	2.63	2.68	2.70	2.69	2.72	2.73	2.79	2.80	2.80	2.82	2.83
65	T.C.	43.3	47.2	47.4	51.7	54.9	45.5	48.5	48.6	52.6	55.9	47.7	49.7	49.9	53.5	56.8
	S.C.	43.3	39.5	33.5	32.7	25.2	45.5	42.5	35.6	34.2	25.9	47.7	45.6	37.7	35.8	26.5
	KW	2.82	2.85	2.85	2.88	2.91	2.93	2.95	2.95	2.98	3.01	3.05	3.06	3.05	3.09	3.11
75	T.C.	42.0	45.7	46.1	50.8	55.1	44.2	47.0	47.3	51.9	56.4	46.5	48.3	48.5	53.0	57.7
	S.C.	42.0	39.0	33.0	32.7	25.8	44.2	42.4	35.4	34.9	26.9	46.5	45.7	37.8	37.1	28.1
	KW	3.07	3.10	3.10	3.14	3.18	3.19	3.21	3.21	3.25	3.29	3.31	3.32	3.31	3.35	3.39
85	T.C.	40.8	43.9	44.1	48.8	53.3	42.8	45.1	45.4	49.9	54.6	44.8	46.4	46.6	51.0	56.0
	S.C.	40.8	38.4	32.2	32.1	25.1	42.8	41.8	34.7	34.4	26.3	44.8	45.2	37.3	36.8	27.4
	KW	3.41	3.44	3.44	3.48	3.51	3.53	3.55	3.55	3.58	3.62	3.64	3.65	3.65	3.69	3.72
95	T.C.	39.6	42.1	42.2	46.9	51.5	41.4	43.3	43.5	48.0	52.9	43.2	44.5	44.7	49.1	54.2
	S.C.	39.6	37.8	31.4	31.4	24.5	41.4	41.3	34.1	33.9	25.6	43.2	44.5	36.7	36.4	26.8
	KW	3.76	3.78	3.78	3.81	3.85	3.87	3.88	3.88	3.92	3.95	3.98	3.99	3.98	4.02	4.06
105	T.C.	37.0	39.7	39.8	44.2	48.6	39.0	40.8	40.9	45.1	49.8	41.0	41.9	42.1	46.0	51.0
	S.C.	37.0	36.5	30.4	30.2	23.5	39.0	39.4	33.0	32.8	24.7	41.0	41.9	35.6	35.3	26.0
	KW	4.24	4.26	4.27	4.30	4.33	4.35	4.37	4.37	4.41	4.44	4.47	4.47	4.47	4.51	4.54
115	T.C.	34.5	37.4	37.4	41.6	45.7	36.7	38.4	38.4	42.3	46.8	38.8	39.4	39.5	43.0	47.9
	S.C.	34.5	35.3	29.5	29.0	22.5	36.7	37.5	31.9	31.6	23.8	38.8	39.4	34.4	34.3	25.1
	KW	4.71	4.74	4.73	4.77	4.80	4.83	4.84	4.84	4.88	4.91	4.94	4.94	4.94	4.99	5.01
125	T.C.	32.0	35.0	35.0	38.9	42.8	34.3	36.0	36.0	39.5	43.8	36.7	36.9	37.0	40.0	44.9
	S.C.	32.0	34.0	28.5	27.8	21.5	34.3	35.7	30.9	30.5	22.9	36.7	36.9	33.3	33.3	24.3
	KW	5.18	5.21	5.20	5.24	5.28	5.30	5.31	5.31	5.35	5.38	5.41	5.41	5.41	5.47	5.48

NOTE: ALL CAPACITIES INCLUDE INDOOR FAN HEAT. KW VALUES ARE FOR THE SYSTEM (OUTDOOR + INDOOR).

Green shaded cells are ACCA (TVA) conditions.

Blue shaded cells are AHRI conditions.

Figure D.2. Performance Data – 4 Tons from a Manufacturer.

AIR TEMP. ENTERING OUTDOOR UNIT (°F)	ID CFM	1500					1750					2000				
	ID DB (°F)	80	80	75	80	80	80	80	75	80	80	80	80	75	80	80
	ID WB (°F)	57	62	62	67	72	57	62	62	67	72	57	62	62	67	72
55	T.C.	55.6	59.6	59.4	61.6	62.0	57.6	60.4	60.2	61.9	62.2	59.6	61.2	61.1	62.1	62.3
	S.C.	54.2	46.9	40.5	37.7	29.2	56.5	48.5	41.8	38.5	29.5	58.7	50.2	43.1	39.3	29.9
	KW	3.11	3.13	3.13	3.14	3.14	3.21	3.23	3.23	3.23	3.23	3.31	3.32	3.32	3.32	3.32
65	T.C.	54.0	58.0	57.8	61.5	64.5	56.1	59.1	58.9	62.2	65.2	58.2	60.3	60.1	62.9	65.9
	S.C.	52.9	46.6	39.8	38.3	30.1	55.1	49.1	41.8	39.9	30.9	57.3	51.6	43.8	41.5	31.7
	KW	3.41	3.45	3.45	3.47	3.49	3.52	3.55	3.55	3.57	3.59	3.63	3.65	3.65	3.67	3.68
75	T.C.	52.5	56.4	56.2	61.4	66.9	54.6	57.8	57.6	62.6	68.2	56.8	59.3	59.0	63.8	69.4
	S.C.	51.6	46.2	39.1	38.8	31.1	53.7	49.7	41.8	41.2	32.3	55.9	53.1	44.4	43.6	33.5
	KW	3.72	3.76	3.76	3.81	3.84	3.83	3.87	3.87	3.91	3.95	3.94	3.98	3.97	4.01	4.05
85	T.C.	51.2	54.4	54.2	59.2	64.2	53.4	55.8	55.6	60.3	65.5	55.6	57.2	56.9	61.4	66.8
	S.C.	50.4	45.7	38.6	38.1	30.2	52.6	49.2	41.3	40.6	31.6	54.7	52.8	44.0	43.1	33.0
	KW	4.14	4.18	4.18	4.22	4.26	4.25	4.28	4.28	4.32	4.37	4.36	4.39	4.38	4.43	4.47
95	T.C.	50.0	52.4	52.2	57.0	61.5	52.2	53.8	53.5	58.0	62.9	54.4	55.2	54.8	59.0	64.3
	S.C.	49.2	45.2	38.0	37.4	29.3	51.4	48.8	40.8	40.0	31.0	53.6	52.4	43.6	42.6	32.6
	KW	4.55	4.59	4.59	4.63	4.68	4.66	4.69	4.69	4.73	4.79	4.77	4.80	4.79	4.84	4.90
105	T.C.	46.7	48.7	48.6	53.2	58.1	48.9	50.1	49.7	54.2	59.1	51.1	51.6	50.9	55.2	60.1
	S.C.	46.0	43.3	36.2	35.9	28.1	48.1	46.4	39.0	38.5	29.7	50.3	49.5	41.7	41.1	31.3
	KW	5.16	5.19	5.19	5.24	5.28	5.27	5.30	5.29	5.34	5.39	5.38	5.40	5.40	5.45	5.50
115	T.C.	43.5	45.1	45.1	49.6	54.8	45.7	46.6	46.1	50.5	55.4	47.8	48.1	47.1	51.5	56.0
	S.C.	42.9	41.4	34.6	34.4	26.9	45.0	44.1	37.2	37.0	28.5	47.1	46.7	39.8	39.6	30.0
	KW	5.75	5.77	5.77	5.83	5.87	5.87	5.88	5.88	5.93	5.97	5.98	5.99	5.99	6.04	6.08
125	T.C.	40.4	41.5	41.6	46.0	51.6	42.5	43.1	42.4	46.8	51.8	44.6	44.7	43.3	47.7	51.9
	S.C.	39.7	39.5	32.9	32.9	25.8	41.8	41.7	35.4	35.5	27.2	43.9	44.0	37.9	38.2	28.7
	KW	6.35	6.36	6.35	6.42	6.45	6.46	6.47	6.47	6.52	6.56	6.57	6.58	6.58	6.63	6.66

NOTE: ALL CAPACITIES INCLUDE INDOOR FAN HEAT. KW VALUES ARE FOR THE SYSTEM (OUTDOOR + INDOOR).

Green shaded cells are ACCA (TVA) conditions.

Blue shaded cells are AHRI conditions.

Figure D.3. Performance Data – 5 Tons from a Manufacturer.